Universitat Autònoma de Barcelona

Chloroperoxidase and D-fructose-6-phosphate aldolase in enzymatic cascade reactions for the synthesis of iminocyclitols

Gerard Masdeu Gámez

ADVERTIMENT. L’accés als continguts d’aquesta tesi queda condicionat a l’acceptació de les condicions d’ús establertes per la següent llicència Creative Commons: http://cat.creativecommons.org/?page_id=184

ADVERTENCIA. El acceso a los contenidos de esta tesis queda condicionado a la aceptación de las condiciones de uso establecidas por la siguiente licencia Creative Commons: http://es.creativecommons.org/blog/licencias/

WARNING. The access to the contents of this doctoral thesis it is limited to the acceptance of the use conditions set by the following Creative Commons license: https://creativecommons.org/licenses/?lang=en

Universitat Autònoma de Barcelona

Escola d’Enginyeria

Departament d’Enginyeria Química, Biològica i Ambiental

Chloroperoxidase and D-fructose-6-phosphate aldolase in enzymatic cascade reactions for the synthesis of iminocyclitols

Memòria per optar al grau de Doctor Internacional
per la Universitat Autònoma de Barcelona,
sota la direcció del Dr. Josep López Santín i el Dr. Gregorio Álvaro Campos

per

Gerard Masdeu Gámez

Bellaterra, setembre 2017

El Dr. Josep López Santín, catedràtic del Departament d'Enginyeria Química, Biològica i Ambiental de la Universitat Autònoma de Barcelona, i el Dr. Gregorio Álvaro Campos, professor agregat del Departament d'Enginyeria Química, Biològica i Ambiental de la Universitat Autònoma de Barcelona,

Certifiquem:

> Que el biotecnòleg Gerard Masdeu Gámez ha dut a terme sota la nostra direcció el treball titulat **Chloroperoxidase and D-fructose-6-phosphate aldolase in enzymatic cascade reactions for the synthesis of iminocyclitols**, que es presenta en aquesta memòria i constitueix la seva Tesi per optar al Grau de Doctor en Biotecnologia per la Universitat Autònoma de Barcelona.

I per tal que se'n prengui coneixement i consti als efectes oportuns, signem la present a Bellaterra, a 13 de setembre de 2017.

Dr. Josep López Santín Dr. Gregorio Álvaro Campos

Resum

Aquest treball de tesi se centra en la viabilitat d'una reacció en cascada formada per una peroxidasa i una aldolasa per a la síntesi d'iminociclitols, que són inhibidors de glicosidases amb un enorme potencial terapèutic en moltes malalties, alterant la glicosilació o el catabolisme de glicoproteïnes. El sistema proposat consisteix en dos enzims –cloroperoxidasa (CPO) i D-fructosa-6-fosfat aldolasa (FSA)– per a la formació del precursor de D-fagomina, seleccionat com l'iminociclitol d'interès per avaluar la viabilitat de l'acoblament d'ambdues reaccions. El substrat inicial és un β-amino alcohol (*N*-Cbz-3-aminopropanol, β-OH), que és oxidat a *N*-Cbz-3-aminopropanal (β-CHO) per CPO, en presència del peròxid. FSA catalitza l'addició aldòlica de dihidroxiacetona a β-CHO per donar lloc al producte final.

Ambdues reaccions són investigades per entendre el mecanisme de reacció, preparar biocatalitzadors estables adequats i trobar les millors condicions per a la seva aplicació. S'analitza la capacitat oxidativa d'amino alcohols de CPO en funció de l'estructura del substrat. Seguidament, es realitzen proves experimentals de l'oxidació de β-OH per determinar les principals condicions d'operació per als primers assaigs de la reacció acoblada. Tanmateix, s'observen la inactivació d'ambdós enzims i l'existència de reaccions no desitjades, com l'oxidació de β-CHO a *N*-Cbz-3-aminopropanoic acid (β-COOH) i la reacció química aldehid-peròxid.

La modelització cinètica de totes les reaccions representa una aproximació a un millor enteniment del sistema i una possible estratègia d'optimitzar-lo. Es desenvolupa i es valida un model matemàtic de la reacció. Paral·lelament, la immobilització d'enzims representa una segona estratègia de millora del sistema, reduint la inactivació de CPO i FSA. S'estudia la immobilització d'ambdós enzims en suports convencionals d'agarosa funcionalitzats i en clústers de nanopartícules magnètiques.

Finalment, el model cinètic és usat per a la intensificació del procés per tal de determinar les condicions òptimes per a l'acoblament de les reaccions. S'avaluen dues configuracions de reactor: un sol reactor (one-pot), i dos reactors en sèrie. Es comparen ambdues estratègies en funció de si s'utilitzen CPO/FSA solubles o immobilitzats.

Abstract

This thesis work is focused on the feasibility of a peroxidase/aldolase cascade reaction for the synthesis of iminocyclitols, which are glycosidase inhibitors with enormous therapeutic potential in many diseases by altering the glycosylation or catabolism of glycoproteins. The proposed system consists of two enzymes –chloroperoxidase (CPO) and D-fructose-6-phosphate aldolase (FSA)– for the formation of the precursor of D-fagomine, selected as target iminocyclitol to evaluate the viability of the coupling of both reactions. The starting substrate is a β-amino alcohol (*N*-Cbz-3-aminopropanol, β-OH), which is oxidized to *N*-Cbz-3-aminopropanal (β-CHO) by CPO in presence of peroxide. FSA catalyzes the aldol addition of dihydroxyacetone to β-CHO to render the final product.

Both reactions are investigated in order to understand the reaction mechanism, prepare suitable stabilized biocatalysts, and find the proper conditions for its application. The amino alcohol oxidative capacity of CPO regarding the substrate structure is discussed, followed by experimental trials on the β-OH oxidation to determine the main operating conditions for the first assays of the coupled reaction. However, the inactivation of both enzymes and the existence of side reactions, such as the further oxidation of β-CHO to *N*-Cbz-3-aminopropanoic acid (β-COOH) and a chemical reaction aldehyde-peroxide, are observed.

Kinetic modeling of all the reactions represents an approach for a better understanding of the system and a possible strategy to optimize it. A mathematical model is systematically developed and validated. Concurrently, enzyme immobilization becomes a second strategy for the system improvement, by reducing the inactivation of CPO and FSA. The immobilization of both enzymes on functionalized conventional supports of agarose and magnetic nanoparticle clusters is studied.

Finally, the kinetic model is employed for process intensification to determine the optimal conditions for the reaction coupling. Two reactor configurations are assayed: one-pot or two-consecutive vessels. Both strategies are compared using soluble and immobilized CPO/FSA.

Abbreviations

β-OH*:* *N*-Cbz-3-anminopropanol
β-CHO: *N*-Cbz-aminopropanal
β-COOH: *N*-Cbz-3-aminopropanoic acid
BSA: bovine serum albumin
Cbz: carboxybenzyl group
CoIDA-agarose: cobalt-iminodiacetic agarose
CPO: chloroperoxidase
DHA: dihydroxyacetone
DHAP: dihydroxyacetone phosphate
DLS: dynamic light scattering
DNPH: dinitrophenylhydrazine phosphoric acid solution
EDAC: 1-ethyl-3-(3-dimethylaminopropyl)carbodiimide
EDTA: ethylenediaminetetraacetic acid
F6P: D-fructose-6-phosphate
FSA: D-fructose-6-phosphate aldolase
FSA A129S: recombinant FSA – Ala 129 substituted by Ser
FSA A129S/A165G: recombinant FSA – Ala 129 substituted by Ser; Ala 165 substituted by Gly.
FucA: L-fuculose 1-phosphate aldolase
G3P: D-glyceraldehyde-3-phosphate
GPD: Glycerophosphate dehydrogenase
H_2O_2: hydrogen peroxide
HEPES :4-(2-hydroxyethyl)-1-piperazineethanesulfonic acid
HA: hydroxyacetone
HAP: hydroxy alkyl peroxide
HLADH: horse liver alcohol dehydrogenase
IDA: iminodiacetic acid
MANA-agarose: monoaminoethyl-*N*-aminoethyl agarose
MCD: monochlorodimedone
MeCN: acetonitrile
MES: 2-(N-morpholino)ethanesulfonic acid
mNC: magnetic nanoparticle clusters (any type)
mNC-R: mNC modified with R functional group (R = PEG, NH_2, COOH, etc.)
MS: mass spectrometry
nCPO: native form of CPO
oxCPO: CPO modified by sugar moieties oxidation
oxDHA: oxidized DHA (1,1,3-trihydroxypropan-2-one)
PA: 4-pentynoic acid
PACPO: CPO modified with PA
PEG: polyethylene glycol
PG: propargylamine
PGCPO: CPO modified with PG
preFagomine: precursor of D-fagomine – (3S,4R)-6-[(benzyloxycarbonyl)amino]-5,6-dideoxyhex-2-ulose
RhuA: L-rhamnulose 1-phosphate aldolase
S.D.: standard deviation
SN: supernatant
SUSP: suspension
$t_{1/2}$: half-life time
t*-BuOH: tert*-butyl alcohol
***t*-BuOO**$^{\cdot}$: radical from the degradation of *t*-BuOOH
t*-BuOOH: tert*-butyl hydroperoxide
TEM: transmission electron microscopy
TPI: triosephosphate isomerase
TFA: trifluoroacetic acid

Nomenclature

[..]	molar concentration, mM
a	CPO inactivation constant, mM min^{-1}
b	FSA inactivation constant, mM min^{-1}
c	FSA inactivation exponent for FSA concentration, -
d	FSA inactivation exponent for DHA concentration, -
k_1	kd_{FSA1} constant (inactivation by r_4), mM^{-1}
k_2	kd_{FSA2} constant (inactivation by r_5), mM^{-1}
k_2’	kd_{FSA2} constant (inactivation by r_5), min^{-1}
k_{3i}	chemical reaction constant, mM^{-1} min^{-1}
k_{3ii}	reverse chemical reaction constant, min^{-1}
k_4	*t*-BuOOH degradation constant, mM
k_a	maximal value of CPO inactivation rate constant, min^{-1}
k_{cat}	maximal reaction rate, µmols min^{-1} (mg enzyme)$^{-1}$
k_d	inactivation rate constant, min^{-1}
ki	inhibition constant, mM
ki_{r3}	chemical reaction exponent, -
K_M	Michaelis-Menten constant in CPO reactions, mM
K_M’	Michaelis-Menten constant in FSA reactions, mM
n	*t*-BuOOH degradation sigmoidal exponent, -
r	reaction rate, mM min^{-1}
Y	enzyme mass concentration, mg mL^{-1}

Contents

Resum i

Abstract iii

Abbreviations v

Nomenclature vii

1 INTRODUCTION 1

1.1 General aspects 1

1.1.1 Biocatalysis in the modern industry 1

1.1.2 Enzyme (in)stability 2

1.1.3 Immobilization methods 3

1.1.4 Why to immobilize? 5

1.1.5 Cascade reactions 5

1.2 Multi-enzymatic cascade for the synthesis of iminocyclitols 7

1.2.1 Iminocyclitols 7

1.2.2 Aldol reactions 8

1.2.3 Aldolases classification 9

1.2.4 Fructose-6-phosphate aldolase 12

1.2.5 FSA for the D-Fagomine synthesis 14

1.2.6 *N*-Cbz-3-aminopropanal synthesis 15

1.2.7 Peroxidases 16

1.2.8 Chloroperoxidase 17

1.2.9 The overall system for the synthesis 20

1.3 Previous work 21

1.4 References 22

2 Objectives 27

3 Chloroperoxidase-catalyzed amino alcohol oxidation: substrate specificity and novel strategy for the synthesis of *N*-Cbz-3-aminopropanal 29

3.1 Introduction 29

3.2 Materials and methods 30

3.2.1 Materials 30

3.2.2 CPO activity 31

3.2.3 HPLC analysis 31

3.2.4 Oxidation of amino alcohols 1–5 32

3.2.5 β-OH oxidation 33

3.2.6 Amino aldehyde–peroxide chemical reaction 33

3.2.7 Identification of side-reaction products 34

3.3 Results and discussion 34

3.3.1 Substrate specificity in amino alcohol oxidations 34
3.3.2 β-OH oxidation 36
3.3.3 β-OH oxidation: Identification of side reactions 40
3.3.4 β-OH oxidation: Intensification 42
3.4 Conclusions 43
3.5 References 44
4 Bottlenecks identification in the coupling of the CPO-catalyzed β-OH oxidation with the FSA-catalyzed aldol addition 47
4.1 Introduction 47
4.2 Materials and methods 48
4.2.1 Materials 48
4.2.2 CPO activity 48
4.2.3 FSA activity 48
4.2.4 FSA production 49
4.2.5 HPLC analysis 49
4.2.6 Peroxide selection 50
4.2.7 Enzyme stability over pH 50
4.2.8 CPO/FSA assays 50
4.2.9 Preliminary coupling 50
4.3 Results and discussion 51
4.3.1 Peroxide 51
4.3.2 pH stability 52
4.3.3 Enzymes compatibility 52
4.3.4 Coupled reaction 53
4.4 Conclusions 55
4.5 References 55
5 Kinetic model for the CPO/FSA-catalyzed β-OH oxidation and DHA aldol addition 57
5.1 Introduction 57
5.1.1 Enzyme kinetics 57
5.1.2 Two-substrate kinetics 60
5.1.3 Parameter estimation 61
5.1.4 Application of a kinetic model 62
5.1.5 CPO/FSA reaction 63
5.2 Materials and methods 63
5.2.1 Materials 63
5.2.2 CPO/FSA activity 63
5.2.3 HPLC analysis 63
5.2.4 Model experiments 64

5.2.5 Model calculations 64
5.3 Results and discussion 64
5.3.1 CPO-catalyzed *t*-BuOOH degradation and enzyme inactivation 67
5.3.2 Chemical reaction aldehyde-peroxide 71
5.3.3 CPO-catalyzed oxidations 79
5.3.4 FSA-catalyzed aldol addition 98
5.3.5 FSA inactivation 103
5.3.6 Model validation 114
5.4 Conclusions 119
5.5 References 120
6 Immobilization of CPO and FSA on functionalized carriers: agarose and magnetic nanoparticle clusters 121
6.1 Introduction 121
6.1.1 Agarose 121
6.1.2 Magnetic nanoparticle clusters 123
6.1.3 CPO and FSA immobilization 124
6.1.4 Objective 126
6.2 Materials and methods 127
6.2.1 Materials 127
6.2.2 Activity assays 127
6.2.3 Preparation of immobilization supports 128
6.2.4 Enzyme modification 131
6.2.5 Enzyme immobilization 132
6.2.6 Application of immobilized derivatives 136
6.2.7 HPLC analysis 138
6.3 Results and discussion 139
6.3.1 CPO immobilization 139
6.3.2 FSA immobilization 157
6.4 Conclusions 169
6.5 Contributions from the collaborations 170
6.6 References 171
7 Kinetic model exploitation for the determination of the coupled reaction conditions 175
7.1 Introduction 175
7.2 Materials and methods 176
7.2.1 Materials 176
7.2.2 CPO/FSA activity 176
7.2.3 Enzyme immobilization 176
7.2.4 HPLC analysis 176

7.2.5 Model calculations 176
7.2.6 Coupled reactions 177
7.3 Results and discussion 177
7.3.1 Two-step coupled reaction 179
7.4 Conclusions 184
7.5 References 185
8 Overall conclusions. Future perspectives 187
9 Acknowledgments 191
10 Scientific contributions 193
11 Appendix 195
11.1 Products from the chemical reaction aldehyde-peroxide 195
11.2 FSA production 198
11.3 SDS-PAGE 201
11.4 FSA purification 202
11.5 Analysis of preFagomine 202
11.6 Analysis of the product of DHA oxidation 203
11.7 Silane-C-C≡H/N_3 synthesis 204
11.8 References 206

1 INTRODUCTION

This brief introduction deals first with general aspects of biocatalysis, biocatalyst stability, immobilization and multi-enzyme synthesis before presenting the thesis work topic. Then the main components of the system (enzyme, substrates, and products) are introduced and discussed.

1.1 General aspects

1.1.1 Biocatalysis in the modern industry

A broad definition of biocatalysis is the use of enzymes (isolated or whole cells) as biocatalysts for the transformation of natural and non-natural compounds.[1,2] Over the years, it has definitely emerged as an alternative to the classic chemical synthesis established in the industry for decades, especially for the production of pharmaceuticals, fine chemicals, and food (Figure 1.1).[3,4] The environmental benefits from the *bio*-based process are well known, such as the lower amount of generated waste, and less required resources and energy due to mild reaction conditions. In catalytic terms, the strength of biocatalysis is related to the enzyme features –high activity, specificity (discrimination between substrates), selectivity (type of reaction)–, which provide a powerful way of producing enantiomerical pure compounds.[5] This purity is notably required for the correct biological activity of the target molecule, because the activity of enantiomers can differ drastically.[6]

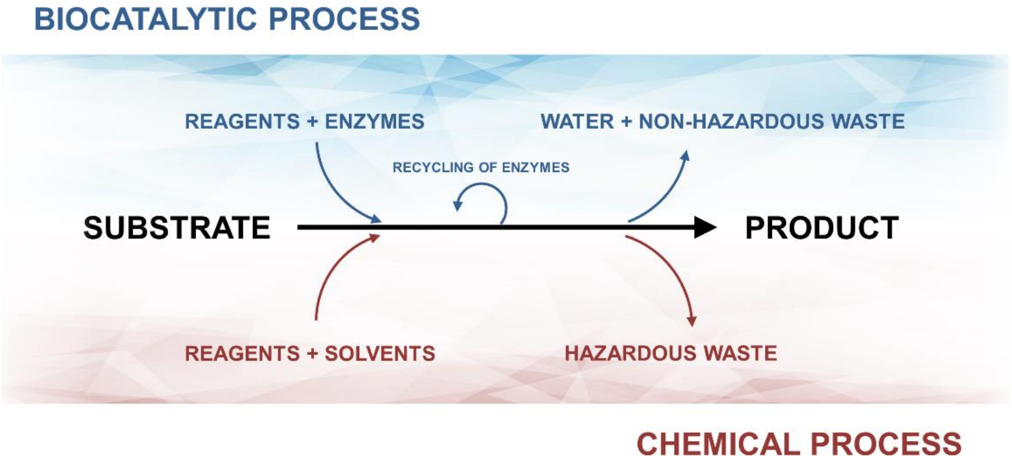
BIOCATALYTIC PROCESS
REAGENTS + ENZYMES
WATER + NON-HAZARDOUS WASTE
RECYCLING OF ENZYMES
SUBSTRATE
PRODUCT
REAGENTS + SOLVENTS
HAZARDOUS WASTE
CHEMICAL PROCESS

Figure 1.1. Graphical representation of the classic chemical synthesis and the biocatalytic process.

Despite all these benefits, some drawbacks are delaying its complete implementation in the industry replacing the conventional process. The time pressures from the pharmaceutical process are incompatible with the long lead times required for engineering a suitable biocatalyst; enzyme identification, test, and optimization are usually slow and tedious steps.[7] Also, one of the main problems in biocatalysis is the low operational stability of wild enzymes with respect to pH, temperature, solvents, and ionic strength, among others. To overcome these limitations, diverse techniques have been developed and are in continuous updating: development of novel enzymes and structural enzyme improvement by new progress in protein engineering, reactor/reaction engineering approaches, and physicochemical enzyme stabilization (enzyme modification, immobilization) (Figure 1.2).[8,9] These two latter strategies will be further discussed and implemented in the target reaction system along this thesis work.

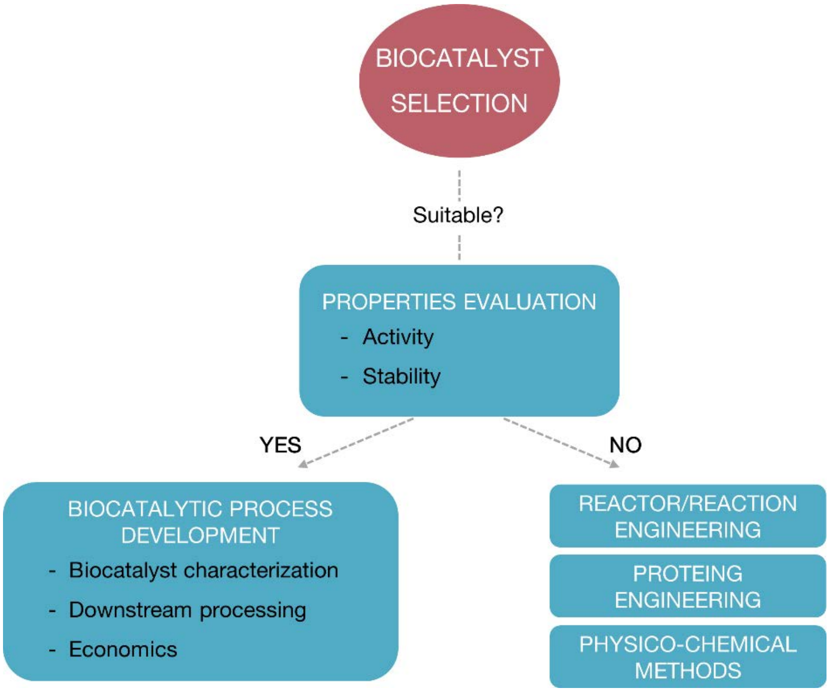
BIOCATALYST SELECTION
Suitable?
PROPERTIES EVALUATION
- Activity
- Stability
YES
NO
BIOCATALYTIC PROCESS DEVELOPMENT
- Biocatalyst characterization
- Downstream processing
- Economics
REACTOR/REACTION ENGINEERING
PROTEING ENGINEERING
PHYSICO-CHEMICAL METHODS

Figure 1.2. The development of the biocatalytic process.

1.1.2 Enzyme (in)stability

Under reaction conditions, enzymes suffer from stability issues. A native enzyme can lose its biological activity by unfolding of its tertiary structure (denaturation), which impedes the active site to recognize and contact the substrate, and further catalysis of the reaction; this process may be reversible by removal of the denaturing influence. The enzyme can also be affected by structural chemical changes that produce irreversible loss of activity (inactivation).[10]

Enzyme stability can be improved by tuning of operating conditions, but also by enzyme modification. This modification includes the chemical modification of some target amino acid side chains, and enzyme immobilization.[11–13] This thesis has been focused on immobilization methods as the tool to enhance the stability, rather than the modification of the enzyme itself.

1.1.3 Immobilization methods

As stated in the first Enzyme Engineering Conference in 1971, immobilized enzymes are 'physically confined or localized in a certain defined region of space with retention of their catalytic activity, and which can be used repeatedly and continuously'.[14] Various factors influence the performance of immobilized enzymes: microenvironment of the carrier, multipoint attachment to a carrier, a spacer or an arm between enzyme–carrier or enzyme–enzyme, diffusion limitations, presence of substrates or inhibitors, the physical structure of the carrier, and, of course, the principle of the immobilization method.[15,16]

Various immobilization supports and methods have been developed to improve the enzyme activity. Regarding the support structure, many conventional carriers are commercially available, and classified into two categories according to their chemical composition: inorganic materials (silica, celite or glass), and organic supports (alginate, chitosan or agarose), which can be further divided into natural and synthetic carriers.[17] With the coming age of nanotechnology, the nanomaterials constitute novel and interesting matrices for enzyme immobilization due to their unique physicochemical properties.[18,19] In particular, magnetic nanoparticles possess additional benefit, as they can be easily recovered from the reaction medium using an external magnetic field. This will be further discussed in Chapter 6.

There are many techniques to immobilize an enzyme to a support (Figure 1.3).[20] Its selection is essential to provide a good overall performance with high immobilization yield, low activity loss, low mass transfer constraints and improved operational stabilities. *Adsorption* is the adherence of the enzyme to the surface of the carrier matrix driven by van der Waals forces, ionic interactions, and hydrogen bonding. This binding enzyme-support is rather weak and reversible, but it does not alter the native enzyme structure, usually minimizing the activity loss after immobilization.[21] One subgroup in adsorption immobilization is via *affinity* interactions between complementary biomolecules (antibody–antigen) or through metal chelation. The most common example is likely the immobilization of a histidine-tagged enzyme, leveraging the specific binding between His and a divalent metal. The enzyme can be easily eluted by addition of imidazole, which competes for the binding to the metal.[22]

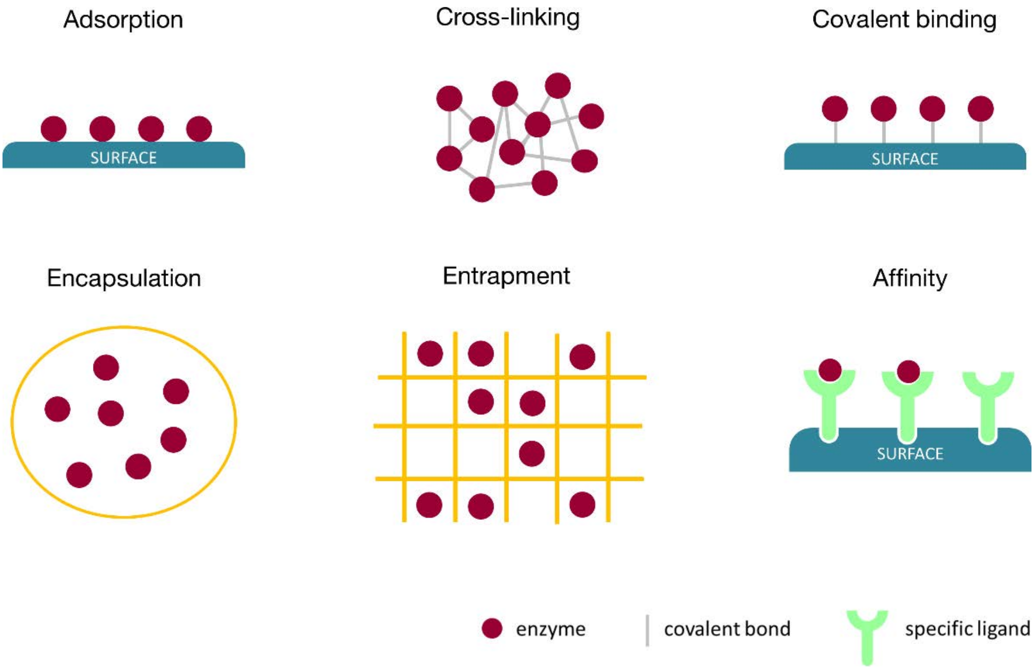

Figure 1.3. General methods for the immobilization of enzymes.

The formation of *covalent bonds* is an irreversible immobilization technique. In this case, the biocatalyst cannot be detached from the support without destroying either the support or the biological activity of the enzyme.[23] The catalyst can then be reused without releasing the enzyme into the solution. Multipoint covalent bonds increase the enzyme rigidity and, consequently, it limits the molecule conformational changes, conferring greater resistance to temperature, denaturing agents, organic solvents, etc. However, sometimes this strong attachment causes enzyme inactivation due to the mentioned rigidity or the binding to the amino acid residues essential for the catalytic activity, blocking the enzyme active site.[24] Another covalent approach is the carrier-free *cross-linked* enzyme (CLE) molecules. The molecular linkages can be formed between soluble enzyme molecules, crystallized (CLEC) or aggregated (CLEA).[25,26] This process, either chemical, enzymatic or chemoenzymatic, often has a low activity retention, low mechanical stability, and poor reproducibility.[27]

Entrapment consists of shutting the enzyme in a polymer network, typically polyacrylamide or a membrane device as a hollow fiber o microcapsule (*encapsulation*), exclusively allowing the diffusion of substrates and products.[28] It commonly requires the formation of the polymeric matrix in the presence of the enzyme. This technique is an easy, fast, cheap, and mostly used in cell immobilization, but it has also been applied with enzymes despite their possible leakage from the gel.[29,30]

1.1.4 Why to immobilize?

One of the main reasons to immobilize an enzyme is the increase in its stabilization to the harsh conditions of the industrial process, as it has been stated above.[31] Moreover, economics is crucial; thus, the reusability of the biocatalyst usually becomes mandatory. The immobilization enables continuous production, without biocatalyst loss during the whole process. Another benefit, perhaps even more important, is the reduction in downstream costs due to a much easier separation of the biocatalyst from the reactor output.[32]

1.1.5 Cascade reactions

The classical chemical synthesis usually involves multi-step reactions carried out in separate reactors. Each intermediate is isolated after each step, purified from the reaction medium and used as the starting material of the following step.[33] As an alternative, *cascade reactions* are defined as a sequential array of reactions in which the product of one reaction serves as the substrate for the next one (Figure 1.4).[34] These reactions can certainly be enzyme-catalyzed. Several examples of multi-enzyme cascade systems already applied in the industry are: coenzyme regeneration,[35] removal of the unwanted enantiomer,[36,37] and sugar production.[38] Enzyme immobilization enables an easy compartmentalization of several reactions, in order to set the proper reaction conditions for each biocatalyst, in separate reactions.

A common operating strategy to avoid the low yields and high costs produced by the intermediate stages is to work in *one-pot* multi-enzyme cascade systems. This is the combination of various cascade enzymatic reactions occurring in the same vessel, lowering operating time, reagents, energy, waste, and, consequently, production costs.

In terms of the target product yield, one-pot may achieve higher yields due to the reduction of side reactions, and equilibrium shift of the first reaction towards products (if applicable).[39,40] The enzymes can be immobilized separately and used together in the same reactor, or they can be previously attached together in the same support. In the latter case, *co-immobilization*, the diffusion time of the first reaction product to the second enzyme may be reduced, increasing the efficiency of the overall system.[41]

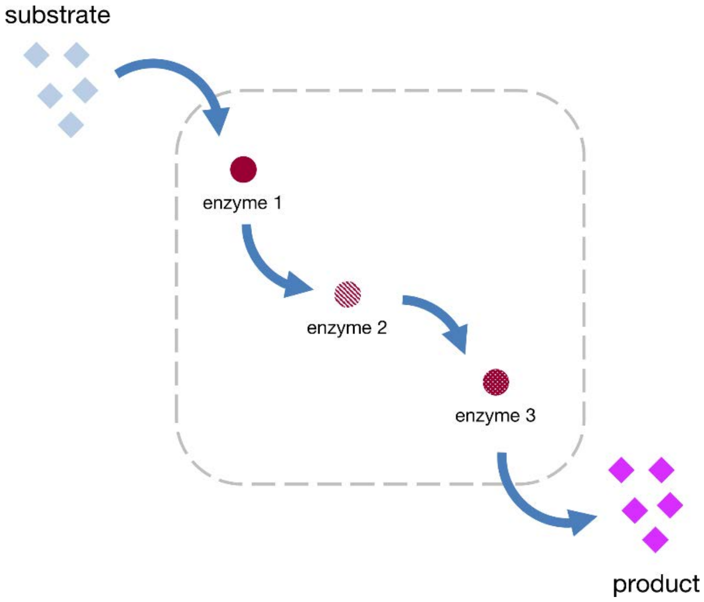

Figure 1.4. Biocatalytic pathway in cascade reactions.

Therefore, in one-pot systems, enzyme compatibility is imperative as all the present enzymes are catalyzing the reaction at the same conditions of pH, temperature, and ionic strength, among others.[42] If the simultaneous catalysis of all reactions is not possible, the coupled system can be performed in consecutive cascade serial steps, minimizing or even eliminating the intermediate purification steps.

Hence there is a compromise between the optimal conditions for each individual reaction. Here is when the immobilization becomes a great advantage in industry: it increases the enzyme stability, and hence it improves the compatibility between various biocatalysts and reactions. However, the stability of the enzyme is not the only compromise to take: the reactants concentrations, as well as the main operating conditions, must be determined to maximize the product yield. Notice that if just a single reaction can be tricky, a multi-enzyme cascade is even more laborious to be optimized. In this case, it could be practical to develop a *mathematical kinetic model* of the system that enables process optimization and can give insight into the process dependencies.[43] A more detailed description is included in Chapter 5.

1.2 Multi-enzymatic cascade for the synthesis of iminocyclitols

The general objective of this thesis work is the feasibility of a multi-enzymatic process for the synthesis of iminocyclitols, catalyzed by a peroxidase and an aldolase in a cascade reaction system. D-fagomine is selected as the target iminocyclitol to evaluate the viability of the coupling of both reactions.

1.2.1 Iminocyclitols

Polyhydroxylated pyrrolidines and piperidines (azasugars), or commonly called iminocyclitols, contain a nitrogen atom in place of the ring oxygen atom of a sugar moiety. These compounds are glycosidases inhibitors with enormous therapeutic potential in many diseases by altering the glycosylation or catabolism of glycoproteins.[44] Accordingly, they have been intensively evaluated as new antibiotics, antimetastatic, antihyperglycemic, or immunostimulating agents.[45]

The biological activity depends on chirality.[46] However, structure-activity relationships for glycosidase inhibitors can be difficult to elucidate.[47] A clear example is reported in the literature: D-iminocyclitols were rationally designed as inhibitors of the D-sugar processing enzymes, but unexpectedly L-iminocyclitols showed higher inhibitory activity.[48]

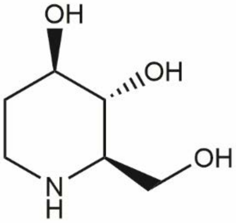

Figure 1.5. D-fagomine.

One valuable iminocyclitol is D-fagomine, which is a member of a small but an important class of glycosidase inhibitors, the 1,2-dideoxy-azasugars family (Figure 1.5).[49] It was isolated from buckwheat seeds (*Fagopyrum esculentum* Moench) and characterized for the first time in 1974.[50] It has shown to possess relevant biological activity; it is a nutraceutical that may be used as a dietary ingredient or a functional food component to reduce various health risks.[51,52] It has been reported to have a significant antihyperglycemic effect in streptozocin-induced diabetic mice and to potentiate markedly immunoreactive insulin release.[53,54] It has also shown some activity as mammalian α-glucosidase and ß-galactosidase inhibitors used for diabetes mellitus type 2, preventing the digestion and absorption of carbohydrates.[55]

The enormous interest of these compounds in the industry has led to many synthetic approaches towards naturally occurring iminocyclitols and structurally modified analogs. Chemical syntheses of D-fagomine usually involve cumbersome protection-deprotection reactions as well as chiral starting materials; therefore, moderate global yields are achieved.[56,57] Several synthetic approaches of D-fagomine have been reported using carbohydrates or carbohydrate precursors as starting materials.[58,59] Other authors started from aldehydes, in six to seven steps with final global yields around 12%.[60] Alternatively, D-fagomine has also been produced enzymatically from amino aldehydes using aldolases.[61]

1.2.2 Aldol reactions

As a start, a definition of an *aldol addition* is the reversible formation of C–C bonds by the stereoselective addition of a donor compound (nucleophile) to an acceptor compound (electrophile) (Figure 1.6).[62] It involves the attack of the deprotonated α-carbon atom of an aldehyde or ketone on the carbonyl atom of another aldehyde or ketone, resulting in a β-hydroxyaldehyde or a β-hydroxyketone, which is commonly called *aldol* adduct (abbreviation of aldehyde and alcohol).

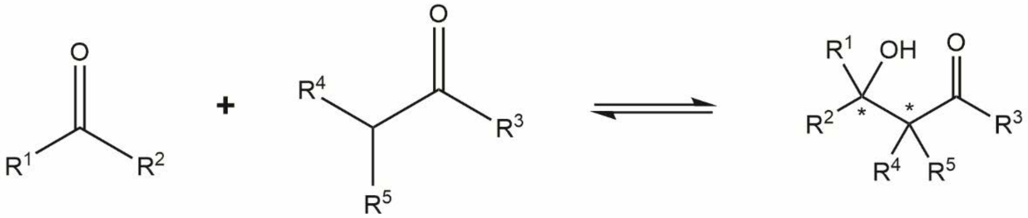

Figure 1.6. The scheme of the general reaction catalyzed by aldolases. R^1–R^5 correspond to the possible carbon substitutions. The symbol * shows the presence of two chiral centers in the final product. This figure has been adapted from the literature.[62]

These reactions are enzymatically catalyzed by aldolases. Nowadays, they represent one of the most powerful tools for carbon–carbon bond formation, obtaining enantiopure multifunctional molecules from simple starting materials.[63,64] It yields a product (aldol) with two chiral centers, being its stereochemistry mainly dependent on the employed specific enzyme and substrates. One stereoisomer is mainly formed with highly predictable conformation.

As a common limitation of enzymes as synthetic catalysts, aldolases show a strict specificity for the donor substrate (ketone) but, however, they can use a broad range of acceptor aldehydes.[65] Ketones frequently need to be phosphorylated to be accepted as a substrate, and small differences in their structure regularly lead to a meaningful reduction in affinity to the active site. These constraints have limited the applicability of aldolases as catalysts for organic synthesis. Various strategies are being used to overcome this limitation: directed evolution, substrate engineering, and discovery of novel enzymes in nature.[66]

1.2.3 Aldolases classification

Aldolases can be classified into two classes according to their mechanism to activate the nucleophilic component (ketone) (Figure 1.7).[62,67] In *class I aldolases* catalysis, a Schiff base intermediate is formed between the substrate and a conserved lysine residue in the active site of the enzyme. *Class II aldolases* rather use a divalent metal cofactor (Zn^{2+}) acting as a Lewis acid in the active site. The catalysis proceeds via the formation of an enediolate intermediate, which attacks the carbonyl carbon of the acceptor substrate (aldehyde) forming the new C–C bond. These class II enzymes are often more stable than class I aldolases.

Another possible discrimination of aldolases is according to the structure of the donor substrate. Main groups are detailed as follows. *Pyruvate/phosphoenolpyruvate-dependent aldolases* are involved in the reversible biosynthesis of α-keto acids. *2-deoxyribose-5-phosphate aldolase* (DERA) is unique among the aldolases in that the donor is not a ketone, but an aldehyde. In vivo, it catalyzes the aldol addition of acetaldehyde to D-glyceraldehyde-3-phosphate (G3P). *Glycine-dependent aldolases* are dependent of pyridoxal 5-phosphate as a cofactor to catalyze the aldol reaction of glycine and an acceptor aldehyde to render a β-hydroxy-α-amino acid. Last main group includes *dihydroxyacetone phosphate (DHAP) dependent aldolases.*

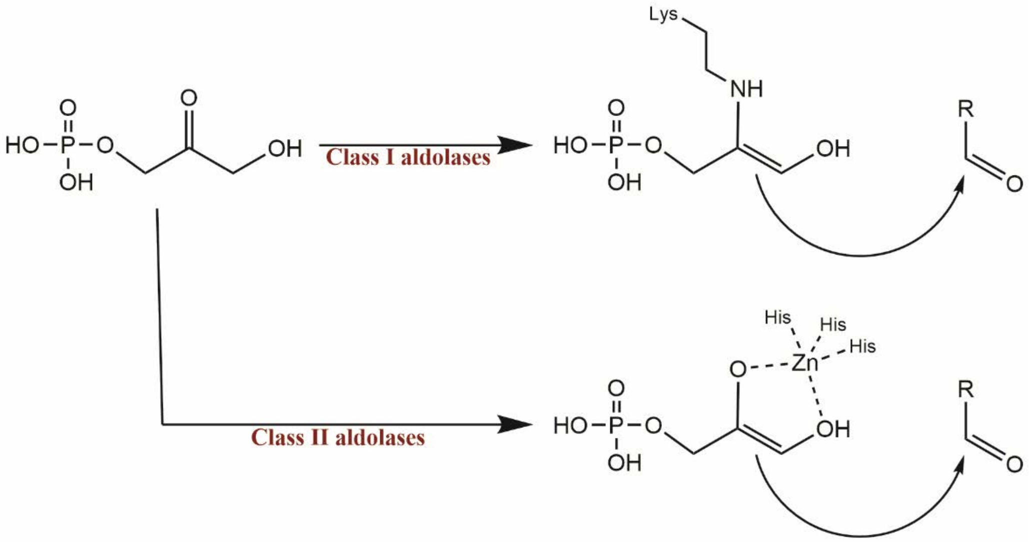

Figure 1.7. Reaction mechanism for Class I and Class II aldolases using DHAP as donor substrate. It has been dapted from the literature.[67]

Four DHAP-dependent aldolases are well-known to catalyze in vivo the reversible asymmetric addition of DHAP to G3P or L-lactaldehyde, leading to four complementary diastereomers (Figure 1.8). These aldolases are L-fuculose 1-phosphate aldolase (FucA, EC 4.1.2.17), fructose 1,6-diphosphate aldolase (FruA, EC 4.1.2.13), L-rhamnulose 1-phosphate aldolase (RhuA, EC 4.1.2.19), and tagatose 1,6-diphosphate aldolase (TagA, EC 4.1.2.2).[68] These enzymes are able to catalyze the addition of DHAP to amino aldehydes containing *N*-amine substitutions. The amino aldehydes are generally amino-protected in order to avoid undesired cyclization; typically, a carboxybenzyl group (Cbz) is added to the *N*-terminal of the compound. Thus, the final product after the aldol reaction is not the iminocyclitol, but its precursor, an aminopolyhydroxyketone. The iminocyclitol can be easily obtained by removal of the phosphate group using acid phosphatase, and posterior hydrogenation to eliminate the amino-protecting group (Figure 1.9).[69,70] The carbon chirality is maintained in the final iminocyclitol.

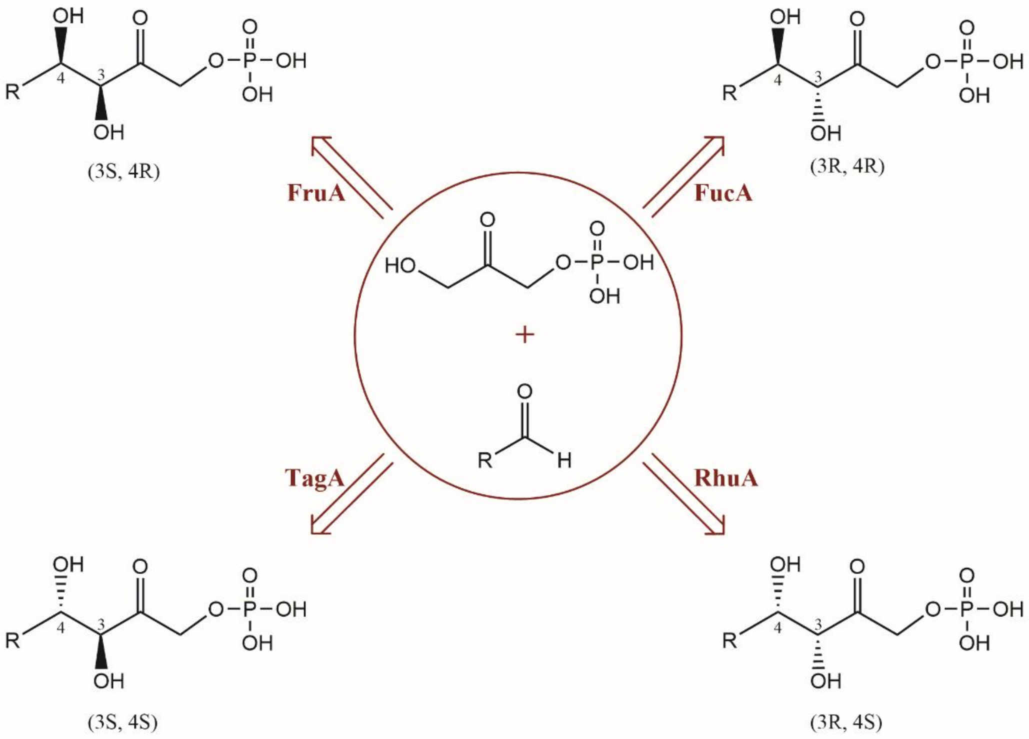

Figure 1.8. Product stereochemistry in aldol additions catalyzed by DHAP-aldolases.

The main disadvantage of DHAP-dependent aldolases is the strict donor substrate specificity toward DHAP. Besides the additional step required for the phosphate removal, and the consequently generated phosphate waste, two more factors hinder the industrial application of DHAP-dependent aldolases: the high cost and instability of DHAP.[71] Thus, significant work has been addressed to find a more practical access to DHAP: various chemical or enzymatic synthetic approaches have been investigated for a scalable and cost-effective production of DHAP.[72,73] Both chemical and enzymatic options need further work to be applicable. A more remarkable alternative is the elimination of the requirement for DHAP. This means enabling the enzyme to accept dihydroxyacetone (DHA) as a donor substrate. This would be achieved by directed evolution of a DHAP-dependent aldolase, modifying the active site to allow the entrance and binding of DHA. Some modifications on aldolases have been already described in the literature.[74,75] Authors also managed to use DHA as a substrate for RhuA.[76] For that, they used borate buffer, which presumably led to the reversible in situ formation of DHA borate ester.

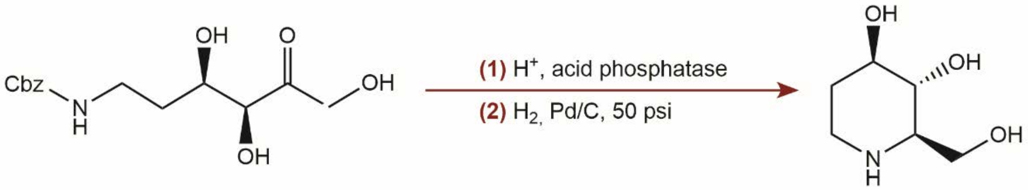

Figure 1.9. Iminocyclitol (D-fagomine) synthesis from a precursor aminopolyhydroxykeone.

Finally, a third approach is the discovery of novel wild enzymes that catalyze the DHA aldol reaction. In 2001, a novel aldolase encoded in the *mipB* sequence from the genome of *Escherichia coli –D-fructose-6-phosphate aldolase* (FSA, EC 4.1.2.-, MW~257KDa)– was found to be able to use DHA as donor substrate.[77] From then, some other DHA aldolases have been discovered.[78]

1.2.4 Fructose-6-phosphate aldolase

The non-strict donor substrate specificity of FSA is unusual for an aldolase, as well as its 3D structure, amino acid sequence and active site topology that are more homologous to transaldolases and more distantly related to fructose-1,6-phosphate aldolases.[79] However, no transaldolase activity (reversible catalysis of sedoheptulose 7-phosphate to glyceraldehyde 3-phosphate to form erythrose 4-phosphate and fructose 6-phosphate) has been observed for this enzyme. It was found that this enzyme was able to catalyze the formation or cleavage of fructose-6-phosphate (F6P) using DHA as donor substrate, and G3P as acceptor aldehyde.[77] Moreover, FSA was not inhibited by ethylenediaminetetraacetic acid (EDTA), which points to a metal-independent mode of action. The Lys85 residue is essential for its action (its mutation to arginine resulted in complete loss of activity). This could indicate a class I aldolase, as the reaction mechanism involves a Schiff base formation through this lysine residue.

The crystal structure of FSA showed a decameric structure of 220-aminoacid monomers.[79] Each subunit consists of a single domain that folds into an α/β barrel (Figure 1.10). In the same report, the active site was characterized by analyzing the surroundings of the catalytic water molecule in the active site. The water molecule formed hydrogen bonds with Gln59, Thr109, and Tyr131.

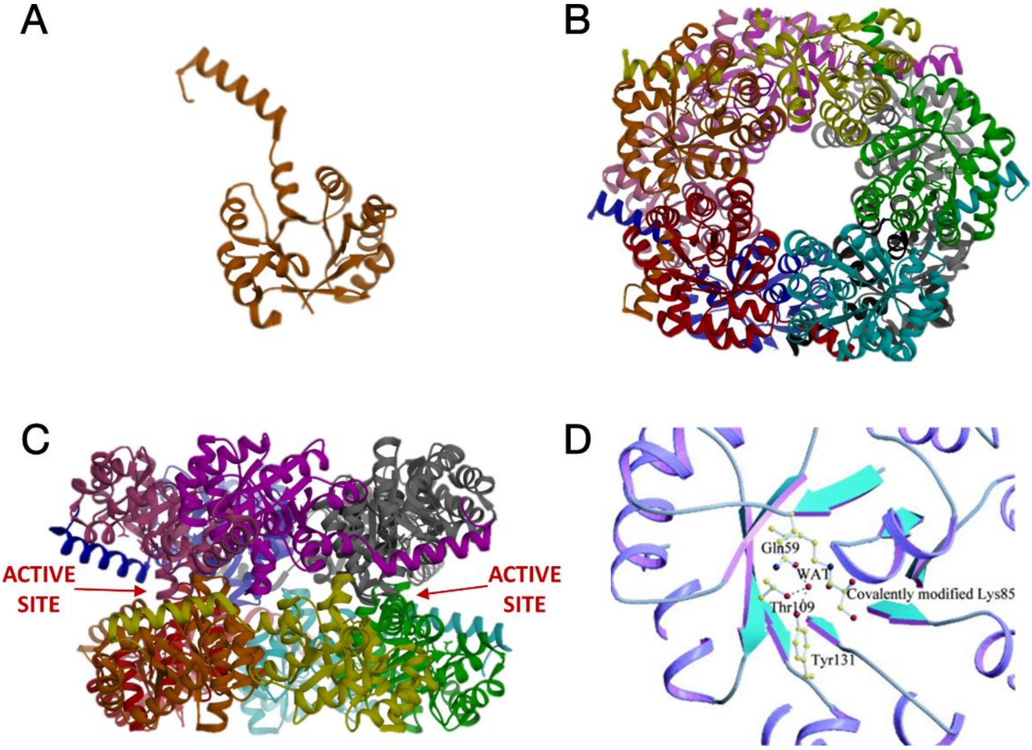

Figure 1.10. The tridimensional structure of FSA. A single monomer (**A**), quaternary structure from the top (**B**) and side (**C**), and a schematic representation of the active site (**D**). Each subunit is drawn with a different color. A-C images are obtained using UCSF Chimera software.[80] D image is reproduced from the literature [79] with permission of Elsevier.

After its discovery, many publications on the use of this enzyme were reported. It was shown that FSA not only catalyzes its natural reaction with F6P, but it could serve as a useful biocatalyst in the organic synthesis of aminopolyhydroxyketones, also allowing the use of hydroxyacetone (HA) as the donor substrate.[81] The stereochemistry of the final product is 3S, 4R. Aside from DHAP-dependent aldolases, FSA represents an exception in substrate specificity. Its unique feature to accept non-phosphorylated donor substrates (the mentioned DHA and HA) has been expanded to hydroxybutanone (HB) and glycolaldehyde, among others.[82,83] Hence, expanding the substrate range by avoiding the need for a phosphorylated substrate has allowed many syntheses of iminocyclitols (the aldol and reductive amination reactions), which have been assayed against a panel of glycosidases.[84]

In order to enhance the productivity, several amino acid site-directed mutations on the FSA gene were designed and evaluated in the aminopolyhydroxyacetone synthesis. A single mutation, FSA A129S (Alanine residue 129 substituted by Serine), improved the reactivity towards DHA; this mutation, however, reduced the affinity towards HA and glycolaldehyde.[85] This differential specificity towards the donor substrate from both FSA and FSA A129S makes them complementary biocatalysts. In a subsequent publication,[86] FSA A129S/A165G (Alanine residue 165 substituted by Glycine) double mutant was produced. This latter substitution was designed to allow more space and flexibility to allocate the aldehydes in the active site. In the same report, other not successful mutations were also tested, such as FSA R134A (Arginine residue 134 substituted by Alanine) that led to lower conversions than the wild-type FSA for the selected aldehydes. In another work, another set of efficient FSA variants was constructed, demonstrating the exceptional malleability of its active site.[87]

1.2.5 FSA for the D-Fagomine synthesis

As stated above, if an amino-protecting group has been used, the direct product from the aldol addition is not the iminocyclitol itself, but its precursor (aminopolyhydroxyketone). This thesis work is focused on the evaluation of the viability of a two-reaction coupling using a peroxidase and an aldolase for the synthesis of the precursor of D-fagomine: (3S,4R)-6-[(benzyloxycarbonyl)amino]-5,6-dideoxyhex-2-ulose, named *preFagomine* from now on.

The synthesis of this specific compound has already been reported in the literature, by the aldol addition of DHA to *N*-Cbz-aminopropanal (β-CHO) catalyzed by FSA (Figure 1.11).[88] In the aforementioned paper, the two successful FSA mutants (A129S and A129S/A165G) were compared in terms of productivity, resulting in very similar values. FSA A129S productivity was slightly higher; the same effect was observed in another report,[89] in which a mathematical model for this reaction was developed. This enzyme catalyzes both aldol and retroaldol additions, but the cleavage of preFagomine was observed to be inhibited by β-CHO. Therefore, in this thesis work, FSA A129S was selected as the biocatalyst to perform the aldol reaction.

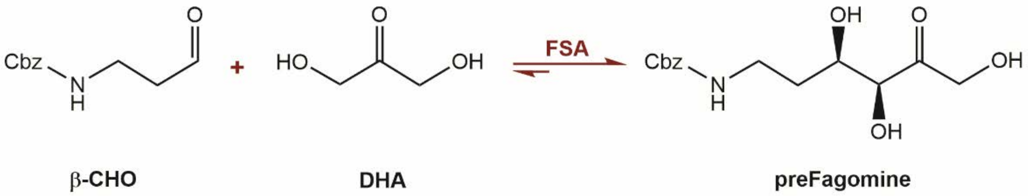

Figure 1.11. Synthesis of preFagomine by the aldol addition of DHA to β-CHO catalyzed by FSA.

1.2.6 N-Cbz-3-aminopropanal synthesis

The aldol addition reaction to yield preFagomine has been defined: donor substrate (DHA), acceptor aldehyde (β-CHO) and enzyme (FSA A129S). The synthesis of the amino aldehyde should be discussed. In the literature, many examples of selective chemical oxidations of alcohols to aldehydes are found, generally with low selectivity and, thus, the lack of control and predictability of the obtained product structure, and the high cost of oxidizing agents. Transition metals are commonly used in these reactions, making the process environmentally unsuitable [90] Hence, the oxidation of alcohols to aldehydes is advantageous to be performed via an enzymatic process.

Besides, the main problem in these reactions is the further oxidation of the aldehyde to the acid, which can be reduced by a one-pot coupling of the aldol addition to this reaction, so that the formed amino aldehyde is rapidly converted to the aminopolyhydroxyketone, minimizing the acid production. Related syntheses have already been catalyzed enzymatically using different systems. For example, the oxidation of an α-amino alcohol (α- indicates the amine position in relation to the hydroxyl), *N*-Cbz-2-aminoethanol, and the subsequent aldol addition of HA catalyzed by FSA: alcohol oxidase using O_2 as co-substrate, and laccase using O_2 with 2,2,6,6-tetramethylpiperidine-*N*-oxyl (TEMPO) as a mediator (Figure 1.12).[91] No oxidation was observed using alcohol oxidase, which was not able to accept this alcohol as a substrate; with the laccase/TEMPO system, the maximum aldehyde yield was below 45% due to higher selectivity to the acid (further oxidation) than to the aldehyde.

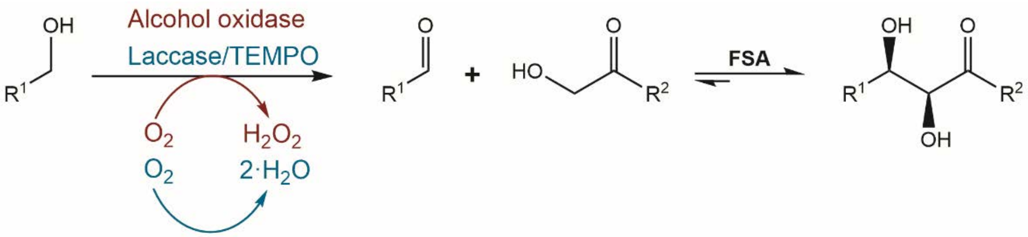

Figure 1.12. Previously reported amino aldehyde synthesis in the cascade reaction for the formation of the aldol adduct. R^1-OH is *N*-Cbz-2-aminoethanol; R^2: H, CH_3, CH_3CH_3, CH_2OH. It has been adapted from the literature.[91]

Another example is catalyzed by horse liver alcohol dehydrogenase (HLADH) (Figure 1.13).[92] Semicarbazide was used to trap the aldehyde product, shifting the equilibrium (this enzyme catalyzes the reaction in both directions) to the product to favor the complete oxidation of the alcohol. However, the main problem is the expensive NAD^+

cofactor requirement, which demands an effective regeneration system to reduce extra costs. The same enzyme was used more recently to yield β-CHO.[93] Again, cofactor regeneration was required; in this case, NADH oxidase was employed.

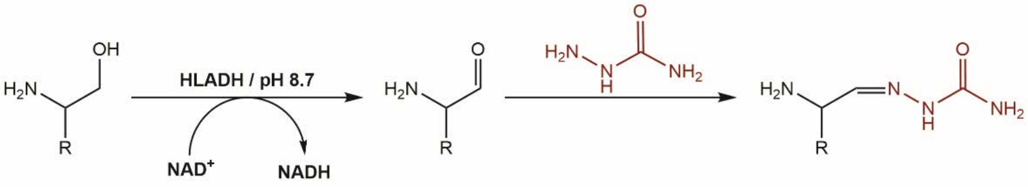

Figure 1.13. The use of semicarbazide to trap the formed aldehyde from the HLADH-catalyzed α-amino alcohol oxidation. Semicarbazide is colored in red. It has been adapted from the literature.[92]

The suitable biocatalyst for the β-CHO synthesis would be an enzyme that does not require any cofactor to catalyze the oxidation and consequently any other enzyme/system to regenerate it. This is the case of peroxidases, which can oxidize a broad range of organic compounds with no cofactor requirement. These oxidoreductases use hydrogen peroxide (H_20_2) or organic peroxides (R-OOH) as oxidants.

1.2.7 Peroxidases

Peroxidases can be widely classified into three groups according to the nature of the catalytic center.[94] *Heme peroxidases* have a heme as the prosthetic group; generally, it is iron(III) chelated by a protoporphyrin ring. *Vanadium peroxidases* contain vanadate as the prosthetic group. Finally, other peroxidases are present with neither heme nor vanadium.

The peroxidase-catalyzed reactions can be divided into four categories.[95,96] *Oxidative dehydrogenation* is mainly restricted to heme peroxidases. It implicates one-electron transfer process with radical cations and radicals as intermediates, which can result in inter- or intra-molecular radical coupling products. *Oxidative halogenation* (halogenation of organic substrates) is catalyzed by the so-called haloperoxidases. This reaction is not limited to a subgroup of peroxidases, and it is believed to proceed via an active halide species. *Catalase activity* involves the hydrogen peroxide decomposition to water and oxygen, and it can be catalyzed by some peroxidases. *Oxygen-transfer reactions* are probably the most interesting biotransformations catalyzed by peroxidases from a synthetic point of view. These reactions include hetero-atom oxidation (*S*-oxidation, *N*-oxidation), epoxidation and CH bond formation (benzylic/allylic oxidation, indole oxidation, and alcohol oxidation. The latter is the most relevant in this work.

1.2.8 Chloroperoxidase

Peroxidases are usually named after their sources (e.g. horseradish peroxidase) or their substrates (e.g. bromoperoxidase). One of the most versatile peroxidases is the *chloroperoxidase* from the ascomycete *Caldariomyces fumago* (CPO, EC 1.11.1.10, MW~42KDa) (Figure 1.14A), which was first isolated in 1961.[97] Its systematic name is chloride:hydrogen-peroxide oxidoreductase. This haloperoxidase catalyzes in vivo the production of the chlorometabolite caldariomycin (1,1-dichloro-2,5-dihydroxy cyclopentane); thus, a well-known standard assay for CPO involves the chlorination of monochlorodimedone to dichlorodimedone.[98]

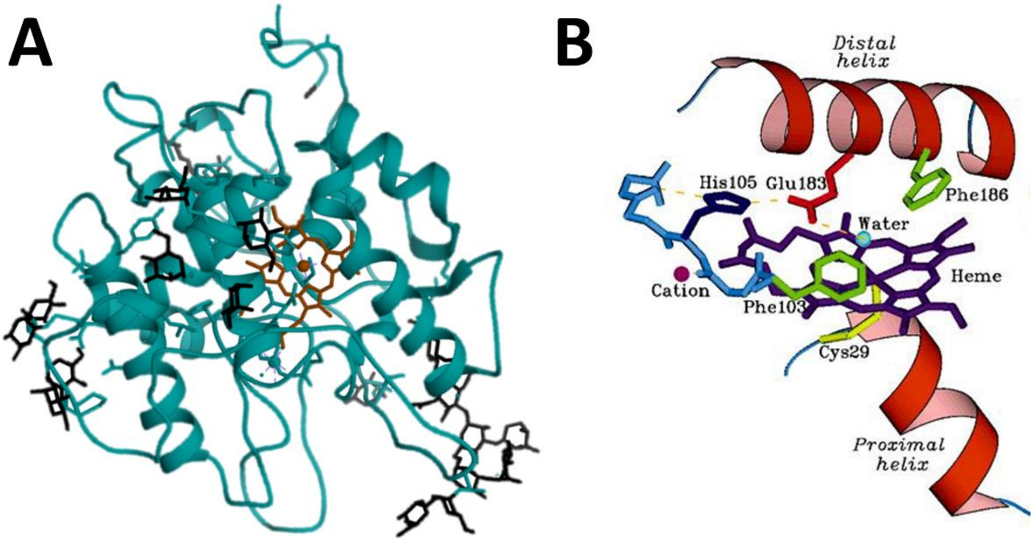

Figure 1.14. Tridimensional CPO structure (**A**) and schematic view of its active site (**B**). Left image has been obtained by UCSF chimera software, coloring the heme group in orange, and sugar moieties in black. The right image is reproduced from the literature with permission of Elsevier.

It is a monomeric glycoprotein that contains 25 to 30% carbohydrate content (the sugar composition depends on the growth conditions),[99] and a great excess of aspartic acid and glutamic acid residues over the total number of basic amino acid residues, and it is rich in serine and proline residues. These four amino acids constitute 45% of the total amino acid content (299 residues). The isoelectric point of CPO has been calculated to be approximately 4.0.[100]

CPO is the most versatile enzyme from heme peroxidases family; it is able to catalyze different types of reactions, mainly using hydrogen peroxide as the oxidant (in addition to H_20_2, the enzyme can use a variety of hydroperoxides and peroxy acids). The principal reaction involves the peroxidative formation of a carbon-halogen bond. For this reaction, the enzyme requires a halogen anion donor (chloride, bromide, and iodide, but not fluoride ions), peroxide, and any suitable nucleophile. These halogenation reactions are catalyzed by the acidic form of the enzyme (pH<3). The neutral form (pH 4–7) catalyzes halide-independent reactions.[101] Thus, CPO is able to catalyze a number of reactions besides its biological function as a peroxide-dependent chlorinating enzyme. This includes the typical reactions for catalase, heme peroxidases, and cytochromes P450 monooxygenases (oxygen insertion activity). CPO exhibits substantial catalase activity when hydrogen peroxide is the only reductant present in the reaction mixture, and it results in the disproportionation of H_2O_2 to molecular oxygen and water.[102] Other halide-independent CPO-catalyzed reactions include enantioselective sulphoxidation, epoxidation, benzylic hydroxylation and *N*-demethylation, oxindole formation from indole, and alcohol oxidation.[103–106] The alcohol oxidation is restricted for almost all the peroxidases to the phenols oxidation to quinones. However, CPO is a particular enzyme that catalyzes the oxidation of primary alcohols to the corresponding aldehydes.[107] Although it was previously stated that CPO oxidation was selective and it did not catalyze the oxidation of an aldehyde to an acid,[106] it also does oxidize aldehydes to acids.[108]

This enormous versatility of CPO showing peroxidase, catalase and cytochrome P450-like activities, in addition to catalyzing halogenation reactions, lies in the structure of its active site (Figure 1.14B).[109] Like P450, the fifth axial heme ligand in CPO derives from the sulfur atom of a cysteine residue, Cys29.[110] This feature is not shared with peroxidases, which have a histidine as a ligand. Another similarity, this time with peroxidases, is the distal heme pocket. This pocket constitutes the peroxide-binding site and is formed mainly by polar amino acids (non-polar amino acids in P450). Finally, the active-site acid-base catalytic group is a glutamate (Glu183) and not a histidine as all peroxidases.[111] However, a histidine residue (His105) is involved indirectly, hydrogen bonded to Glu183. Probably, the role of His105 is to correctly orient Glu183 and to provide charge-charge interactions.

The general mechanism for the CPO-catalyzed reactions is summarized in Figure 1.15. The active site of CPO contains a ferric heme center (Fe^{III}), to which hydrogen peroxide is bonded to initiate the reaction.[112–114] This interaction causes a two-electron transfer, resulting in the cleavage of H_2O_2, and the formation of a water molecule and an oxygen-activated heme intermediate, *compound I*, $(Fe^{IV}=O)^{\cdot+}$. This compound is responsible for catalyzing different chemical reactions. For instance, for the catalase activity, it will interact with a second H_2O_2 molecule to form molecular oxygen and water and to reduce the heme iron to the ferric resting state (Fe^{III}). For the peroxidase activity, compound I can convert organic molecules (HA) to radical products ($A^{\cdot}$), and then be reduced to *compound II* ($Fe^{IV}=O$) by transferring one electron to the organic substrate. Another one-electron oxidation is catalyzed, and the ferric resting state is regenerated. At last, in halogenation activity, compound I and a halide ion (X^-) form the *compound X* ($Fe^{III}=O$—X), which decomposes to result in Fe^{III} and halogenates an organic molecule.

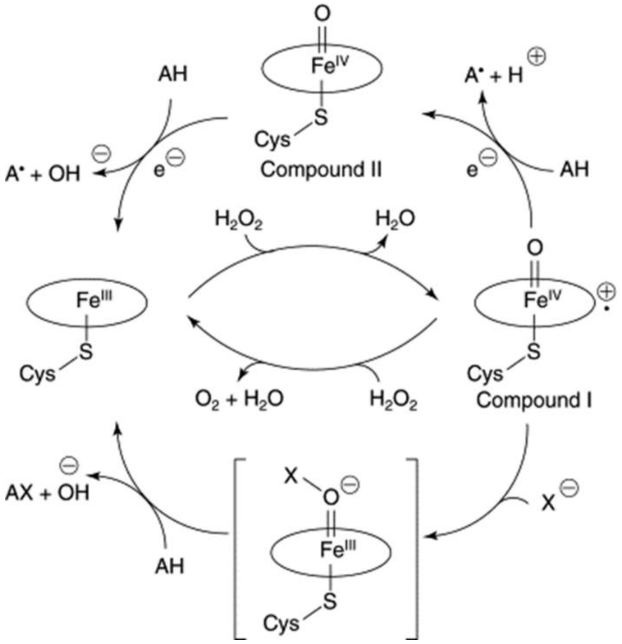

Figure 1.15. The proposed mechanism for the CPO-catalyzed reactions. It is reproduced from the literature[95] with permission of Elsevier.

As already stated above, CPO is a promising enzyme for synthetic applications and has no need for the cofactor, but for peroxide. However, despite their requirement for the reaction, peroxides or derivate radical species cause a rapid deactivation of chloroperoxidase, probably by oxidation of Cys29 causing the heme group destruction.[115–119] This low operational stability has been reduced through many strategies in the literature (addition of stabilizing agents[120] or antioxidants,[121] chemical modification,[122] controlled addition of the peroxide during the reaction[123,124]), but this work is more focused in the immobilization of CPO to enhance its stability. This will be further discussed in Chapter 6.

1.2.9 The overall system for the synthesis

The main aspects of the proposed multi-enzymatic synthesis of preFagomine as the combination of an oxidation step and an aldol addition have been discussed (Figure 1.16). The design and implementation of a system for the multi-enzymatic cascade reaction can be performed using several or one single (one-pot configuration) reactors. The starting material is a β-amino alcohol (*N*-Cbz-3-anminopropanol, β-OH), which would be oxidized to β-CHO. It is reported that CPO is able to catalyze the peroxide-mediated oxidation of alcohols to aldehydes, and thus it is a suitable candidate for this oxidation. Oxidation of β-amino alcohols by CPO has not been reported prior to this thesis work. Finally, FSA would catalyze the aldol addition of DHA to β-CHO to render the final product.

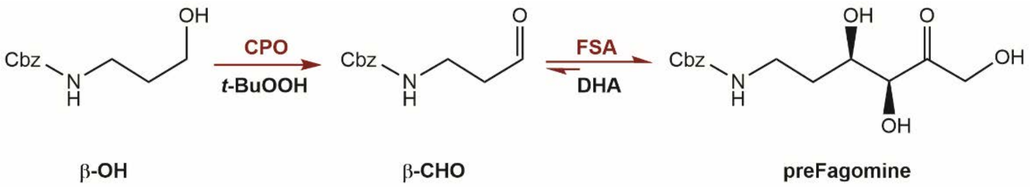

Figure 1.16. Multi-enzyme synthesis of preFagomine catalyzed by CPO and FSA, using *t*-BuOOH and DHA as co-substrates.

This work is addressed to investigate these two reactions, understand the reaction mechanism, prepare suitable stabilized biocatalysts through immobilization, and ideally find the proper conditions for its application. To that end, the key points will be further studied and discussed, such as peroxide nature (use of various peroxides as oxidants for the reaction), peroxide addition (one pulse, continuous addition), and enzyme immobilization (type of support and binding), among others. The possibility of side reactions in the system should be considered, as for example the likely oxidation of β-CHO to *N*-Cbz-3-aminopropanoic acid (β-COOH). In that case, a kinetic modeling of all the reactions present in the system would be an approach for a better understanding of the system, and a possible way to optimize it. As mentioned before, CPO/FSA immobilization is also an issue to consider, as it may enhance their operational stability increasing the final productivity. Besides, the enzyme compatibility is expanded, so it could help to find the operating conditions for a possible one-pot system.

All these elements will be discussed in this thesis. In the first chapter, a preliminary study on the CPO-catalyzed β-OH oxidation is investigated, highlighting the substrate specificity of CPO and its stability in front of organic solvent, peroxide and the substrate itself. The second chapter is addressed to the first trials on coupling CPO and FSA reactions, analyzing the possible bottlenecks of the system. This is followed by a third chapter, in which all the reactions of the system are indicated and analyzed in order to estimate the kinetic parameters of each reaction, and to develop a kinetic model of the whole system. In the fourth chapter, the immobilization of CPO and FSA onto magnetic nanoparticles and other conventional supports is discussed. In a final fifth chapter, an exploitation of the kinetic model for the coupled CPO/FSA reaction is presented.

1.3 Previous work

It is always necessary to place a scientific work in a context, locating its starting point. This thesis project should be referred to all the previous work from the research group of Bioprocess Engineering and Applied Biocatalysis at Universitat Autònoma de Barcelona.

The oxidation step from α-amino alcohol to amino aldehyde has been studied with *N*-Cbz-ethanolamine and (*S*)-Cbz-alaninol as substrates. After a wide screening of potential biocatalysts, most of the tested oxidoreductases were not able to catalyze the oxidation reaction. Finally, only HLADH and CPO recognized the target substrates, and they were selected. Thus, the CPO-oxidation of an amino alcohol (*N*-Cbz-ethanolamine) has been performed and coupled to an aldolase(RhuA)-catalyzed aldol reaction to produce a α-aminohydroxyketone in acetate buffer in presence of dioxane.[125,126] For the first reaction, an optimized peroxide addition rate of 3 mM/h was used. In this case, *tert*-butyl hydroperoxide (*t*-BuOOH) was selected as the peroxide. Hydrogen peroxide was also employed as oxidant, but results were unsuccessful due to very low reaction rates. CPO inactivation caused by the peroxides was studied and, consequently, CPO was immobilized in order to improve the enzyme stabilization, as indicated before.[127] Its stability was improved, and the reaction yield, initial reaction rate and half-life time of the enzyme were greatly improved.

HLADH has also been evaluated for the oxidation of β-OH to yield β-CHO.[128] In this case it was not possible to direct the reaction to the aldehyde formation; however, the obtained acid byproducts were valuable β-amino acids.

Besides, in the research group, there are also many publications regarding the immobilization of aldolases, like the attachment of FucA to a cobalt-chelated agarose,[129] and the application of these immobilized biocatalysts in the aldol addition of DHAP to *S*-Cbz-alaninal catalyzed by immobilized FucA and RhuA, developing a kinetic model for the reaction.[22,130] The reaction mechanism and kinetics were determined, and free and immobilized reactors were operated with high yields and selectivity. RhuA has also been immobilized in gold nanoparticles, and this immobilized derivative was tested in aldol additions.[131]

1.4 References

[1] T. W. Johannes, M. R. Simurdiak, H. Zhao, in *Encycl. Chem. Process.* (Ed.: S. Lee), Taylor & Francis, New York, USA, **2006**, pp. 101–110.

[2] L. Gardossi, F. Molinari, in *Catalysis* (Ed.: G. Centi), Encyclopedy Of Life Support Systems-EOLSS, UNESCO, **2009**.

[3] G. M. Whitesides, C. H. Wong, *Angew. Chemie - Int. Ed.* **1985**, *24*, 617–718.

[4] N. J. Turner, M. D. Truppo, *Curr. Opin. Chem. Biol.* **2013**, *17*, 212–214.

[5] K. M. Koeller, C. H. Wong, *Nature* **2001**, *409*, 232–240.

[6] L. A. Nguyen, H. He, C. Pham-Huy, *Int. J. Biomed. Sci.* **2006**, *2*, 85–100.

[7] M. D. Truppo, *ACS Med. Chem. Lett.* **2017**, DOI 10.1021/acsmedchemlett.7b00114.

[8] A. S. Bommarius, *Annu. Rev. Chem. Biomol. Eng.* **2015**, *6*, 319–345.

[9] K. M. Polizzi, A. S. Bommarius, J. M. Broering, J. F. Chaparro-Riggers, *Curr. Opin. Chem. Biol.* **2007**, *11*, 220–225.

[10] A. Illanes, *Enzyme Biocatalysis: Principles and Applications*, **2008**.

[11] G. DeSantis, J. B. Jones, *Curr. Opin. Biotechnol.* **1999**, *10*, 324–330.

[12] R. C. Rodrigues, C. Ortiz, Á. Berenguer-Murcia, R. Torres, R. Fernández-Lafuente, *Chem. Soc. Rev.* **2013**, *42*, 6290–6307.

[13] C. Mateo, J. M. Palomo, G. Fernandez-Lorente, J. M. Guisan, R. Fernandez-Lafuente, *Enzyme Microb. Technol.* **2007**, *40*, 1451–1463.

[14] I. Chibata, L. B. Wingard, Eds. , *Applied Biochemistry and Bioengineering, Vol. 4: Immobilized Microbial Cells*, Academic Press, Cambridge, USA, **1983**.

[15] L. Cao, in *Carrier-Bound Immobil. Enzym. Princ. Appl. Des.*, Wiley-VCH, Weinheim, Germany, **2006**, pp. 1–52.

[16] S. Datta, L. R. Christena, Y. R. S. Rajaram, *3 Biotech* **2013**, *3*, 1–9.

[17] V. Sirisha, A. Jain, A. Jain, in *Adv. Food Nutr. Res. Vol. 79* (Eds.: S.-W. Kim, F. Toldrá), Academic Press, Cambridge, USA, **2016**, pp. 179–211.

[18] R. A. Meryam Sardar, *Biochem. Anal. Biochem.* **2015**, *4*, 1–8.

[19] S. A. Ansari, Q. Husain, *Biotechnol. Adv.* **2012**, *30*, 512–523.

[20] S. D. Minteer, Ed. , *Enzyme Stabilization and Immobilization: Methods and Protocols*, Humana Press, New York, USA, **2011**.

[21] T. Jesionowski, J. Zdarta, B. Krajewska, *Adsorption* **2014**, *20*, 801–821.

[22] I. Ardao, G. Álvaro, M. D. Benaiges, *Biochem. Eng. J. j* **2011**, *56*, 190–197.

[23] J. M. Guisán, Ed. , *Immobilization of Enzymes and Cells*, Humana Press, New York, USA, **2006**.

[24] U. Guzik, K. Hupert-Kocurek, D. Wojcieszynska, *Molecules* **2014**, *19*, 8995–9018.

[25] T. Heck, G. Faccio, M. Richter, L. Thöny-Meyer, *Appl. Microbiol. Biotechnol.* **2013**, *97*, 461–475.

[26] G. Matheis, J. R. Whitaker, *J. Food Biochem.* **1987**, *11*, 309–327.

[27] R. A. Sheldon, S. Van Pelt, *Chem. Soc. Rev.* **2013**, *42*, 6223–6235.

[28] M. D. Trevan, in *New Protein Tech.* (Ed.: J.M. Walker), Humana Press, New York, USA, **1988**, pp. 491–494.

[29] M. A. Nawaz, A. Karim, Z. Bibi, H. U. Rehman, A. Aman, D. Hussain, M. Ullah, S. A. U. Qader, *J. Taiwan Inst. Chem. Eng.* **2015**, *64*, 31–38.

[30] P. Li, S. Y. Moon, M. A. Guelta, S. P. Harvey, J. T. Hupp, O. K. Farha, *J. Am. Chem. Soc.* **2016**, *138*, 8052–8055.

[31] N. R. Mohamad, N. H. C. Marzuki, N. A. Buang, F. Huyop, R. A. Wahab, *Biotechnol. Biotechnol. Equip.* **2015**, *29*, 205–220.

[32] R. DiCosimo, J. McAuliffe, A. J. Poulose, G. Bohlmann, *Chem. Soc. Rev.* **2013**, *42*, 6437.

[33] V. Gotor-Fernández, R. Brieva, V. Gotor, in *Multi-Step Enzym. Catal. Biotransformations Chemoenzymatic Synth.* (Ed.: E. García-Junceda), Wiley-VCH, Weinheim, Germany, **2008**, pp. 213–233.

[34] H. C. Hemker, P. W. Hemker, *Proc. R. Soc. B* **1969**, *173*, 411–420.

[35] R. Wichmann, D. Vasic-Racki, in *Technol. Transf. Biotechnol.* (Ed.: U. Kragl), Springer, Heidelberg, Germany, **2005**, pp. 225–260.

[36] N. Nakajima, D. Conrad, H. Sumi, K. Suzuki, N. Esaki, C. Wandrey, K. Soda, *J. Ferment. Bioeng.* **1990**, *70*, 322–325.

[37] Z. Findrik, D. Vasić-Rački, B. Geueke, M. Kuzu, W. Hummel, *Eng. Life Sci.* **2005**, *5*, 550–555.

[38] Y. Ge, Y. Wang, H. Zhou, S. Wang, Y. Tong, W. Li, *J. Biotechnol.* **1999**, *67*, 33–40.

[39] E. Ricca, B. Brucher, J. H. Schrittwieser, *Adv. Synth. Catal.* **2011**, *353*, 2239–2262.

[40] P. A. Santacoloma, G. Sin, K. V. Gernaey, J. M. Woodley, *Org. Process Res. Dev.* **2011**, *15*, 203–212.

[41] J. Mansfeld, H. Dautzenberg, in *Immobil. Enzym. Cells* (Ed.: G.F. Bickerstaff), Humana Press, New York, USA, **1997**, pp. 319–326.

[42] C. A. Denard, J. F. Hartwig, H. Zhao, *ACS Catal.* **2013**, *3*, 2856–2864.

[43] Z. Findrik, D. Vasic-Racki, *Chem. Biochem. Eng. Quarte* **2009**, *23*, 545–553.

[44] A. E. Stütz, *Iminosugars as Glycosidase Inhibitors*, Wiley-VCH, Weinheim, Germany, **1999**.

[45] L. J. Whalen, C. H. Wong, *Aldrichimica Acta* **2006**, *39*, 63–71.

[46] J. Calveras, M. Egido-Gabás, L. Gómez, J. Casas, T. Parella, J. Joglar, J. Bujons, P. Clapés, *Chem. - A Eur. J.* **2009**, *15*, 7310–7328.

[47] T. M. Gloster, P. Meloncelli, R. V. Stick, D. Zechel, A. Vasella, G. J. Davies, *J. Am. Chem. Soc.* **2007**, *129*, 2345–2354.

[48] N. Asano, K. Ikeda, L. Yu, A. Kato, K. Takebayashi, I. Adachi, I. Kato, H. Ouchi, H. Takahata, G. W. J. Fleet, *Tetrahedron Asymmetry* **2005**, *16*, 223–229.

[49] M. S. M. Pearson, M. Mathé-Allainmat, V. Fargeas, J. Lebreton, *European J. Org. Chem.* **2005**, 2159–2191.

[50] M. Koyama, S. Sakamura, *Agric. Biol. Chem.* **1974**, *38*, 1111–1112.

[51] L. Gómez, E. Molinar-Toribio, M. Á. Calvo-Torras, C. Adelantado, M. E. Juan, J. M. Planas, X. Cañas, C. Lozano, S. Pumarola, P. Clapés, et al., *Br. J. Nutr.* **2012**, *107*, 1739–1746.

[52] A. Kato, N. Asano, H. Kizu, K. Matsui, A. A. Watson, R. J. Nash, *J. Nat. Prod.* **1997**, *60*, 312–314.

[53] H. Nojima, I. Kimura, F. J. Chen, Y. Sugihara, M. Haruno, a Kato, N. Asano, *J. Nat. Prod.* **1998**, *61*, 397–400.

[54] S. Taniguchi, N. Asano, F. Tomino, I. Miwa, *Horm. Metab. Res.* **1998**, *30*, 679–683.

[55] J. Q. Fan, S. Ishii, N. Asano, Y. Suzuki, *Nat. Med.* **1999**, *5*, 112–115.

[56] G. W. J. Fleet, L. E. Fellows, P. W. Smith,

Tetrahedron **1987**, *43*, 979–990.

[57] G. Pandey, M. Kapur, *Tetrahedron Lett.* **2000**, *41*, 8821–8824.

[58] N. Kumari, B. G. Reddy, Y. D. Vankar, *European J. Org. Chem.* **2009**, 160–169.

[59] J. Y. Goujon, D. Gueyrard, P. Compain, O. R. Martin, K. Ikeda, A. Kato, N. Asano, *Bioorganic Med. Chem.* **2005**, *13*, 2313–2324.

[60] Y. Banba, C. Abe, H. Nemoto, A. Kato, I. Adachi, H. Takahata, *Tetrahedron Asymmetry* **2001**, *12*, 817–819.

[61] J. A. Castillo, J. Calveras, J. Casas, M. Mitjans, M. P. Vinardell, T. Parella, T. Inoue, G. a. Sprenger, J. Joglar, P. Clapés, *Org. Lett.* **2006**, *8*, 6067–6070.

[62] S. Barberis, F. Guzmán, A. Illanes, J. López-Santín, L. Wilson, G. Álvaro, J. M. Guisán, R. Fernández-Lafuente, C. Mateo, P. Clapés, et al., in *Enzym. Biocatal. Princ. Appl.* (Ed.: A. Illanes), Springer, Dordrecht, Netherlands, **2008**, pp. 253–378.

[63] T. Machajewski, C. Wong, *Angew. Chemie Int. Ed.* **2000**, *39*, 1352–1375.

[64] D. Franke, C. C. Hsu, C. H. Wong, *Methods Enzymol.* **2004**, *388*, 224–238.

[65] P. Clapés, W.-D. Fessner, G. A. Sprenger, A. K. Samland, *Curr. Opin. Chem. Biol.* **2010**, *14*, 154–167.

[66] S. M. Dean, W. A. Greenberg, C. H. Wong, *Adv. Synth. Catal.* **2007**, *349*, 1308–1320.

[67] J. Mlynarski, J. Paradowska, *Chem. Soc. Rev.* **2008**, *37*, 1502–1511.

[68] M. G. Silvestri, G. Desantis, M. Mitchell, C.-H. Wong, in *Top. Stereochem.* (Ed.: S.E. Denmark), John Wiley & Sons, New York, USA, **2003**, pp. 267–342.

[69] L. Espelt, T. Parella, J. Bujons, C. Solans, J. Joglar, A. Delgado, P. Clapés, *Chem. Eur. J.* **2003**, *9*, 4887–4899.

[70] A. K. Samland, G. A. Sprenger, *Appl. Microbiol. Biotechnol.* **2006**, *71*, 253–264.

[71] M. Brovetto, D. Gamenara, P. Saenz Méndez, G. A. Seoane, *Chem. Rev.* **2011**, *111*, 4346–4403.

[72] T. Gefflaut, M. Lemaire, M. L. Valentin, J. Bolte, *J. Org. Chem.* **1997**, *62*, 5920–5922.

[73] I. Sánchez-Moreno, J. F. García-García, A. Bastida, E. García-Junceda, *Chem. Commun.* **2004**, 1634–1635.

[74] M. Cheriyan, E. J. Toone, C. A. Fierke, *Protein Sci.* **2007**, *16*, 2368–77.

[75] S. Fong, T. D. Machajewski, C. C. Mak, C. H. Wong, *Chem. Biol.* **2000**, *7*, 873–883.

[76] M. Sugiyama, Z. Hong, L. J. Whalen, W. A. Greenberg, C. H. Wong, *Adv. Synth. Catal.* **2006**, *348*, 2555–2559.

[77] M. Schürmann, G. A. Sprenger, *J. Biol. Chem.* **2001**, *276*, 11055–11061.

[78] C. Guérard-Hélaine, V. De Berardinis, M. Besnard-Gonnet, E. Darii, M. Debacker, A. Debard, C. Fernandes, V. Hélaine, A. Mariage, V. Pellouin, et al., *ChemCatChem* **2015**, *7*, 1871–1879.

[79] S. Thorell, M. Schürmann, G. A. Sprenger, G. Schneider, *J. Mol. Biol.* **2002**, *319*, 161–171.

[80] E. F. Pettersen, T. D. Goddard, C. C. Huang, G. S. Couch, D. M. Greenblatt, E. C. Meng, T. E. Ferrin, *J. Comput. Chem.* **2004**, *25*, 1605–1612.

[81] M. Schürmann, M. Schürmann, G. A. Sprenger, *J. Mol. Catal. B Enzym.* **2002**, *19–20*, 247–252.

[82] P. Clapés, X. Garrabou, *Adv. Synth. Catal.* **2011**, *353*, 2263–2283.

[83] R. Roldán, I. Sanchez-Moreno, T. Scheidt, V. Hélaine, M. Lemaire, T. Parella, P. Clapés, W. D. Fessner, C. Guérard-Hélaine, *Chem. - A Eur. J.* **2017**, *23*, 5005–5009.

[84] M. Sugiyama, Z. Hong, P.-H. Liang, S. M. Dean, L. J. Whalen, W. A. Greenberg, C.-H. Wong, *J. Am. Chem. Soc.* **2007**, *129*, 14811–14817.

[85] J. A. Castillo, C. Guérard-Hélaine, M. Gutiérrez, X. Garrabou, M. Sancelme, M. Schürmann, T. Inoue, V. Hélaine, F. Charmantray, T. Gefflaut, et al., *Adv. Synth. Catal.* **2010**, *352*, 1039–1046.

[86] M. Gutierrez, T. Parella, J. Joglar, J. Bujons, P. Clapés, *Chem. Commun.* **2011**, *47*, 5762–5764.

[87] A. Szekrenyi, A. Soler, X. Garrabou, C. Guérard-Hélaine, T. Parella, J. Joglar, M. Lemaire, J. Bujons, P. Clapés, *Chem. - A Eur. J.* **2014**, *20*, 12572–12583.

[88] M. Sudar, Z. Findrik, D. Vasić-Rački, P. Clapés, C. Lozano, *Enzyme Microb. Technol.* **2013**, *53*, 38–45.

[89] M. Sudar, Z. Findrik, C. Lozano, *J. Biotechnol.* **2013**, *167*, 191–200.

[90] D. Lenoir, *Angew. Chemie - Int. Ed.* **2006**, *45*, 3206–3210.

[91] M. Mifsud, A. Szekrényi, J. Joglar, P. Clapés, *J. Mol. Catal. B Enzym.* **2012**, *84*, 102–107.

[92] L. Andersson, R. Wolfenden, *Anal. Biochem.* **1982**, *124*, 150–157.

[93] M. Sudar, Z. Findrik, Đ. Vasić-Rački, A. Soler, P. Clapés, *RSC Adv.* **2015**, *5*, 69819–69828.

[94] M. P. J. Van Deurzen, F. Van Rantwijk, R. A. Sheldon, *Tetrahedron* **1997**, *53*, 13183–13220.

[95] S. Colonna, N. Gaggero, C. Richelmi, P. Pasta, *Trends Biotechnol.* **1999**, *17*, 163–168.

[96] M. C. . Franssen, H. C. van der Plas, *Adv. Appl. Microbiol.* **1992**, *37*, 41–99.

[97] P. D. Shaw, L. P. Hager, *J. Biol. Chem.* **1961**, *236*, 1626–1630.

[98] D. R. Morris, L. P. Hager, *J. Biol. Chem.* **1966**, *241*, 1763–1768.

[99] M. A. Pickard, A. Hashimoto, *Can. J. Microbiol.* **1988**, *34*, 998–1002.

[100] Y. J. Han, J. T. Watson, G. D. Stucky, A. Butler, *J. Mol. Catal. B Enzym.* **2002**, *17*, 1–8.

[101] J. A. Thomas, D. R. Morris, L. P. Hager, *J. Biol. Chem.* **1970**, *245*, 3129–3134.

[102] W. Sun, T. A. Kadima, B. Dunford, *Biochem. Cell Biol.* **1994**, *72*, 321–31.

[103] F. Van Rantwijk, R. A. Sheldon, *Curr. Opin. Biotechnol.* **2000**, *11*, 554–564.

[104] V. M. Dembitsky, *Tetrahedron* **2003**, *59*, 4701–4720.

[105] W. Adam, M. Lazarus, C. R. Saha-Möller, O. Weichold, U. Hoch, D. Häring, P. Schreier, in *Biotransformations* (Ed.: K. Faber), Springer, Heidelberg, Germany, **1999**, pp. 73–108.

[106] J. Geigert, D. J. Dalietos, S. L. Neidleman, T. D. Lee, J. Wadsworth, *Biochem. Biophys. Res. Commun.* **1983**, *114*, 1104–1108.

[107] E. Kiljunen, L. T. Kanerva, *J. Mol. Catal. B Enzym.* **2000**, *9*, 163–172.

[108] M. P. J. van Deurzen, F. van Rantwijk, R. A. Sheldon, *J. Carbohydr. Chem.* **1997**, *16*, 299–309.

[109] J. A. Thomas, D. R. Morris, P. Hager, *J. Biol. Chem.* **1970**, *245*, 3135–3142.

[110] S. R. Blanke, L. P. Hager, *J. Biol. Chem.* **1988**, *263*, 18739–18743.

[111] M. Sundaramoorthy, J. Terner, T. L. Poulos, *Structure* **1995**, *3*, 1367–1378.

[112] H. B. Dunford, J. S. Stillman, *Coord. Chem. Rev.* **1976**, *19*, 187–251.

[113] J. F. Kennedy, C. A. White, *Advances in Inorganic and Bioinorganic Mechanisms*, Academic Press, New York, USA, **1984**.

[114] M. Hofrichter, R. Ullrich, *Appl. Microbiol. Biotechnol.* **2006**, *71*, 276–288.

[115] A. N. Shevelkova, A. D. Ryabov, *Biochem Mol Biol Int* **1996**, *39*, 665–670.

[116] M. Andersson, M. M. Andersson, P. Adlercreutz, *Biocatal. Biotransformation* **2000**, *18*, 457–469.

[117] M. Ayala, C. V Batista, R. Vazquez-Duhalt, *J. Biol. Inorg. Chem.* **2011**, *16*, 63–68.

[118] W. Chamulitrat, N. Takahashi, R. P. Mason, *J. Biol. Chem.* **1989**, *264*, 7889–7899.

[119] J.-B. Park, D. S. Clark, *Biotechnol. Bioeng.* **2006**, *93*, 1190–1195.

[120] N. Spreti, R. Germani, A. Incani, G. Savelli, *Biotechnol. Prog.* **2004**, *20*, 96–101.

[121] C. E. Grey, F. Rundbäck, P. Adlercreutz, *J. Biotechnol.* **2008**, *135*, 196–201.

[122] J.-Z. Liu, M. Wang, *BMC Biotechnol.* **2007**, *7*, 23.

[123] K. Seelbach, M. P. J. Van Deurzen, F. Van Rantwijk, R. A. Sheldon, U. Kragl, *Biotechnol. Bioeng.* **1997**, *55*, 283–288.

[124] M. P. J. Van Deurzen, K. Seelbach, F. van Rantwijk, U. Kragl, R. a. Sheldon, *Biocatal. Biotransformation* **1997**, *15*, 1–16.

[125] M. Pešić, C. López, G. Álvaro, *Biochem. Eng. J.* **2012**, *67*, 218–224.

[126] M. Pešić, C. López, J. López-Santín, G. Álvaro, *Appl. Microbiol. Biotechnol.* **2013**, *97*,

7173–7183.

[127] M. Pešić, C. López, G. Álvaro, J. López-Santín, *J. Mol. Catal. B Enzym.* **2012**, *84*, 144–151.

[128] R. A. Rodriguez-Hinestroza, C. Lopez, J. Lopez-Santin, C. Kane, M. Dolors Benaiges, T. Tzedakis, *Chem. Eng. Sci.* **2017**, *158*, 196–207.

[129] I. Ardao, M. D. Benaiges, G. Caminal, G. Álvaro, *Enzyme Microb. Technol.* **2006**, *39*, 22–27.

[130] T. Suau, G. Alvaro, M. D. Benaiges, *Biochem. Eng. J.* **2008**, *41*, 95–103.

[131] I. Ardao, J. Comenge, M. D. Benaiges, G. Álvaro, V. F. Puntes, *Langmuir* **2012**, *28*, 6461–6467.

2 Objectives

The main aim of this thesis work is the study of the feasibility of a multi-enzymatic cascade composed by a peroxidase and an aldolase for the synthesis of iminocyclitols, using amino alcohols as the starting material. In particular, CPO would catalyze the β-OH oxidation, and the further DHA addition would be catalyzed by FSA to render preFagomine.

The specific objectives are:

- Study of the substrate specificity of CPO in front of amino alcohols. To this end, several amino alcohols would be assayed in the CPO-catalyzed oxidation, relating the final conversions of the substrate to its structure.
- Evaluation of the suitability of CPO for the β-OH oxidation. A preliminary study of the main operating conditions for the β-OH oxidation would be detailed, prior to the coupling with the aldol addition. The reaction medium, the substrate concentration, and the peroxide nature should be investigated. For the reaction, various peroxides would be employed as oxidants, analyzing the effect on the enzyme operational stability.
- Coupling of the CPO-catalyzed β-OH oxidation and the FSA-catalyzed aldol addition of DHA to the formed amino aldehyde. The bottlenecks of the process should be investigated.
- Development of a mathematical model of the coupled reaction. All the observed reactions would be characterized, estimating the kinetic parameters of each reaction.
- Immobilization of CPO and FSA onto magnetic nanoparticle clusters (mNC). Different strategies for the attachment would be develop using variously functionalized clusters to link the enzyme through different functional groups on its surface.
- Immobilization of CPO and FSA on other conventional supports, such as amino/aldehyde-functionalized or metal-chelated agarose.
- Exploitation of the kinetic model to find the proper conditions for the coupling of both reactions catalyzed by soluble/immobilized CPO and FSA.

3 Chloroperoxidase-catalyzed amino alcohol oxidation: substrate specificity and novel strategy for the synthesis of *N*-Cbz-3-aminopropanal

3.1 Introduction

As stated in previous pages, the oxidation of amino alcohols to yield amino aldehydes is intended using CPO. Amino aldehydes are used as the substrates of aldolases for the aldol addition of DHA or DHAP to yield aldol adducts.[1–5] These compounds are precursors of the well-known iminocyclitols, which have been extensively studied for their antiviral, anticancer, and antidiabetic effects.[6–9]

Only a few studies have been published on the oxidation of amino alcohols catalyzed by CPO and exclusively restricted to α-amino alcohols.[10,11] The ability of this enzyme to oxidize amino alcohols in other configurations –particularly focusing on β-amino alcohols– is worth investigating, so as to discover new valuable intermediates and products. In the present chapter, the substrate specificity in the amino alcohol oxidation catalyzed by CPO is analyzed.

Enzymes are generally very specific in relation to the substrate, which is provided with the chemical bonds that can be attacked by the functional groups from the active site of the enzyme. In that way, the substrate is anchored in the active site for the reaction. Thus, any chemical modification[12] or amino acid mutation[13,14] at the active site may vary the enzyme specificity. To study the specificity of CPO, several amino alcohol compounds are intended to be oxidized by targeting their molecular substituents, employing CPO and peroxide. Different configurations according to the amine position toward the hydroxyl (α to ε) are tested. The effect of the amino-protecting group and other substituents (i.e., methyl and hydroxyl) is also examined, evaluating feasible steric hindrance due to the effect of bulky substituents.

The peroxide nature is crucial in the CPO-catalyzed reactions, affecting not only the stability of the enzyme but the overall synthesis. As a substrate, the peroxide influences the net oxidation rate depending on the enzyme affinity toward the specific peroxide. Many reports in the literature describe the use of various peroxides as oxidants in these reactions, such as *t*-BuOOH and cumene hydroperoxide.[15] In order to see this effect, the oxidation of each amino alcohol is catalyzed using either H_2O_2 or *t*-BuOOH, analyzing the effect of the peroxide nature in terms of the initial reaction rate, substrate conversion, and CPO operational stability.

Concurrently to the study of CPO substrate specificity, one reaction of particular interest is the CPO-catalyzed oxidation of β-OH in order to yield β-CHO. This aldehyde is an intermediate for the aldol addition of DHA catalyzed by FSA, with preFagomine as the final product.[16–19] Hence, the oxidation of β-OH to β-CHO is investigated, using CPO as the biocatalyst, and H_2O_2 or *t*-BuOOH as the peroxide. In this reaction, the substrate solubility is a restricting step, which limits the process intensification. This could be alleviated by the use of organic solvents. The presence of such organic solvents has been previously found to alter CPO catalysis by changing the protein conformation (it usually leads to enzyme inactivation) and the local environment at the active site.[20,21] In the case of using immobilized CPO, the enzyme instability caused by solvents could be reduced.[22] Despite the inactivation, organic solvents increase the substrate solubility, and therefore they have been used in many CPO reactions to improve the productivity of the system.[23,24]

To this end, the main operating conditions, such as the reaction medium, the initial amino alcohol concentration and the peroxide nature, are determined prior to the coupling with the FSA-catalyzed aldol addition.

3.2 Materials and methods

3.2.1 Materials

CPO from *C. fumago* was supplied by Chirazyme Labs (Greenville, NC, USA) as a solution of partially purified enzyme (9.54 mg protein ml^{-1}) with a specific activity of 1400 U mg^{-1} protein. Monochlorodimedone (MCD, 1,1-dimethyl-4-chloro-3,5-cyclohexadione) and 1-fluoro-2,4-dinitrobenzene (DNFB) were obtained from Fluka (Milwaukee, WI, USA). *N*-Cbz-2-aminoethanol (benzyl *N*-(2-hydroxyethyl)carbamate) (**1**, Table 3.1), β-OH (benzyl *N*-(3-hydroxypropyl)carbamate) (**2.a**), 3-amino-1-propanol (**2.b**), *N*-Fmoc-4-aminobutanol (**3**), *N*-Cbz-5-aminopentanol (**4**), *N*-Cbz-6-aminohexanol (**5**), β-CHO (3-[(Benzyloxycarbonyl)amino] propionaldehyde), β-COOH (Z-β-Ala-OH), *t*-BuOOH (70 wt. % in H_2O), H_2O_2 (30 wt. % in H_2O), and trifluoroacetic acid (TFA) were purchased from Sigma Aldrich (St. Louis, MO, USA). 4-Amino-2-butanol (**2.c**) was procured from Acros Organics (Geel, Belgium). *N*-Cbz-2-hydroxy-3-aminoethanol (**2.d**) was supplied by Dr. Clapés from the Biotransformation and Bioactive Molecules Research Group (CSIC, Barcelona, Spain). HPLC-grade acetonitrile was obtained from Carlo Erba (Milan, Italy). Milli-Q-grade water was used for analytical HPLC.

Table 3.1. List of amino alcohols used as substrates in CPO-catalyzed oxidation reactions.

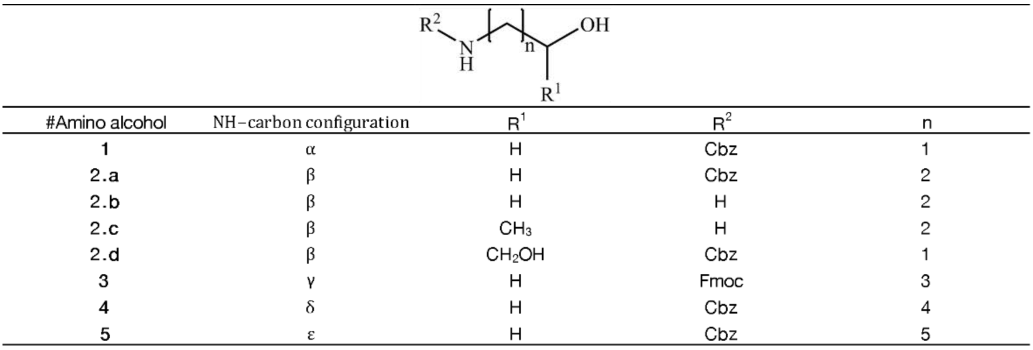

#Amino alcohol	NH–carbon configuration	R^1	R^2	n
1	α	H	Cbz	1
2.a	β	H	Cbz	2
2.b	β	H	H	2
2.c	β	CH_3	H	2
2.d	β	CH_2OH	Cbz	1
3	γ	H	Fmoc	3
4	δ	H	Cbz	4
5	ε	H	Cbz	5

3.2.2 CPO activity

The CPO stability was determined by measuring its activity along time. For simplicity, the chlorination activity test was performed. The CPO half-life time ($t_{1/2}$) was experimentally estimated from activity versus time data. The enzymatic activity was determined by the decrease in absorbance at 278 nm due to the conversion of MCD (ε_{278} =12.2 mM^{-1} cm^{-1})[25] to dichlorodimedone (DCD), according to the method of Hager and Morris.[26] The enzymatic assay contained 100 mM potassium phosphate buffer of pH 2.75, 0.16 mM MCD, 20 mM KCl, 2 mM hydrogen peroxide, and 50 µL of the sample with CPO, in a total volume of 1 mL. The absorbance was measured at 25 °C, using a Cary 50 Bio UV–Visible Spectrophotometer (Varian, Palo Alto, CA, USA). One activity unit of CPO is defined as the amount of enzyme required for the conversion of 1 µmol of MCD per minute at pH 2.75 and 25 °C. The standard deviation of the CPO activity test was calculated from measurements performed by duplicate.

3.2.3 HPLC analysis

The concentrations of amino alcohols and the oxidized products from β-OH (β-CHO, β-COOH) were measured by HPLC analysis in an HPLC Dionex UltiMate 3000 with

UltiMate 3000 Variable Wavelength Detector. For chromatographic separation, a reversed-phase column (XBridge BEH C18, 130Å, 5 µm, 4.6 × 250 mm) from Waters (Milford, MA, USA) was used. The reaction samples were dissolved in acetonitrile (MeCN), which deactivates the enzyme and arrests the reaction. All separations were performed by injecting 30 µL of the sample at a flow rate of 1 mL min^{-1} at 30 °C. For all substrates, the solvent system consisted of solvent A (0.1% (v/v) TFA in H_2O) and solvent B (0.095% (v/v) TFA in MeCN/H_2O 4:1 (v/v)). Samples were eluted using a specific multistep gradient for each substrate molecule: (**1**) gradient from 20% to 36% in 24 min, λ = 200 nm; (**2.a**, β-CHO, β-COOH) gradient from 5% to 31% B in 0.35 min and isocratic elution at 30% B over 14.65 min, λ = 254 nm; (**2.d**) gradient from 5% to 28% B in 0.35 min and isocratic elution at 30% B over 9.65 min, λ = 254 nm; (**3**) gradient from 20% to 50% B in 1.5 min and isocratic elution at 30% B over 18.5 min, λ = 200 nm; (**4**) gradient from 20% to 60% B in 1.5 min and isocratic elution at 30% B over 7.5 min, λ = 200 nm; and (**5**) gradient from 20% to 65% B in 1.5 min and isocratic elution at 30% B over 8.5 min, λ = 200 nm.

2.b and **2.c** were analyzed via a well-established derivatization method with DNFB.[27] In both cases, 50 µL of the sample was mixed with 80 µL of DNFB (37.6 mM in acetone) and 20 µL of 1 M $NaHCO_3$. The mixture was incubated for 1.5 h at 40 °C. The reaction was terminated by the addition of 40 µL of 1 M HCl and 200 µL of MeCN. Samples were eluted with a gradient from 31.3% to 48.8% in 25 min, λ = 360 nm.

A quantitative analysis of all compounds was performed by prior calibration with standards of known concentration. The concentration values were converted into the molar amount (µmol); that is, the volume of the peroxide added in pulses via a microburette and the volume of the reaction medium withdrawn for each analysis (<10% of the initial volume) were considered. The standard deviation of molar quantities was calculated from HPLC measurements performed by duplicate.

*3.2.4 Oxidation of amino alcohols **1–5***

The reaction conditions were adapted from a previous study in the research group.[10] The reaction medium was prepared by dissolving the amino alcohol in 100 mM sodium acetate buffer (pH 5.0) and ethyl acetate (90:10 v/v) in a final volume of 5 mL. The substrate concentration range was 5 mM for α/β-amino alcohols or 0.5 mM for γ/δ/ε-amino alcohols. This difference in the order of magnitude was due to solubility restrictions. All reactions were performed at 25 °C and 1000 rpm of orbital stirring (MultiTherm™, Benchmark Scientific, Edison, NJ, USA), and 450 U mL^{-1} of CPO was used. The reaction was initiated by a pulse of 0.8 mM peroxide and carried out by continuous addition of 3 mM h^{-1} peroxide using a single-syringe automatic microburette (Crison Instruments, Barcelona, Spain). A linear fitting of substrate concentration versus time, at a substrate conversion <10%, was used to estimate initial reaction rates.

Two reaction controls were performed for each substrate oxidation to prevent false-positive results: (a) the substrate was incubated in a reaction buffer, without enzyme or peroxide. This control checked the stability of the substrate itself under reaction conditions. (b) The substrate was incubated in a reaction buffer with peroxide (H_2O_2/*t*-BuOOH) addition at 3 mM h^{-1} and in the absence of enzyme. This second control accounted for possible chemical reactions between the substrate and peroxide, in the absence of enzyme, as it has been observed in the literature.[28–32]

3.2.5 β-OH oxidation

The reaction medium contained β-OH dissolved in 100 mM sodium acetate buffer (pH 5.0) in a final volume of 5 mL, with an initial substrate concentration of 5–38 mM. For the first trials of reactions performed with an organic solvent (ethyl or butyl acetate) in monophasic or biphasic systems, the initial β-OH concentration was set at maximum solubility in each medium: 38 mM in aqueous buffer, 53 mM in acetate buffer saturated with ethyl acetate, 69 mM in acetate buffer saturated with butyl acetate, and 85 mM in a biphasic medium of aqueous buffer and ethyl acetate (90:10 v/v). In all cases, 450 U mL^{-1} of CPO was used. The reaction performance (peroxide addition, temperature, and agitation) was the same as previously mentioned.

Oxidation reactions at high enzyme load and high peroxide–substrate ratio were carried out at an initial substrate concentration of 15 mM. β-OH was dissolved in 100 mM sodium acetate buffer (pH 5.0) in a final volume of 0.3 mL, containing 350 mM *t*-BuOOH. For this purpose, 15 kU mL^{-1} of CPO was used. The reaction was performed in duplicate at 25 °C and 1000 rpm of orbital stirring.

3.2.6 Amino aldehyde–peroxide chemical reaction

β-OH, β-CHO and β-COOH were incubated at maximum concentration (38, 17, and 11 mM, respectively) in 5 mL of 100 mM sodium acetate buffer (pH 5.0). The reaction was allowed to take place under orbital agitation in a MultiTherm™ device overnight for 19 h. Peroxide was continuously added to the reactor at 3 mM h^{-1}.

3.2.7 Identification of side-reaction products

Products **6**–**8** were identified either by HPLC–mass spectrometry (MS)–MS or by MS, at *Servei d'Anàlisi Química* from *Universitat Autònoma de Barcelona* (Barcelona, Spain). NMR analyses of the three molecules confirmed the proposed structure (*Servei de Ressonància Magnètica Nuclear* from *Universitat Autònoma de Barcelona*). Further information is presented in the Appendix.[33]

3.3 Results and discussion

3.3.1 Substrate specificity in amino alcohol oxidations

The amino alcohol oxidative capacity of CPO was investigated by the oxidation of compounds **1**–**5** to amino aldehydes (Table 3.1). These compounds are amino alcohols with similar hydrocarbon chains selected due to (i) the distinct the amine position toward the hydroxyl, (ii) presence or absence of an amino-protecting group, and (iii) other specific carbon substitutions. Each substrate oxidation was performed by continuous addition of oxidants (H_2O_2 or *t*-BuOOH).

As seen in Table 3.2, CPO accepts nearly all compounds **1**–**5** as substrates to catalyze their oxidation, with **2.d** and **3** being the only non-converted molecules. For all substrates, the initial reaction rates (r_0) and conversion at the reaction end point (time at which all substrate was converted or no remaining CPO activity was detected) are described in relation to compound structural issues. The operational stability of CPO toward the peroxide nature was also compared.

The chemical structures of compounds **1**, **2.a**, **4**, and **5** differ only in the *n* value of CH_2 groups and therefore in the amine position toward the hydroxyl. According to the initial reaction rate analysis, the highest r_0 was observed for substrate **1** and the lowest for **5** using either H_2O_2 or *t*-BuOOH as the oxidant. Thus, these results revealed that the further the amino group from the hydroxyl in the substrate molecule, the lower the r_0.

Table 3.2. Amino alcohol oxidations catalyzed by CPO using H_2O_2 or *t*-BuOOH as oxidant at an addition rate of 3 mM h^{-1} in 5 mL of monophasic medium with 100 mM acetate buffer of pH 5.0 (ethyl acetate 10%, v/v).

#Amino alcohol	Oxidant: H_2O_2			Oxidant: *t*-BuOOH		
	r_0 (μmol h^{-1})	Conversion (%)[a]	CPO $t_{1/2}$ (h)	r_0 (μmol h^{-1})	Conversion (%)[a]	CPO $t_{1/2}$ (h)
1	2.2	24.4	2.0	3.3	18.8	0.9
2.a	1.2	9.7	1.3	2.5	10.9	0.8
2.b	1.6	44.0	7.0	7.8	83.6	3.1
2.c	16.6	25.7	2.5	4.6	77.9	3.0
2.d	0.0	0.0	5.6	0.0	0.0	1.0
3[b]	0.0	0.0	0.9	0.0	0.0	1.1
4[b]	1.1	16.3	0.9	1.3	16.8	1.1
5[b]	0.1	12.3	6.0	0.1	9.4	1.0

[a] Substrate conversion was determined at the reaction end point by HPLC analysis of the corresponding amino alcohols.

[b] Initial reaction rate (r_0) values were normalized according to initial substrate concentrations: 5 mM for compounds 1-2.d; 0.5 for compounds 3-5.

The presence of amino-protecting groups altered the reaction course in terms of the initial rate and maximum substrate conversion. Thus, the Cbz group in substrate **2.a** reduced r_0 compared with the non-protected substrate **2.b**; due to non-amino protection, r_0 increased 1.4-fold with H_2O_2 as the oxidant and 3.1-fold with *t*-BuOOH. Moreover, for compound **3**, which was protected by fluorenylmethyloxycarbonyl (Fmoc) instead of Cbz, no oxidation was observed, presumably because the protecting group was bulky.

The extra methyl substituent in substrate **2.c** R^1 compared with **2.b** had a different impact on the initial rate depending on the oxidant used. The lower initial rate with *t*-BuOOH can be attributed to the steric hindrance produced by the methyl group. Finally, no conversion was observed for substrate **2.d** with any peroxide, probably due to steric hindrance or changes in electron density caused by the presence of the CH_2OH group.

The oxidant selection affected the operational stability of CPO and consequently the reaction time course, as reflected by enzyme half-life values obtained in each case. In many substrate reactions, $t_{1/2}$ of CPO was higher with H_2O_2 than with *t*-BuOOH, thus achieving longer reaction periods; in other cases, $t_{1/2}$ was practically the same for both peroxides. For Cbz-protected substrates, conversion of a similar order of magnitude was achieved for both oxidants, due to lower reaction rates and higher enzyme stability with H_2O_2 as the peroxide.

Substrate species were also found to have a modulatory effect on enzyme stability. Under the same reaction conditions, the specific substrate determined the CPO deactivation degree. As an example, $t_{1/2}$ of CPO was 7.8-fold higher for compound **2.b** than **4** with H_2O_2 as the oxidant. This stabilizing effect of the substrate toward the enzyme is well established.[34,35]

3.3.2 *β-OH oxidation*

As previously mentioned, the first reaction in the present work is the enzymatic oxidation of β-OH (also compound **2.a**) to yield β-CHO (Figure 3.1). The possible CPO-catalyzed oxidation of the amino aldehyde can yield β-COOH. The acid is an undesirable compound if the target product is the amino aldehyde, but its formation could be reduced with an eventual coupling with the FSA-catalyzed aldol addition. Several assays were performed to determine the main operating conditions for β-OH oxidation. According to CPO-catalyzed oxidation of amino alcohols discussed above, *t*-BuOOH was preliminarily chosen as the peroxide for the main reaction, as higher r_0 values were obtained with this oxidant.

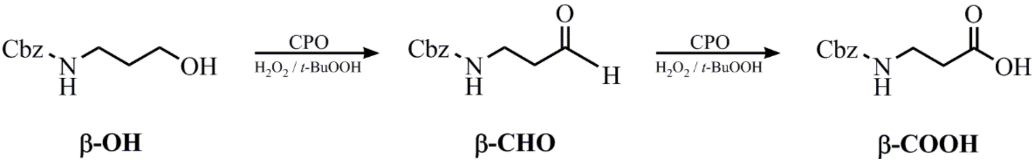

Figure 3.1. CPO-catalyzed oxidation of β-OH to β-CHO and β-COOH.

The solubility of β-OH in an aqueous buffer is moderate (maximum 38 mM in 100 mM sodium acetate buffer of pH 5.0). To overcome this limitation, three other media with selected eco-friendly solvents were used: (i) acetate buffer saturated with ethyl acetate, (ii) acetate buffer saturated with butyl acetate, and (iii) a biphasic medium of aqueous buffer and ethyl acetate (90:10 v/v). All four media were tested for the CPO operational stability and the substrate oxidation. The reactions were performed at an initial β-OH concentration corresponding to maximum solubility in each medium.

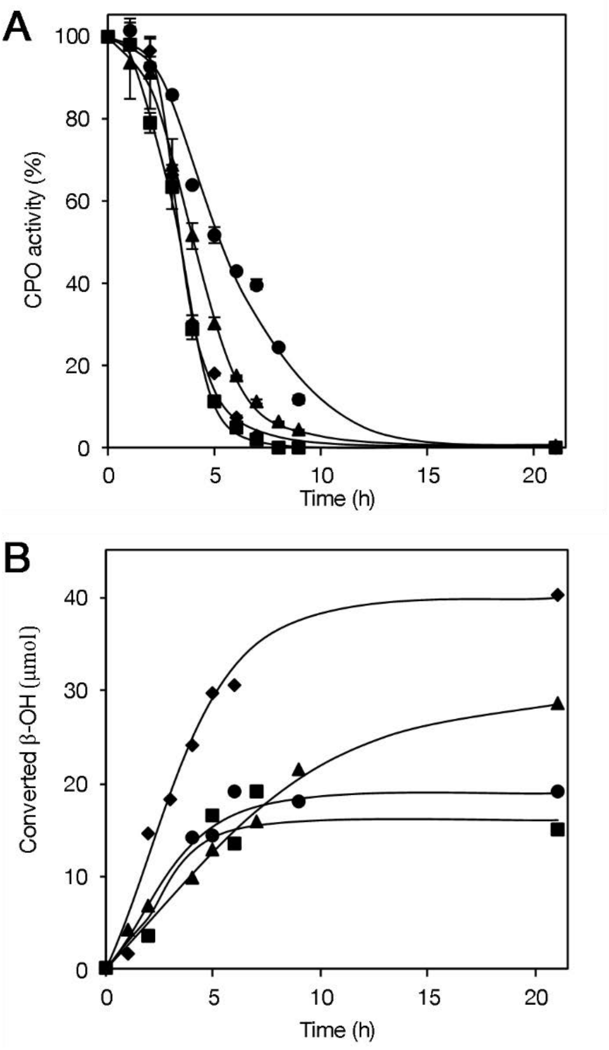

Figure 3.2. CPO-catalyzed β-OH oxidation by addition of *t*-BuOOH at 3 mM h^{-1} in 5 mL of the four assayed reaction media: 100 mM sodium acetate buffer (pH 5.0) (◆), acetate buffer saturated with ethyl acetate (■), acetate buffer saturated with butyl acetate (▲), and biphasic medium buffer/ethyl acetate 90:10 v/v (●). Initial substrate concentrations corresponded to maximum solubility in each medium: 38, 53, 68, and 85 mM. 450 U mL^{-1} of CPO was used. **(A)** Operational stability of soluble CPO. **(B)** β-OH consumption.

The enzyme half-life time increased from 3.4 h in an aqueous buffer to 5.1 h in a biphasic medium, as presented in Figure 3.2A. The stabilities in saturated media were similar to that measured in acetate buffer. However, the oxidation curves of the reactions catalyzed in ethyl or butyl acetate (saturated or biphasic) were not as expected with low β-OH conversion (Figure 3.2B). Maximum initial rate and final β-OH conversion were noted for the aqueous buffer. The conversion in acetate buffer was 21%, but <10% in other cases. This result can be attributed to two possible factors: (a) a protective effect of the substrate toward the enzyme (maximum initial substrate concentration in each case) or (b) a likely *t*-BuOOH partition between the two phases leading to lower peroxide concentration in the aqueous phase. In turn, this would explain the lower deactivation of CPO observed as well as the low oxidation rate in the presence of an organic phase.

To establish the appropriate initial β-OH concentration for the biotransformation, several reactions in the aqueous buffer were carried out at different initial substrate concentrations: 10, 16, 19, 26, and 36 mM. The half-life time of CPO increased with the initial substrate concentration in the range studied (Figure 3.3). It was 1.6-fold higher at 38 mM than at 11 mM. These results were in concordance with the low $t_{1/2}$ values obtained for the oxidation of compounds **1**–**5** (initial substrate concentration was 0.5–5 mM). Again, the data revealed the protective effect of the substrate on the operational stability of the enzyme.

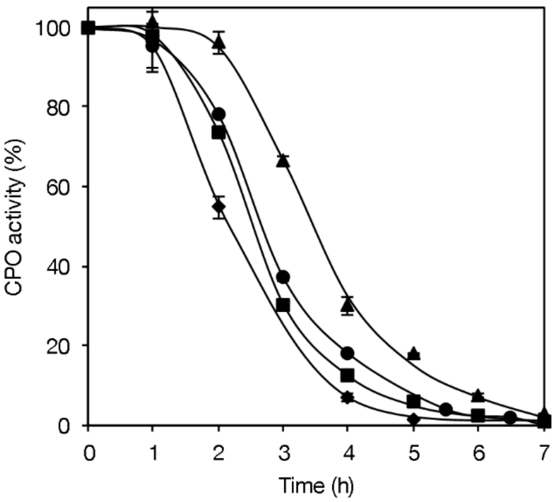

Figure 3.3. Operational stability of CPO in relation to initial β-OH concentration: 11 mM (◆), 21 mM (■), 34 mM (●), and 38 mM (▲). Experiment conditions: 100 acetate buffer (pH 5.0), *t*-BuOOH was added at 3 mM h^{-1}.

However, substrate inhibition in CPO-catalyzed reactions has been reported previously.[36,37] Nevertheless, it was not significant in the solubility range of β-OH in acetate buffer. The initial reaction rates were calculated and adjusted to a Michaelis–Menten model (Figure 3.4). The estimated $K_{M,\beta\text{-OH}}$ and r_{max} values were 34.0 mM and 5.4 mM h^{-1}, respectively.

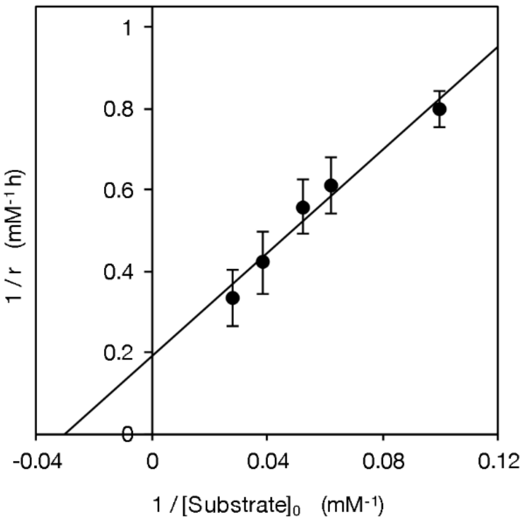

Figure 3.4. Lineweaver–Burk plot from the Michaelis–Menten adjustment of CPO-catalyzed oxidation of β-OH. Reactions were performed at initial substrate concentrations of 10, 16, 19, 26, and 36 mM β-OH in 5 mL of 100 mM acetate buffer (pH 5.0) with the addition of 3 mM h^{-1} *t*-BuOOH. 450 U mL^{-1} of CPO was used.

Two reactions were carried out in 100 mM acetate buffer at the same substrate concentration (38 mM β-OH) and peroxide addition rate (3 mM h^{-1}), each one with a different oxidant (*t*-BuOOH or H_2O_2). The evolution of enzymatic activity over time (Figure 3.5A), β-OH conversion, and formation of β-CHO and β-COOH (Figure 3.5B) were evaluated.

The CPO half-life time increased 2.4-fold when hydrogen peroxide was used instead of *t*-BuOOH; however, as expected, the initial β-OH oxidation rate was lower with H_2O_2. Nevertheless, both oxidants led to similar degrees of final β-OH conversion degree (CPO remained active for a longer time with H_2O_2). β-CHO production was faster and higher with *t*-BuOOH, but it conducted to high amino acid yield.

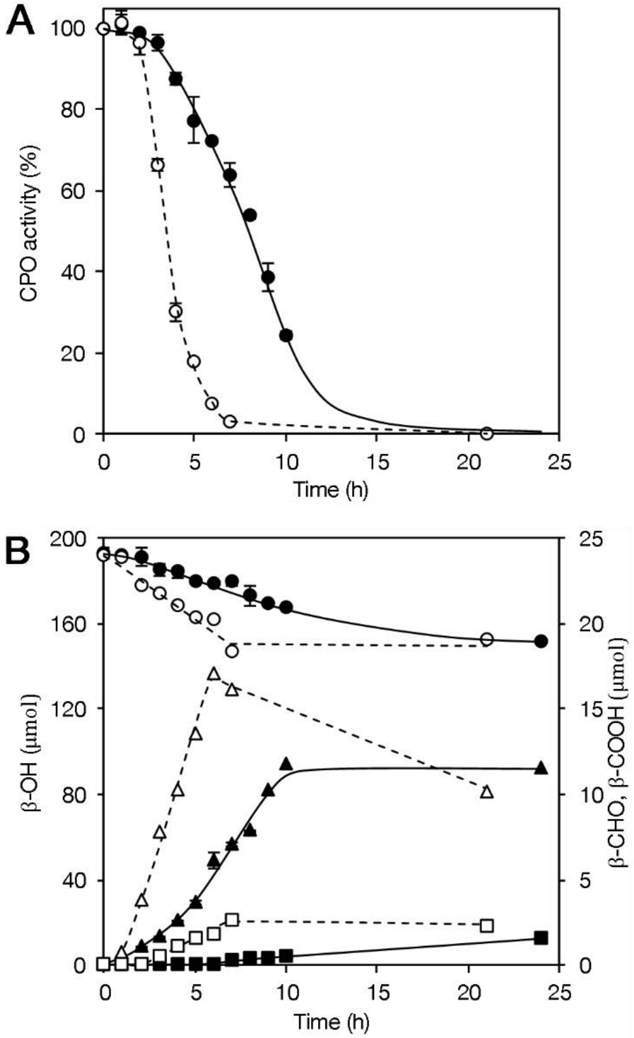

Figure 3.5. Oxidation of β-OH in 5 mL of 100 mM sodium acetate buffer (pH 5.0) with initial substrate concentration set at 38 mM, with addition of 3 mM h^{-1} *t*-BuOOH or H_2O_2. 450 U mL^{-1} of CPO was used. **(A)** Operational stability of CPO. *t*-BuOOH (○); H_2O_2 (●). (**B**) Substrate consumption and oxidized product formation. *t*-BuOOH: β-OH (○), β-CHO (△), β-COOH (□); H_2O_2: β-OH (●), β-CHO (▲), β-COOH (■).

3.3.3 β-OH oxidation: Identification of side reactions

On carefully evaluating the mole number of converted substrate and products obtained with reaction time (Figure 3.5B), a mass imbalance was observed: (a) using *t*-BuOOH at *t*=7h, 45.5 µmol of oxidized β-OH yielded only 18.7 µmol of products (16.1 µmol β-CHO and 2.6 µmol β-COOH). (b) Using H_2O_2 at *t*=24h, 41.3 µmol of oxidized β-OH yielded only 13 µmol of products (11.5 µmol β-CHO and 1.5 µmol β-COOH).

Therefore, in addition to the reactions presented in Figure 3.1, secondary reactions conducting to by-products were assumed to take place. It was hypothesized to be a chemical reaction between any of the three compounds and the peroxide. To confirm this, each molecule was incubated separately in acetate buffer for 19 h with the addition of 3 mM h^{-1} H_2O_2 or *t*-BuOOH. Both β-OH and β-COOH were not oxidized by any peroxygen species, but the amino aldehyde did react with the two peroxides: (i) 13.5% of initial β-CHO reacted with *t*-BuOOH after 19-h incubation, and (ii) 87.1% of β-CHO reacted with H_2O_2. A white precipitate was observed in the reactor when hydrogen peroxide was used. This chemical reaction between the amino aldehyde and the peroxide could explain the mass balance non-closure. This type of reaction has been previously described elsewhere.[38,39]

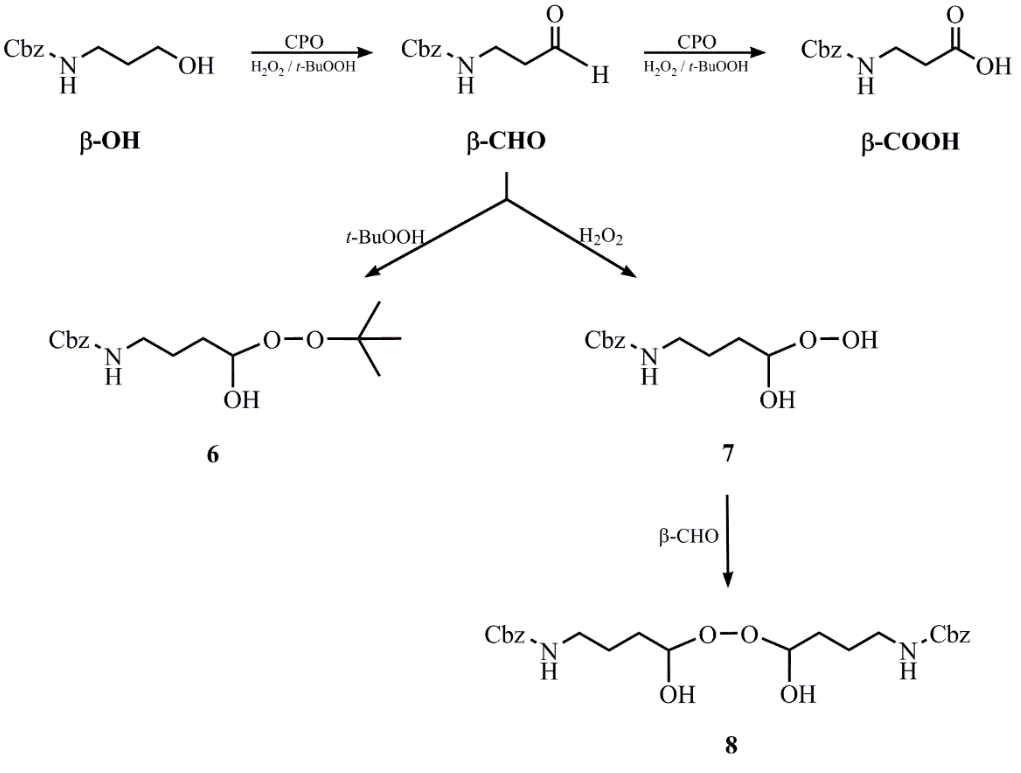

Figure 3.6. Novel proposed reaction scheme for β-OH oxidation catalyzed by CPO with the addition of peroxide (H_2O_2/*t*-BuOOH)

Thus, a novel reaction scheme was proposed (Figure 3.6). It includes one by-product when the selected oxidant is *t*-BuOOH, and two with H_2O_2. Then, for *t*-BuOOH, the putative product is benzyl (3-(*tert*-butylperoxy)-3-hydroxypropyl)carbamate ($C_{15}H_{23}NO_5$, compound **6**). For H_2O_2 reactions, the proposed hydroxy alkyl peroxide –benzyl (3-hydroperoxy-3-hydroxypropyl)carbamate ($C_{11}H_{15}NO_5$, compound **7**)– can further react with another amino aldehyde molecule to form a dialkyl peroxide (dibenzyl (peroxybis(3-hydroxypropane-3,1-diyl))dicarbamate; $C_{22}H_{28}N_2O_8$, compound **8**). The dialkyl peroxide is only formed with H_2O_2, as the hydroxy peroxy intermediate formed by *t*-BuOOH is not chemically reactive enough to attack another aldehyde. To characterize these molecules, all three compounds were obtained in the absence of salts, which might interfere with the identification analysis. The concentration of each target compound was maximized for the identification according to the mole ratio of peroxide/β-CHO. Compounds **6**–**7** were soluble under reaction conditions, whereas **8** was highly insoluble and formed a solid precipitate. The three compounds were identified by MS and NMR spectroscopy.[33]

An experimental verification of the proposed reaction mechanism was required to ensure its consistency. The test was performed using hydrogen peroxide because, in this case, the secondary reactions are more significant. β-OH (380 µmol) in 10 mL of acetate buffer was oxidized by CPO with the addition of 3 mM h^{-1} H_2O_2. After 24 h, 82.1 µmol of β-OH underwent conversion. Only 63.6 µmol of aldehyde and acid products were obtained; 18.5 µmol was missing. The 18.5 µmol represented compounds **7** and **8**. Under the reaction conditions, the concentration of by-product **7** was negligible (HPLC analysis quantification). Applying the proposed mechanism scheme and the molecular weight of by-product **8**, 4.15 mg was missing (equivalent to 9.25 µmol of by-product **8**). The reaction medium was carefully filtered, the filter and the empty reactor vessel were dried at 35 °C overnight, and the weight increase was considered to be the weight of compound **8** (4.0 ± 0.6 mg). Hence, the proposed mechanism was confirmed.

3.3.4 β-OH oxidation: Intensification

The above-mentioned results of β-OH oxidation indicated a necessary compromise between CPO stability, rates of substrate oxidation and key product formation, and the presence of side reactions. High substrate conversion was achieved by increasing the enzyme load and the peroxide/substrate ratio. Although hydrogen peroxide is an eco-friendly oxidant with a weaker enzyme-deactivating effect, *t*-BuOOH was the chosen peroxide because it leads to higher initial oxidation rate and a lower degree of side reactions.

The reaction was performed increasing the enzyme and substrates concentrations. The results are shown in Figure 3.7. In this case, 87% β-OH conversion was achieved after

60 min of reaction. In terms of the target product formation, yields of 16% β-CHO and 47% β-COOH were obtained. The product selectivity was in favor of the acid product. It could be driven toward the amino aldehyde by coupling the CPO-catalyzed reaction with a consecutive one (aldol addition), thus preventing the formation of compound **6**.

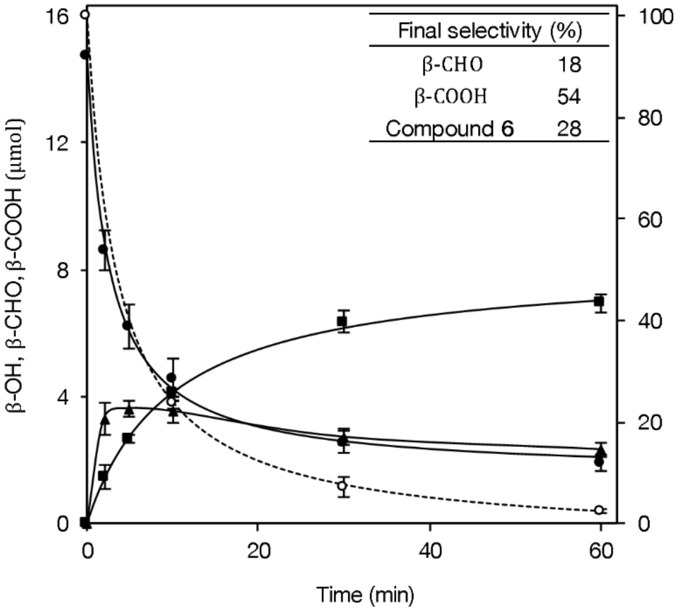

Figure 3.7. The extent of the β-OH oxidation. Reaction carried out in 0.3 mL of 100 mM sodium acetate buffer (pH 5.0) with 15 mM β-OH and 350 mM *t*-BuOOH as initial concentrations. 15,000 U mL^{-1} of CPO was used. β-OH (●), β-CHO (▲), β-COOH (■), operational stability of CPO (○). Inset: Measured selectivity for β-CHO and β-COOH products. Selectivity for compound **6** (Figure 3.6) was calculated by difference.

3.4 Conclusions

The amino alcohol oxidative capacity of CPO regarding substrate structure was studied. It is worth noting that CPO accepts α to ε configurations as substrates for the reaction. The effect of this configuration on enzyme catalysis was investigated, and it was found that the further the amino group from the hydroxyl in the substrate molecule, the lower the initial reaction rate. The influence of substituents on the amino alcohol molecule was also discussed, especially with respect to the amino-protecting group. The presence of this substituent was significant in the reaction progression, which prevented the chemical reaction between the amino alcohol and the peroxide. However, the reaction rates and final conversions were lower when the amino group was protected.

The deactivation of CPO by peroxides was also examined. Higher stability was observed with hydrogen peroxide than *t*-BuOOH in many reactions. Nevertheless, the substrate species influenced enzyme operational stability: the substrate was found to have a modulatory effect. Therefore, the exact deactivation of CPO should be determined case by case, depending on the substrate.

Furthermore, β-CHO was successfully synthesized by a novel strategy using β-OH as the starting material and CPO as the biocatalyst. Main operational conditions, such as reaction medium and initial substrate concentration, were studied. The Michaelis–Menten kinetics parameters were estimated. A secondary chemical reaction between the formed amino aldehyde and peroxides was identified, and a new reaction scheme was proposed and validated.

Finally, the extent of the target oxidation was determined: high amino alcohol conversion was achieved, but with an amino aldehyde selectivity of only 18%. Hence, further research must focus on driving the oxidation in the desired synthetic direction (preFagomine synthesis), avoiding the mentioned undesirable reaction.

3.5 References

[1] L. J. Whalen, C. H. Wong, Aldrichimica Acta 2006, 39, 63–71.

[2] K. M. Koeller, C.-H. Wong, Glycobiology 2000, 10, 1157–1169.

[3] M. H. Fechter, A. E. Stütz, A. Tauss, Curr. Org. Chem. 1999, 3, 269–285.

[4] L. Espelt, T. Parella, J. Bujons, C. Solans, J. Joglar, A. Delgado, P. Clapés, Chem. Eur. J. 2003, 9, 4887–4899.

[5] M. Sugiyama, Z. Hong, P.-H. Liang, S. M. Dean, L. J. Whalen, W. A. Greenberg, C.-H. Wong, J. Am. Chem. Soc. 2007, 129, 14811–14817.

[6] I. Lundt, R. Madsen, in Iminosugars as Glycosidase Inhib. Nojirimycin Beyond (Ed.: A.E. Stütz), Wiley-VCH, 1999, pp. 93–109.

[7] Q. Li, X. S. Ye, *Isr. J. Chem.* **2015**, *55*, 336–346.

[8] B. Winchester, G. W. J. Fleet, *Glycobiology* **1992**, *2*, 199–210.

[9] P. Sears, C. H. Wong, *Angew. Chemie - Int. Ed.* **1999**, *38*, 2300–2324.

[10] M. Pešić, C. López, G. Álvaro, *Biochem. Eng. J.* **2012**, *67*, 218–224.

[11] M. Pešić, C. López, J. López-Santín, G. Álvaro, *Appl. Microbiol. Biotechnol.* **2013**, *97*, 7173–7183.

[12] S. K. Wright, R. E. Viola, *J. Biol. Chem.* **2001**, *276*, 31151–31155.

[13] T. D. Colby, B. J. Bahnson, J. K. Chin, J. P. Klinman, B. M. Goldstein, *Biochemistry* **1998**, *37*, 9295–9304.

[14] J. L. Jestin, S. Vichier-Guerre, *Res. Microbiol.* **2005**, *156*, 961–966.

[15] W. Chamulitrat, N. Takahashi, R. P. Mason, *J. Biol. Chem.* **1989**, *264*, 7889–7899.

[16] J. A. Castillo, J. Calveras, J. Casas, M. Mitjans, M. P. Vinardell, T. Parella, T. Inoue, G. a. Sprenger, J. Joglar, P. Clapés, *Org. Lett.* **2006**, *8*, 6067–6070.

[17] L. Gómez, E. Molinar-Toribio, M. Á. Calvo-Torras, C. Adelantado, M. E. Juan, J. M. Planas, X. Cañas, C. Lozano, S. Pumarola, P. Clapés, et al., *Br. J. Nutr.* **2012**, *107*, 1739–1746.

[18] H. Nojima, I. Kimura, F. J. Chen, Y. Sugihara, M. Haruno, a Kato, N. Asano, *J. Nat. Prod.* **1998**, *61*, 397–400.

[19] A. Kato, N. Asano, H. Kizu, K. Matsui, A. A. Watson, R. J. Nash, *J. Nat. Prod.* **1997**, *60*, 312–314.

[20] W. A. Loughlin, D. B. Hawkes, *Bioresour. Technol.* **2000**, *71*, 167–172.

[21] M. P. J. van Deurzen, B. W. Groen, F. van Rantwijk, R. A. Sheldon, *Biocatalysis* **1994**, *10*, 247–255.

[22] M. Andersson, B. K. Samra, H. Holmberg, P. Adlercreutz, *Biocatal. Biotransformation* **1999**, *17*, 293–303.

[23] B. K. Samra, M. Andersson, P. Adlercreutz, *Biocatal. Biotransformation* **1999**, *17*, 381–391.

[24] F. Van De Velde, M. Bakker, F. Van Rantwijk, R. A. Sheldon, *Biotechnol. Bioeng.* **2001**, *72*, 523–529.

[25] P. Toti, A. Petri, T. Gambicorti, A. M. Osman, C. Bauer, *Biophys. Chem.* **2005**, *113*, 105–113.

[26] D. R. Morris, L. P. Hager, *J. Biol. Chem.* **1966**, *241*, 1763–1768.

[27] A. Casablancas, M. Cárdenas-Fernández, G. Álvaro, M. D. Benaiges, G. Carminal, C. De Mas, G. González, C. López, J. López-Santín, *Electron. J. Biotechnol.* **2013**, *16*, 1–13.

[28] H. Tumma, N. Nagaraju, K. V. Reddy, *J. Mol. Catal. A Chem.* **2009**, *310*, 121–129.

[29] R. D. Bach, M.-D. Su, H. B. Schlegel, *J. Am. Chem. Soc.* **1994**, *116*, 5379–5391.

[30] M. Mečiarová, M. Mojzesová, R. Šebesta, *Chem. Pap.* **2013**, *67*, 51–58.

[31] G. L. K. Hoh, D. O. Barlow, A. F. Chadwick, D. B. Lake, S. R. Sheeran, *J. Am. Oil Chem. Soc.* **1963**, *40*, 268–271.

[32] A. A. Oswald, D. L. Guertin, *J. Org. Chem.* **1963**, *28*, 651–657.

[33] G. Masdeu, M. Pérez-Trujillo, J. López-Santín, G. Álvaro, *Data Br.* **2016**, *8*, 659–665.

[34] M. B. Arnao, M. Acosta, J. A. del Río, F. García-Cánovas, *Biochim. Biophys. Acta* **1990**, *1038*, 85–89.

[35] G. Álvaro, R. Fernández-Lafuente, R. M. Blanco, J. M. Guisán, *Enzyme Microb. Technol.* **1991**, *13*, 210–214.

[36] L. Casella, S. Poli, M. Gullotti, C. Selvaggini, T. Beringhelli, a Marchesini, *Biochemistry* **1994**, *33*, 6377–6386.

[37] R. D. Libby, N. S. Rotberg, T. Emerson, T. C. White, G. M. Yen, S. H. Friedman, N. S. Sun, R. Goldowski, *J. Biol. Chem.* **1989**, *264*, 15284–15292.

[38] C. W. Jones, in *Appl. Hydrog. Peroxide Deriv.* (Ed.: J.H. Clark), Royal Society Of Chemistry, Cambridge, **1999**, pp. 79–177.

[39] C. N. Satterfield, L. C. Case, *Ind. Eng. Chem.* **1954**, *46*, 998–1001

4 Bottlenecks identification in the coupling of the CPO-catalyzed β-OH oxidation with the FSA-catalyzed aldol addition

4.1 Introduction

For the coupling of the CPO-catalyzed amino alcohol oxidation and the FSA-catalyzed aldol addition of DHA to the formed amino aldehyde, some issues should be analyzed, such as the selection of the oxidation, buffer, pH, and the concentrations of enzymes and substrates.

As shown in previous pages, in contrast to *t*-BuOOH, the environmentally friendly H_2O_2 leads to a higher stability of CPO in reaction, but also to a lower oxidation rate.[1] The peroxide selection is crucial for the oxidation, as there is a compromise between eco-friendship, stability, and reaction rate.

The reaction buffer is also important for the synthesis course.[2] Each enzyme stability has a strict dependence on the pH; thus, in the case of the coupling of reactions, the buffer selection will determine the stability of all the present enzymes. In particular, the operational pH range of CPO for the oxidation of substrates in the absence of a halogen anion is reported to be from pH 4 to 7; below that, it catalyzes halogen-dependent reactions.[3] Contrarily, FSA catalyzes aldol additions at a more basic pH range (from 5.5 to 11).[4] Then, theoretically, there would be a common pH (between 5.5 and 7) in which the target coupled reaction could be performed.

In the case of one-pot synthesis, the coupling of the FSA reaction to the CPO oxidation could reduce the formation of the amino acid towards the synthesis of preFagomine. However, it is necessary to consider the behavior of the by-products from the chemical side reaction aldehyde–peroxide that was described in the previous chapter. Besides, inhibitions could take place from substrates of one enzyme to the other one, or even between substrates of the same enzyme, like the amino alcohol and the aldehyde in the case of CPO.

The inactivation of both enzymes is also an issue to consider. The CPO inactivation caused by the use of peroxides has been observed in previous reactions.[5–7] It should be fully characterized for the reaction coupling, analyzing other possible activity losses. Besides, FSA could also be inactivated by any reagents in the reaction medium. All these possible interactions are examined in the following pages.

4.2 Materials and methods

4.2.1 Materials

Recombinant FSA A129S was produced in *Escherichia coli* BL21 (DE3) from plasmid pET22-fsaA, which was generously supplied by Dr. Clapés from the Biotransformation and Bioactive Molecules Research Group (IQAC-CSIC, Barcelona). 2,4-Dinitrophenylhydrazine phosphoric acid solution (DNPH, 0.2M), α-Glycerophosphate dehydrogenase (GPD)–Triosephosphate isomerase (TPI), F6P and NADH were purchased from Sigma Aldrich. The origin of other important reagents and enzymes is detailed in Chapter 3.

4.2.2 CPO activity

The enzymatic activity of CPO was measured following the activity test detailed in Materials and Methods in Chapter 3.

4.2.3 FSA activity

FSA catalyzes the cleaving of F6P to G3P and DHA. Enzymatic activity was determined by a three-enzyme-catalyzed system according to the literature.[4] TPI converts G3P into DHAP, which is further reduced by GPD using NADH. FSA activity is monitored by the decrease in absorbance due to the conversion of NADH to NAD^+ (ε_{340} = 6.2 mM^{-1} cm^{-1}). The mixture for the enzymatic assay contained 5 mM F6P, 0.1 mM NADH, 50 mM imidazole, 10 U mL^{-1} of GPD-TPI, and 50 µl of the sample with FSA, in a total volume of 1 mL.

Absorbance at 340 nm was measured at 30 °C in a UV-visible Spectrophotometer Cary 50. One activity unit of FSA is defined as the amount of enzyme required for the conversion of 1 µmol of F6P per minute at pH 8.0, 25°C. The standard deviation of the CPO activity test was calculated from measurements performed by duplicate.

4.2.4 FSA production

The protocols for the production and purification of FSA are fully described in the Appendix. After its purification, the measured specific activity of FSA was 15.0 U (mg FSA)$^{-1}$. The specific activity has been fixed at this value for further experiments in the thesis.

4.2.5 HPLC analysis

Concentrations of β-OH and its oxidized products –β-CHO, β-COOH–, *t*-BuOOH, and preFagomine were measured by HPLC analysis in a Dionex UltiMate 3000 with variable wavelength detector. The reversed-phase column CORTECS C18+ 2.7 µm 4.6×150 mm from Waters was employed. Reaction samples were dissolved in MeCN, which deactivates the enzyme and stops the reaction. The analyses were performed by injecting 15 µL of the sample at a flow rate of 0.7 mL min^{-1}, 30 °C. The solvent system consisted of solvent A –0.1% (v/v) TFA in H2O– and solvent B –0.095% (v/v) TFA in MeCN/H2O 4:1 (v/v)–. Samples were eluted using a gradient from 5 to 28.5% B in 0.5 min, and an isocratic elution at 28.5% B over 15 min (λ=254 nm).

The proposed structure of preFagomine was confirmed by HPLC-MS analyses performed by *Servei d'Anàlisi Química, UAB*. Results are shown in the Appendix.

For DHA quantification, sample derivatization was required prior to HPLC analysis. DNPH was employed to add a chromophore group to DHA. To that end, a new protocol was adapted from a published work.[8] 30 µL of DHA (at a concentration of 0–2 mM) were mixed with 30 µL of DNPH 0.2 M, and incubated for 60 min. The reaction was stopped by addition of 180 µL of 3 M sodium acetate (pH 9.0). For HPLC analysis, the derivatized compound was extracted into an organic phase using 240 µL of MeCN. The abovementioned reversed-phase column and solvent system were used, injecting 15 µL of the sample at a flow rate of 0.7 mL min^{-1}, 30 °C. Samples were eluted with an isocratic method at 50% B for 2 min, followed by a gradient from 50 to 65% B over 5 min (λ=260 nm).

Prior calibration with standards of known concentration was used for quantitative analysis of all compounds. The standard deviation was calculated from duplicated measurements from a single sample.

4.2.6 Peroxide selection

Two peroxides (H_2O_2, *t*-BuOOH) were tested in the CPO-catalyzed β-OH oxidation. The reaction was performed for 60 min in 100 mM acetate buffer (pH 5.0), with an initial β-OH concentration of 15 mM, and a single addition of peroxide. 15 or 30 mM H_2O_2 or *t*-BuOOH was used in a final volume of 0.2 mL. All reactions were performed at 25 °C and 1000 rpm of orbital stirring (MultiThermTM), and 1000 U mL^{-1} of CPO was used.

4.2.7 Enzyme stability over pH

Various buffer solutions were prepared in the pH range 5–8 according to their pKa value: 100 mM sodium buffer (pH 5.0, 5.5), 100 mM 2-(*N*-morpholino)ethanesulfonic acid (MES) buffer (pH 6.0, 6.5), and 100 mM 4-(2-hydroxyethyl)-1-piperazineethanesulfonic acid (HEPES) buffer (pH 7.0, 7.5, 8.0).

To determine the pH stability of each enzyme, 2 U mL^{-1} of CPO or FSA was incubated in 1 mL of each buffer for 60 min, at 25 °C and 1000 rpm of orbital stirring. The stability was determined as the relative activity in the final sample in relation to the initial one.

4.2.8 CPO/FSA assays

At pH 5.0 (100 mM acetate buffer), 6.0 (100 mM MES) and 7.0 (100 mM HEPES), both enzymes were incubated together for 60 min to check for any interaction between them, in presence of 30 mM *t*-BuOOH. 5000 U mL^{-1} of CPO and 200 U mL^{-1} of FSA were used in 0.2 mL, at 25 °C and 1000 rpm of orbital stirring. As a control, both enzymes were incubated at the same conditions for 60 min, but without peroxide. Another control was the 60-min incubation of FSA separately in buffer with peroxide (same concentrations).

4.2.9 Preliminary coupling

A coupled one-pot reaction with CPO and FSA was carried out in 0.2 mL of 100 mM MES (pH 6.5), using 1000 U mL^{-1} of CPO and 5 U mL^{-1} of FSA, at 25 °C and 1000 rpm of orbital stirring. The initial substrates concentrations were 48 mM β-OH, 78 mM *t*-BuOOH and 175 mM DHA. Another reaction at the same concentrations, without DHA and FSA, was performed to evaluate their effect in the amino alcohol oxidation. As a control, DHA and *t*-BuOOH were incubated at similar molar ratio (1.0:2.3 of *t*-BuOOH to DHA) in the reaction buffer for 150 min to check for a possible chemical reaction.

4.3 Results and discussion

4.3.1 Peroxide

Prior to the reaction coupling, the peroxide nature was evaluated in the CPO-catalyzed β-OH oxidation in terms of amino alcohol conversion and enzyme stability. The reaction was performed using two different concentrations of the two peroxides (H_2O_2, *t*-BuOOH): equimolar with β-OH (15 mM peroxide), or in 2:1 molar ratio of peroxide to alcohol (30 mM peroxide).

When hydrogen peroxide was added to the reaction medium (in which CPO was already present), a lot of air bubbles were formed. This could be explained by a side reaction already described in the literature: peroxide degradation by CPO catalase activity, leading to oxygen formation.[9] Almost all the oxidant was consumed and, thus, no substrate conversion was observed with H_2O_2, and the enzyme remained completely active (Table 4.1). In the previous chapter, however, some amino alcohol conversion was observed. The main difference was the peroxide addition: if H_2O_2 was added slowly at a semi-continuous rate, some β-OH was converted although at a low reaction rate; if H_2O_2 was added in a single pulse to speed the reaction, its decomposition rate was very high, and no β-OH conversion was observed.

With *t*-BuOOH, CPO did convert β-OH into β-CHO. Results indicate that a two-fold higher peroxide concentration increased the alcohol conversion, but only from 23.0% to 26.9%. This slight increment was probably caused by inactivation of the enzyme by *t*-BuOOH. According to this, *t*-BuOOH was finally selected as the oxidant for the amino alcohol oxidation. For a better performance of the reaction, this enzyme inactivation should be investigated and characterized.

Table 4.1. Substrate conversion and CPO activity after 60 min of 15 mM β-OH oxidation, using H_2O_2 or *t*-BuOOH as peroxide. 1000 U mL^{-1} of CPO was used in 100 mM acetate buffer (pH 5.0).

Peroxide	Peroxide : β-OH (molar ratio)	β-OH conversion (%)	CPO activity (%)
H_2O_2	1:1	<1	>99
	2:1	<1	>99
t-BuOOH	1:1	23.0 ± 0.7	34.7 ± 3.1
	2:1	26.9 ± 0.5	13.5 ± 0.7

4.3.2 pH stability

As mentioned before, the reaction could be performed at pH interval 5.5 to 7, as reported in the literature. To select the proper pH, several buffer solutions were prepared to evaluate the stability of both enzymes over the pH range 5–8.

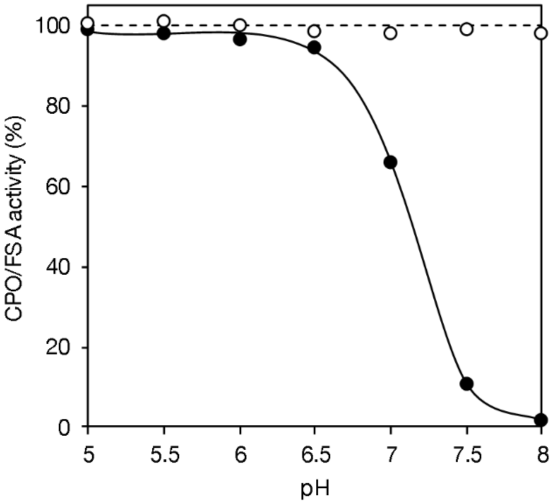

Figure 4.1. pH stability of CPO (●) and FSA (○). 2 U mL^{-1} of CPO or FSA was used in 100 mM sodium buffer (pH 5.0, 5.5), 100 mM MES (pH 6.0, 6.5), and 100 mM HEPES (pH 7.0, 7.5, 8.0). in 1 mL of total volume, for 60 min.

The stability after 60 min is plotted in Figure 4.1. CPO remained >95% stable at pH below 6.5. At higher pH, CPO activity dropped fast, becoming completely inactivated at pH 8.0. Regarding the stability of FSA, it was very stable within all the tested pH range; activity loss was negligible. For further stability experiments, only the pH range 5–7 (pH 5.0, 6.0 and 7.0) was evaluated, since almost no CPO activity was present at pH 7.5–8.0.

4.3.3 Enzymes compatibility

The compatibility of CPO and FSA in the reaction medium was assayed. To this end, both enzymes were incubated together at the three mentioned pH (5.0, 6.0, 7.0), in presence of 30 mM *t*-BuOOH. The peroxide altered the activity of both enzymes (Table 4.2). It has already been discussed the inactivation of CPO by the peroxide in the previous chapter. FSA was also inactivated at the three tested conditions, especially at pH 5.0. The explanation of this FSA inactivation could be some interaction between both enzymes, but it was discarded after both enzymes were incubated together without peroxide at the three pH. In this case, no negative effect on activity was measured and activity loss was only observed for CPO at pH 7.0 (55% remaining activity after 60 min), in accordance with data shown in Figure 4.1.

Another hypothesis could be the effect of peroxide on the enzyme structure. To check this hypothesis, FSA alone was incubated with *t*-BuOOH at the same conditions (30 mM *t*-BuOOH at the three pH). This time, no meaningful inactivation was observed. Therefore, the more plausible explanation would be that the inactivation of FSA is caused by the presence of CPO and the peroxide, likely in a similar mechanism that CPO inactivation by the formation of a peroxyl radical. This inactivation of CPO and peroxide to FSA should be investigated in detail for the correct performance of the system.

Table 4.2. CPO and FSA activities after together incubation with or without peroxide. The last column shows the FSA activity after incubation with peroxide (no CPO). Experiment conditions: 60-min incubation with 0/30 mM *t*-BuOOH at pH 5.0 (100 mM acetate buffer), 6.0 (100 mM MES) and 7.0 (100 mM HEPES).

pH	CPO + FSA + *t*-BuOOH		CPO + FSA		FSA + *t*-BuOOH
	CPO Act. (%)	FSA Act. (%)	CPO Act. (%)	FSA Act. (%)	FSA Act. (%)
5.0	60.7	1.8	>99	>99	98.1
6.0	52.2	16.1	>99	98.4	>99
7.0	12.5	19.7	55.4	>99	98.9

Another phenomenon was observed: FSA precipitated in all experiments at pH 6.0 and below. Thus, although FSA was stable after precipitation, the selected pH for the coupling system was finally set at 6.5 to avoid the undesired presence of non-soluble solids in the medium. Therefore, as primary selection, the reaction medium consists of 100 mM MES (pH 6.5), with the use of *t*-BuOOH as the peroxide for the oxidation.

4.3.4 Coupled reaction

Once the buffer and peroxide have been defined, it is required to test the feasibility of the coupled reaction performed in one-pot. Substrates and enzymes concentrations were defined arbitrarily at the values indicated in Section 4.2.9, as no reference to this system was reported in the literature. According to previous work with these enzymes (data not shown), the employed FSA activity (5 U mL^{-1}) employed in the reaction should have been enough to totally convert the amino aldehyde formed by the CPO-catalyzed oxidation. However, no preFagomine formation was observed, probably by the inactivation of FSA caused by CPO and *t*-BuOOH (no FSA activity was measured after 5 min).

A parallel reaction at the same conditions without DHA and FSA is also presented. It was performed to search for any positive/negative effect of DHA on the β-OH oxidation. The time profiles for the first 30 min of the coupled reaction and the parallel one are presented in Figure 4.2. As it can be seen, with DHA in the medium, the initial β-OH oxidation rate was reduced, and more peroxide was consumed. This could indicate a possible side reaction, the oxidation of DHA catalyzed by CPO using *t*-BuOOH. This reaction is not chemically-catalyzed as no peroxide consumption was observed after 150 min of the incubation of DHA and peroxide in buffer (reaction control), without using CPO. Another evidence of this side reaction could be the difference in the remaining activity of CPO in the medium. The inactivation was slower with DHA, probably due to a protective effect of DHA on the CPO stability, as it was observed for other substrates in Chapter 3.

Another issue to consider in Figure 4.2 is the degradation of *t*-BuOOH catalyzed by CPO. In the non-coupled reaction, around 9.6 mM β-OH was consumed in 30 min. Only 2.4 mM β-COOH was formed (not shown in the graph). As the reaction stoichiometry is mole-to-mole, 12.0 mM *t*-BuOOH should have been consumed for the oxidation of β-OH and β-CHO; however, 33.2 mM was consumed. This could be explained by the degradation of the peroxide catalyzed by CPO.

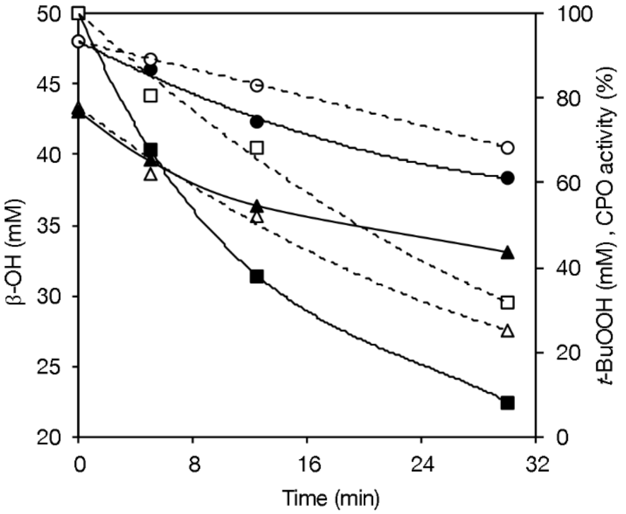

Figure 4.2. Comparison on the β-OH oxidation with or without a coupled FSA-catalyzed DHA addition. Coupled: β-OH (○), *t*-BuOOH (△), CPO activity (□); not coupled: β-OH (●), *t*-BuOOH (▲), CPO activity (■). 1000 U mL^{-1} of CPO and 5 U mL^{-1} of FSA were used in 100 mM MES (pH 6.5).

4.4 Conclusions

This preliminary study on the coupling of the CPO-catalyzed β-OH oxidation and the FSA-catalyzed DHA addition has permitted to select the proper peroxide and buffer for the coupled reaction. It has been proved that, despite its environmentally friendly nature, hydrogen peroxide is not adequate for this system. *t*-BuOOH, instead, allows a higher reaction rate of the amino alcohol oxidation. The coupled reaction can be performed in 100 mM MES buffer (pH 6.5). This medium has shown the best qualities for the coupling: both enzymes remain stable, and it does not cause the precipitation of FSA.

FSA is inactivated by incubation with CPO and *t*-BuOOH. This reaction should be further investigated if both enzymes are used together in a one-pot system. Besides, the coupled reaction has been tested, but no preFagomine has been obtained, probably by the inactivation of FSA. Nevertheless, it has been used to identify various side reactions on the system: the likely oxidation of DHA in presence of *t*-BuOOH and CPO –which competes with FSA for the use of DHA–, and the degradation of *t*-BuOOH catalyzed by CPO.

All these observed phenomena hinder the simultaneous coupling of these two reactions. An exhaustive study of each reaction performed separately could enhance the understanding of the whole reaction mechanism, and eventually permit the reaction coupling. To this end, the development of a mathematical kinetic model is proposed as the work strategy. Concurrently, enzyme immobilization is suggested as an alternative to reduce the inactivation of both enzymes. Both strategies will be further discussed in the following chapters.

4.5 References

[1] G. Masdeu, M. Pérez-Trujillo, J. López-Santín, G. Álvaro, *Process Biochem.* **2016**, *51*, 1204–1211.

[2] H. Bisswanger, *Perspect. Sci.* **2014**, *1*, 41–55.

[3] J. A. Thomas, D. R. Morris, L. P. Hager, *J. Biol. Chem.* **1970**, *245*, 3129–3134.

[4] M. Schürmann, G. A. Sprenger, *J. Biol. Chem.* **2001**, *276*, 11055–11061.

[5] A. N. Shevelkova, A. D. Ryabov, *Biochem Mol Biol Int* **1996**, *39*, 665–670.

[6] M. Ayala, C. V Batista, R. Vazquez-Duhalt, *J. Biol. Inorg. Chem.* **2011**, *16*, 63–68.

[7] J.-B. Park, D. S. Clark, *Biotechnol. Bioeng.* **2006**, *93*, 1190–1195.

[8] V. Ferioli, E. Vezzalini, C. Rustichelli, G. Gamberini, *Chromatographia* **1995**, *41*, 61–65.

[9] W. Sun, T. A. Kadima, B. Dunford, *Biochem. Cell Biol.* **1994**, *72*, 321–31.

5 Kinetic model for the CPO/FSA-catalyzed β-OH oxidation and DHA aldol addition

5.1 Introduction

5.1.1 Enzyme kinetics

Enzymes are biocatalysts that enhance rates of natural or non-natural reactions.[1] Their kinetics refers to the quantitative analysis of all factors that determine the catalytic potential of an enzyme.[2] A kinetic description of their activity is usually required to design and evaluate the reactor performance for its process application. Consider an enzyme (E) that catalyzes the biotransformation from a substrate (S) to a product (P). An enzyme–substrate complex (ES) is formed, and it can be dissociated into S and E, or P, through the following pathway:[3]

$$E + S \underset{k_{-1}}{\overset{k_1}{\rightleftharpoons}} ES \underset{k_{-2}}{\overset{k_2}{\rightleftharpoons}} P$$

Assuming that almost none of the product reverts to the initial substrate (k_{-2} is negligible), this mechanism is generally simplified to:

$$E + S \underset{k_{-1}}{\overset{k_1}{\rightleftharpoons}} ES \xrightarrow{k_2} P$$

The enzyme-catalyzed transformation rate of S to P (r) could be expressed as a constant term (k_2 or k_{cat}) multiplied by the concentration of ES (Equation 5.1). The initial concentration of enzyme (E_0) is equal to the total uncombined enzyme (E) and ES (Equation 5.2). Typically for many enzymes, this pathway can be described by the Michaelis-Menten kinetics, first reported in 1913.[4,5] Under the steady-state assumption, the Michaelis-Menten (K_M) constant is defined in Equation 5.3.

$$r = \frac{dP}{dt} = k_{cat} \cdot ES \tag{5.1}$$

$$E_0 = E + ES \tag{5.2}$$

$$K_M = \frac{k_{-1} + k_2}{k_1} \tag{5.3}$$

The principal equation for a one-substrate enzyme is indicated in Equation 5.4, where

r_{max} is the maximum value of r. At low [S], it can be simplified to a first-order reaction in which the rate is directly proportional to [S] (Figure 5.1); at high [S], it is a zero-order reaction in which r_{max} is expected, since the catalytic sites on the enzyme are saturated with substrate (E_0 = ES), leading to Equations 5.5 and 5.6. K_M corresponds to [S] at which r = 0.5 r_{max}; hence it is a measure of binding affinity of the substrate to the enzyme. A low K_M value corresponds to tight binding between E and S.

$$r = \frac{r_{max} \cdot [S]}{K_M + [S]} \tag{5.4}$$

$$r_{max} = k_{cat} \cdot E_0 \tag{5.5}$$

$$r = \frac{k_{cat} \cdot E_0 \cdot [S]}{K_M + [S]} \tag{5.6}$$

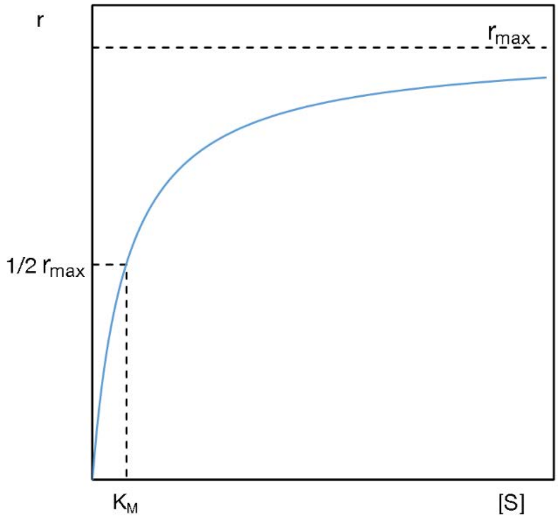

Figure 5.1. The Michaelis-Menten relation between the substrate concentration and the reaction rate.

Most enzymatic reactions of industrial relevance are altered by substrate and/or product inhibition.[6] Thus, the mathematical description of the inhibition kinetics is crucial. By definition, an inhibitor (I) is a modulator substance that reversibly interacts with the enzyme, and slowdowns its reaction rate.

Inhibition mechanisms are classified into three categories according to their interaction with the enzyme (Figure 5.2).[2,3] In *competitive inhibition*, both S and I resemble in structure so that they compete for the binding at the enzyme active site. Although partial inhibition might occur in a few cases, generally this inhibition excludes simultaneous binding of S and I. This inhibition increases the apparent K_M constant, but it does not affect the r_{max} value, as the modulatory effect can be reduced by raising the substrate concentration (Figure 5.3). Equation 5.7 indicates how the reaction rate is affected by the inhibition constant (k_I).

In the *non-competitive* type, S and I structures are unlikely to be similar. They do not compete for the active site, both compounds can be attached to the enzyme simultaneously. Therefore, an increase in [S] does not reduce the inhibition. Unchanged K_M and lower apparent r_{max} are expected, as expressed in Equation 5.8.

Mixed-type inhibition shows competitive and non-competitive behaviors. S and I can be attached to the enzyme simultaneously in two different sites, in a dependent way. This is, the affinity of binding S or I affects the binding of the other. A particular case of mixed inhibition is *uncompetitive inhibition*, in which there is no preformed site for binding the inhibitor. The inhibitor only binds to the enzyme after the attachment of S. In this case, both apparent K_M and r_{max} are reduced (Equation 5.9).

$$r = \frac{k_{cat} \cdot E_0 \cdot [S]}{K_M \cdot \left(1 + \frac{I}{k_I}\right) + [S]} \tag{5.7}$$

$$r = \frac{k_{cat} \cdot E_0 \cdot [S]}{K_M + [S] \cdot \left(1 + \frac{I}{k_I}\right)} \tag{5.8}$$

$$r = \frac{k_{cat} \cdot E_0 \cdot [S]}{(K_M + [S]) \cdot \left(1 + \frac{I}{k_I}\right)} \tag{5.9}$$

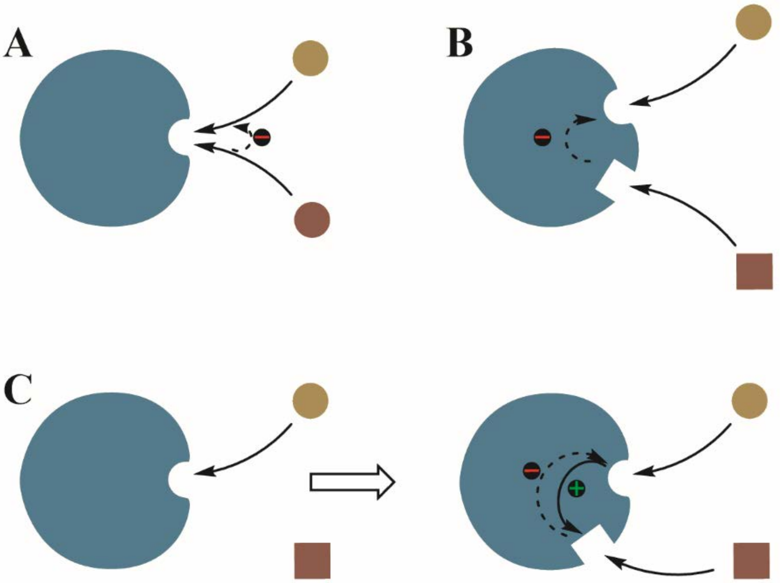

Figure 5.2. Types of enzyme inhibition: competitive (**A**), non-competitive (**B**), uncompetitive (**C**). Enzyme ●; substrate ●; inhibitor ●, ■ .

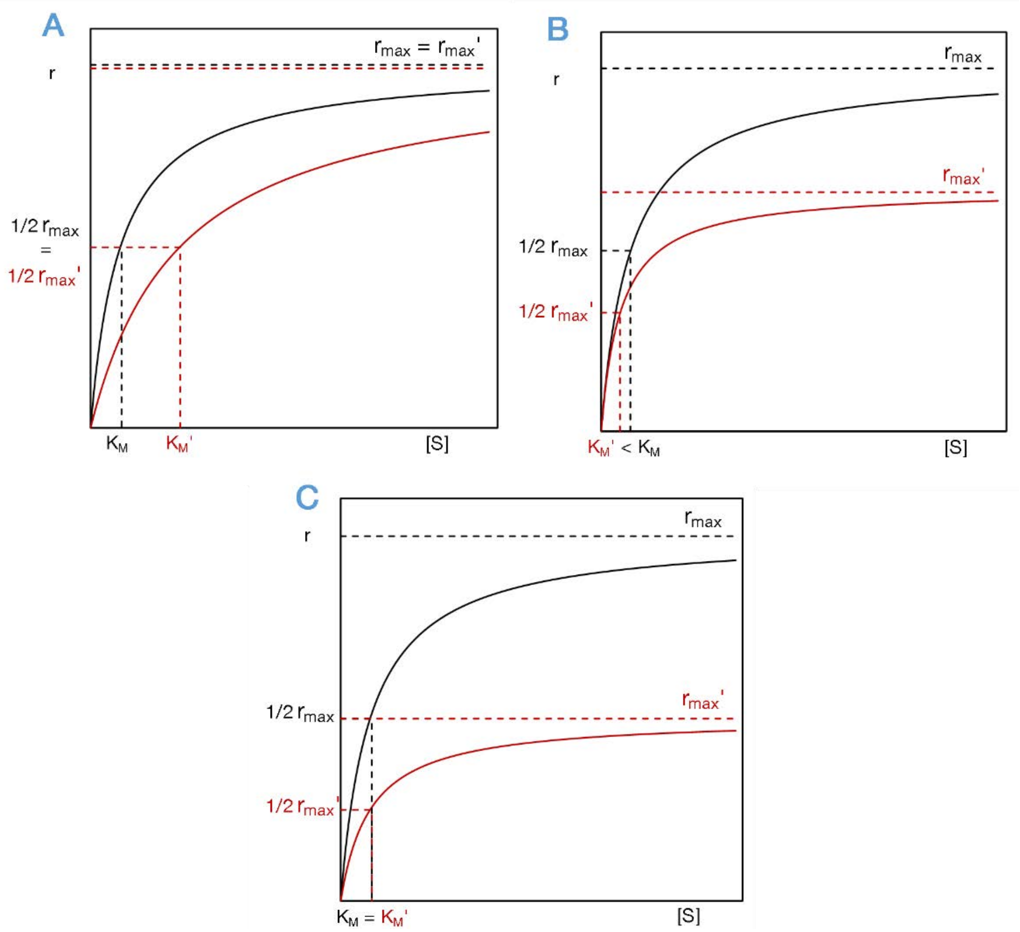

Figure 5.3. Variation of K_M and r_{max} depending on the inhibition: competitive (**A**), non-competitive (**B**), uncompetitive (**C**). A non-inhibited reaction is plotted in black; the inhibited, in red.

5.1.2 *Two-substrate kinetics*

Complex molecules are usually produced in reactions involving more than one substrate.[7] The selected enzymes for this project work (CPO and FSA) catalyze a two-substrate reaction. CPO oxidizes the amino alcohol in presence of *t*-BuOOH, and FSA performs the DHA aldol addition to the amino aldehyde to render preFagomine.

Reaction mechanisms of a two-substrate reaction can be divided into two main categories.[8,9] In *sequential* mechanisms, the two substrates must combine with the enzyme before the reaction can take place. Their interaction with the enzyme can be ordered or random. In *ping-pong* mechanisms, before all substrates can react with the enzyme, one or more products must be released modifying the enzyme to E'. These three pathways are schematically described in Figure 5.4, where an irreversible bi-bi two-substrate reaction is considered –two substrates (A, B), two products (P, Q)–. A simple mathematical description has been adapted from the literature.[2,10] Equations 5.10–5.12 detail the three mechanisms: ordered sequential, random sequential and ping-pong, respectively.

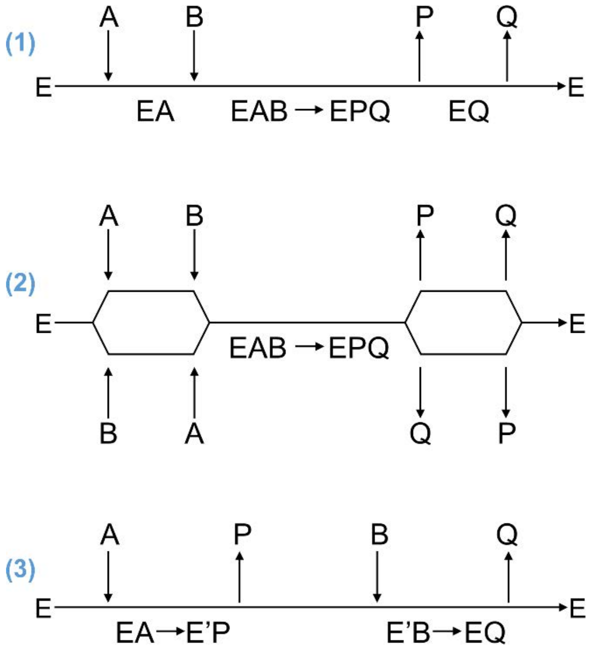

Figure 5.4. Characteristic mechanism from each inhibition type: ordered sequential (**1**), random sequential (**2**), ping-pong (**3**). Substrates: A, B; products: P, Q; enzyme: E; modified enzyme: E'.

$$r = \frac{k_{cat} \cdot E_0 \cdot [A] \cdot [B]}{[A] \cdot [B] + K_{M,B} \cdot [A] + K_{M,A} \cdot K_{M,B}} \tag{5.10}$$

$$r = \frac{k_{cat} \cdot E_0 \cdot [A] \cdot [B]}{[A] \cdot [B] + K_{M,B} \cdot [A] + K_{M,A} \cdot [B] + K_{M,A} \cdot K_{M,B}} \tag{5.11}$$

$$r = \frac{k_{cat} \cdot E_0 \cdot [A] \cdot [B]}{[A] \cdot [B] + K_{M,B} \cdot [A] + K_{M,A} \cdot [B]} \tag{5.12}$$

5.1.3 Parameter estimation

Several methods are described in the literature to estimate the kinetic parameters of a model. Most of them are based on measurements of the initial reaction rate varying substrate concentrations. Linear transformations of data and linear regression have been the most used methods for parameter estimation for years, as it does not require the help of computational tools.[11] K_M and r_{max} can be easily determined with the Lineweaver-Burk linearization, plotting 1/r over 1/[S] (Equation 5.13).[12] This method has several benefits: (a) the substrate concentration remains almost unaltered, as the initial rate should be calculated before much substrate is converted (i.e. less than 10%); (b) no modulatory effect from the product (low concentration) can affect the initial rate; (c) the enzyme activity loss should be negligible. However, since the inverses are used, the experimental error gets magnified.

$$\frac{1}{r} = \frac{1}{r_{max}} + \frac{K_M}{r_{max}} \cdot \frac{1}{[S]} \tag{5.13}$$

As an alternative, parameters can be already estimated from the progress curve analysis of an enzymatic reaction.[13] Its use has increased in the recent years due to computational resources.[14,15] Contrarily to the initial rate estimations, the entire time course is used. This means more data is obtained from the experiments, so that fewer experimental assays could be necessary to estimate all parameters. For instance, the effect of product concentration is analyzed in the same experiment. Nevertheless, in a complex system (e.g. multiple inhibitions), the difficulty to study single parameters could impede a correct parameter determination. An initial rate analysis could be helpful in that case to separately determine kinetic parameters or its initial value for time profiles fitting. In both methodologies, the experimental design is essential for an efficient estimation of kinetic parameters.

5.1.4 Application of a kinetic model

Through the kinetic investigation of a process, a mathematical model can be constructed. With the use of a model, alternative routes and changes to an existing process can be explored *in silico*, before experimentation.[16] Thus, models can speed up bioprocess development and control strategies design. The optimal operating strategy of a complex system can be approximated in order to maximize the reaction rates and product yield, minimizing the formation of side products.

Models can be classified by many criteria: mathematical structure (deterministic, empirical), temporal resolution (steady-state, dynamic), complexity (simple, complex), scope (catalyst, reaction, reactor, process), application purpose (design, analysis, control, optimization), among others.[17]

5.1.5 CPO/FSA reaction

There are many examples of reactions catalyzed by CPO in the literature that exhibit an undeniable ping-pong mechanism.[18–20] The reaction pathway of this enzyme was already schemed in Figure 1.15. The peroxide acts as the first substrate (A), activating the enzyme (E) to E' with the release of a reduced peroxide form (P). Then the substrate B (β-OH in the particular case) reacts with the activated enzyme to form the target product Q (β-CHO).

FSA is a class I aldolase and, therefore, the conserved active lysine in the enzyme active site forms a Schiff base intermediate with DHA (substrate A), which attacks the carbonyl carbon of substrate B (β-CHO).[21] This can be described as an ordered sequential mechanism.

Along this chapter, all the identified reactions in the previous chapter are further investigated and characterized in order to develop an efficient kinetic model that describes the whole system. Each reaction is studied separately (if applicable) to minimize interactions with other reagents.

5.2 Materials and methods

5.2.1 Materials

All the reagents used in this chapter have been already presented in previous chapters.

5.2.2 CPO/FSA activity

The enzymatic activities of CPO and FSA were measured following the activity test detailed in Materials and Methods in Chapter 3 and Chapter 4, respectively.

5.2.3 HPLC analysis

Concentrations of β-OH, β-CHO, β-COOH, *t*-BuOOH, DHA, and preFagomine were measured by HPLC analysis according to the protocol described in Chapter 4. 1,1,3-trihydroxypropan-2-one ($_{ox}$DHA) structure was confirmed by MS analyses performed by *Servei d'Anàlisi Química, UAB* (Appendix).

5.2.4 Model experiments

All reactions were performed in 100 mM MES buffer (pH 6.5) at 25 °C, 1000 rpm of orbital stirring, in 0.5 mL of total volume. Withdrawn volume was always kept below 10% vol. Substrates and enzymes concentrations are specified in the corresponding text, figures or tables in *Results and discussion.*

5.2.5 Model calculations

All simulations and estimations using progress curve analysis have been performed using PSE gPROMS® Model Builder 5.0.0, which allows the simultaneous estimation of multiple parameters from multiple experiments. MicroMath® Scientist® 2.0 was exclusively used for initial reaction rate analysis.

5.3 Results and discussion

The proposed reaction pathway of the enzymatic system CPO/FSA in the synthesis of preFagomine is detailed in Figure 5.5, as a result of the preliminary coupling study in the previous chapter. The reaction rates (**r**) are named according to the corresponding reaction (**R**). r_1 is the reaction rate of $\mathbf{R_1}$, which is CPO-catalyzed oxidation of β-OH to β-CHO, which can be further oxidized to β-COOH by the same enzyme and peroxide ($\mathbf{R_2}$). $\mathbf{R_3}$ represents the chemical reaction aldehyde-peroxide that has been previously identified in Chapter 1. The product of this reaction is a hydroxy alkyl peroxide (HAP). $\mathbf{R_4}$ is the degradation of *t*-BuOOH by CPO to render *tert*-butyl alcohol (*t*-BuOH) and a radical (*t*-BuOO$^{\cdot}$). $\mathbf{R_5}$ states for the likely oxidation of DHA catalyzed by CPO leading to $_{ox}$DHA. Its structure has been identified by MS measurements (Appendix). $\mathbf{R_6}$ and $\mathbf{R_7}$ are the aldol and retroaldol additions by FSA, respectively.

The inactivations of both enzymes are also depicted in the same figure. $\mathbf{kd_{CPO}}$ is the first-order inactivation rate constant of CPO in presence of *t*-BuOOH; $\mathbf{kd_{FSA1}}$ is the first-order inactivation rate constant of FSA caused by CPO and peroxide; $\mathbf{kd_{FSA2}}$ was not identified in the previous chapter, but when incubating FSA with CPO, *t*-BuOOH, and DHA this inactivation was observed.

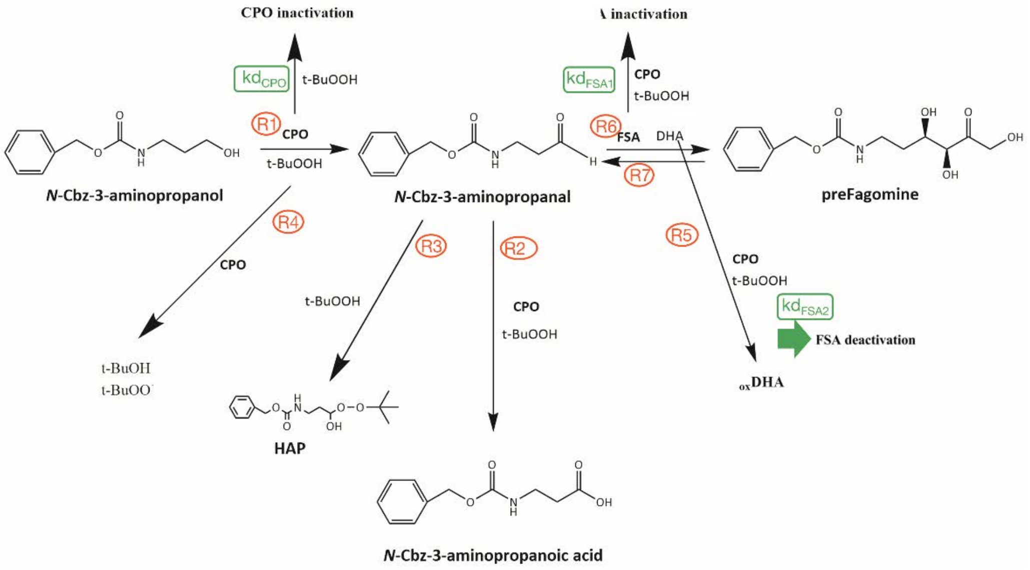
CPO inactivation
kdCPO
t-BuOOH
R1
CPO
t-BuOOH
N-Cbz-3-aminopropanol
N-Cbz-3-aminopropanal
inactivation
kdFSA1
CPO
t-BuOOH
R6
FSA
DHA
R7
preFagomine
R4
CPO
t-BuOH
t-BuOO
R3
t-BuOOH
HAP
R2
CPO
t-BuOOH
N-Cbz-3-aminopropanoic acid
R5
CPO
t-BuOOH
kdFSA2
FSA deactivation
oxDHA

Figure 5.5. Reaction pathway in the CPO/FSA-catalyzed synthesis of preFagomine.

In order to develop a mathematical model of the overall system, if applicable, each reaction and inactivation rate is studied individually in order to reduce the disturbing effects of the other reactions, such as substrate or product inhibitions. A model for each enzyme can be firstly developed separately. Thus, the steps followed to build the CPO model are: (**1**) inactivation of CPO (kd_{CPO}) should be determined by incubation of CPO and *t*-BuOOH. In this case, r_4 is also taking place in the system. (**2**) The chemical reaction between *t*-BuOOH and β-CHO (r_3) that renders the hydroxy alkyl peroxide (HAP) can be investigated. (**3**) The oxidation of β-CHO can be then described, as kd_{CPO}, r_4 and r_3 would be already determined. (**4**) After estimating all the parameters of the previous reactions, the oxidation of β-OH can be analyzed. With these 4 steps, the CPO model can be developed. Regarding the FSA model, it only includes two reactions: r_6 and r_7, which cannot be separated. However, when mixing the two parts of the system (CPO and FSA reactions), other reactions should be investigated: the non-desired oxidation of DHA by CPO, and the inactivation of FSA (kd_{FSA}) caused by the products from r_4 and r_5. With this, the model should be completed.

The experimental distribution of each set of experiments is indicated in each case. The criteria to select this distribution has been the variation on the concentration of substrates/enzymes of the corresponding reaction.

The stoichiometry and mass balances from all reactions are written in Equations 5.14–5.32. The stoichiometry of R_4 is based on the literature.[22] The units of each parameter are compiled in the nomenclature section at the first pages of this work.

Stoichiometry

$$R_1:\ \beta\text{-OH} + t\text{-BuOOH} \xrightarrow[\text{CPO}]{} \beta\text{-CHO} + t\text{-BuOH} \tag{5.14}$$

$$R_2:\ \beta\text{-CHO} + t\text{-BuOOH} \xrightarrow[\text{CPO}]{} \beta\text{-COOH} + t\text{-BuOH} \tag{5.15}$$

$$R_3:\ \beta\text{-CHO} + t\text{-BuOOH} \rightarrow \text{HAP} \tag{5.16}$$

$$R_4:\ 3\ t\text{-BuOOH} \xrightarrow[\text{CPO}]{} t\text{-BuOH} + 2\ t\text{-BuOO}^{\cdot} \tag{5.17}$$

$$R_5:\ \text{DHA} + t\text{-BuOOH} \xrightarrow[\text{CPO}]{} \text{oxDHA} + t\text{-BuOH} \tag{5.18}$$

$$R_6:\ \text{DHA} + \beta\text{-CHO} \xrightarrow[\text{FSA}]{} \text{preFagomine} \tag{5.19}$$

$$R_7:\ \text{preFagomine} \xrightarrow[\text{FSA}]{} \text{DHA} + \beta\text{-CHO} \tag{5.20}$$

Mass balances

$$\frac{d[\beta\text{-OH}]}{dt} = -\ r_1 \tag{5.21}$$

$$\frac{d[\beta\text{-CHO}]}{dt} = r_1 - r_2 - r_3 - r_6 + r_7 \tag{5.22}$$

$$\frac{d[\beta\text{-COOH}]}{dt} = r_2 \tag{5.23}$$

$$\frac{d[\text{HAP}]}{dt} = r_3 \tag{5.24}$$

$$\frac{d[t\text{-BuOOH}]}{dt} = -\ r_1 - r_2 - r_3 - 3 \cdot r_4 - r_5 \tag{5.25}$$

$$\frac{d[t\text{-BuOH}]}{dt} = r_1 + r_2 + r_4 + r_5 \tag{5.26}$$

$$\frac{d[t\text{-BuOO}^{\cdot}]}{dt} = 2 \cdot r_4 \tag{5.27}$$

$$\frac{d[\text{DHA}]}{dt} = -\ r_5 - r_6 + r_7 \tag{5.28}$$

$$\frac{d[\text{oxDHA}]}{dt} = r_5 \tag{5.29}$$

$$\frac{d[\text{preFagomine}]}{dt} = r_6 - r_7 \tag{5.30}$$

Enzyme inactivation

$$\frac{d(\text{CPO activity})}{dt} = kd_{\text{CPO}} \cdot \text{CPO activity} \tag{5.31}$$

$$\frac{d(\text{FSA activity})}{dt} = (kd_{FSA1} + kd_{FSA2}) \cdot \text{FSA activity} \tag{5.32}$$

5.3.1 CPO-catalyzed t-BuOOH degradation and enzyme inactivation

With the incubation of *t*-BuOOH and CPO, r_4 and kd_{CPO} can be determined. In this case, a study of initial reaction rates was not easy to perform due to the inactivation of CPO. For that, a progress curve analysis was carried out from many trials following the experimental distribution from Figure 5.6. Each reaction was analyzed in terms of peroxide concentration and CPO activity along time. Results showed a perceptible sigmoidal behavior in r_4 (data not shown). Therefore, the measured values (Figure 5.7) were fitted to the proposed mathematical expression written in Equations 5.33 and 5.34, where Y_{CPO} corresponds to the CPO concentration.

The inactivation of CPO has been expressed as a function of the degradation of *t*-BuOOH, since the possible cause of its inactivation is the formed peroxyl radical, *t*-BuOO$^{\cdot}$.[22,23] As a radical, this compound is not stable and it is supposed to be degraded in a few seconds. Therefore, its concentration can be considered negligible. Hence, in Equation 5.34 kd_{CPO} has been related to r_4. According to the mass balance (Equation 5.27), $2 \cdot r_4$ can be understood as the instant concentration of the radical before its degradation. From all these experiments, the five unknown parameters from Equations 5.33 and 5.34 were estimated (Table 5.1).

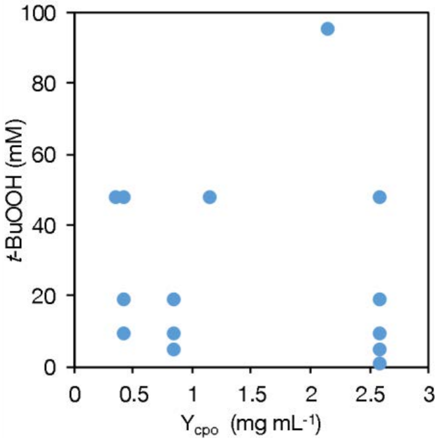

Figure 5.6. Experimental distribution of the incubations of *t*-BuOOH and CPO for the study of r_4 and kd_{CPO}.

$$r_4 = \frac{k_{cat4} \cdot Y_{CPO} \cdot e^{-kd_{CPO} \cdot t} \cdot [t\text{-BuOOH}]^n}{k_4^{\,n} + [t\text{-BuOOH}]^n} \tag{5.33}$$

$$\mathrm{kd_{CPO}} = \frac{k_a \cdot 2 \cdot r_4}{a + 2 \cdot r_4} \qquad (5.34)$$

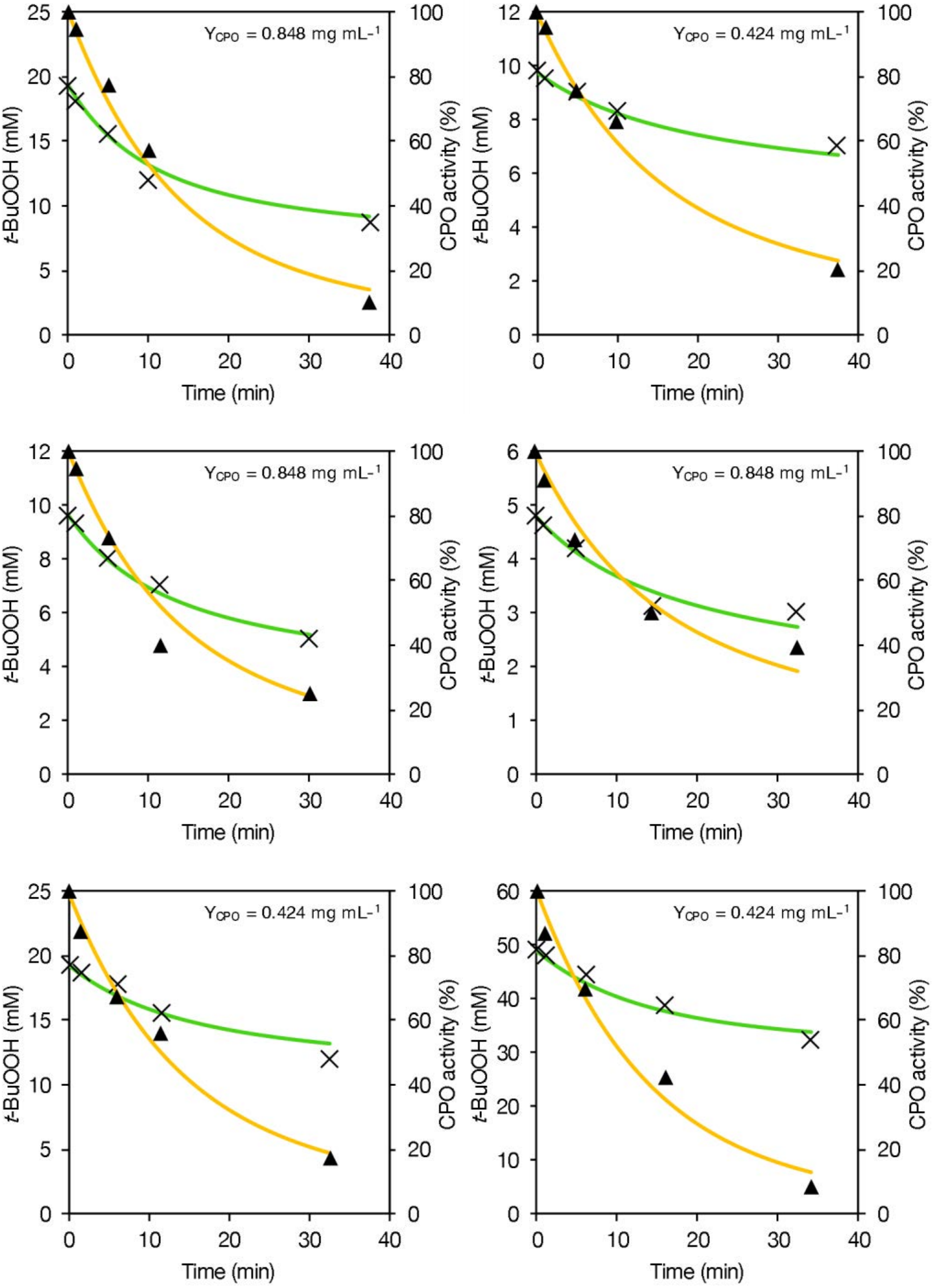

(It continues on the following page)

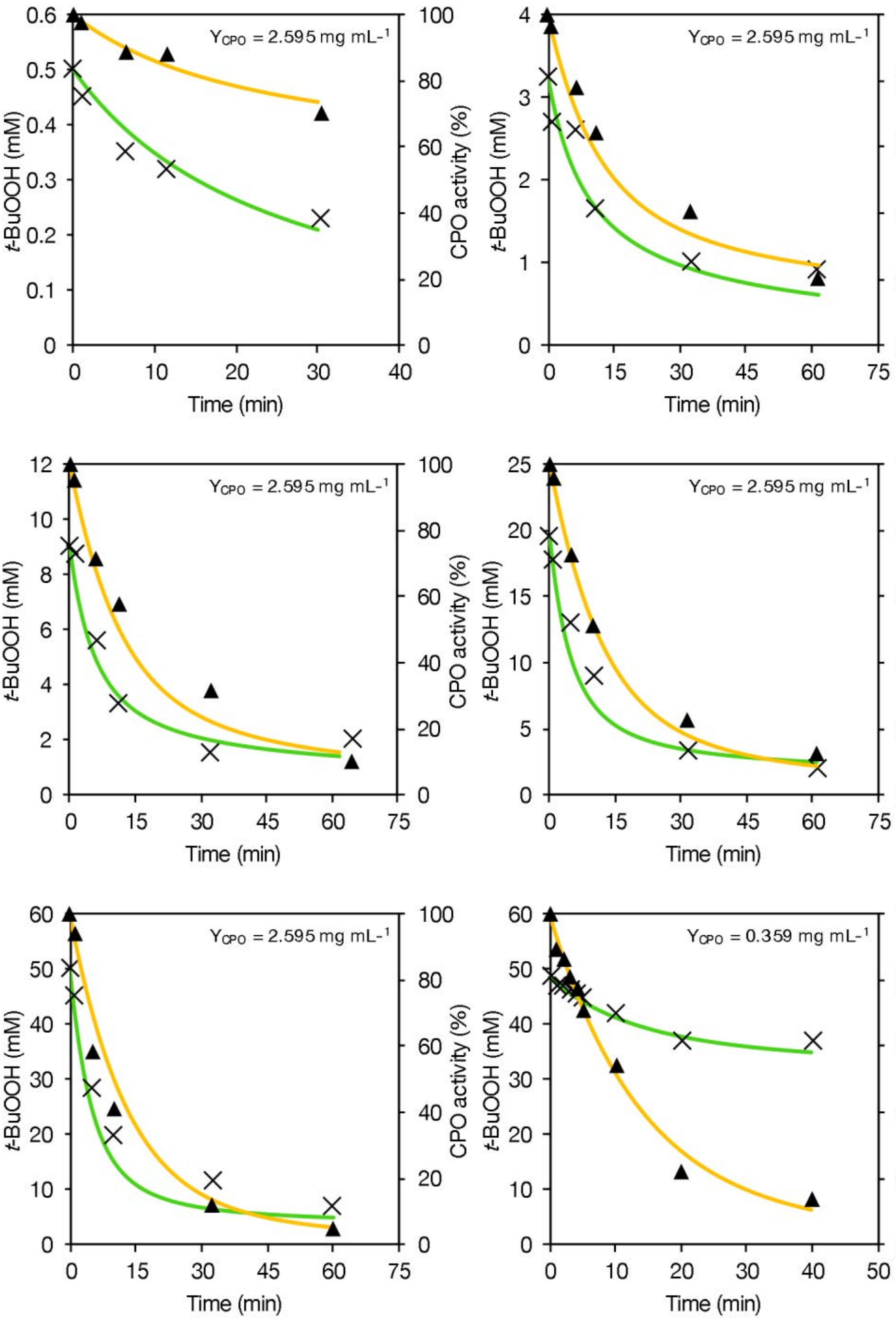

(It continues on the following page)

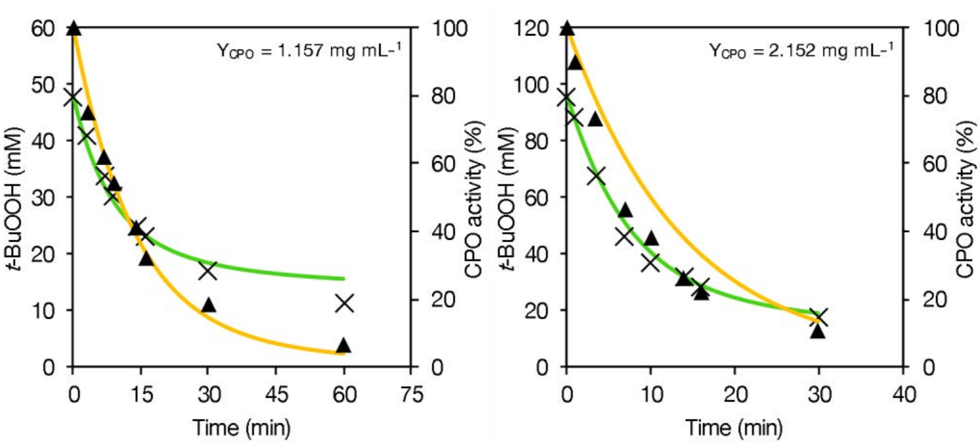

Figure 5.7. Degradation of *t*-BuOOH catalyzed by CPO, and CPO inactivation caused by *t*-BuOO·. The amount of CPO used in each reaction is detailed in each graph. All reactions were performed in 100 mM MES pH 6.5, 25 ºC. Experimental data: *t*-BuOOH (×), CPO activity (▲); model simulation: *t*-BuOOH (🟩), CPO activity (🟨).

Table 5.1. Estimated values of the parameters from Equations 5.33 and 5.34. 95% conf. intervals are given.

Parameter	Value	Units
k_{cat4}	2.068 ± 0.095	$\mu mol \cdot min^{-1} \cdot mgCPO^{-1}$
k_4	51.54 ± 3.40	mM
n	1.433 ± 0.018	-
k_a	$7.038 \cdot 10^{-2} \pm 0.172 \cdot 10^{-2}$	min^{-1}
a	$3.656 \cdot 10^{-2} \pm 0.409 \cdot 10^{-2}$	$mM \cdot min^{-1}$

Regarding inhibitions affecting r_4 or modulations over kd_{CPO}, it was not checked with β-OH, β-CHO or DHA, as they are substrates of the same enzyme and consequently another reaction (r_1, r_2, r_5) could interfere with the result. Inhibition/modulation was evaluated with various concentrations of β-COOH and preFagomine. No effect was observed as shown in Figure 5.8 (no additional term was needed in the model equations).

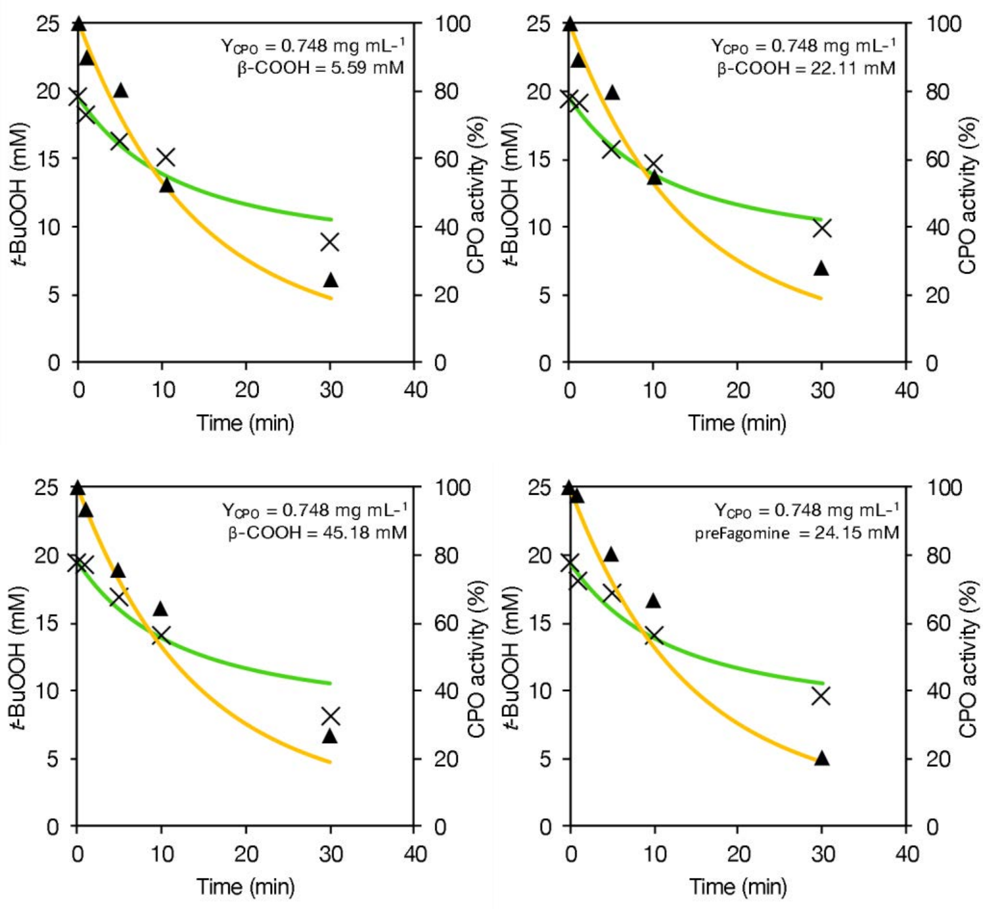

Figure 5.8. Evaluation of β-COOH and preFagomine as inhibitors in the degradation of *t*-BuOOH catalyzed by CPO, and CPO inactivation caused by *t*-BuOO$^{\cdot}$. The amount of CPO and inhibitor used in each reaction is detailed in each graph. All reactions were performed in 100 mM MES pH 6.5, 25 ºC. Experimental data: *t*-BuOOH (×), CPO activity (▲); model simulation: *t*-BuOOH (➡), CPO activity (➡).

5.3.2 Chemical reaction aldehyde-peroxide

To describe the chemical aldehyde-peroxide reaction rate, various concentrations of both compounds were mixed and left for incubation, according to the experimental distribution from Figure 5.9. Each reaction was analyzed in terms of concentrations of β-CHO and *t*-BuOOH along time. Experimental data from Figure 5.10 showed a typical equilibrium behavior from a reversible reaction. With this, the reaction equation was formulated as indicated in Equation 5.35, and the parameters were estimated accordingly (Table 5.2).

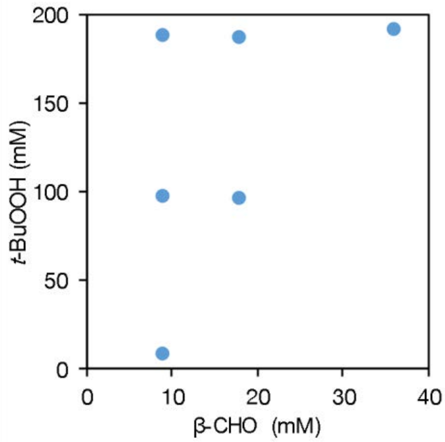

Figure 5.9. Experimental distribution of the incubations of β-CHO and *t*-BuOOH for the study of r_3.

$$r_3 = k_{3i} \cdot [\beta\text{-CHO}] \cdot [t\text{-BuOOH}] - k_{3ii} \cdot [\text{HAP}] \tag{5.35}$$

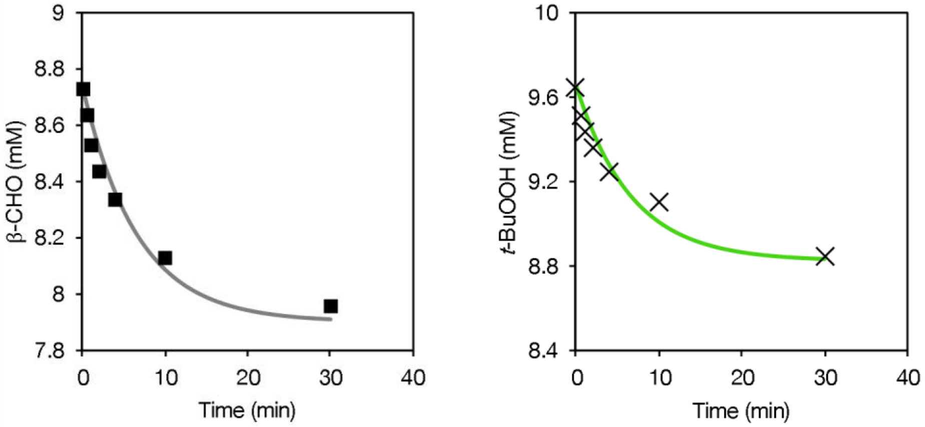

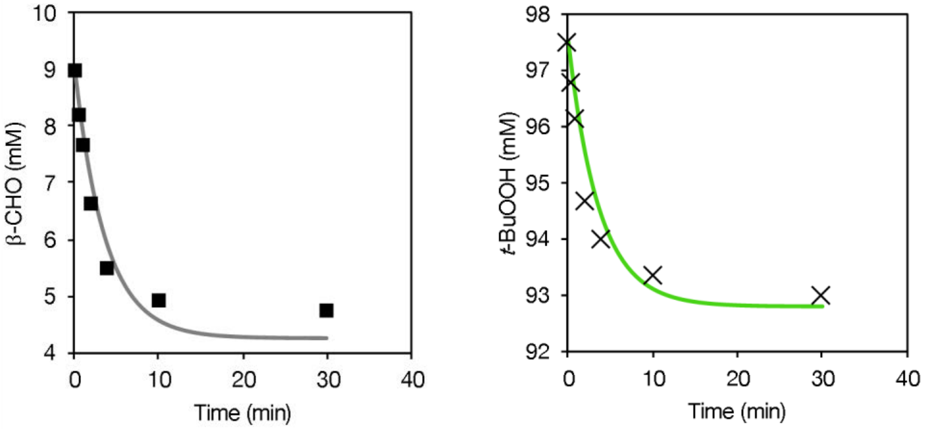

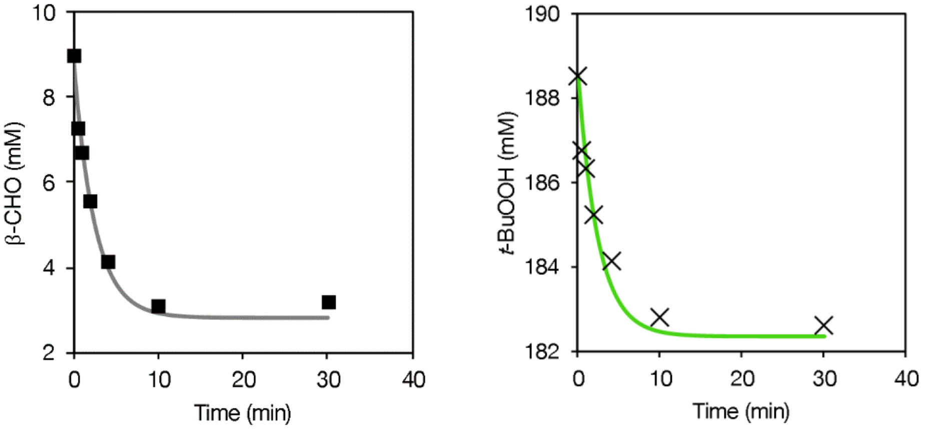

(It continues on the following page)

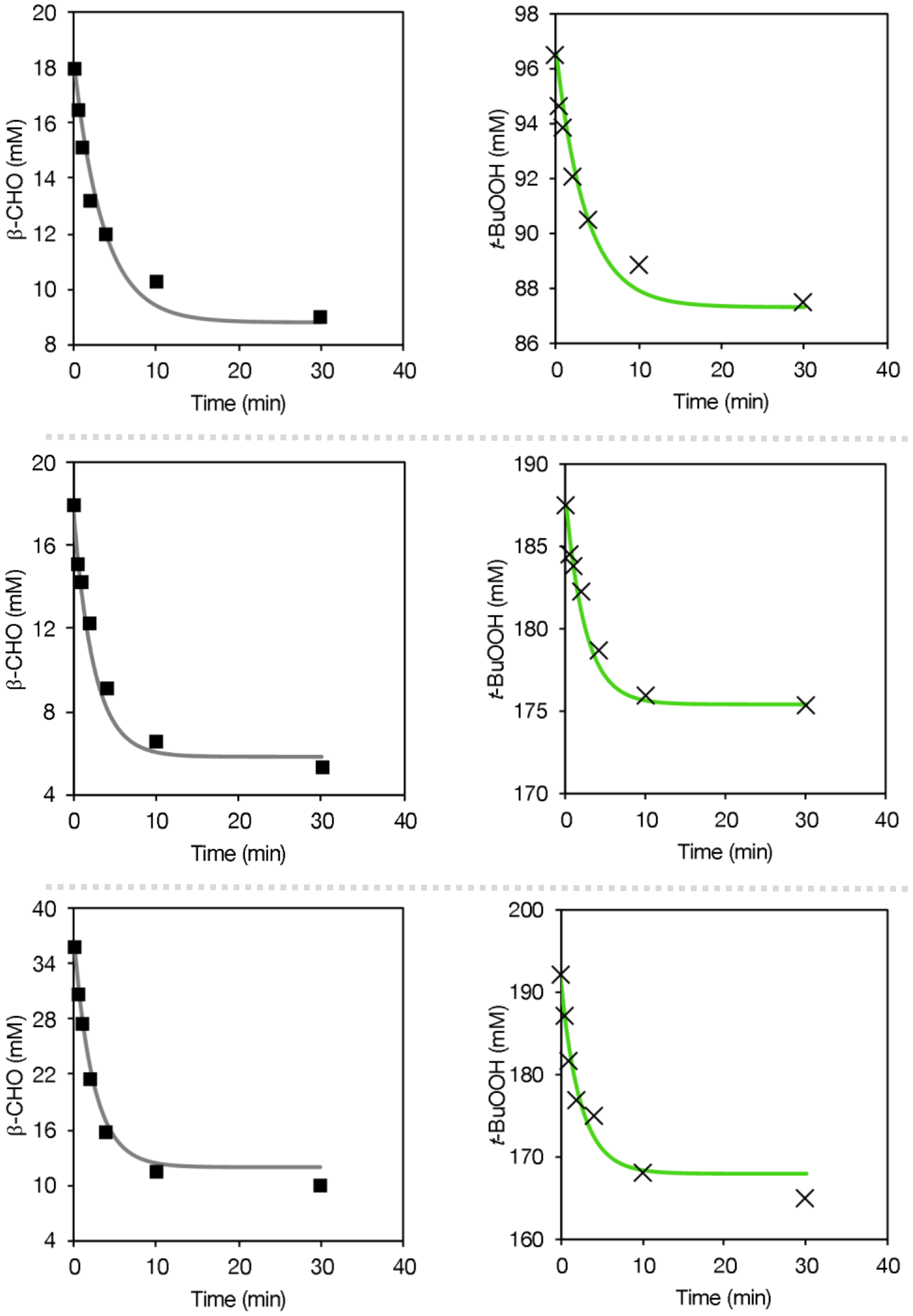

Figure 5.10. Chemical reaction between β-CHO and *t*-BuOOH. All reactions were performed in 100 mM MES pH 6.5, 25 ºC. The dotted line separates individual experiments. Experimental data: β-CHO (■), *t*-BuOOH (×); model simulation: β-CHO (➡), *t*-BuOOH (➡).

Table 5.2. Estimated values of the parameters from Equation 5.35. 95% conf. intervals are given.

Parameter	Value	Units
k_{3i}	$1.489{\cdot}10^{-3} \pm 4.8{\cdot}10^{-5}$	$mM^{-1}\ min^{-1}$
k_{3ii}	$1.248{\cdot}10^{-1} \pm 5.6{\cdot}10^{-3}$	min^{-1}

Several compounds were tested for inhibition of this reaction: β-OH, β-COOH, *t*-BuOH, DHA, preFagomine. As plotted in Figure 5.11, no inhibition was observed in any case, except for β-COOH. An inhibition term (ki_{r3}) was added to Equation 5.35 leading to Equation 5.36. With this new term, the model simulation fitted the experimental data in Figure 5.12, with the parameter estimation detailed in Table 5.3.

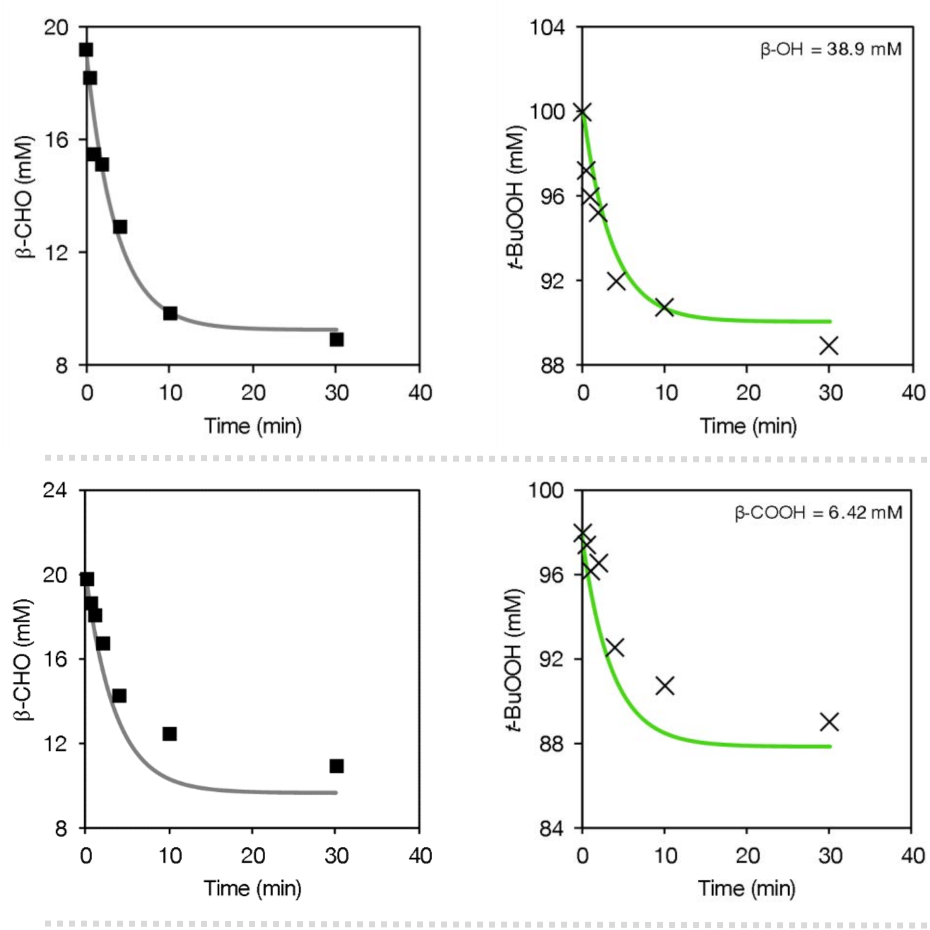

(It continues on the following page)

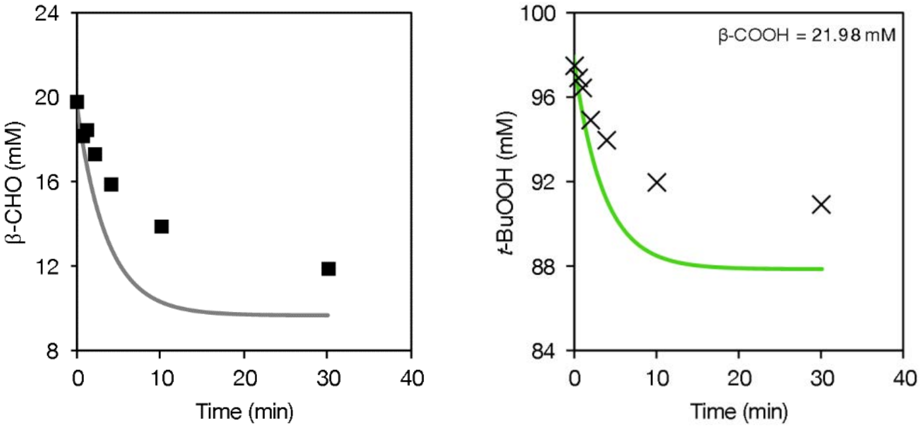

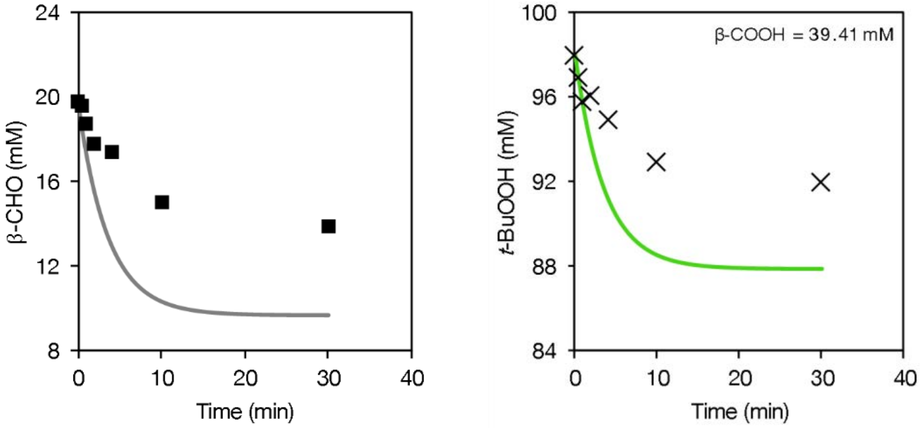

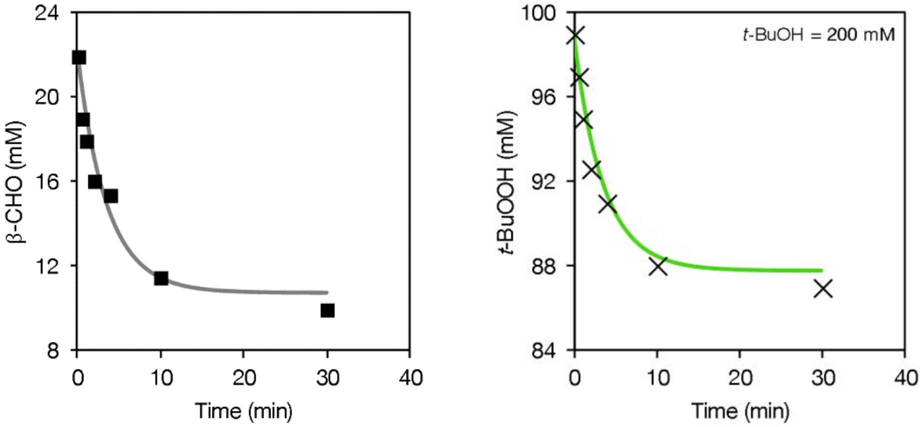

(It continues on the following page)

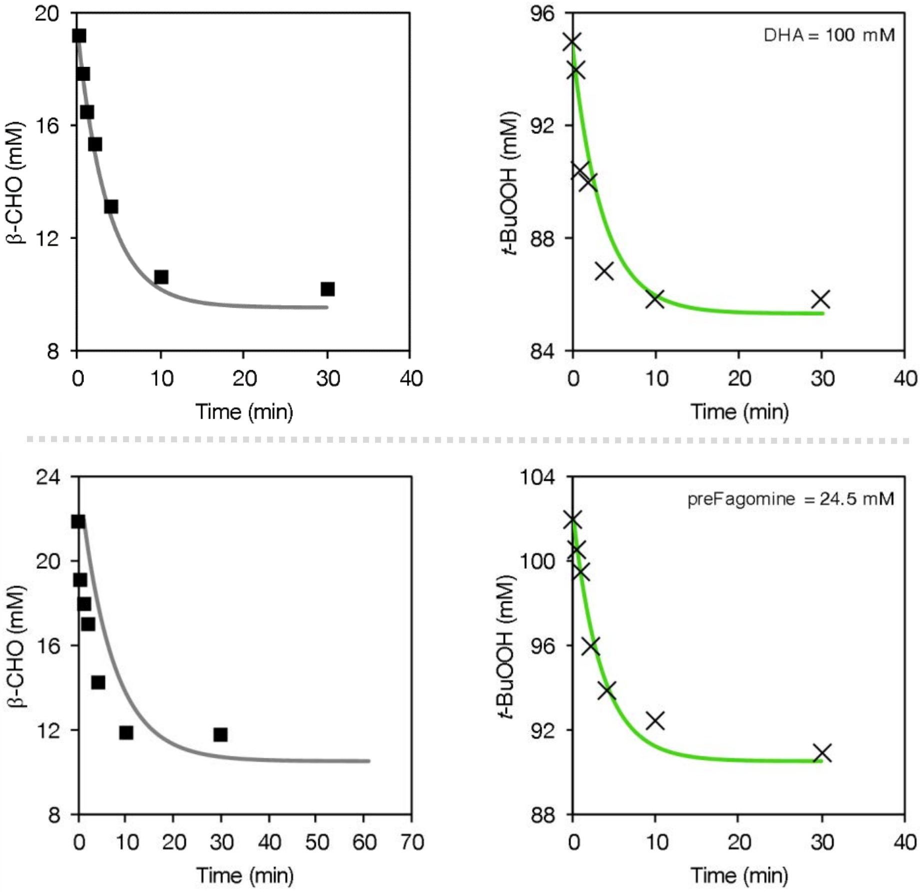

Figure 5.11. Evaluation of β-COOH, *t*-BuOH, β-OH, DHA and preFagomine as inhibitors in the chemical reaction between β-CHO and *t*-BuOOH. All reactions were performed in 100 mM MES pH 6.5, 25 ºC. The dotted line separates individual experiments. Experimental data: β-CHO (■), *t*-BuOOH (×); model simulation: β-CHO (➡), *t*-BuOOH (➡).

$$r_3 = k_{3i} \cdot [\beta\text{-CHO}] \cdot [t\text{-BuOOH}] \cdot (1 + [\beta\text{-COOH}])^{-ki_{r3}} - k_{3ii} \cdot [\text{HAP}] \qquad (5.36)$$

Table 5.3. Estimated values of the parameters from Equation 5.36. 95% conf. intervals are given.

Parameter	Value	Units
ki_{r3}	$2.178{\cdot}10^{-1} \pm 1.40{\cdot}10^{-2}$	-

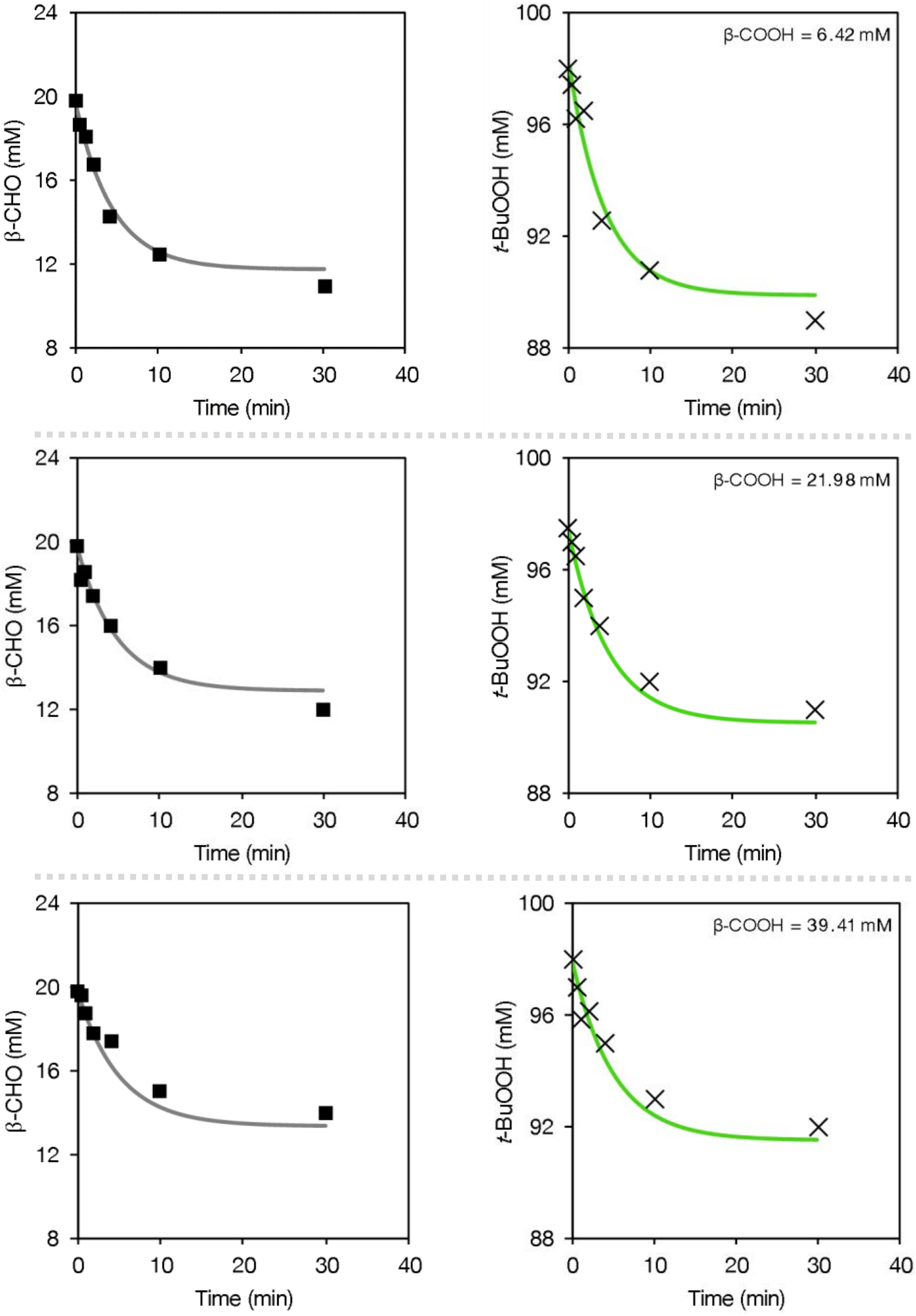

Figure 5.12. Inhibition of β-COOH in the chemical reaction between β-CHO and *t*-BuOOH. In this case, an inhibition term has been used for the model simulations. All reactions were performed in 100 mM MES pH 6.5, 25 ºC. The dotted line separates individual experiments. Experimental data: β-CHO (■), *t*-BuOOH (×); model simulation: β-CHO (▬), *t*-BuOOH (🟩).

5.3.3 *CPO-catalyzed oxidations*

As it has been mentioned in previous lines, the oxidation reaction of CPO reported in the literature is based on a ping-pong mechanism. The estimation of the kinetic parameters in these systems can be hindered by the tight relation between them. To overcome this limitation, a preliminary study of initial reaction rates was performed in order to find a proper value of each parameter to be used as initial value for the model calculations. The mathematical description of r_1, r_2, and r_5 is detailed in Equations 5.37–5.39.

$$r_1 = \frac{k_{cat1} \cdot Y_{CPO} \cdot e^{-kd_{CPO} \cdot t} \cdot [\beta\text{-OH}] \cdot [t\text{-BuOOH}]}{K_{M,\beta\text{-OH}} \cdot [t\text{-BuOOH}] + K_{M,t\text{-BuOOH}} \cdot [\beta\text{-OH}] + [t\text{-BuOOH}] \cdot [\beta\text{-OH}]} \tag{5.37}$$

$$r_2 = \frac{k_{cat2} \cdot Y_{CPO} \cdot e^{-kd_{CPO} \cdot t} \cdot [\beta\text{-CHO}] \cdot [t\text{-BuOOH}]}{K_{M,\beta\text{-CHO}} \cdot [t\text{-BuOOH}] + K_{M,t\text{-BuOOH}} \cdot [\beta\text{-CHO}] + [t\text{-BuOOH}] \cdot [\beta\text{-CHO}]} \tag{5.38}$$

$$r_5 = \frac{k_{cat5} \cdot Y_{CPO} \cdot e^{-kd_{CPO} \cdot t} \cdot [\text{DHA}] \cdot [t\text{-BuOOH}]}{K_{M,\text{DHA}} \cdot [t\text{-BuOOH}] + K_{M,t\text{-BuOOH}} \cdot [\text{DHA}] + [t\text{-BuOOH}] \cdot [\text{DHA}]} \tag{5.39}$$

Initial reactions rates r_1, r_2 and r_5 were studied together as one unknown parameter is common in the three equations, $K_{M,t\text{-BuOOH}}$. All the experiments performed to estimate the initial values for the calculations are included in the experimental distributions of Figure 5.13. The obtained initial values are given in Table 5.4.

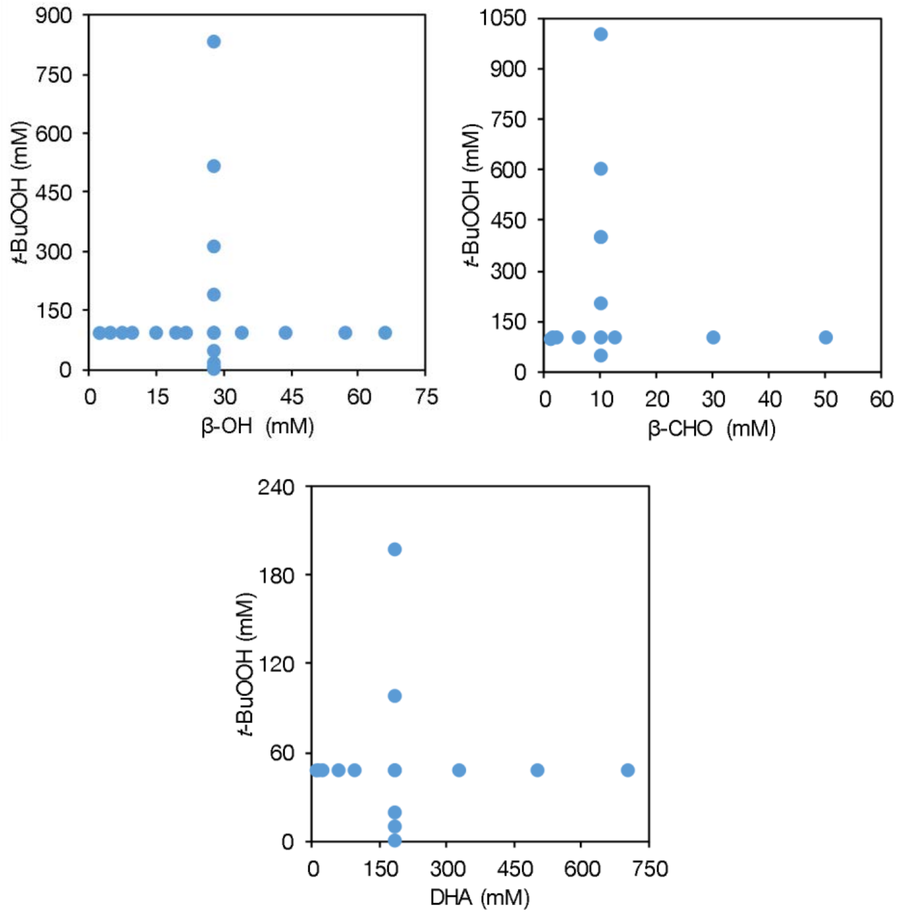

Figure 5.13. Experimental distribution of the incubations of β-OH, β-CHO or DHA with *t*-BuOOH and CPO for the study of the initial value for $r_{1,}$ $r_{2,}$ r_5 calculations.

Table 5.4. Estimated initial values of the further calculation of parameters from Equations 5.37–5.39.

Parameter	Estimated initial value	Units
k_{cat1}	11.23	$\mu mol \cdot min^{-1} \cdot mgCPO^{-1}$
k_{cat2}	3.973	$\mu mol \cdot min^{-1} \cdot mgCPO^{-1}$
k_{cat5}	50.34	$\mu mol \cdot min^{-1} \cdot mgCPO^{-1}$
$K_{M,t\text{-BuOOH}}$	66.18	mM
$K_{M,\beta\text{-OH}}$	311.3	mM
$K_{M,\beta\text{-CHO}}$	42.53	mM
$K_{M,DHA}$	779.6	mM

5.3.3.1 β-CHO

The oxidation of the amino aldehyde into the amino acid catalyzed by CPO is now discussed. When mixing the peroxide, the amino aldehyde and the enzyme, four reactions should be considered: degradation of the peroxide (r_4), inactivation of CPO

(kd_{CPO}), the chemical reaction (r_3), and β-CHO oxidation (r_2). The four reaction rate equations have already been written: Equations 5.33, 5.34, 5.36 and 5.38. Several reactions were carried out in order to estimate the final value of the parameters of r_2 (Figure 5.14). However, an inhibition mechanism in r_4 caused by the amino aldehyde was observed from the experimental data. Thus, an inhibition term was added to Equation 5.33, leading to Equation 5.40. The best results were obtained considering a competitive inhibition of β-CHO to the binding of the peroxide at the active site. The experimental data and model simulations for the parameter estimation are shown in Figure 5.15, and the parameters values are detailed in Table 5.5.

$$r_4 = \frac{k_{cat4} \cdot Y_{CPO} \cdot e^{-kd_{CPO} \cdot t} \cdot [t\text{-BuOOH}]^n}{k_4^n \cdot (1 + \frac{[\beta\text{-CHO}]}{ki_{r4a}}) + [t\text{-BuOOH}]^n} \tag{5.40}$$

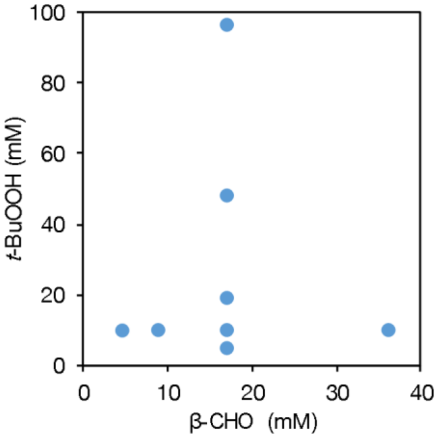

Figure 5.14. Experimental distribution of the incubations of β-CHO, *t*-BuOOH and CPO for the study of r_2.

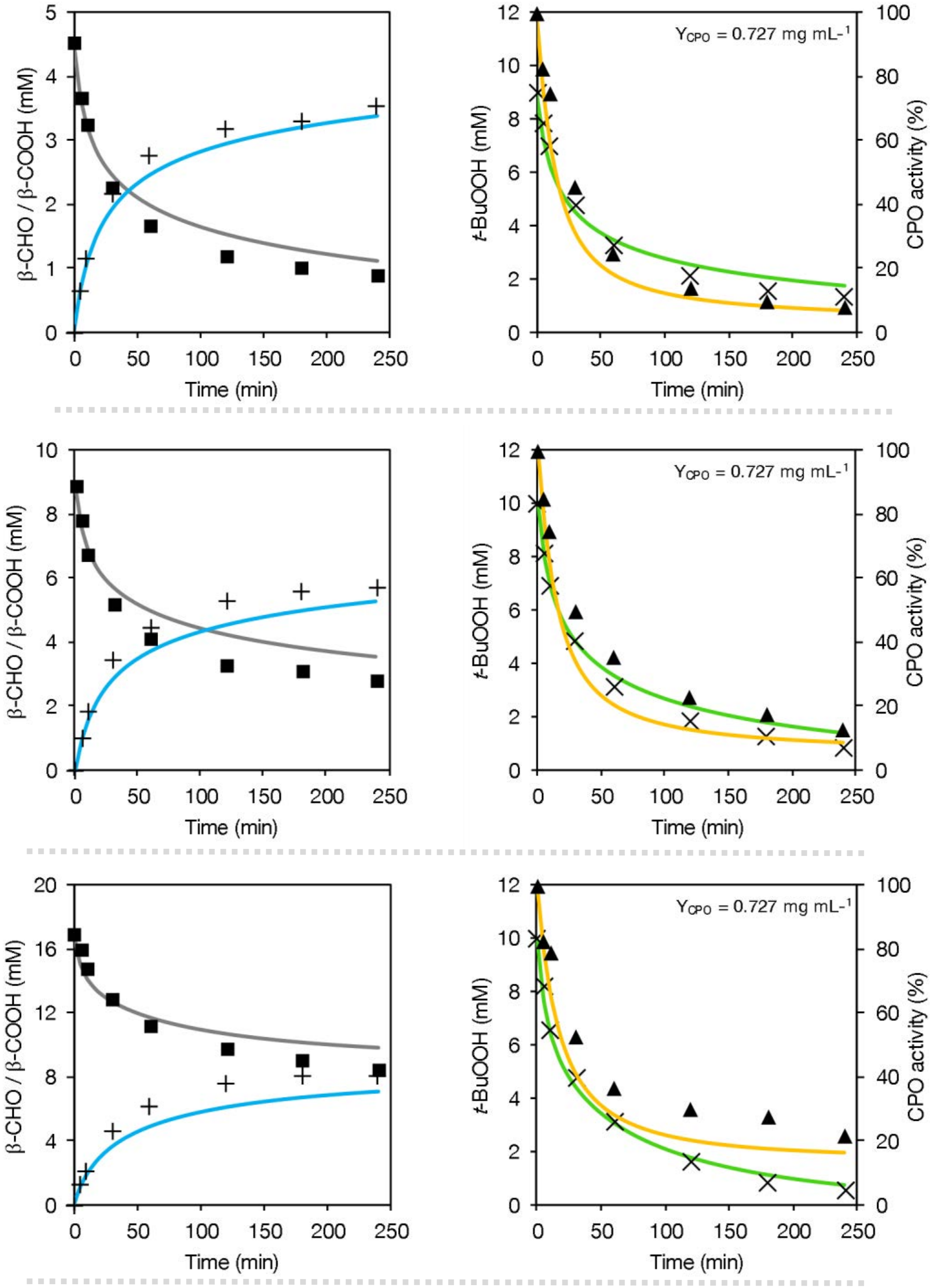

(It continues on the following page)

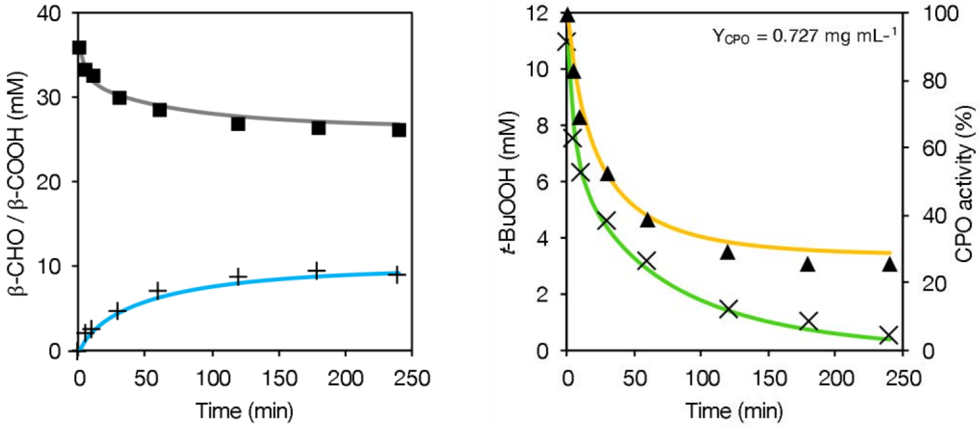

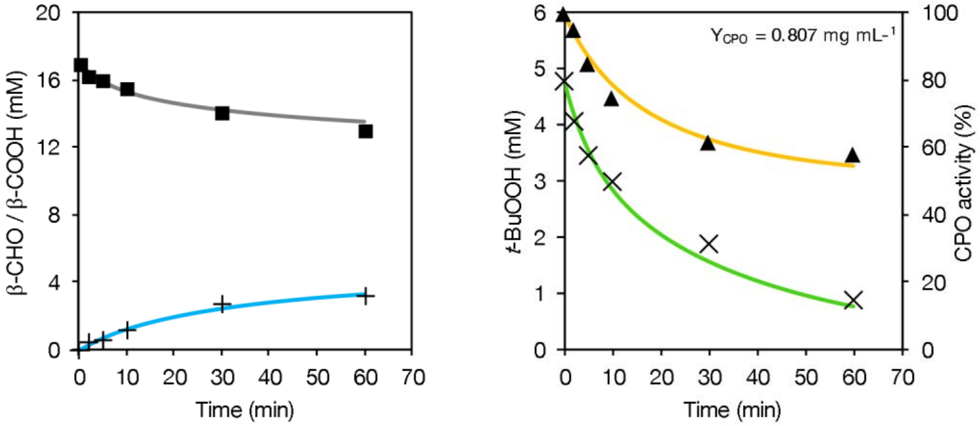

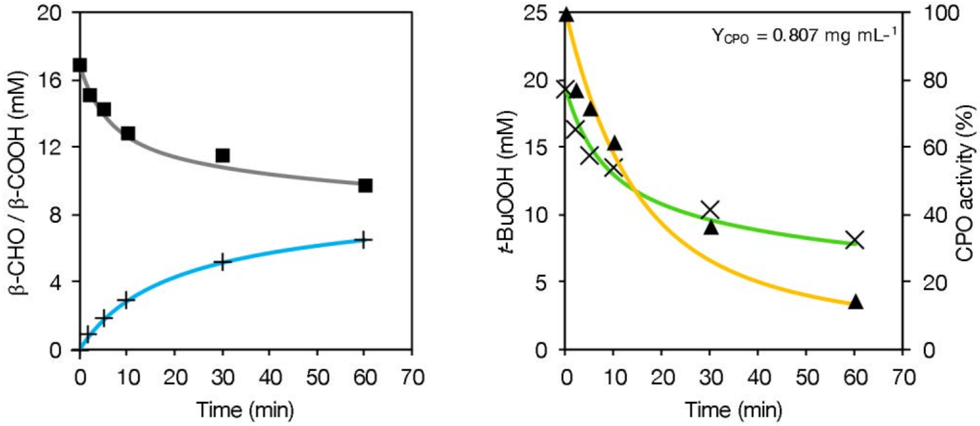

(It continues on the following page)

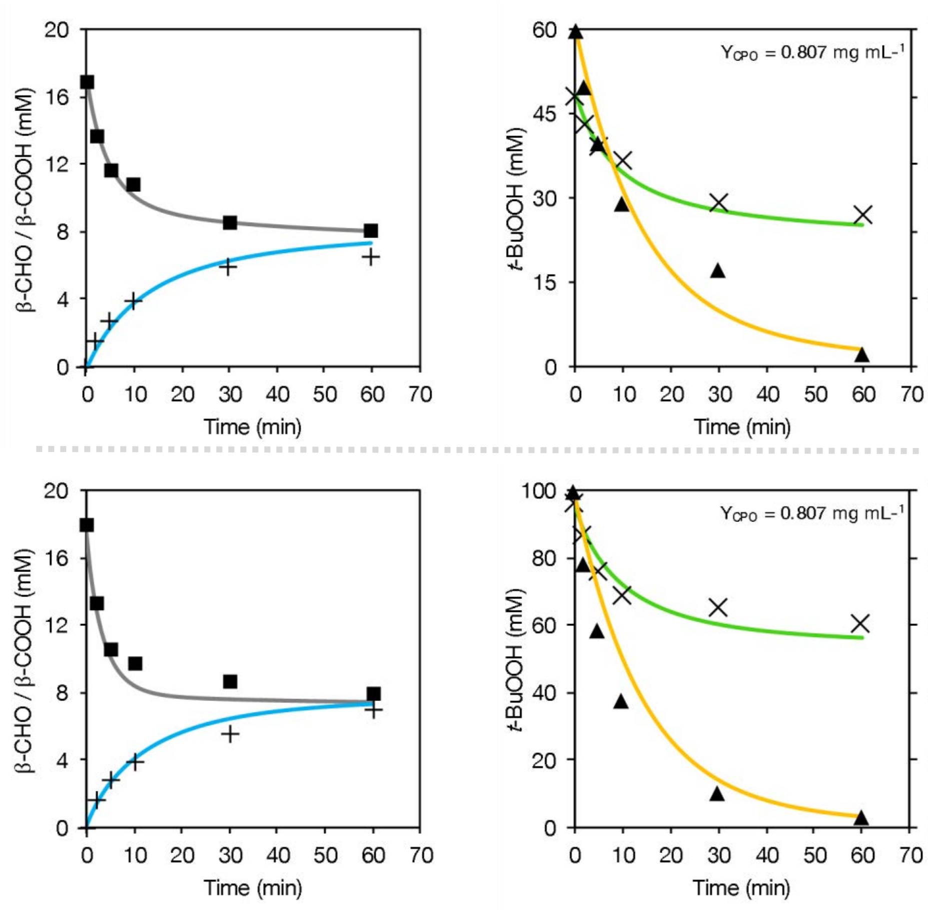

Figure 5.15. Oxidation of β-CHO and degradation of *t*-BuOOH catalyzed by CPO, and CPO inactivation caused by *t*-BuOO$^{\cdot}$. The amount of CPO used is detailed in each reaction (two graphs). All reactions were performed in 100 mM MES pH 6.5, 25 ºC. The dotted line separates individual experiments. Experimental data: β-CHO (■), β-COOH (+), *t*-BuOOH (×), CPO activity (▲); model simulation: β-CHO (◼), β-COOH (🟦), *t*-BuOOH (🟩), CPO activity (🟨).

Table 5.5. Estimated values of the parameters from Equations 5.34, 5.36, 5.38, and 5.40. 95% conf. intervals are given.

Parameter	Value	Units
k_{cat2}	3.417 ± 0.292	$\mu mol \cdot min^{-1} \cdot mgCPO^{-1}$
$K_{M,t\text{-BuOOH}}$	58.83 ± 5.18	mM
$K_{M,\beta\text{-CHO}}$	36.38 ± 3.84	mM
ki_{r4a}	6.518 ± 0.043	mM

The inhibition from other compounds of the reaction system, such as β-COOH, *t*-BuOH, and preFagomine on r_2 was evaluated. To this end, more reactions were performed with different concentrations of these compounds, as shown in Figure 5.16. No inhibition was observed in any case.

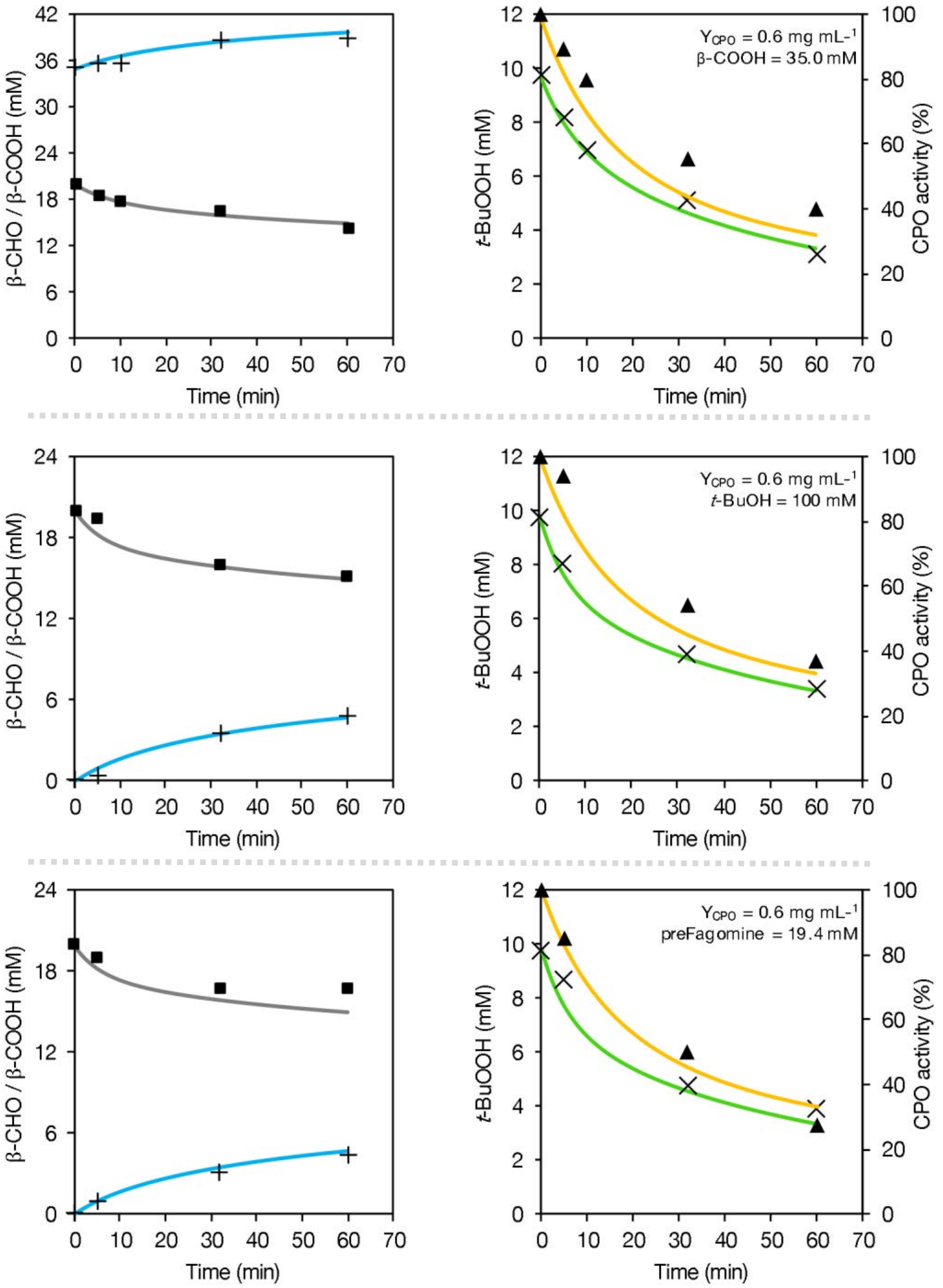

Figure 5.16. Evaluation of β-COOH, *t*-BuOH, and preFagomine as inhibitors in the oxidation of β-CHO catalyzed by CPO. The amount of CPO and inhibitor used in each reaction is detailed in each graph. All reactions were performed in 100 mM MES pH 6.5, 25 ºC. The dotted line separates individual experiments. Experimental data: β-CHO (■), β-COOH (+), *t*-BuOOH (×), CPO activity (▲); model simulation: β-CHO (➡), β-COOH (➡), *t*-BuOOH (➡), CPO activity (➡).

5.3.3.2 β-OH

To investigate the CPO-catalyzed oxidation of the amino alcohol into the amino aldehyde, several reactions were carried out in order to estimate the final value of the parameters of r_1 from Equation 5.37 (Figure 5.17). Apart from r_1, in this case, r_2, r_3, r_4, and kd_{CPO} should be also considered. Nevertheless, no inhibitions were observed between them. The experimental data and model simulations for the parameter estimation are shown in Figure 5.18, and the parameters values are detailed in Table 5.6.

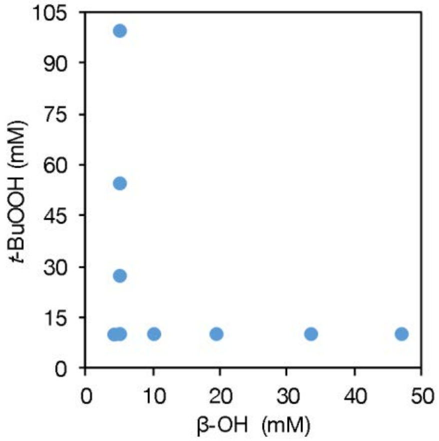

Figure 5.17. Experimental distribution of the incubations of β-OH, *t*-BuOOH and CPO for the study of r_1.

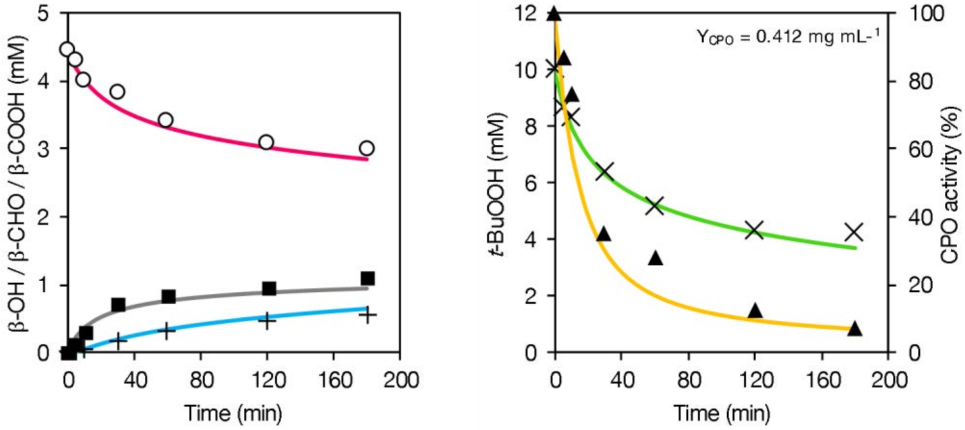

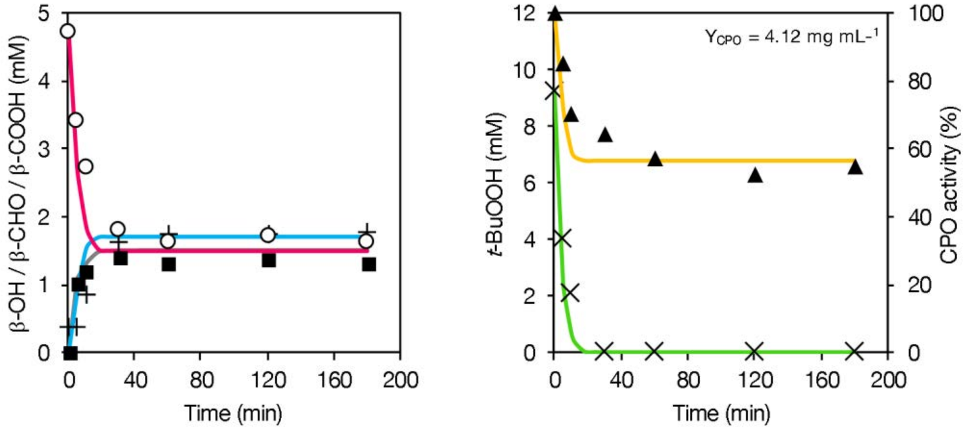

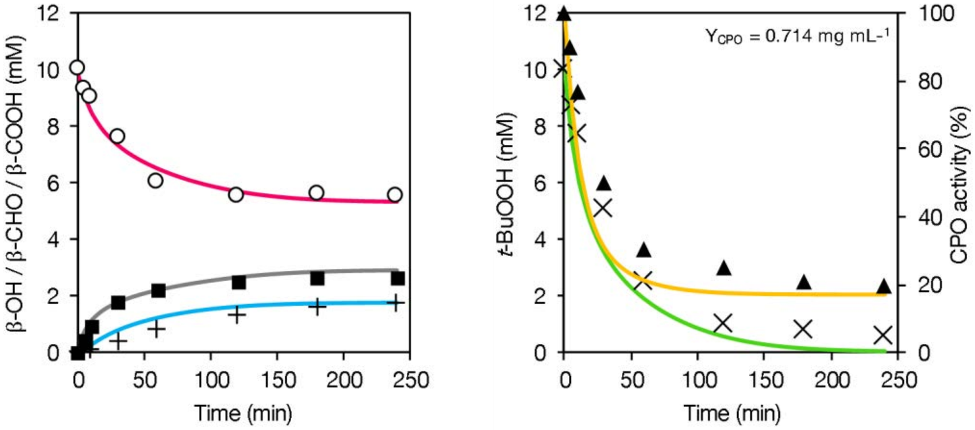

(It continues on the following page)

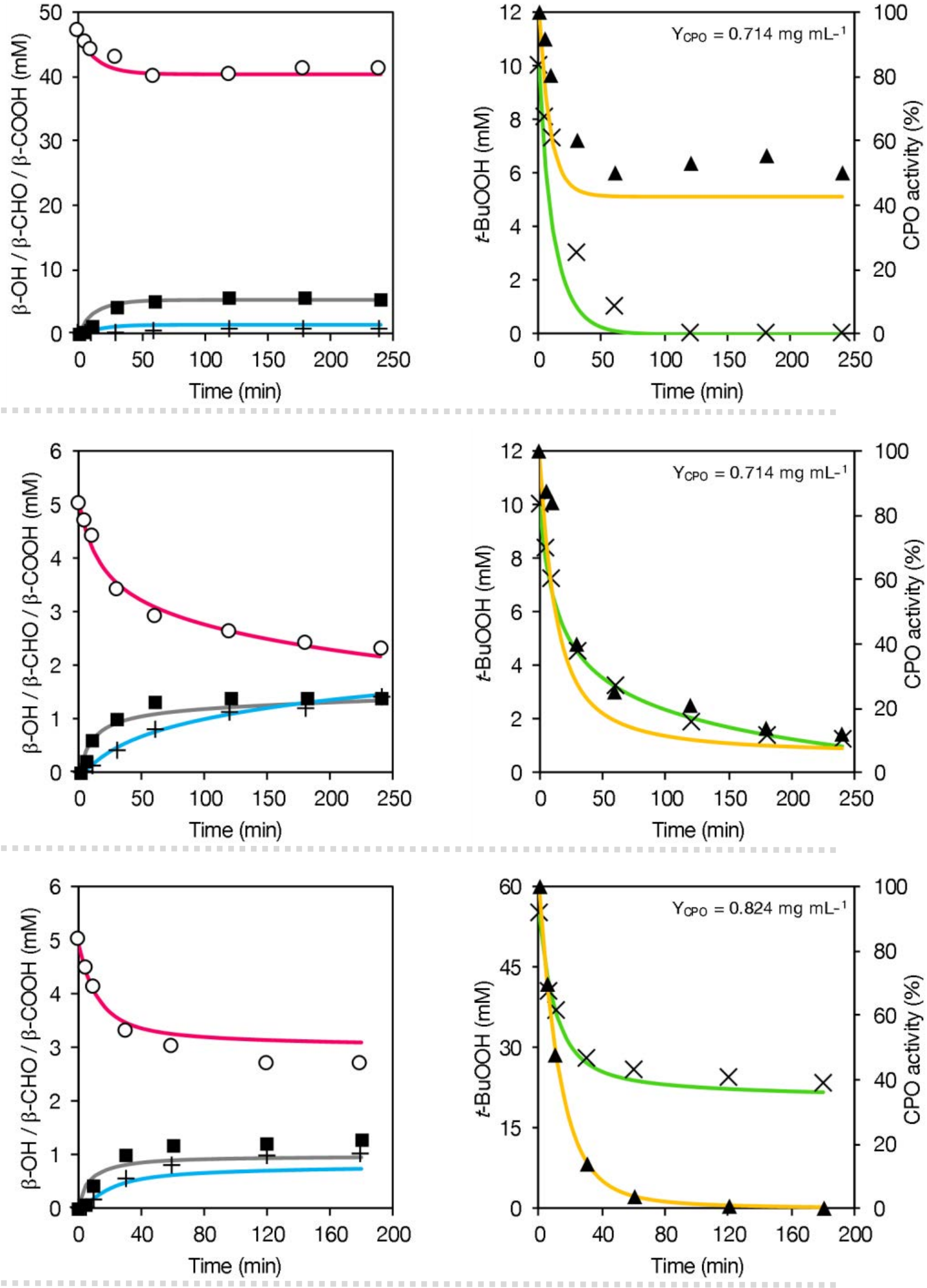

(It continues on the following page)

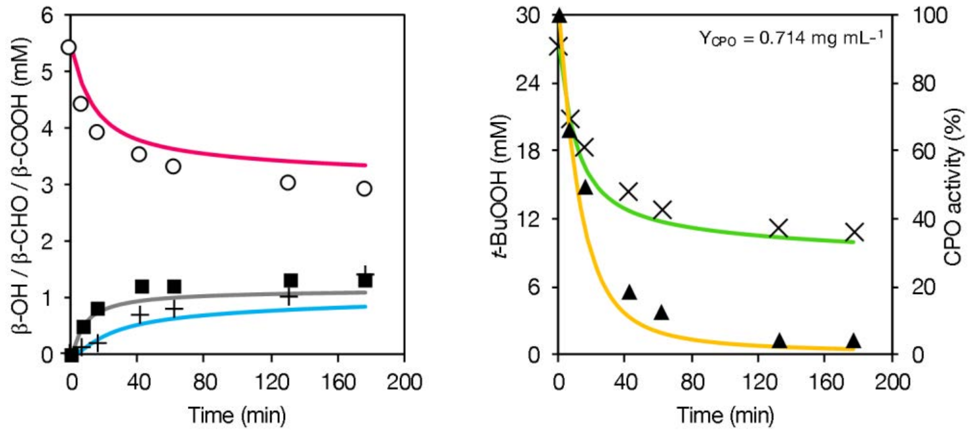

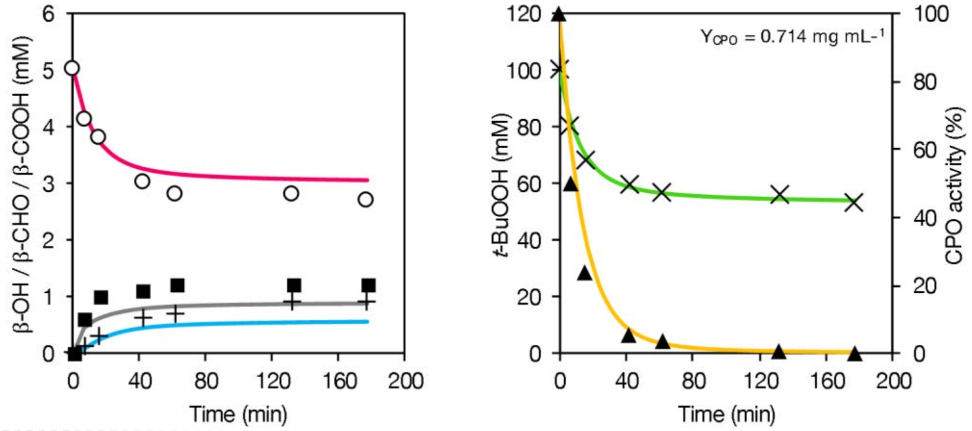

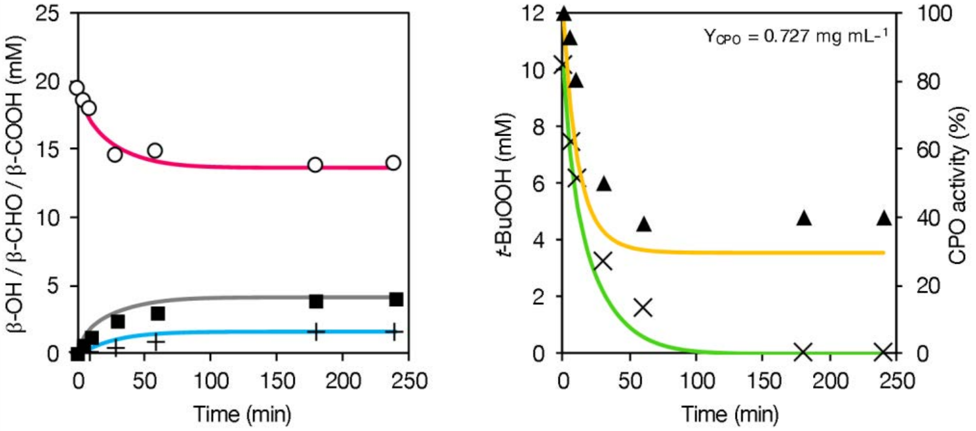

(It continues on the following page)

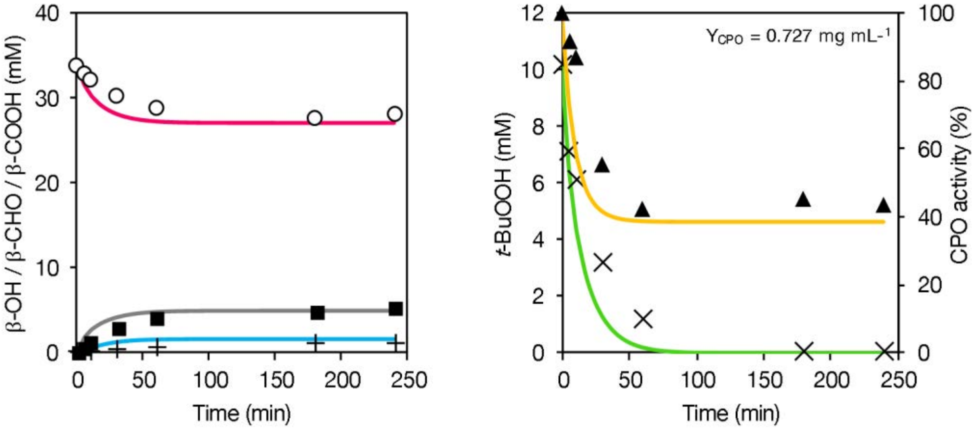

Figure 5.18. CPO-catalyzed oxidation of β-OH and β-CHO, degradation of *t*-BuOOH, and CPO inactivation caused by *t*-BuOO˙. The amount of CPO used is detailed in each reaction (two graphs). All reactions were performed in 100 mM MES pH 6.5, 25 ºC. The dotted line separates individual experiments. Experimental data: β-OH (○), β-CHO (■), β-COOH (+), *t*-BuOOH (×), CPO activity (▲); model simulation: β-OH (➡), β-CHO (➡), β-COOH (➡), *t*-BuOOH (➡), CPO activity (➡).

Table 5.6. Estimated values of the parameters from Equation 5.37. 95% conf. intervals are given.

Parameter	Value	Units
k_{cat1}	10.88 ± 0.37	$\mu mol \cdot min^{-1} \cdot mgCPO^{-1}$
$K_{M\beta\text{-}OH}$	309.5 ± 12.0	mM

Regarding inhibitions affecting r_1, it was not evaluated with various concentrations of β-COOH and preFagomine, for similarity with r_2, in which any inhibitory effect was observed.

5.3.3.3 DHA

Once the CPO model is completed, it is necessary to investigate the DHA oxidation catalyzed by this enzyme, since this side reaction will be important when coupling the second reaction catalyzed by FSA. In order to estimate the kinetic parameters from Equation 5.39, many reactions were performed according to Figure 5.19. Apart from r_5, in this case, r_4 and CPO inactivation should be also considered.

However, an inhibition mechanism in r_4 caused by DHA was observed from the experimental data. Thus, an inhibition term was added to Equation 5.40, leading to Equation 5.41. The best results were obtained considering a competitive inhibition of DHA to the binding of the peroxide at the active site. The experimental data and model simulations for the parameter estimation are shown in Figure 5.20, and the parameters values are detailed in Table 5.7.

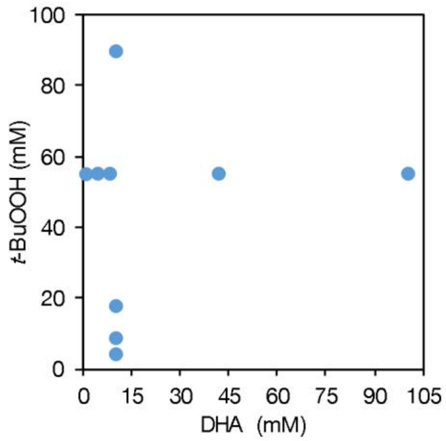

Figure 5.19. Experimental distribution of the incubations of DHA, *t*-BuOOH, and CPO for the study of r_1.

$$r_4 = \frac{k_{cat4} \cdot Y_{CPO} \cdot e^{-kd_{CPO} \cdot t} \cdot [t\text{-BuOOH}]^n}{k_4{}^n \cdot \left(1 + \frac{[\beta\text{-CHO}]}{ki_{r4a}} + \frac{[DHA]}{ki_{r4b}}\right) + [t\text{-BuOOH}]^n} \tag{5.41}$$

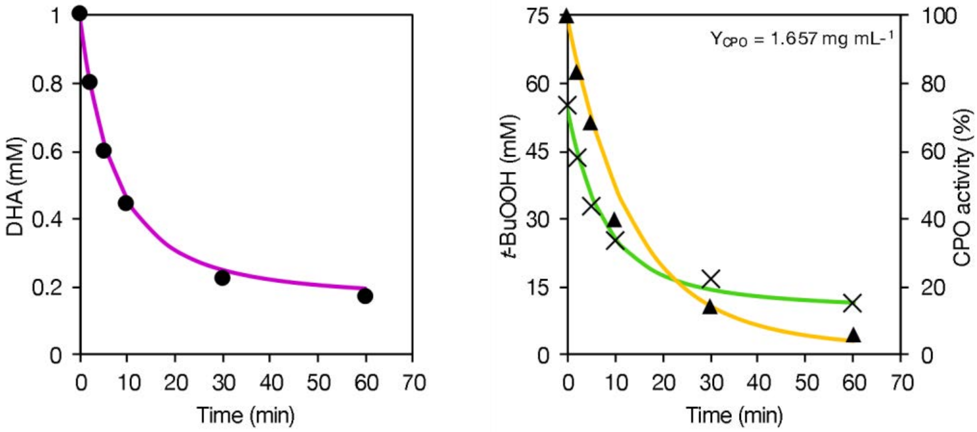

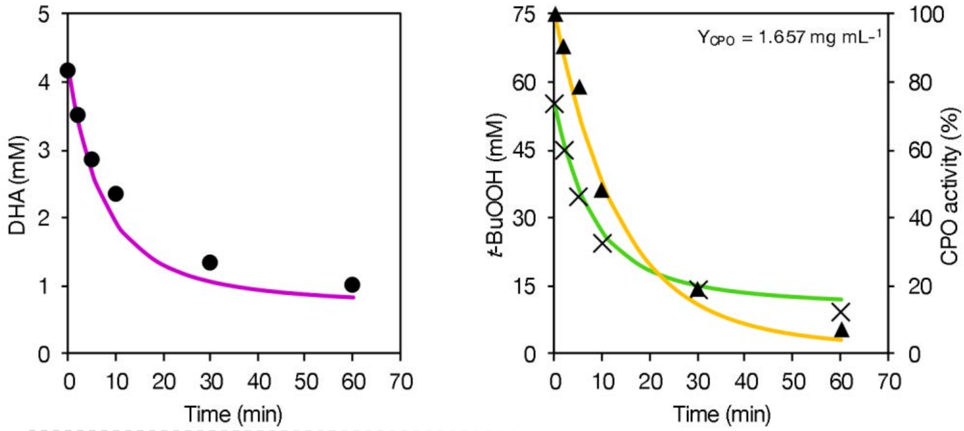

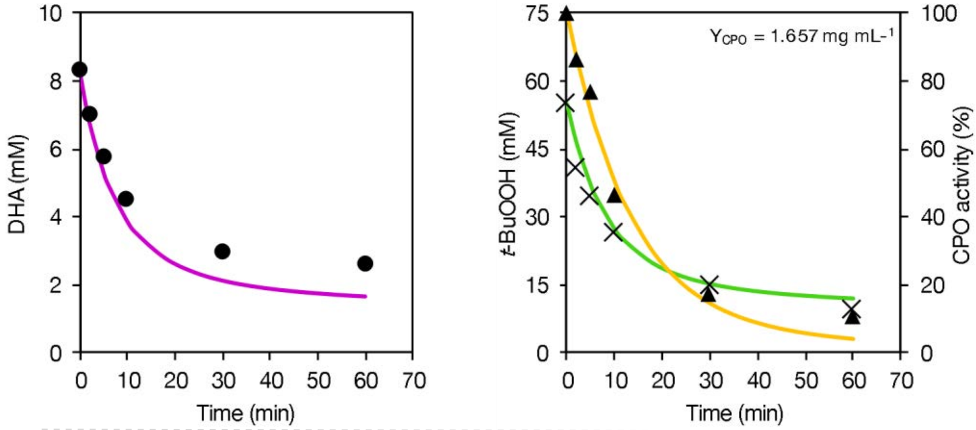

(It continues on the following page)

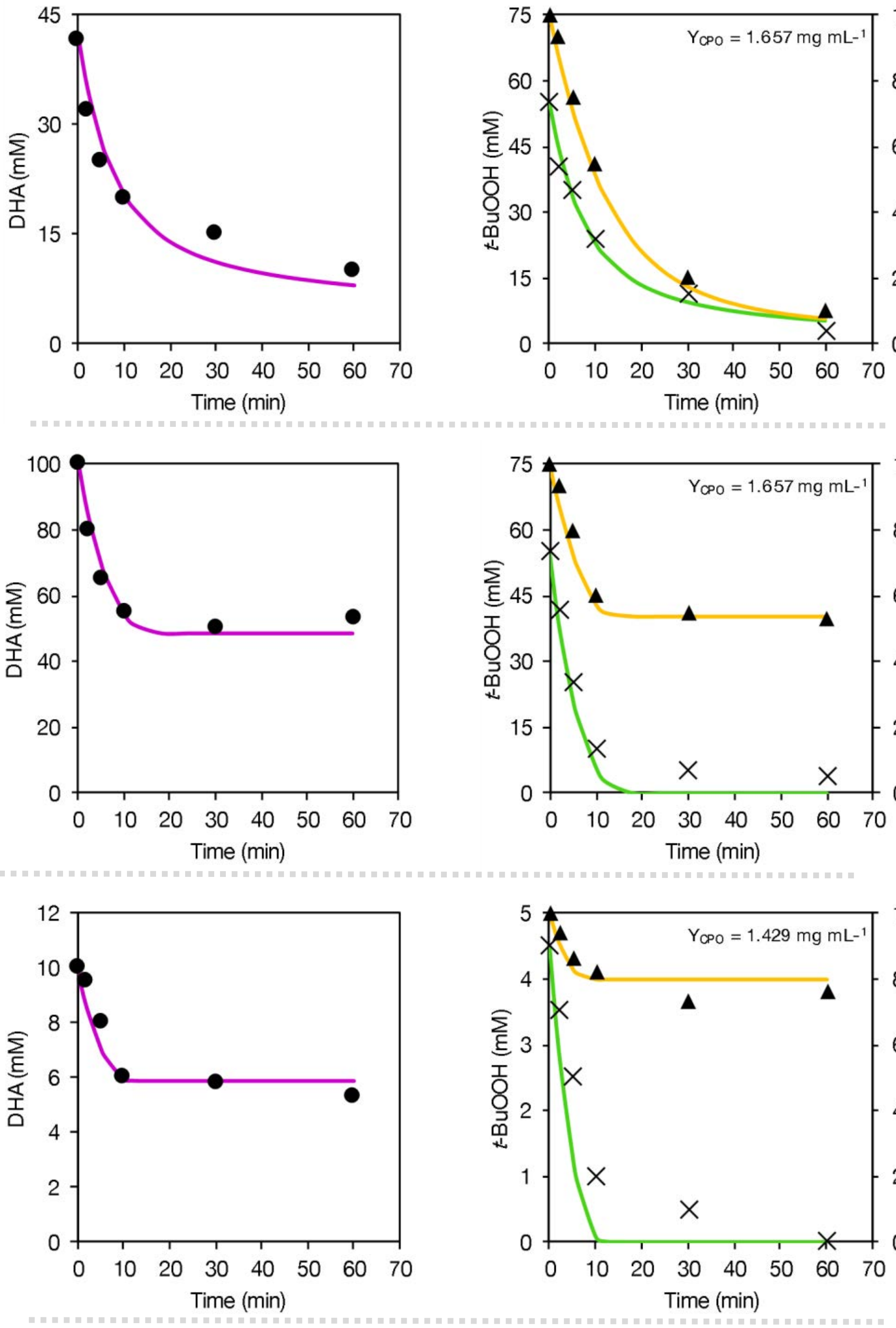

(It continues on the following page)

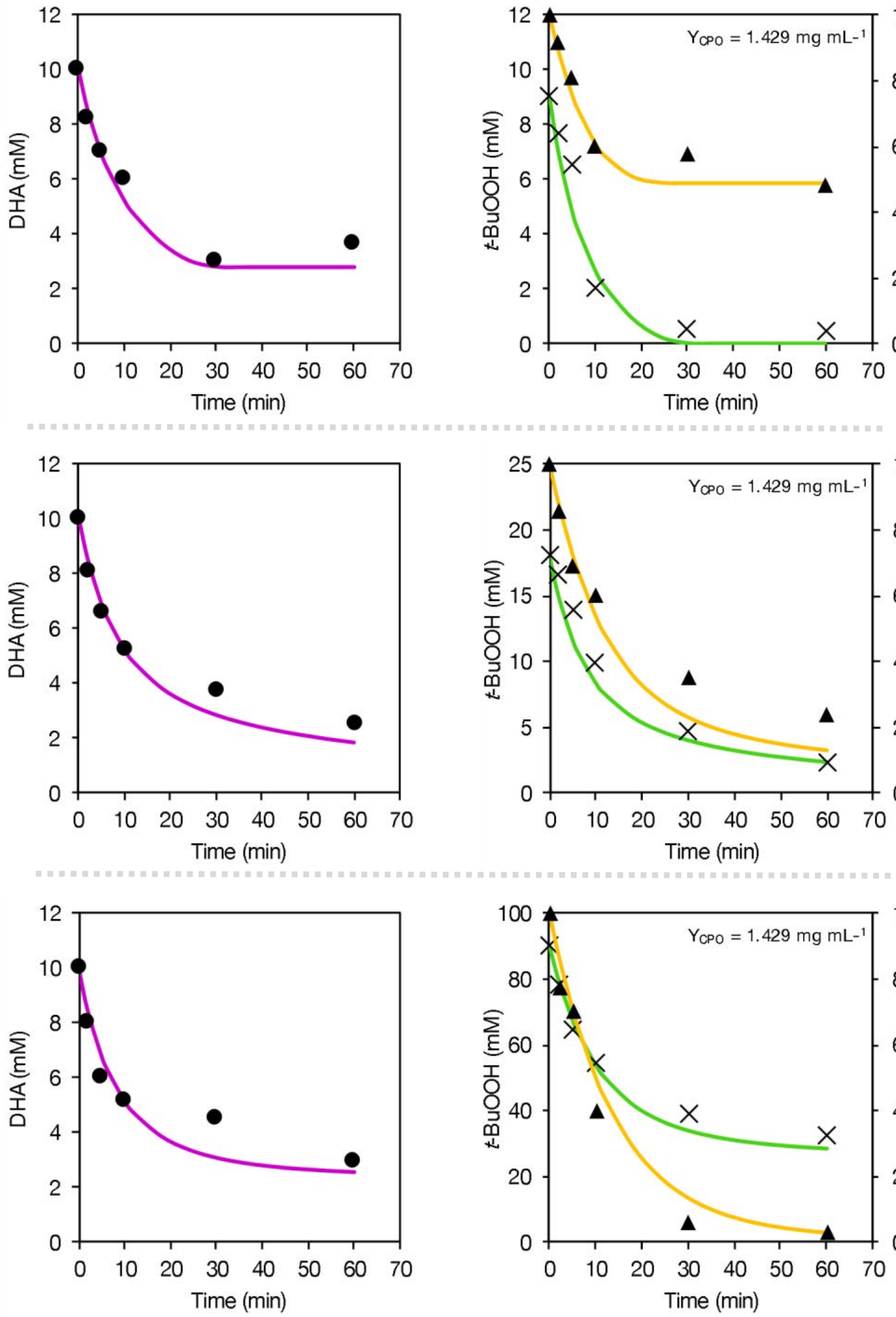

Figure 5.20. CPO-catalyzed oxidation of DHA, degradation of *t*-BuOOH, and CPO inactivation caused by *t*-BuOO$^{\cdot}$. The amount of CPO used is detailed in each reaction (two graphs). All reactions were performed in 100 mM MES pH 6.5, 25 ºC. The dotted line separates individual experiments. Experimental data: DHA (●), *t*-BuOOH (×), CPO activity (▲); model simulation: DHA (🟪), *t*-BuOOH (🟩), CPO activity (🟨).

Table 5.7. Estimated values of the parameters from Equations 5.39 and 5.41. 95% conf. intervals are given.

Parameter	Value	Units
k_{cat5}	54.18 ± 4.11	$\mu mol \cdot min^{-1} \cdot mgCPO^{-1}$
$K_{M,DHA}$	833.6 ± 71.2	mM
ki_{r4b}	11.26 ± 0.64	mM

In order to check for possible interactions of r_5 with r_1 or r_2, five reactions with a fixed concentration of CPO, β-OH, and *t*-BuOOH, but with a variable amount of DHA, were performed. Inhibitions were observed, and hence three terms were added to the mathematical model: two competitive inhibition of DHA to the binding of β-OH or β-CHO to the active site (ki_{r1}, ki_{r2}); and the competitive inhibition of β-OH to the binding of DHA (ki_{r5}). Thus, Equations 5.37–5.39 have been modified to Equations 5.42–5.44. The experimental data and model simulation to find the value of these parameters are plotted in Figure 5.21. The estimated values are detailed in Table 5.8.

$$r_1 = \frac{k_{cat1} \cdot Y_{CPO} \cdot e^{-kd_{CPO} \cdot t} \cdot [\beta\text{-OH}] \cdot [t\text{-BuOOH}]}{K_{M,\beta\text{-OH}} \cdot \left(1 + \frac{[DHA]}{ki_{r1}}\right) \cdot [t\text{-BuOOH}] + K_{M,t\text{-BuOOH}} \cdot [\beta\text{-OH}] + [t\text{-BuOOH}] \cdot [\beta\text{-OH}]} \tag{5.42}$$

$$r_2 = \frac{k_{cat2} \cdot Y_{CPO} \cdot e^{-kd_{CPO} \cdot t} \cdot [\beta\text{-CHO}] \cdot [t\text{-BuOOH}]}{K_{M,\beta\text{-CHO}} \left(1 + \frac{[DHA]}{ki_{r2}}\right) \cdot [t\text{-BuOOH}] + K_{M,t\text{-BuOOH}} \cdot [\beta\text{-CHO}] + [t\text{-BuOOH}] \cdot [\beta\text{-CHO}]} \tag{5.43}$$

$$r_5 = \frac{k_{cat5} \cdot Y_{CPO} \cdot e^{-kd_{CPO} \cdot t} \cdot [DHA] \cdot [t\text{-BuOOH}]}{K_{M,DHA} \left(1 + \frac{[\beta\text{-OH}]}{ki_{r5}}\right) \cdot [t\text{-BuOOH}] + K_{M,t\text{-BuOOH}} \cdot [DHA] + [t\text{-BuOOH}] \cdot [DHA]} \tag{5.44}$$

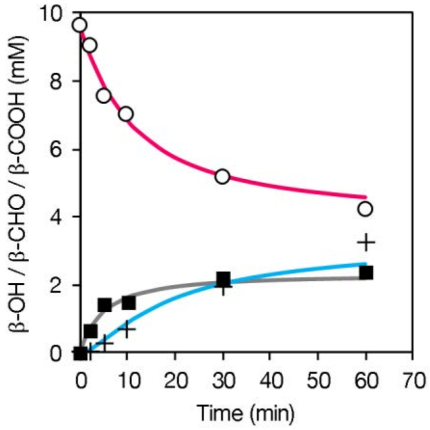

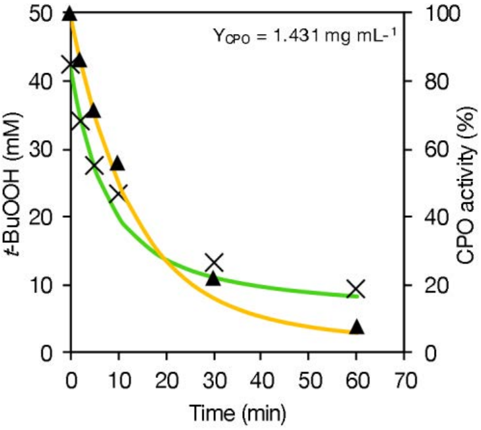

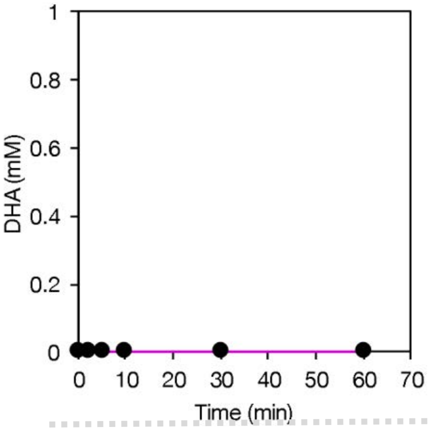

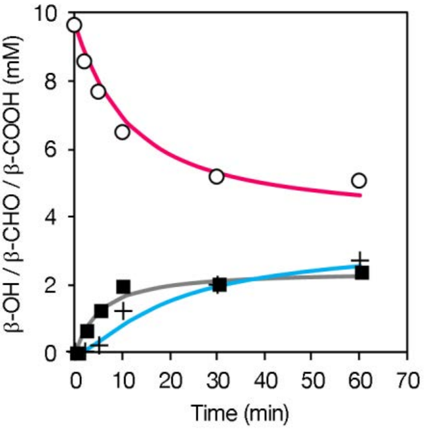

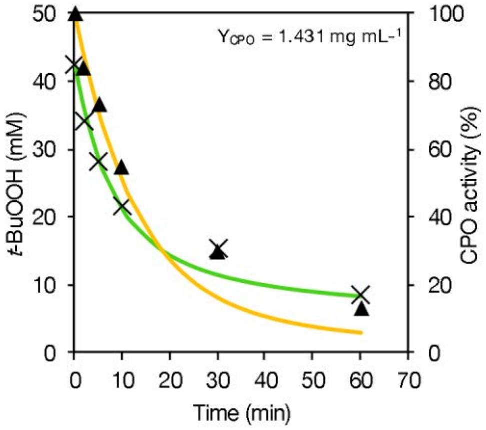

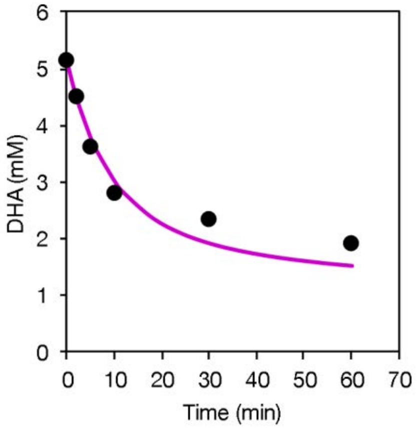

(It continues on the following page)

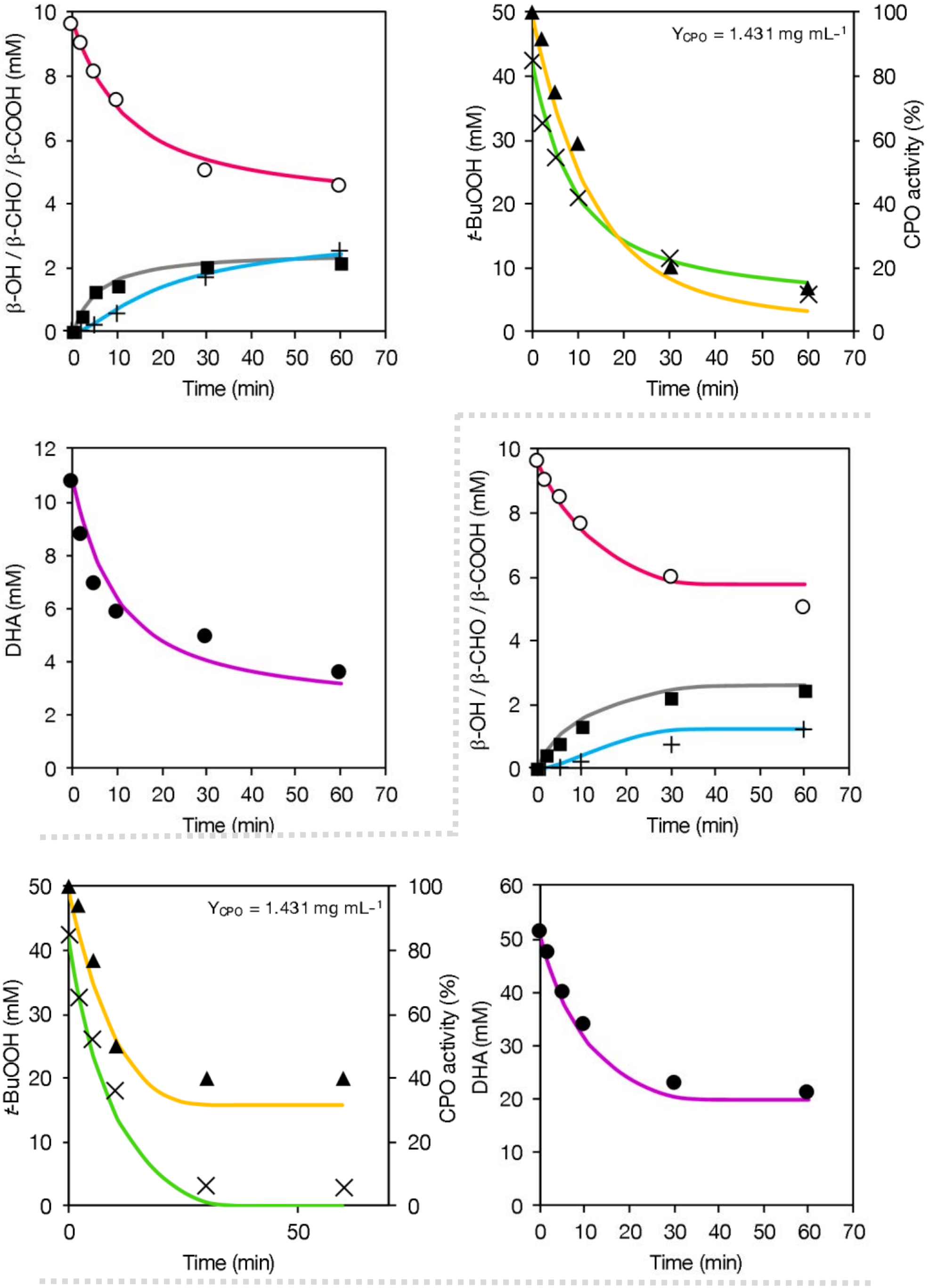

(It continues on the following page)

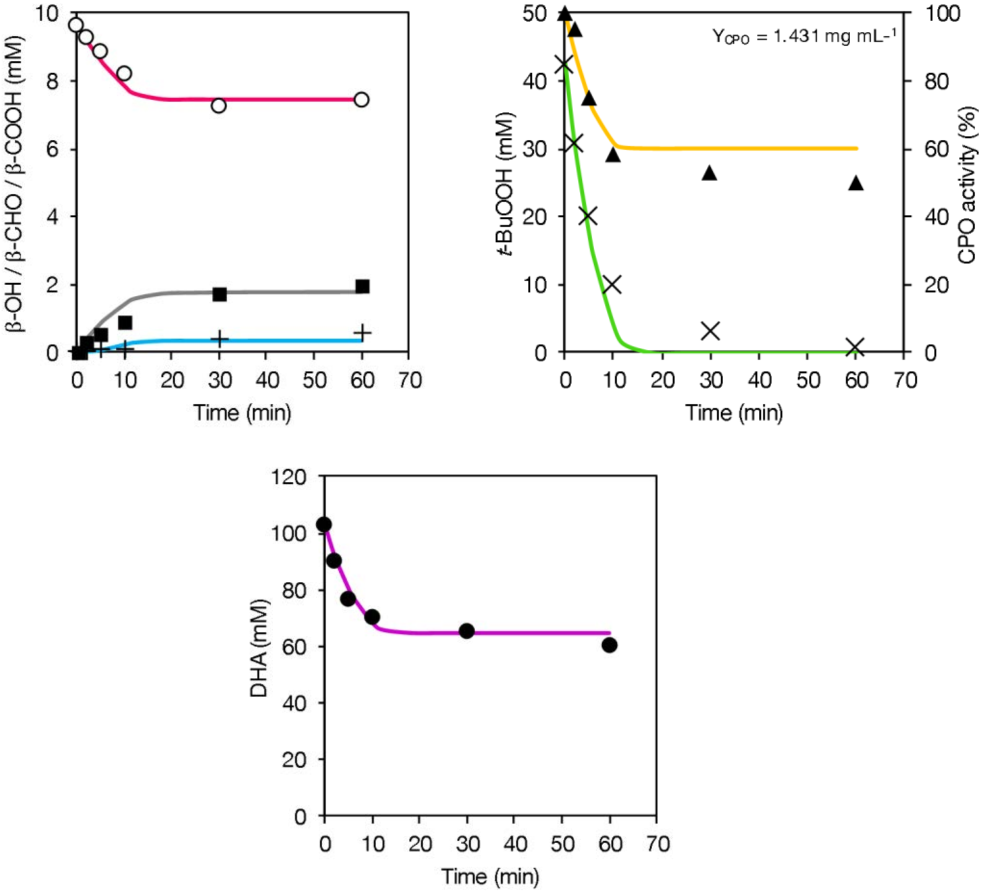

Figure 5.21. CPO-catalyzed oxidation of β-OH, β-CHO, DHA, degradation of *t*-BuOOH, and CPO inactivation caused by *t*-BuOO$^{\cdot}$. The amount of CPO used is detailed in each reaction (three graphs). All reactions were performed in 100 mM MES pH 6.5, 25 ºC. The dotted line separates individual experiments. Experimental data: β-OH (○), β-CHO (■), β-COOH (+), DHA (●), *t*-BuOOH (×), CPO activity (▲); model simulation: β-OH (➡), β-CHO (➡), β-COOH (➡), DHA (➡), *t*-BuOOH (➡), CPO activity (➡).

Table 5.8. Estimated values of the parameters from Equations 5.42–5.44. 95% conf. intervals are given.

Parameter	Value	Units
ki_{r1}	108.2 ± 8.5	mM
ki_{r2}	38.21 ± 8.08	mM
ki_{r5}	32.15 ± 0.76	mM

5.3.4 FSA-catalyzed aldol addition

Once the CPO model is completed, the mathematical expression for the FSA reaction should be written. As stated before, FSA catalyzes the aldol addition of DHA following an ordered sequential mechanism. Thus, considering the aldol and retroaldol additions (r_6, r_7), its kinetics could be written with Equations 5.45 and 5.46.

$$r_6 = \frac{k_{cat6} \cdot Y_{FSA} \cdot [\mathrm{DHA}] \cdot [\beta\text{-CHO}]}{K'_{M,\beta\text{-CHO}} \cdot [\mathrm{DHA}] + K'_{M,\mathrm{DHA}} \cdot K'_{M,\beta\text{-CHO}} + [\mathrm{DHA}] \cdot [\beta\text{-CHO}]} \tag{5.45}$$

$$r_7 = \frac{k_{cat7} \cdot Y_{FSA} \cdot [\mathrm{preFagomine}]}{K_{M,\mathrm{preFagomine}} + [\mathrm{preFagomine}]} \tag{5.46}$$

Contrarily to CPO estimations, no inactivation of FSA is expected along its own reaction. Therefore, an initial reaction rate analysis can be easily performed to obtain the parameters values. To this end, several reactions were performed varying the concentration of DHA or β-CHO, and preFagomine, analyzing the reaction rate before 10% of substrate conversion has been achieved (Figure 5.22, Figure 5.23). The estimated parameter values are given in Table 5.9.

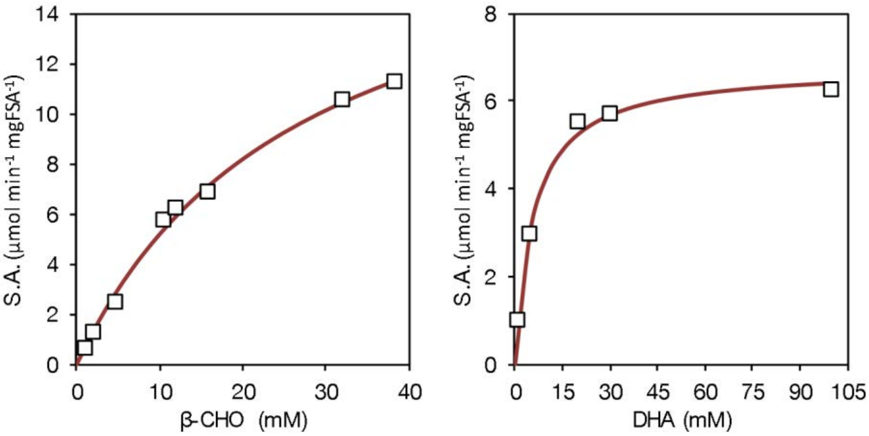

Figure 5.22. Initial reaction rate analysis of the aldol addition of DHA to β-CHO catalyzed by FSA. Specific activity (S.A.) has been calculated from the slope in product formation from each reaction. All reactions were performed in 100 mM MES pH 6.5, 25 ºC, using 0.5 U FSA mL^{-1}.

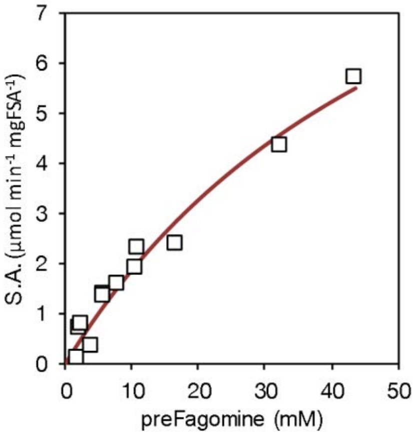

Figure 5.23. Initial reaction rate analysis of the preFagomine cleavage catalyzed by FSA. Specific activity (S.A.) has been calculated from the slope in product formation from each reaction. All reactions were performed in 100 mM MES pH 6.5, 25 ºC, using 2.0 U FSA mL^{-1}.

Table 5.9. Estimated values of the parameters from Equations 5.45 and 5.46. 95% conf. intervals are given.

Parameter	Value	Units
k_{cat6}	19.31 ± 1.00	$\mu mol \cdot min^{-1} \cdot mgFSA^{-1}$
k_{cat7}	13.06 ± 0.69	$\mu mol \cdot min^{-1} \cdot mgFSA^{-1}$
$K'_{M.DHA}$	9.004 ± 1.703	mM
$K'_{M,\beta\text{-}CHO}$	20.94 ± 2.25	mM
$K_{M,preFagomine}$	59.68 ± 1.93	mM

To check if there is any inhibition between both reactions, various reactions were carried out, as shown in Figure 5.25. As it has been already reported in the literature, some product inhibition was observed in the retroaldol addition by the amino aldehyde.[24] Thus, another term was included in Equation 5.46, leading to Equation 5.47. The fitted data and the estimated parameter value are shown in Figure 5.25 and Table 5.10.

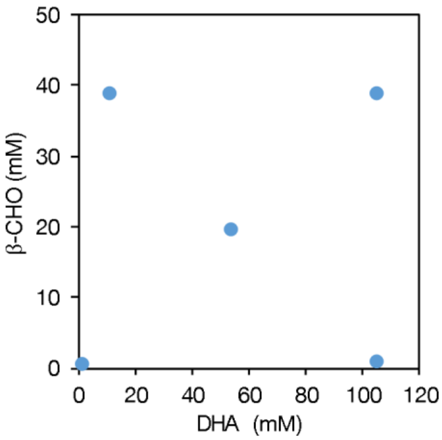

Figure 5.24. Experimental distribution of the incubations of DHA, β-CHO and FSA for the study of r_6 and r_7.

$$r_7 = \frac{k_{cat7} \cdot Y_{FSA} \cdot [\text{preFagomine}]}{K_{M,\text{preFagomine}} \cdot \left(1 + \frac{[\beta\text{-CHO}]}{ki_{r7}}\right) + [\text{preFagomine}]} \tag{5.47}$$

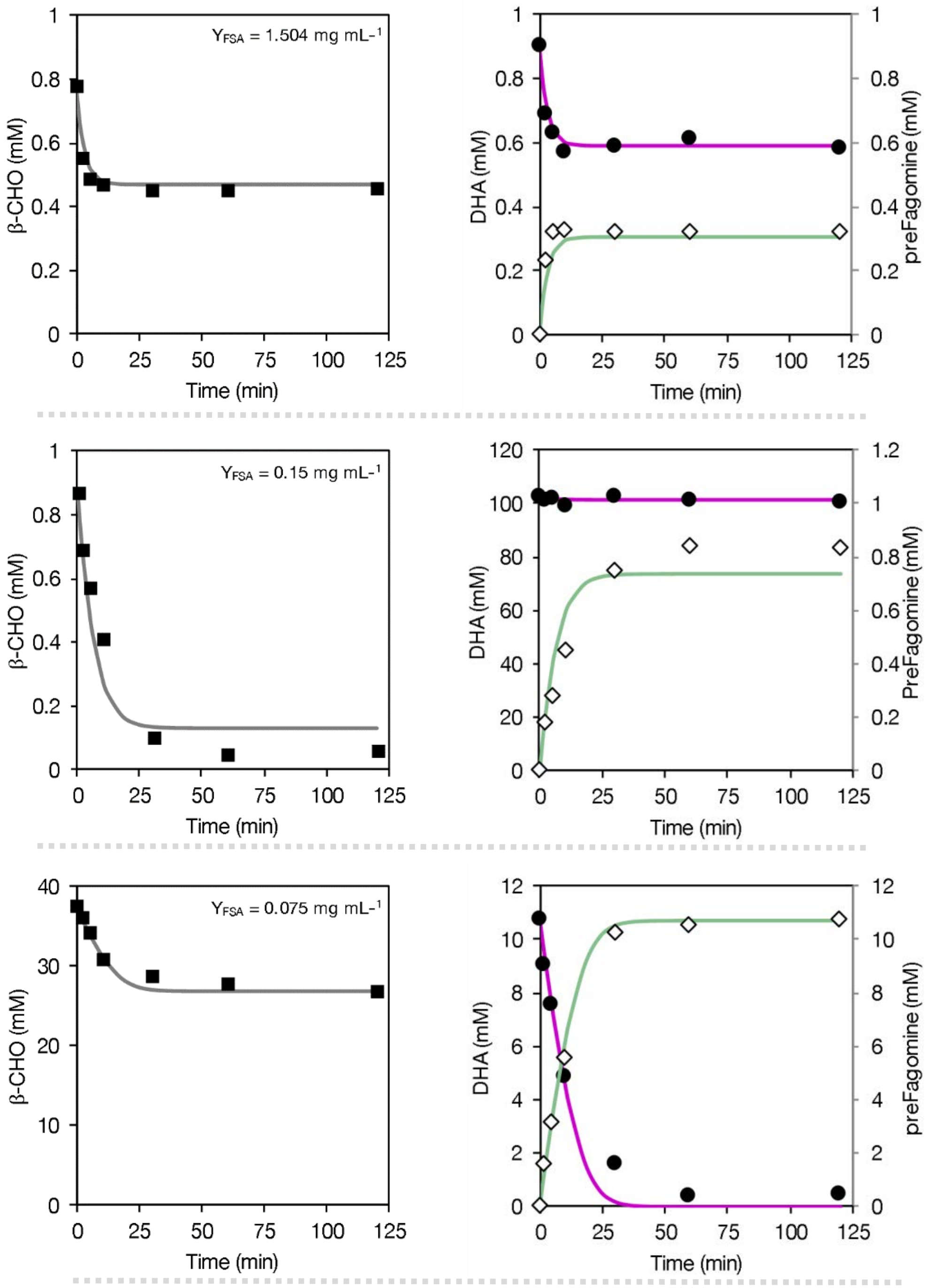

(It continues on the following page)

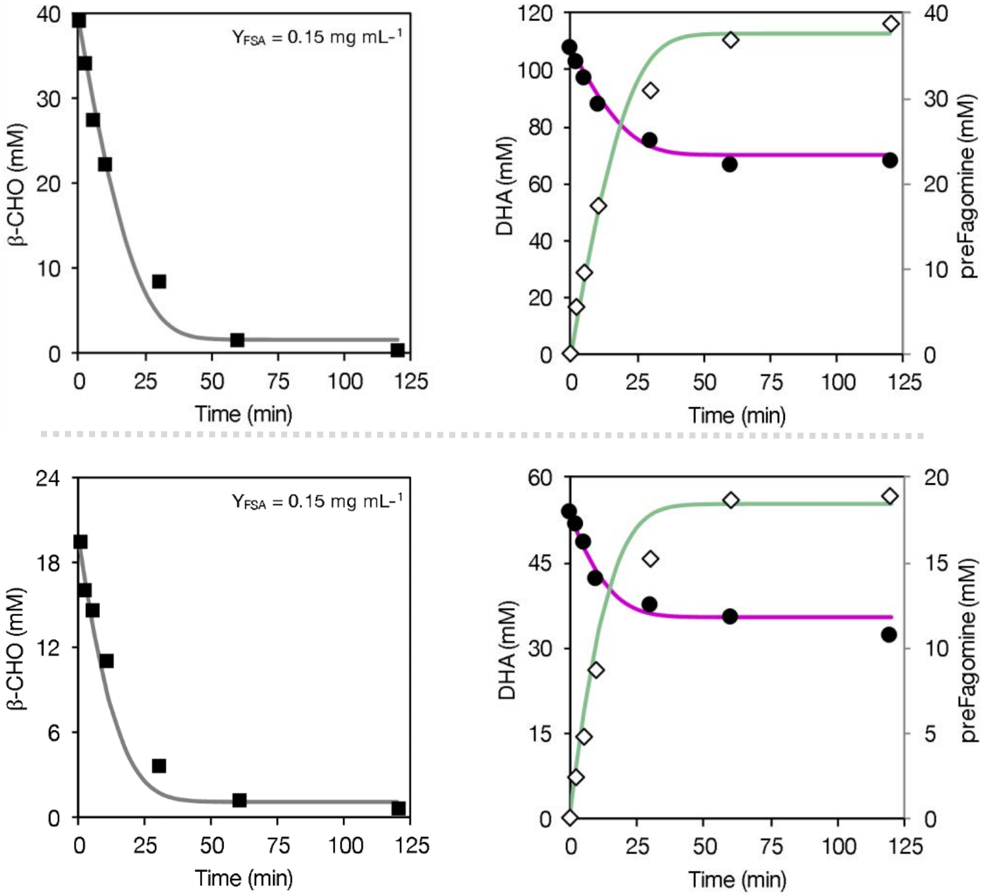

Figure 5.25. FSA-catalyzed aldol addition of DHA to β-CHO and preFagomine cleavage. The amount of FSA used is detailed in each reaction (two graphs). The dotted line separates individual experiments. All reactions were performed in 100 mM MES pH 6.5, 25 ºC. Experimental data: β-CHO (■), DHA (●), preFagomine (◇); model simulation: β-CHO (➡), DHA (➡), preFagomine (➡).

Table 5.10. Estimated values of the parameters from Equation 5.47. 95% conf. intervals are given.

Parameter	Value	Units
ki_{r7}	$3.092{\cdot}10^{-1} \pm 5.41{\cdot}10^{-2}$	mM

5.3.5 FSA inactivation

Both models are completed separately, supposed to predict the experimental data for the specific reaction of each enzyme. However, in order to employ this model for the coupled reaction prediction, the modeling of the FSA inactivation is required. Two inactivations should be distinguished: (1) inactivation by the peroxyl radical formed by the degradation of *t*-BuOOH by CPO, and (2) inactivation by the oxidation of DHA catalyzed by CPO in presence of *t*-BuOOH.

Regarding the first inactivation (kd_{FSA1}), incubations of FSA with different concentrations of *t*-BuOOH and CPO (Figure 5.26) were used to write Equation 5.48, which properly predicts the experimental data from Figure 5.27. The estimated parameter value is given in Table 5.11.

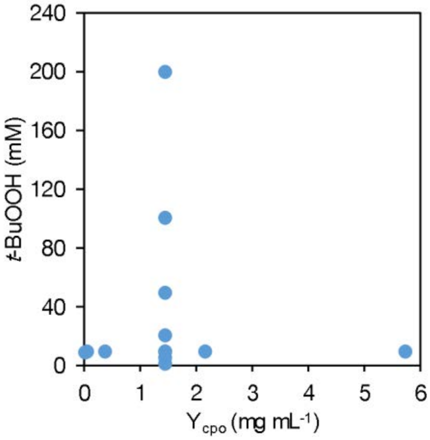

Figure 5.26. Experimental distribution of the incubations of FSA with different concentrations of *t*-BuOOH and CPO for the study of kd_{FSA1}.

$$kd_{FSA1} = k_1 \cdot 2 \cdot r_4 \tag{5.48}$$

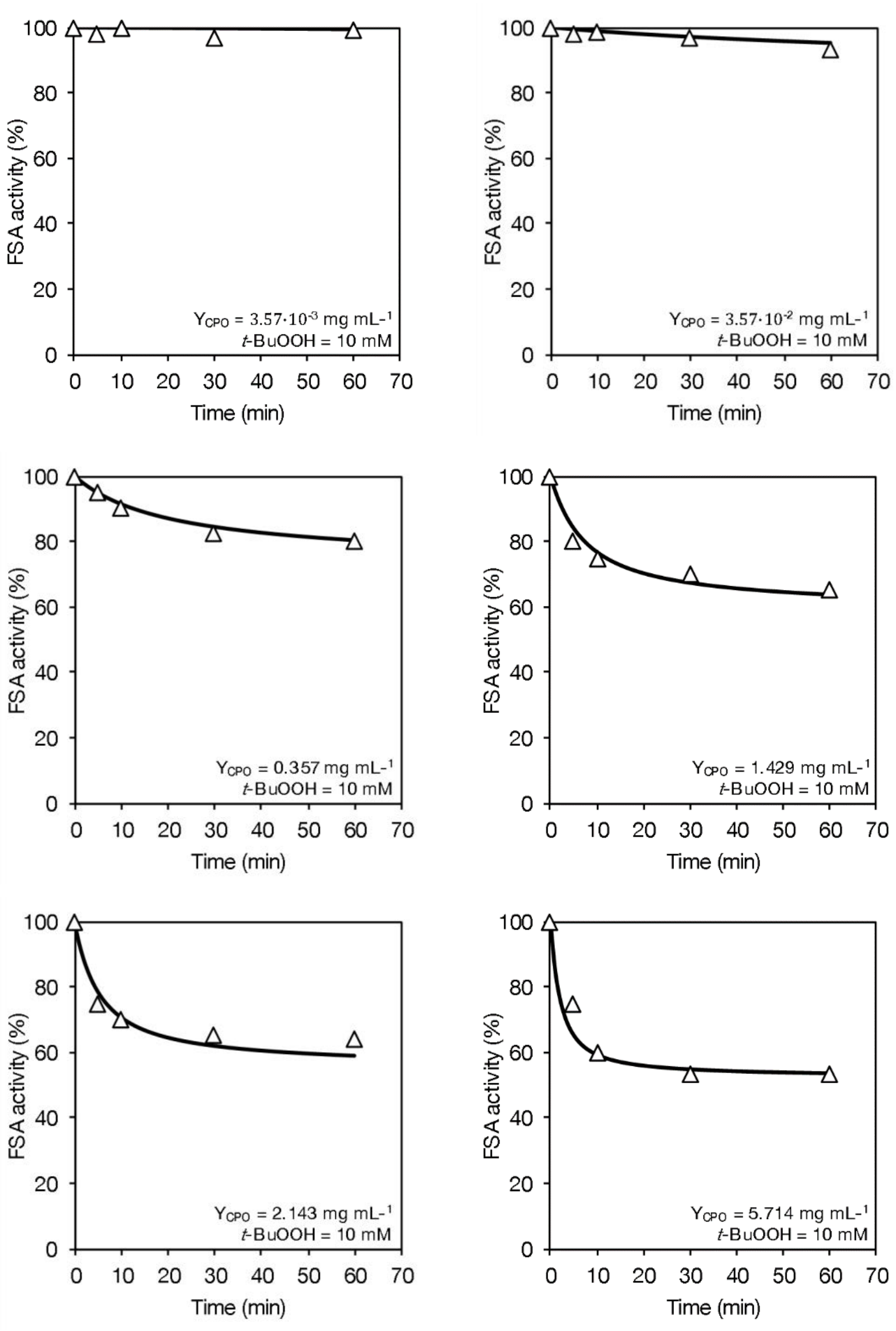

(It continues on the following page)

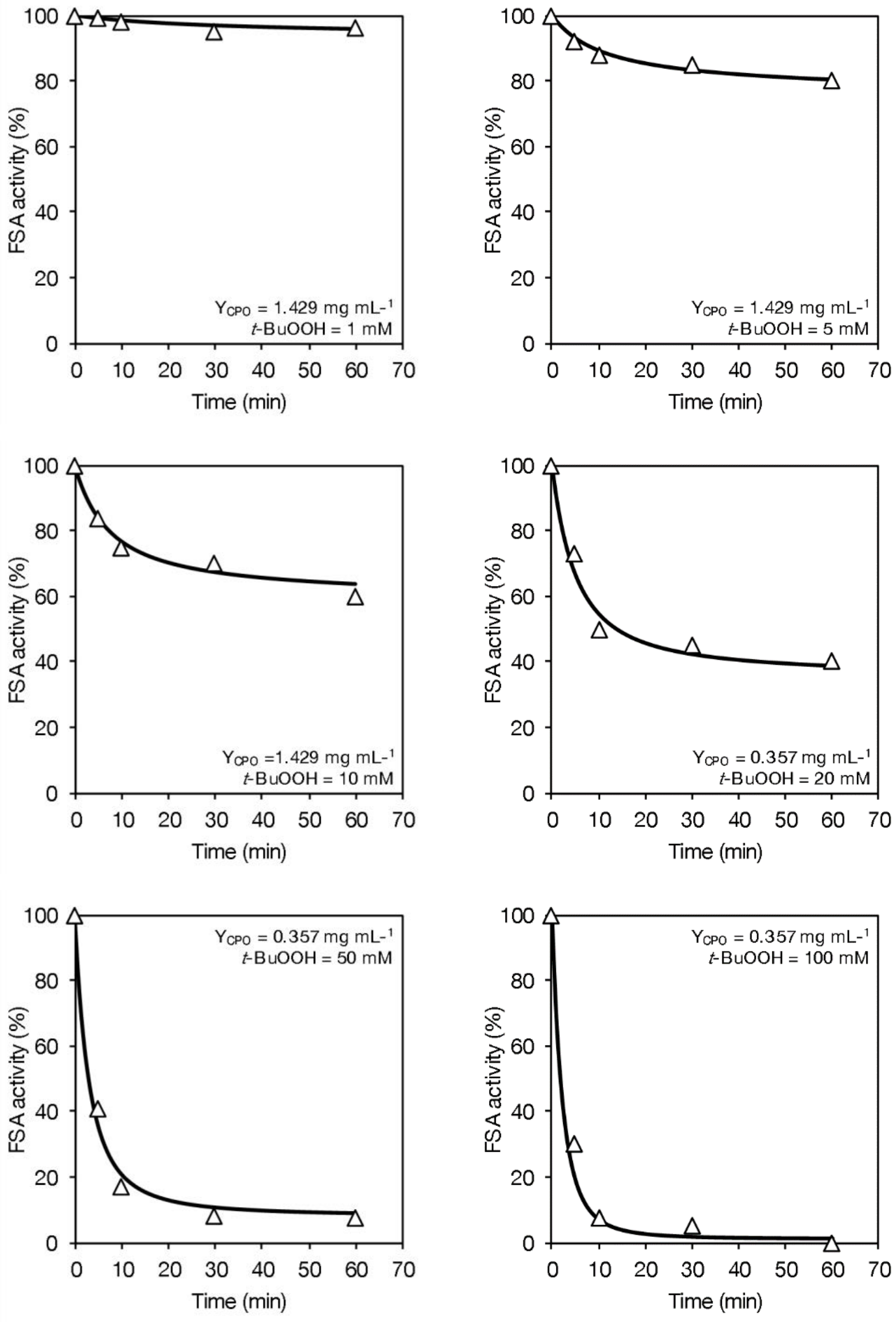

(It continues on the following page)

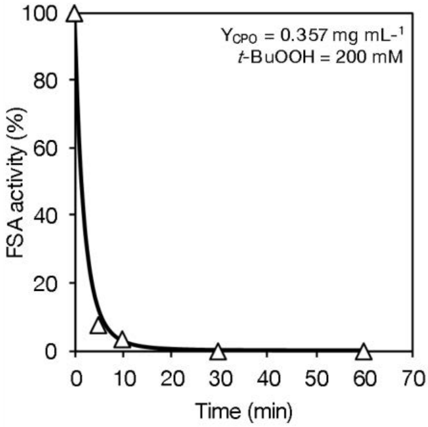

Figure 5.27. Inactivation of FSA catalyzed by the peroxyl radical formed from the degradation of *t*-BuOOH by CPO. 0.34 mgFSA mL^{-1} was used. The amount of CPO and *t*-BuOOH used is specified in each graph. All reactions were performed in 100 mM MES pH 6.5, 25 ºC. Experimental data: FSA activity (△); model simulation: FSA activity (➨).

Table 5.11. Estimated values of the parameters from Equation 5.48. 95% conf. intervals are given.

Parameter	Value	Units
k_1	$9.792 \cdot 10^{-2} \pm 3.57 \cdot 10^{-3}$	mM^{-1}

Regarding the second inactivation (kd_{FSA2}), incubations of FSA and CPO with different concentrations of *t*-BuOOH and DHA (Figure 5.28) were used to write Equation 5.49, which properly predicts the experimental data from Figure 5.29. Again, the inactivation was proposed as a linear function. In this case, it is not related to r_4, but to the oxidation of DHA by CPO, r_5. The estimated parameter value is given in Table 5.12.

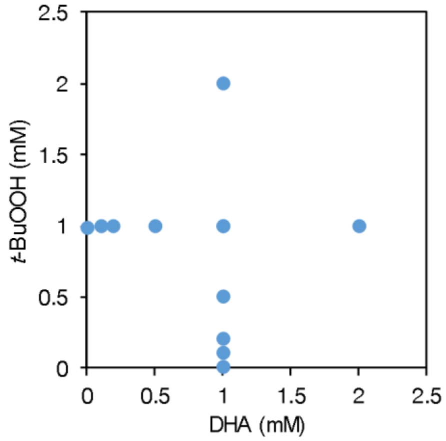

Figure 5.28. Experimental distribution of the incubations of FSA and CPO with different concentrations of *t*-BuOOH and DHA for the study of kd_{FSA2}.

$$kd_{FSA2} = k_2 \cdot r_5 \tag{5.49}$$

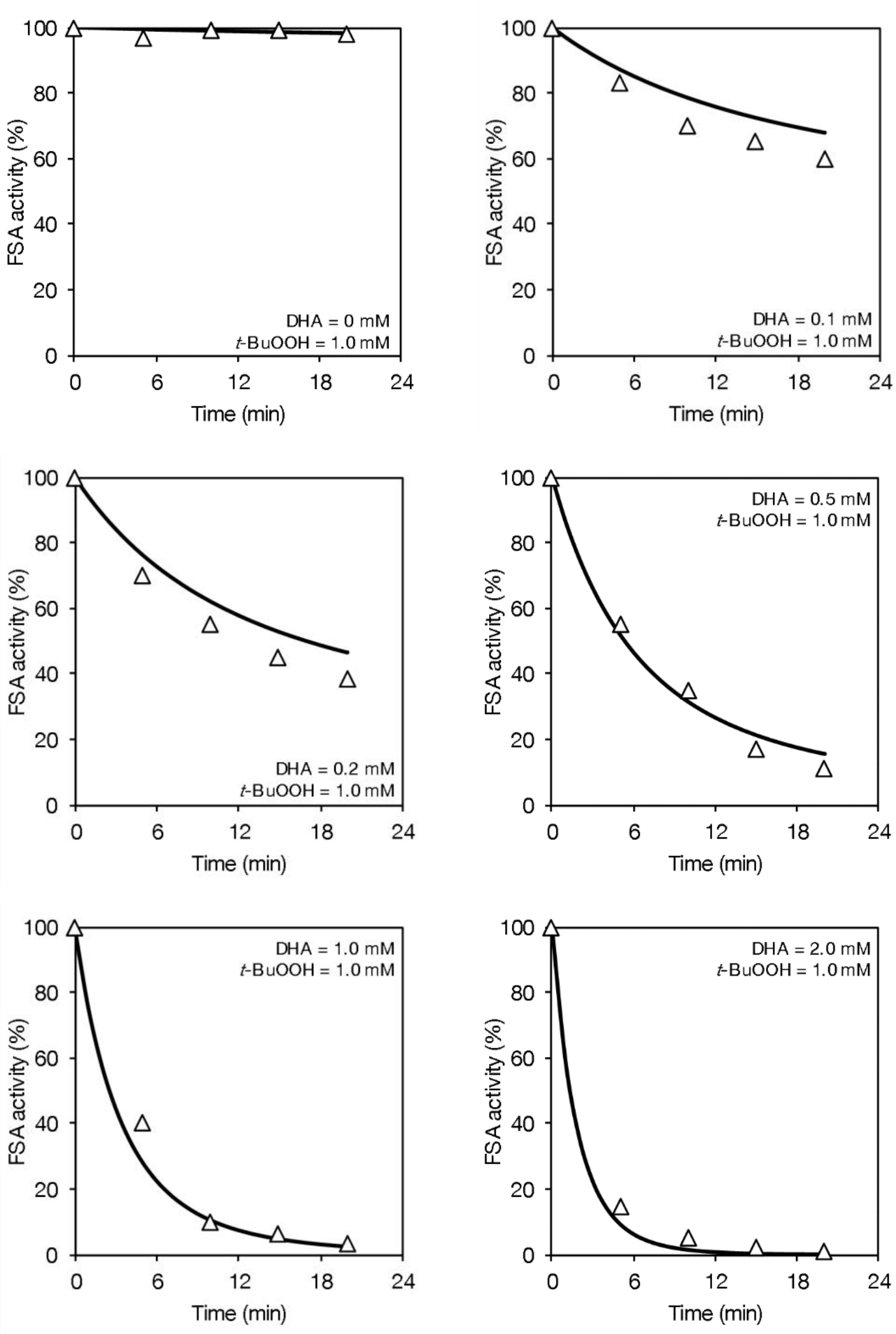

(It continues on the following page)

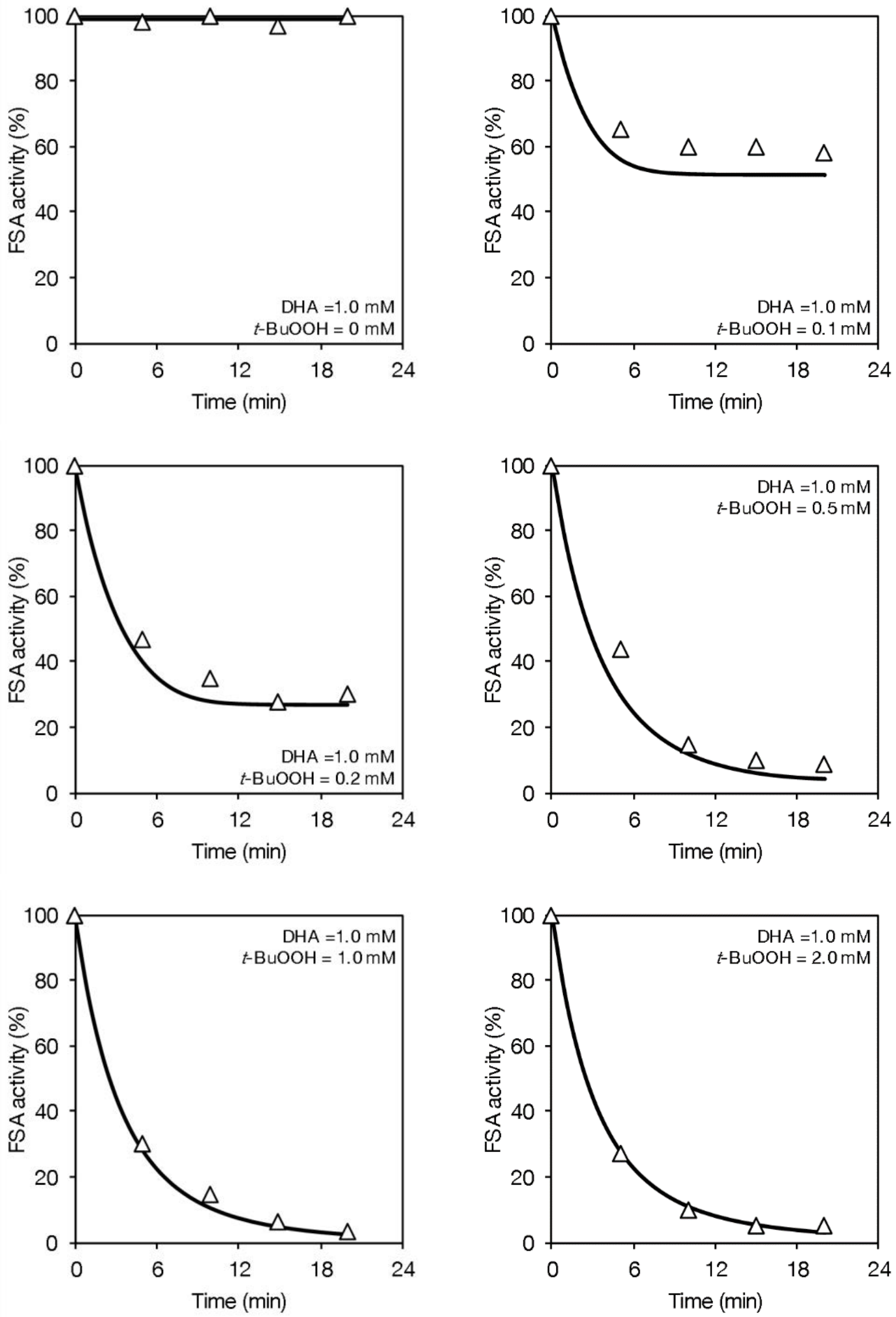

Figure 5.29. Inactivation of FSA by the oxidation of DHA in presence of *t*-BuOOH and CPO. 0.38 mgFSA mL^{-1} and 0.714 mgCPO mL^{-1} were used. The amount of DHA and *t*-BuOOH used is specified in each graph. All reactions were performed in 100 mM MES pH 6.5, 25 ºC. Experimental data: FSA activity (△); model simulation: FSA activity (➨).

Table 5.12. Estimated values of the parameters from Equation 5.49. 95% conf. intervals are given.

Parameter	Value	Units
k_2	6.704 ± 0.240	mM^{-1}

In order to confirm the obtained kinetic values for the inactivation of FSA, another series of experiments was performed, mixing different concentrations of β-OH, DHA, *t*-BuOOH, CPO and FSA, according to Table 5.13. Results from these experiments indicated: (1) kd_{FSA1} was confirmed to be a linear function of $2 \cdot r_4$ (2) kd_{FSA2} was not a linear function of r_5; (3) an increase of Y_{FSA} acts as a positive modulator effect on FSA activity, lowering kd_{FSA2}; (4) an increase of the DHA concentration leads a higher r_5, which produces a more rapid inactivation of FSA. However, DHA is a natural substrate of FSA and protects the active site of FSA from inactivation.

Therefore, Equation 5.49 should be rewritten to Equation 5.50. With this equation, the model is able to predict correctly the experimental data (Figure 5.30). Final estimated parameters are given in Table 5.14.

$$kd_{FSA2} = \frac{k_2 \cdot r_5}{b + r_5} \cdot (1 + Y_{FSA})^{-c} \cdot (1 + [DHA])^{-d} \tag{5.50}$$

Table 5.13. List of performed experiments for the study of kd_{FSA1} and kd_{FSA2}.

#	β-OH (mM)	DHA (mM)	*t*-BuOOH (mM)	CPO (mg mL^{-1})	FSA (mg mL^{-1})
A	10	20	25	0.714	6.67
B	10	20	25	1.429	6.67
C	10	20	25	0.714	33.33
D	10	20	25	0.714	46.67
E	10	20	25	0.714	20.00
F	10	20	25	0.357	46.67
G	10	20	25	0.179	46.67
H	10	20	25	0.000	46.67
I	10	20	25	1.429	46.67
J	0	20	25	0.714	46.67
K	20	20	25	0.714	46.67
L	10	0	25	0.714	46.67
M	10	20	0	0.714	46.67
N	10	20	125	0.714	46.67
O	0	20	25	0.714	46.67
P	0	20	25	0.714	46.67
Q	0	10	25	0.714	46.67
R	0	20	25	0.714	46.67
S	0	140	25	0.714	46.67
T	0	550	25	0.714	46.67
U	0	1000	25	0.714	46.67
V	0	1390	25	0.714	46.67

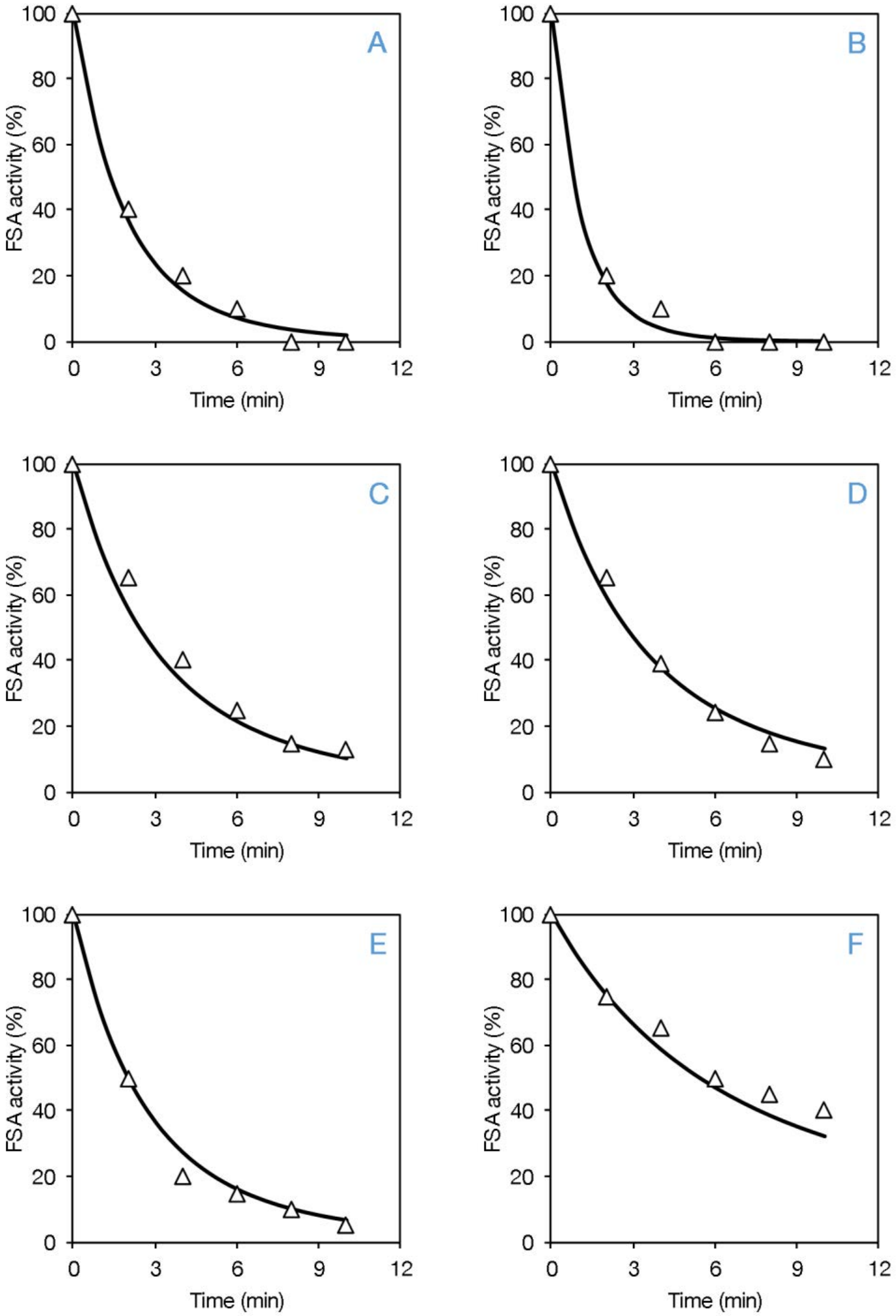

(It continues on the following page)

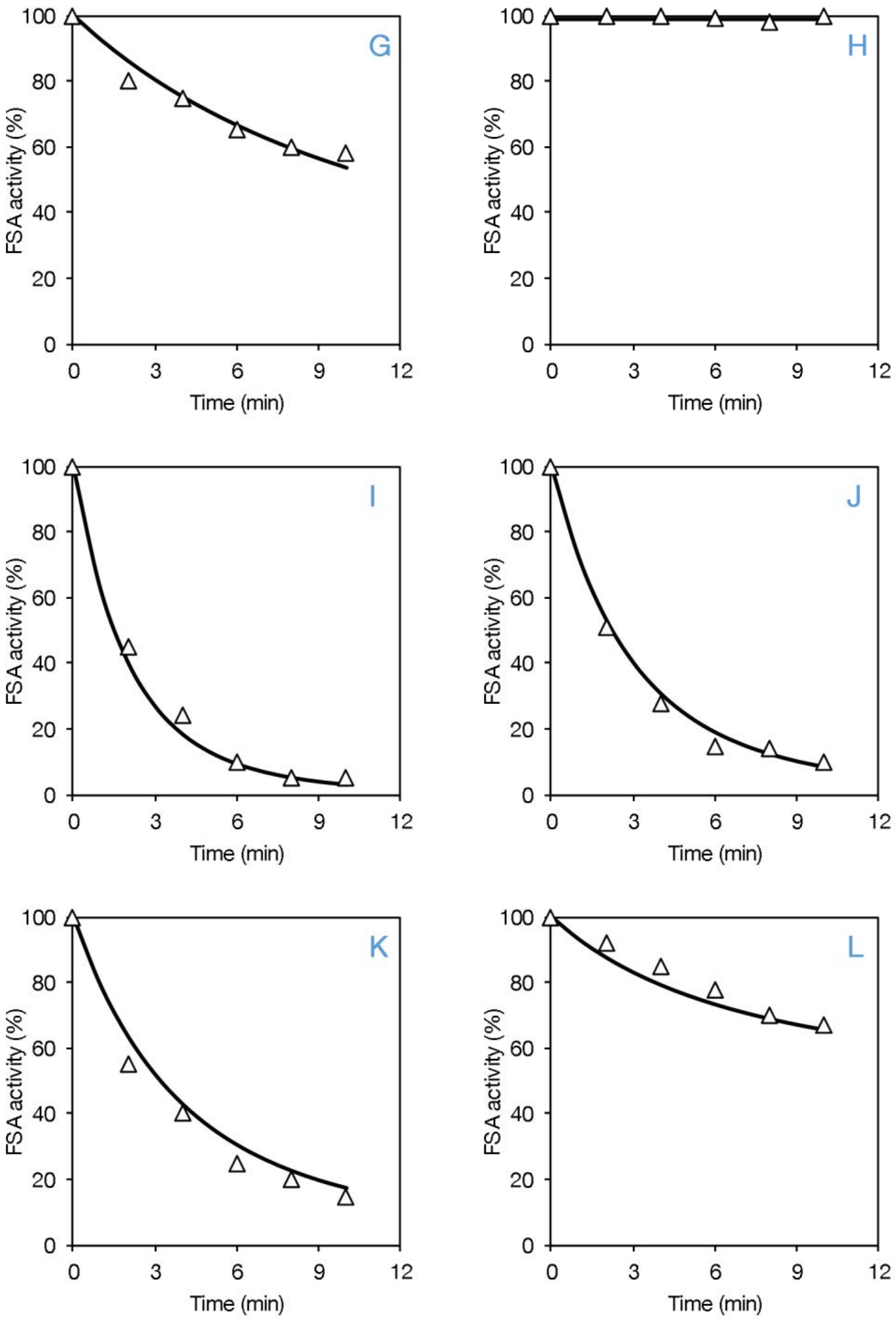

(It continues on the following page)

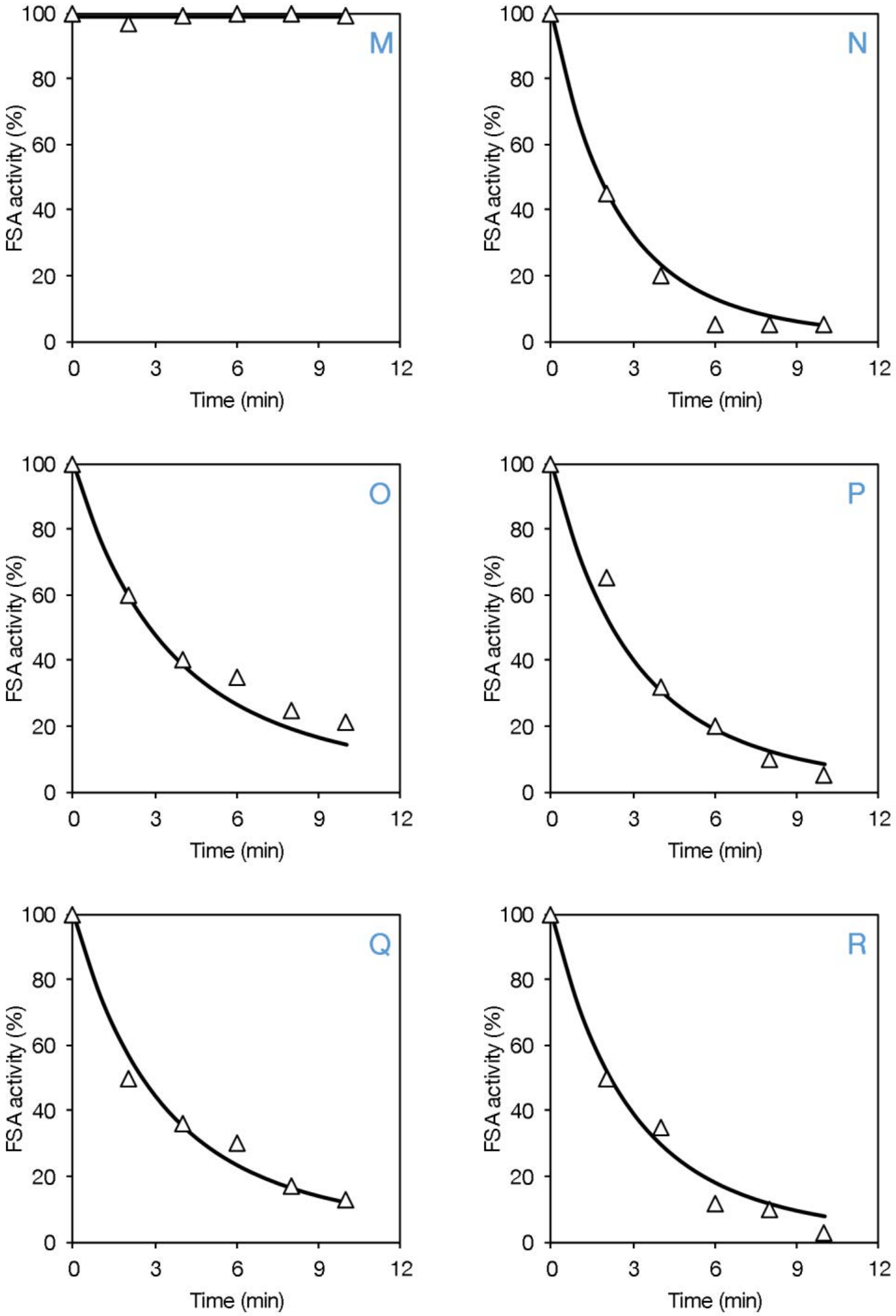

(It continues on the following page)

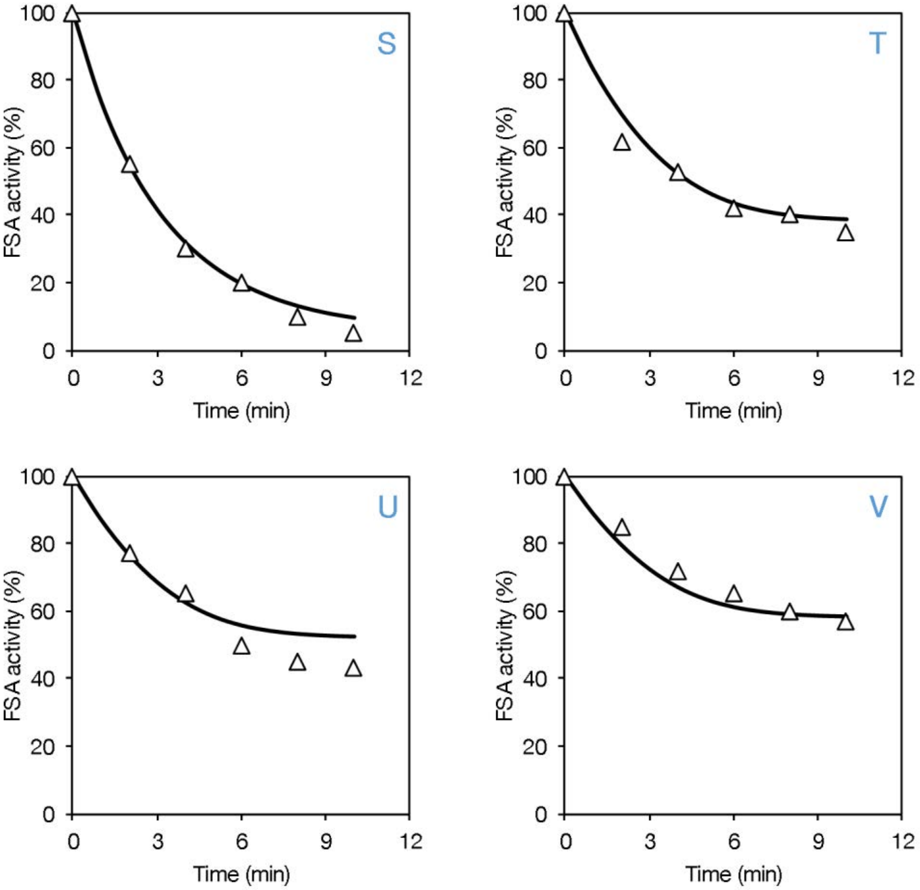

Figure 5.30. Inactivation of FSA by incubation with *t*-BuOOH, DHA, and CPO. β-OH was also added in some cases to check for any effect. The amount of each compound is specified in Table 5.13. All reactions were performed in 100 mM MES pH 6.5, 25 ºC. Experimental data: FSA activity (△); model simulation: FSA activity (➨).

Table 5.14. Estimated values of the parameters from Equation 5.50. 95% conf. intervals are given.

Parameter	Value	Units
k_2'	33.75 ± 4.20	min^{-1}
b	3.454 ± 0.413	$mM \cdot min^{-1}$
c	$3.852 \cdot 10^{-1}$ ± $7.0 \cdot 10^{-3}$	-
d	$5.314 \cdot 10^{-1}$ ± $1.42 \cdot 10^{-2}$	-

5.3.6 Model validation

Finally, after estimation of all kinetic parameters, a validation step of the model is required. To this end, several reactions were performed. β-OH, *t*-BuOOH, and CPO were fixed at 47.0 mM, 77.7 mM and 0.714 mg mL^{-1}, respectively. The alcohol and peroxide concentrations were set at high values in order to increase the productivity of preFagomine. According to the results presented along this chapter, DHA concentration and FSA load are the more important variables to determine, since the inactivation of FSA is extremely related to them. Thus, up to seven reactions were carried out with different concentrations of these two variables, as it can be observed from Figure 5.31. The model predicted all the data correctly. However, very low concentrations of preFagomine were obtained.

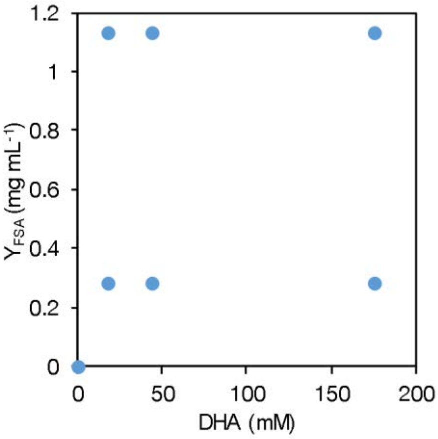

Figure 5.31. Experimental distribution of the reactions used for model validation.

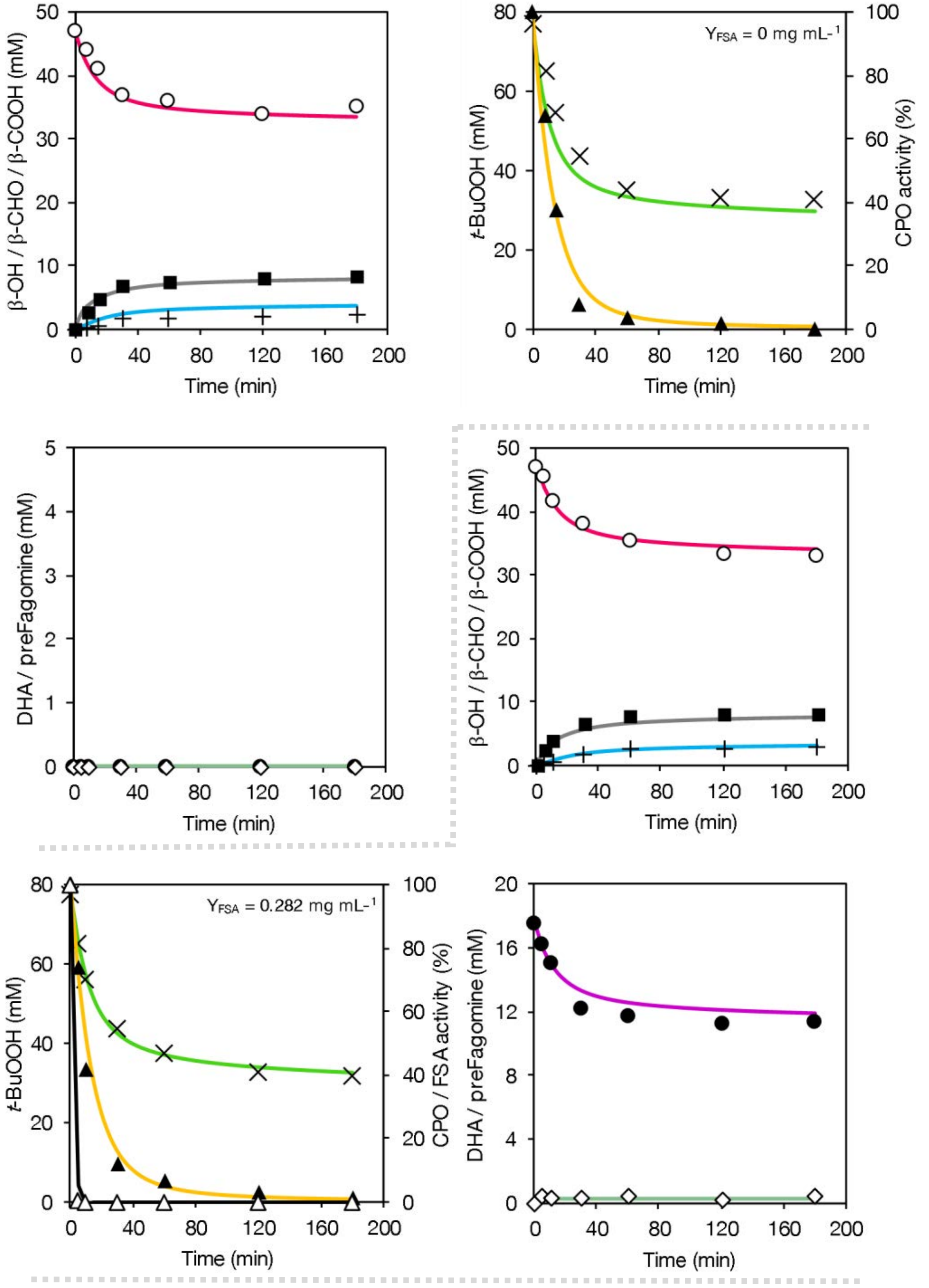

(It continues on the following page)

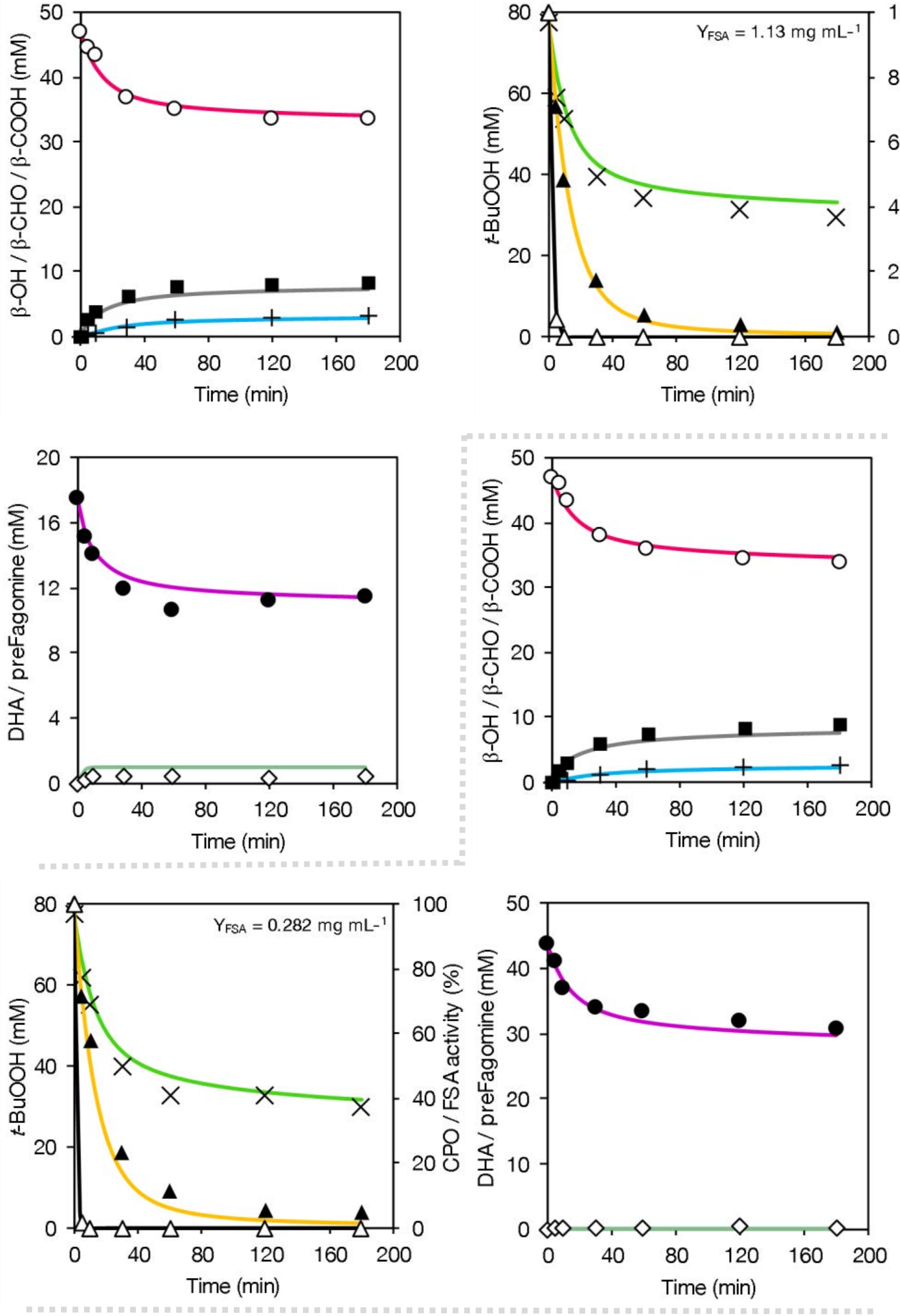

(It continues on the following page)

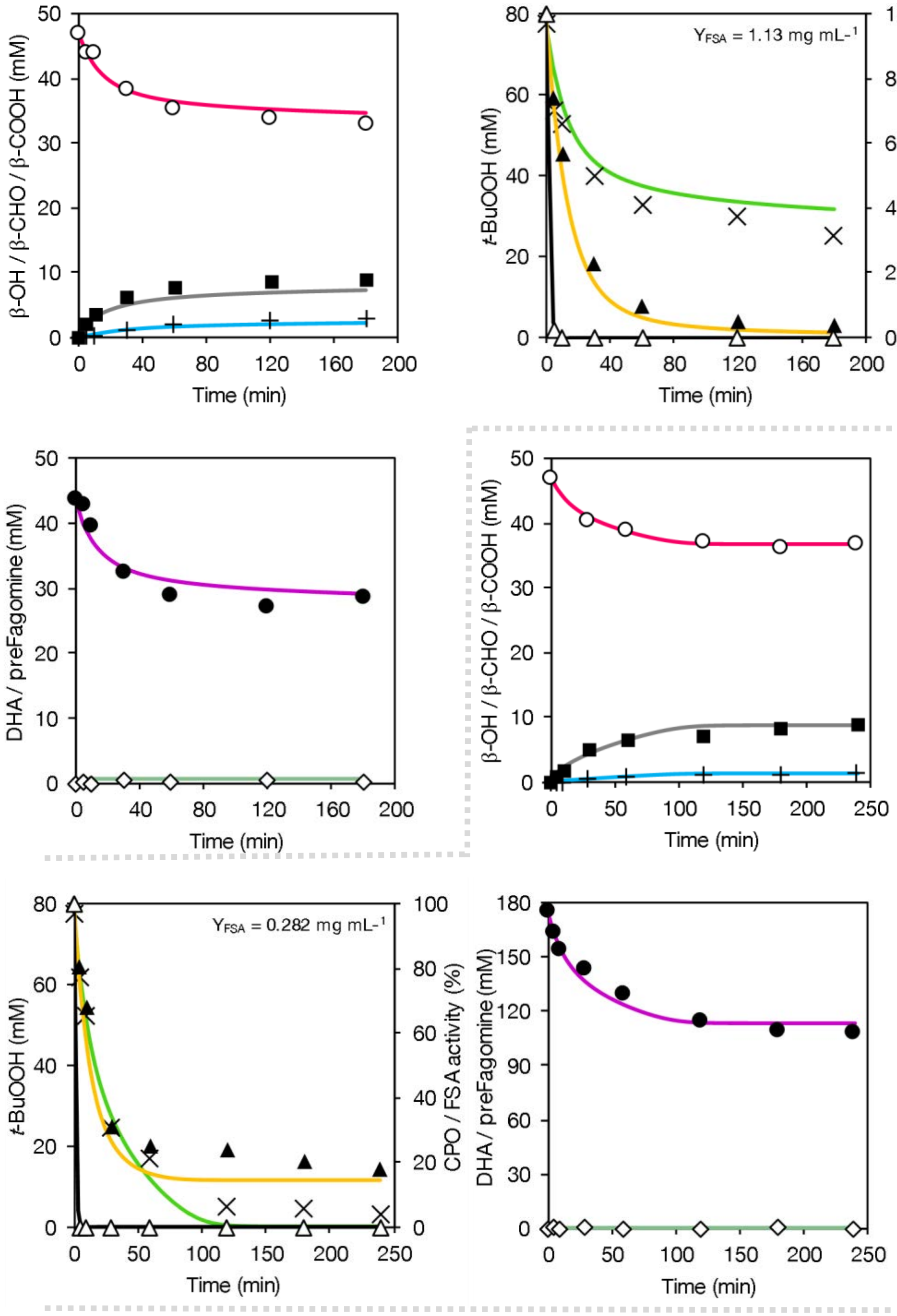

(It continues on the following page)

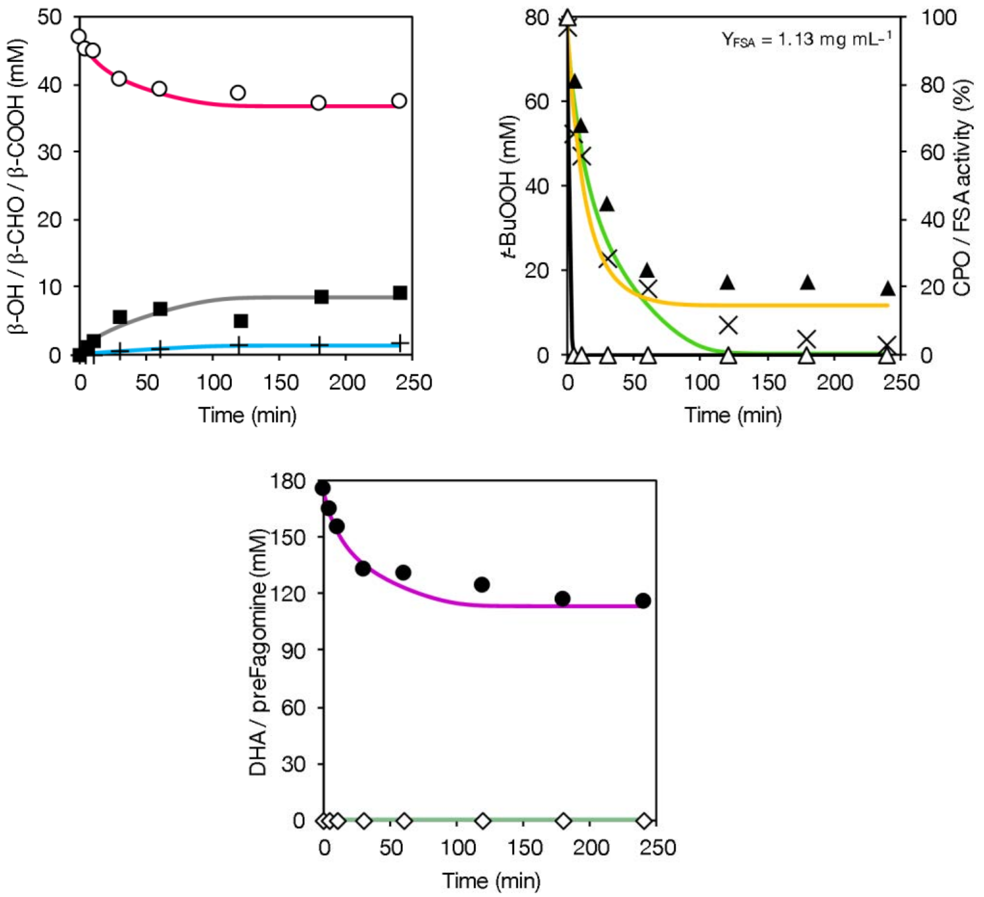

Figure 5.32. Model validation of the CPO/FSA-catalyzed synthesis of preFagomine. The dotted line separates individual experiments. 47.0 mM β-OH, 77.7 mM *t*-BuOOH, and 0.714 mgCPO mL^{-1} were used. The amount of FSA used is detailed in each reaction (three graphs). All reactions were performed in 100 mM MES pH 6.5, 25 ºC. Experimental data: β-OH (○), β-CHO (■), β-COOH (+), DHA (●), *t*-BuOOH (×), preFagomine (◇), CPO activity (▲), FSA activity (△); model simulation: β-OH (➨), β-CHO (➨), β-COOH (➨), DHA (➨), *t*-BuOOH (➨), preFagomine (➨), CPO activity (➨), FSA activity (➨).

5.4 Conclusions

A kinetic model for the coupled reactions of CPO and FSA to produce preFagomine has been developed. Each reaction has been separated from the whole system in order to study the kinetic individually, avoiding undesired interactions between reactions which could hinder the analysis of the results. Up to 7 reactions have been investigated, estimating their kinetic parameters: degradation of peroxide, chemical reaction, amino aldehyde oxidation, alcohol oxidation, DHA oxidation, aldol addition, retroaldol addition. Moreover, the inactivation of both enzymes has been also discussed. Finally, the kinetic model has been validated, although a very low amount of preFagomine has been obtained. This could be overcome by model exploitation to optimize the reaction conditions, increasing the product yield. Besides, the use of immobilized enzymes could enhance the compatibility between both enzymes, lowering their inactivation rates. This will be further discussed in the fifth chapter.

5.5 References

[1] A. S. Bommarius, *Annu. Rev. Chem. Biomol. Eng.* **2015**, *6*, 319–345.

[2] A. Illanes, C. Altamirano, L. Wilson, in *Enzym. Biocatal. Princ. Appl.* (Ed.: A. Illanes), Springer, Dordrecht, Netherlands, **2008**, pp. 107–153.

[3] J. Berg, J. Tymoczko, L. Stryer, in *Biochemistry*, W H Freeman, New York, USA, **2002**, pp. 117–144.

[4] L. Michaelis, M. L. Menten, *Biochem. Z.* **1913**, *49*, 333–369.

[5] K. A. Johnson, R. S. Goody, *Biochemistry* **2011**, *50*, 8264–8269.

[6] J. G. Robertson, *Biochemistry* **2005**, *44*, 5561–5571.

[7] R. L. Stein, in *Kinet. Enzym. Action Essent. Princ. Drug Hunters*, John Wiley & Sons, NJ, USA, **2011**, pp. 141–168.

[8] W. W. Cleland, *Biochim. Biophys. Acta* **1963**, *67*, 104–137.

[9] W. W. Cleland, *Annu. Rev. Biochem.* **1967**, *36*, 77–112.

[10] A. G. Marangoni, in *Enzym. Kinet. A Mod. Approach* (Ed.: A.G. Marangoni), John Wiley & Sons, NJ, USA, **2003**.

[11] K. A. Johnson, *FEBS Lett.* **2013**, *587*, 2753–2766.

[12] H. Lineweaver, D. Burk, *J. Am. Chem. Soc.* **1934**, *56*, 658–666.

[13] R. G. Duggleby, J. F. Morrison, *Biochim. Biophys. Acta* **1977**, *481*, 297–312.

[14] R. G. Duggleby, C. Wood, *Biochem. J.* **1989**, *258*, 397–402.

[15] C. T. Goudar, S. K. Harris, M. J. McInerney, J. M. Suflita, *J. Microbiol. Methods* **2004**, *59*, 317–326.

[16] J. Almquist, M. Cvijovic, V. Hatzimanikatis, J. Nielsen, M. Jirstrand, *Metab. Eng.* **2014**, *24*, 38–60.

[17] G. Sin, J. M. Woodley, K. V. Gernaey, *Biotechnol. Prog.* **2009**, *25*, 1529–1538.

[18] G. L. Kedderis, P. F. Hollenberg, *J. Biol. Chem.* **1983**, *258*, 12413–12419.

[19] L. Casella, S. Poli, M. Gullotti, C. Selvaggini, T. Beringhelli, a Marchesini, *Biochemistry* **1994**, *33*, 6377–6386.

[20] H. B. Dunford, *Peroxidases and Catalases: Biochemistry, Biophysics, Biotechnology and Physiology*, John Wiley & Sons, NJ, USA, **2010**.

[21] M. Schürmann, G. A. Sprenger, *J. Biol. Chem.* **2001**, *276*, 11055–11061.

[22] W. Chamulitrat, N. Takahashi, R. P. Mason, *J. Biol. Chem.* **1989**, *264*, 7889–7899.

[23] J.-B. Park, D. S. Clark, *Biotechnol. Bioeng.* **2006**, *93*, 1190–1195.

[24] M. Sudar, Z. Findrik, C. Lozano, *J. Biotechnol.* **2013**, *167*, 191–200.

6 Immobilization of CPO and FSA on functionalized carriers: agarose and magnetic nanoparticle clusters

6.1 Introduction

Soluble enzymes need to be immobilized in order to facilitate its reuse in industrial reactors. Additionally, some other enzyme properties such as operation and storage stability, and selectivity towards non-natural substrates can be improved and/or changed.[1] Moreover, enzyme immobilization facilitates product recovery and avoids product contamination by the enzyme, reducing allergenicity charge in the final product, which has capital importance for the pharmaceutical industry.[2] Every each enzyme has different structural features and, therefore, no universally applicable method for immobilization has been developed. The immobilization procedure is selected especially regarding the enzyme characteristics –surface functional groups, pH stability, etc.– and the desired support-enzyme attachment (i.e. physical adsorption, ionic/affinity linkages, irreversible stable covalent bonds).[3] It determines the overall immobilization efficiency. *Immobilization yield* is the parameter that refers to the percentage of the enzyme mass that has been immobilized. *Retained activity* describes the final activity of the immobilized enzyme, as some activity loss by the binding process may occur.

The carrier structure also influences the immobilization process, according to its chemical composition, functional groups, pore size, and maximum enzyme load capacity, among others.[4] It affects the final biochemical, mechanical and kinetic properties of the immobilized derivative.[5] The presented work in this chapter is particularly focused on the use of a conventional carrier (agarose) and a more trending support (magnetic nanoparticle clusters) for the immobilization of the target CPO and FSA, which have shown in previous pages some stability incompatibilities in the coupled system. The use of the latter carrier with the application of magnetic forces for the recovery of immobilized biocatalysts is becoming a novel field of interest in biotechnology.[6]

6.1.1 Agarose

Enzymes are generally unstable in hydrophobic environments and, therefore, hydrophilic materials are the most employed supports for enzyme immobilization.[7] A well-known hydrophilic, inert (to prevent uncontrolled carrier-enzyme interactions) and highly porous support are agarose-based beads.[8] These polysaccharide beads show low mechanical resistance to magnetic stirring; however, their flexibility allows high resistance to mechanical stirring.[9]

Agarose is commercially available as a cross-linked matrix with increased mechanical resistance. Its physical or chemical cross-linking has been reported in the literature for decades.[10–13] It can be purchased within a wide range of particle diameters, depending on the particular application required.

For a specific immobilization, some reactive groups may be incorporated into the support or the enzyme. In the case of agarose, the presence of numerous hydroxyl groups on its surface permits an easy functionalization with a vast variety of reagents. To this end, many protocols for agarose derivatization have been developed. For example, glyoxal agarose is an immobilization carrier based on agarose functionalized with aldehyde groups, suitable to get a very strong support-enzyme linkage by multipoint covalent attachment.[14] The binding is expected to occur through Schiff-base complexes, which may be very stable after bond reduction with periodate.

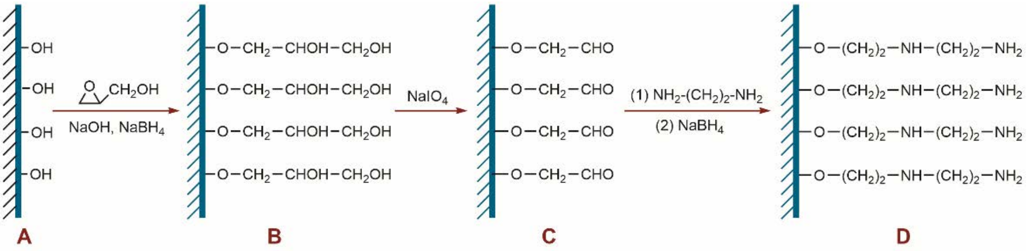

Figure 6.1. Agarose derivatization to synthesize MANA-agarose gels.

Glyoxal agarose can be prepared by etherification of the primary hydroxyl groups of the support with glycidol to introduce diols (glyceryl agarose), which are later oxidized with sodium periodate to obtain the aldehyde group (Figure 6.1).[15] The aldehyde group can be further converted into amino groups using ethylenediamine; this is commonly called MANA-agarose (monoaminoethyl-*N*-aminoethyl agarose).[16] In this case, the covalent enzyme binding is driven by prior carbodiimide activation of carboxyl groups of the protein.

Another habitual derivatization of agarose consists in the introduction of divalent metals –Co^{2+}, Ni^{2+}, Zn^{2+}– on its surface to bind the histidine residues from a His-tagged protein.

The metal functionalization is achieved by the use of metal-chelating agents, like iminodiacetic acid (IDA). This type of support is commonly employed in purification by affinity chromatography; thus, the enzyme can be purified and immobilized in a single step.[17]

6.1.2 Magnetic nanoparticle clusters

Enzyme immobilization onto magnetic carriers has been widely proposed to prepare biocatalysts easy-to-separate from the reaction medium[18–20] and, noteworthy, superparamagnetic nanoparticles are a promising alternative. Superparamagnetism is a phenomenon related to ferromagnetic particles when their size is reduced below a certain limit where thermal excitation induces rapid fluctuations of the nanoparticles' magnetic moments. The superparamagnetic limit is around 20 nm for soft-magnetic materials such as frequently used magnetic iron oxides. The use of the superparamagnetic nanoparticles is beneficial for dispersing the magnetic carriers into a liquid reaction medium. As they do not show spontaneous magnetic moments, they do not agglomerate due to magnetic dipole-dipole interactions like larger ferromagnetic particles. Inexpensive magnetic iron oxides (maghemite γ-Fe_2O_3 or magnetite Fe_3O_4) are usually used as magnetic materials for the carriers.[21]

Enzyme immobilization onto superparamagnetic nanoparticles has emerged as a promising approach rendering hybrid enzyme-particle complexes useful in biomedicine, biosensing, and bioremediation.[22–24] Recently, their possible application in biotransformations is being evaluated because, in addition to their easy recovery under a magnetic field, the bioconversions with those immobilized biocatalysts would behave like homogeneous catalysis; the easy dispersibility of the particles facilitates contact with the substrate, avoiding mass-transfer limitations.[25–28] As with other immobilization methods, the biocatalyst stability is expected to be improved under reactive conditions.

Effective magnetic manipulation of enzyme-loaded carriers requires strong magnetic force acting on the individual magnetic particle in a magnetic-field gradient.[29] The magnetic force should prevail over the thermal energy and hydrodynamic drag in the complex reaction medium. It is proportional to both particle's magnetization and volume. Since the magnetization is mainly defined by the type of magnetic material, the particle size has a crucial impact on the magnetic force. Due to the small size, the force acting on the individual superparamagnetic nanoparticles in the magnetic-field gradient is generally too weak to enable their efficient magnetic separation. The conventional techniques of magnetic separation are based on relatively large micron-sized beads containing superparamagnetic nanoparticles dispersed in a polymer matrix.[30] Such superparamagnetic microspheres display good magnetic responsiveness; however, their disadvantage is in the relatively low specific surface. An excellent compromise between the smallest possible size of the carrier particles that still enables effective magnetic guidance and the large surface area is achieved by assembling individual superparamagnetic nanoparticles into clusters. Such magnetic nanoparticles clusters (mNC) with the size of approximately 100 nm retain the superparamagnetic nature of the individual nanoparticle, whereas their relatively large volume enables their effective manipulation with the magnetic field.[31]

6.1.3 CPO and FSA immobilization

All the above characteristics may contribute to significant bioprocess improvements in the case of poorly stable enzymes performing complex biotransformations. This is the case of CPO and FSA, which require an improvement in stability in order to achieve a higher preFagomine yield due to their inactivation in the reaction conditions. However, although a huge amount of articles about enzyme immobilization are reported, it is difficult to choose the proper immobilization method and support for each case. Hence, here various techniques and carriers are evaluated for the immobilization of both enzymes, analyzing the yield and final activity of each derivative.

6.1.3.1 CPO

Several procedures for CPO immobilization have been reported, including encapsulation,[32,33] adsorption on mesoporous materials,[34,35] on celite,[36] and cross-linked enzyme aggregates (CLEA),[37,38] with some stability improvements. Covalent methods for CPO have been developed, most of them involving the formation of bonds between the support surface and the amino groups from lysine residues of CPO. Nevertheless, immobilization yields were relatively low, probably because CPO surface is not rich in Lys, but in Asp and Glu.[39] To take advantage of its structure, in the current research group, it was previously performed the immobilization of CPO via carboxyl groups of the protein surface, using MANA-agarose gels, with high yield and nearly 50% retained activity.[40] These supports contain very low pK primary amino groups, and hence they are very suitable supports for immobilization of enzymes at low pH values.[16]

Immobilization process consisted of a previous step of ionic adsorption between enzyme–support, followed by covalent attachment using carbodiimide.

In the same article, CPO was also immobilized through its sugar moieties (glycoprotein) on MANA-agarose. These sugar residues were oxidized using sodium periodate to aldehyde groups, which were reactive to amines from MANA-agarose. Similar yield and activity were achieved with this method, but this latter derivative was less stable to peroxide inactivation. Finally, the native CPO covalently attached to MANA-agarose was used as a biocatalyst for the oxidation of Cbz-ethanolamine to Cbz-glycinal, with higher substrate conversion and stability than the soluble enzyme.[40]

Concerning magnetic nanoparticles, Wang et al. reported the preparation of chloroperoxidase-conjugated magnetic nanoparticles with iron oxide core and polymer shell for the sulfoxidation of thioanisole assisted by H_2O_2.[41] Moreover, Cui et al immobilized CPO on the surface of Fe_3O_4 functionalized with avidin and biotin for the decolorization of soluble aniline blue.[42] In both cases, not much data about immobilization yield or activity recovery are presented and, although stability improvement is claimed, reaction cycles were performed at very low substrate concentration within only a few minutes.

6.1.3.2 FSA

Regarding the immobilization of aldolases, only a few works are reported in the literature. For example, D-fructose-1,6-bisphosphate (FBP) aldolase from pig muscle was covalently attached to a silica-based support functionalized with aldehyde groups.[43] Another FBP aldolase, from *Haloferax mediterranei* was immobilized by cross-linking in a proteinic matrix with bovine serum albumin (BSA), which protected the enzyme from inactivation.[44] More recently, 2‑Deoxy‑D-ribose-5-phosphate aldolase (DERA) has been immobilized in polymeric thin films.[45]

In the research group, there is also some related work on aldolase immobilization. FucA has been immobilized on glyoxal-agarose gels by multipoint covalent attachment,[46] and reversibly on metal-chelated supports, such as CoIDA (IDA-functionalized agarose with cobalt) and NiIDA (nickel).[17] The immobilized derivatives were applied in the aldol addition of DHAP to *N*-Cbz-alaninal. RhuA has been also immobilized on CoIDA,[47] and onto gold nanoparticles without the need of any coupling agent.[48]

Only a few publications on the immobilization of the model aldolase for this work, FSA, have been found in the literature.[49] They correspond to the use of layered double hydroxide (LDH) as a carrier. LDH is an inorganic nanostructure with positively charged layers composed of metal hydroxides that bind the enzyme in between. Another variant of this procedure was further developed: polysaccharide-layered double hydroxide–aldolase biohybrid beads.[50] This encapsulation of FSA-LDH in polysaccharide beads leveraged the interesting properties of a polysaccharide support.

6.1.4 Objective

In the present chapter, the immobilization of CPO on MANA-agarose is reproduced from literature conditions.[40] The immobilized biocatalyst is tested in the β-OH oxidation to yield the target β-CHO, and compared to the soluble enzyme. Besides, a systematic study of the CPO immobilization onto an innovative type of superparamagnetic carriers is presented.

This study is the fruit of the collaboration with the Jožef Stefan Institute, Nanos SCI, and the University of Trieste. They synthesized and characterized the carriers with assembling around 100 individual superparamagnetic iron-oxide nanoparticles with the size of ~10 nm into the spherical cluster with the size of ~100 nm.[51–54] After the assembly, the nanoparticle clusters are coated with a silica layer which improves the structural stability and enables facile further functionalization with alkoxysilanes. The technology for the preparation of stable colloidal mNC suspensions was developed by Nanos SCI.[52] In this work, variously functionalized clusters were linked to the enzyme through different amino acid residues on its surface. The obtained hybrid biocatalysts are also tested in the β-OH oxidation.

The second block of results includes the immobilization of FSA on CoIDA, through the His-tag of the enzyme (recombinant FSA A129S) in one step purification-immobilization. The use of mNC to attach FSA is also investigated, as an extension of the above mentioned collaboration, also joint by a lab partner from the research group, Luis Miguel Vázquez. The derivatives are used in the DHA aldol addition to β-CHO to render preFagomine.

6.2 Materials and methods

6.2.1 Materials

N-(3-dimethylaminopropyl)-*N'*-ethylcarbodiimide, 4-pentynoic acid, propargylamine, polyacrylic acid (PAA, 25 kDa), (3-aminopropyl)triethoxysilane (APS; silane-NH_2, 99%), ethylenediamine, ethyl acetate (EA), polyvinyl pyrrolidone (PVP, 40 kDa), and trifluoroacetic acid were obtained from Sigma Aldrich (St. Louis, MO, USA). Iron (III) sulfate hydrate, iron (II) sulfate heptahydrate (ACS, 99%), citric acid (99%), tetraethoxysilane (TEOS, 99.9%), NH_4OH (28-30%) was supplied by Alfa Aesar (Lancashire, UK). (Hydroxy(polyethyleneoxy)propyl) triethoxysilane (silane-PEG), triethoxysilylpropylmaleamic acid (silane-COOH), *O*-(propargyl)-*N*-(triethoxysilylpropyl) carbamate (commercial silane-C≡CH), 3-mercaptopropyltrimethoxy silane (silane-SH), *N*-(trimethoxysilylpropyl) ethylenediaminetriacetate (silane-EDTA) were purchased by Gelest, USA. 10% cross-linked agarose beads, and IDA-agarose were supplied by Agarose Bead Technologies, ABT (Madrid, Spain). All other reagents were commercial products of analytical grade. Silane-C≡CH and silane-N_3 were synthesized in collaboration with Dr. Stane Pajk; the protocol is described in the Appendix. FSA A129S was obtained from *E.coli* by fed-batch fermentation and purified by affinity chromatography (CoIDA-agarose), as described in Chapter 4. Other reagents are already mentioned in previous chapters.

6.2.2 Activity assays

6.2.2.1 CPO

The enzymatic activity of CPO was measured following the activity test detailed in Materials and Methods in Chapter 3. Note (a) when using CPO immobilized on MANA-agarose, 100 µL of sample were added in a total volume of 2 mL at the same reagents concentrations. Magnetic stirring inside the cuvette was used; (b) no interference of the agarose/nanoparticle support was observed in the assay when measuring the immobilized enzyme activity. The standard deviation was calculated from duplicated measurements from a single sample.

6.2.2.2 FSA

The activity of soluble FSA and FSA immobilized on CoIDA-agarose was measured according to the activity test described in Chapter 4. In the case of using immobilized enzyme, 100 µL of sample were added in a total volume of 2 mL at the same reagents concentrations, and magnetic stirring was used.

The retained activity from mNC-FSA derivatives was quantified using alternative tests employing either the natural substrate or the target aldol addition. Two assays were developed: (**A**) The decoupled activity test was performed as follows: 50 mM imidazole, 50 mM F6P and 0–0.062 U FSA mL^{-1} (soluble or immobilized) were mixed for 50 min in a total volume of 650 µL. Using a magnetic field, mNC were separated (if applicable), and the SN was ultrafiltrated using 10 KDa centrifugal filters to remove any soluble enzyme molecule. 450 µL of the filtrated liquid was added to a spectrophotometric cuvette, in which 50 µL of a mixture with NADH and TPI/GPD was present. The final concentrations in the cuvette were 1 mM NADH and 5 U TPI/GPD. The decay rate of the absorbance at 340 nm was used to quantify the FSA activity. (**B**) The aldol addition reaction was monitored by HPLC. The immobilized enzyme was concentrated up to 50 µL by removing of supernatant using a magnetic field. This volume was added to the reaction mixture, containing 40 mM β-CHO and 100 mM DHA in 50 mM HEPES pH 8.0, in a final volume of 1 mL. It was left for 90 min at 30 °C, 1000 rpm of orbital stirring. The reaction was stopped by pH change: 100 µL of sample was mixed for 1 min with 150 µL of 1 M sodium phosphate buffer pH 2.5. The sample was neutralized with 150 µL of 2 M sodium phosphate buffer pH 7.0. The percentage of activity was determined by HPLC analysis of the preFagomine concentration.

6.2.3 Preparation of immobilization supports

6.2.3.1 MANA-agarose gels

MANA-agarose support was prepared from agarose gels by three-step chemical modification:[15,16] (1) etherification of 10% cross-linked agarose gels with glycidol obtaining glyceryl-agarose, (2) periodate oxidation of glyceryl-agarose leading to glyoxal-agarose, and (3) reaction of glyoxal-agarose gels with ethylenediamine and further reduction with sodium borohydride ($NaBH_4$).

15 ml of agarose gels (16.05 g) were vacuum-filtered and washed with distilled water and suspended in 11.6 mL of a solution that contained NaOH, $NaBH_4$, and glycidol at final concentrations of 0.32 M, 0.14 M and 2.04 M, respectively. The mixture was left under mild stirring for 19 h at room temperature. Glyceryl-agarose gel was obtained after vacuum-filtering and washing with distilled water.

The next step was the oxidation of the 15 mL of obtained glyceryl-agarose with 30 mL of 0.1 M sodium periodate (200 $NaIO_4$ µmoles mL^{-1} of glyceryl-agarose) in a final volume of 180 mL in H_2O. The mixture was left under gentle stirring until $NaIO_4$ was consumed, which corresponds to the formation of aldehyde groups on the support. In order to monitor the oxidation, aliquots of supernatant were periodically withdrawn and analyzed by a colorimetric parallel reaction. The reaction consisted of a mixture of 1 mL of potassium iodide (KI) 10% w/v in H_2O, 1 mL of saturated sodium hydrogen carbonate ($NaHCO_3$) and 1 mL of glyceryl-agarose oxidation supernatant. The iodine liberated from KI by oxidation with the remaining $NaIO_4$ in presence of $NaHCO_3$ was monitored at 500 nm. The approximated time for the oxidation of glyceryl-agarose was nearly 30-45 min. The glyoxal-agarose mixture was vacuum-filtered and washed with distilled water.

The final step was the reaction between aldehyde groups from glyoxal-agarose and ethylenediamine. This reaction, which involves the formation of unstable Schiff bases, lasted around 2 hours. For this purpose, the 15 mL of obtained glyoxal-agarose were suspended in 135 mL of 0.1 M bicarbonate buffer pH 10.0, 2 M ethylenediamine. After 2 h under mild stirring, 1.5 g of $NaBH_4$ was added at final concentration of 0.26 M in order to allow the complete conversion of Schiff bases into stable secondary amino bonds. $NaBH_4$ also ensured the complete reduction of the few still remaining aldehyde groups into inert hydroxyl compounds.

The obtained MANA-agarose gels were vacuum filtered and washed first with 150 ml of 100 mM sodium acetate pH 5.0 (1 M NaCl), then with 150 mL of 0.1 M sodium bicarbonate pH 10.0 (1 M NaCl), and finally with 750 ml of distilled water.

6.2.3.2 CoIDA-agarose

CoIDA-agarose gels were prepared from high-density metal-chelated supports (20–40 µmol divalent metal mL^{-1} gel, with IDA as the residue to chelate the metal). In order to load the metal, 100 mL of IDA-agarose were incubated with 300 mL of 0.2 M $CoCl_2$ pH

4.7 for 12h.[17] After washing with water to remove the excess of metal, the support was stored in EtOH 20% v/v at 4 °C.

6.2.3.3 Functionalized silica-coated mNC

mNC was obtained by the self-assembly of primary maghemite nanoparticles followed by coating of the magnetic cluster with a layer of silica. In brief, maghemite (γ-Fe_2O_3) nanoparticles were synthesized using precipitation of Fe^{3+}/Fe^{2+} from an aqueous solution. The nanoparticle clusters were prepared by emulsification of the hydrophobic ethyl acetate suspension (~ 5 vol% of the continuous phase) as a dispersed phase with water as the continuous phase. The poly(acrylic acid) (Mw ~ 25kDa) was mainly used as a surfactant for stabilization of emulsion droplets. The residual ethyl acetate in droplets was removed using rotary evaporator. As a result, the clusters containing ~ 100 nanoparticles were formed. Finally, the clusters were coated with a layer of silica using hydrolysis and polycondensation of tetraethyl orthosilicate. All procedures were developed exclusively by the company Nanos SCI and were fully described in the literature.[52,55]

To enable conjugation of the enzyme, the magnetic nanoparticle clusters mNC-Si were functionalized by grafting different organic molecules onto their surfaces. In general, the functionalization followed the same procedure, where the alkoxysilane molecules (silane-PEG, $-NH_2$, -COOH, -SH, $-N_3$, -C≡CH) formed covalent bonds with the silanol –OH groups at the mNC-Si surface. For ensuring the colloidal stability of the conjugate, mNC-Si was grafted with a mixed layer of silane molecules. The functionalization mixtures for all functionalized mNC (with the exception of mNC-PEG, where only silane-PEG was used) were composed of ~83 mol. % functional silanes, providing different types of specific functional groups for conjugation with the CPO, and ~17 mol. % of the silane-PEG for the additional steric stabilization of the particles' suspensions.

The general procedure for the alkoxysilane grafting was as follows. First, the desired alkoxysilane (0.9 mmol) was dissolved in a mixture composed of 60 mL EtOH, 1.5 mL NH_4OH, 0.18 mmol silane-PEG and then the aqueous suspension of mNC-Si (12 mL; 150 mg) was added. The reaction mixture was heated to 50 °C and stirred for 5 h. After completion, the nanoparticle clusters were thoroughly washed with ethanol and distilled water using magnetic separation to remove any unbound silane from the suspension.

Finally, the functionalized magnetic nanoparticle clusters (mNC-PEG, mNC-NH_2, mNC-COOH, mNC-SH, mNC-N_3, mNC-C≡CH) were directly re-dispersed in distilled water.

Aldehyde-functionalized mNC (mNC-CHO) for CPO immobilization was prepared using a two-step procedure: glycidol etherification and further periodate oxidation.[15] Amount of 3 mg mNC-PEG was suspended in 5 mL of a solution containing 6.4 mM NaOH, 2.8 mM $NaBH_4$, 40.8 mM glycidol (variant #**a**). Four more variants were prepared increasing the solution concentration 5, 10, 20 and 50-fold (#**b**, #**c**, #**d**, #**e**). The mixtures were left under mild agitation for 19 hours. The functionalized particles were then washed with 10 volumes of distilled H_2O. All 5 variants were oxidized with an excess of periodate (10 mM) in 5 mL final volume. Finally, as-synthesized mNC-CHO was washed with 10 volumes of distilled H_2O. For the mNC-CHO preparation to immobilize FSA, 3 mg mNC-PEG was suspended for 19 h in 5 mL of a solution containing 64 mM NaOH, 28 mM $NaBH_4$, 408 mM glycidol. The functionalized particles were washed with 10 volumes of distilled H_2O, and oxidized with 2 mM $NaIO_4$ in the case of mNC-CHO for pH 5.0 immobilizations (other periodate concentrations were not successful), or 90 mM for pH 8.0. Finally, mNC-CHO was washed with 10 volumes of distilled H_2O.

The synthesized mNC were characterized using transmission electron microscopy (TEM, Jeol, JEM 2100, Japan) operated at 200 kV. For the TEM analyses, the magnetic nanoparticle clusters were deposited by drying a suspension on a copper-grid-supported, perforated, transparent carbon foil. The magnetic properties of the magnetic nanoparticle clusters were measured with a vibrating-sample magnetometer (VSM, Lake Shore 7307, USA). The suspensions of functionalized magnetic nanoparticle clusters were monitored with electro-kinetic measurements of the zeta-potential (Brookhaven Instruments Corporation, ZetaPALS, USA). The surface concentration of amino groups was estimated using conductometric titration as precisely described in our previous paper.[56] The hydrodynamic size distributions of as-synthesized mNC were measured in the aqueous suspension (pH 7.4; 1 mg mL^{-1}) and 10 mM phosphate buffer (pH 5.0; 1 mg mL^{-1}), respectively, using dynamic light scattering (DLS, Fritsch, Analysette 12 DynaSyzer, Germany).

6.2.4 Enzyme modification

Sugar moieties on the surface of the CPO native form ($_n$CPO) were oxidized according to previous work.[40] 232 U $_n$CPO mL^{-1} was incubated with 0, 5, 25, 50, 100 and 200 mM sodium periodate in 50 mM phosphate buffer pH 5.0 for 60 min to obtain oxidized CPO ($_{ox}$CPO) variants #**A**-**F**, respectively. Total volume was 0.5 mL. It was performed in the dark to reduce $NaIO_4$ degradation induced by light. Propylene glycol was added to stop the reaction at 2-fold higher concentration than the corresponding $NaIO_4$. Remaining reactants were finally removed using 0.5 mL Amicon 10 kDa ultracentrifugal filters (Merck Millipore, Billerica, MA, USA).

R-C≡CH groups were introduced on the CPO surface using 4-pentynoic acid (PA) or propargylamine (PG) to render $_{PA}$CPO or $_{PG}$CPO. All modifications were performed for 2 h at a final volume of 0.5 mL 10 mM phosphate buffer, pH 5.0 with 2000 U $_{n}$CPO mL^{-1}. Initial PA or PG concentrations were 10, 100 and 200 mM in each case (variants #**G**, #**H**, #**I** for PA; #**J**, #**K**, #**L** for PG). *N*-(3-dimethylaminopropyl)-*N'*-ethylcarbodiimide (EDAC) was added to form the covalent bond at a concentration 2-fold higher than the corresponding PA or PG. PA, PG or EDAC were previously adjusted to pH 5.0 in the same buffer. The remaining reactants were removed using 0.5 mL Amicon 10 kDa ultracentrifugal filters.

6.2.5 Enzyme immobilization

6.2.5.1 $_{n}$CPO on MANA-agarose

The immobilization was performed in 30-milliliter vials. Prior the immobilization, these vials were incubated with 15 mL of BSA (2 mg mL^{-1}) for 10 min in order to reduce the undesired spontaneous binding of the proteins to the plastic surface.[57] Unbound BSA was eliminated by decantation and pipetting to avoid interferences in the immobilization by BSA attachment on MANA-agarose.

The immobilization of $_{n}$CPO was achieved by covalent attachment using EDAC (1-ethyl-3-(3-dimethylaminopropyl)carbodiimide). 1 mL of MANA-agarose (1.07 g) was mixed with 9 mL of 10 mM sodium phosphate buffer pH 5.0. After readjusting pH to 5.0, different loads of $_{n}$CPO were employed: 20 U mL^{-1} of agarose for low enzymatic load immobilization; 5625 U mL^{-1} of agarose for high enzymatic load immobilization. The mixture was stirred at room temperature within 15 min for the ionic adsorption of $_{n}$CPO on the support. Then, 2.5 mL of 0.2 M EDAC in the same buffer was added to the mixture at a final concentration of 50 mM to form covalent bonds between enzyme and support. After 3 h under mild stirring, NaCl in a final concentration of 1 M was added to eliminate the ionic interactions between $_{n}$CPO and MANA-agarose. The mixture was left under mild stirring for 1 h. Final $_{n}$CPO immobilized on the support was vacuum-filtered and washed with buffer in order to eliminate the remaining reagents.

A blank containing water instead of the support was monitored in parallel in this procedure. In order to monitor the immobilization time course, aliquots of the supernatant (SN) and suspension (SUSP), as well as samples of blank, were withdrawn periodically, and the enzymatic activity was tested. The immobilization yield and retained activity were calculated according to Equations 6.1 and 6.2.

$$\text{Immobilization yield (\%)} = \frac{\text{Initial activity - SN activity}}{\text{Initial activity}} \cdot 100 \tag{6.1}$$

$$\text{Retained activity (\%)} = \frac{\text{SUSP activity - SN activity}}{\text{Initial activity}} \cdot 100 \tag{6.2}$$

6.2.5.2 mNC-CPO

Various conjugation/immobilization strategies were developed for the binding of CPO to the functionalized mNC. For all conjugations, 0.5 mg of functionalized mNC was suspended in 10 mM phosphate buffer at pH 5.0 in 1 mL of total volume. Prior the conjugation, the 2 mL-microcentrifuge tubes were incubated with 1 mL of BSA (2 mg mL^{-1}) for 10 min; unbound BSA was eliminated by decantation and centrifugation.

The buffer and pH were selected due to previous work on CPO immobilization.[40] During conjugations, the pH was always kept at acidic values because low CPO stability was observed at neutral or basic pH. The CPO (native or modified) loading was 2-4 U mL^{-1}, except when otherwise indicated. All immobilizations were carried out at 25 °C under mild orbital stirring (MultiTherm™, Benchmark Scientific, Edison, NJ, USA). 1 M NaCl was added at the end and left for 60 min to validate the bonding strength by the elimination of electrostatic interactions between the enzyme and particles. Final mNC-CPO conjugates were washed with buffer in order to eliminate the remaining reagents.

1) Non-covalent immobilization of $_{n}$CPO to mNC-Si, mNC-PEG, mNC-NH$_2$, mNC-COOH, mNC-SH, mNC-C≡CH: With mNC-Si/PEG/NH$_2$/COOH, the enzyme-support mixture was left to contact during 60 min. Onto mNC-SH, $_{n}$CPO was immobilized for 2 h and 0.1 mg CoCl$_2$ was added to oxidize the SH, allowing enzyme-support linking.[58] For $_{n}$CPO immobilization onto mNC-C≡CH, the mixture was incubated for 2 h.

2) Covalent immobilization of ${}_{n}$CPO to mNC-NH_2, mNC-COOH: It was achieved by 2-hour incubation with a pH-adjusted EDAC solution. This solution consisted of EDAC in 10 mM sodium phosphate buffer; pH was adjusted to 5.0. Final EDAC concentration was 25 mM.

mNC-COOH activation was accomplished by prior 25 mM EDAC incubation for 5-60 min, followed by mNC washing to remove reagents excess and ${}_{n}$CPO immobilization for 2h.

3) Two-step (ionic, covalent) ${}_{n}$CPO immobilization onto mNC-NH_2, mNC-COOH: Onto mNC-NH_2, it was performed for 15 min to achieve the ionic interaction, followed by 1-50 mM EDAC 2 h incubation. With mNC-COOH: 1 h ionic interaction, 2 h with 25 mM EDAC.

4) ${}_{n}$CPO immobilization onto mNC-CHO: The mixture was left under agitation for 2 h. The formed Schiff base was reduced by 0.1 mg $NaBH_4$ mL^{-1} for 30 min.

5) Covalent immobilization of ${}_{ox}$CPO to mNC-NH_2: The immobilization was carried out for 2 h to and then 0.1 mg $NaBH_4$ mL^{-1} was added to reduce the formed Schiff base for 30 min.

6) Click chemistry between ${}_{PA}$CPO, ${}_{PG}$CPO and mNC-N_3: It was carried out for 2 h. 0.1 mg CuBr mL^{-1} catalyst was added to start the click reaction. Copper effect on ${}_{n}$CPO stability was studied by a 2-hour incubation with copper at immobilization conditions.

In order to characterize the immobilization course, aliquots of SN and SUSP were periodically withdrawn applying a magnetic field, to test the enzymatic activity. Soluble CPO activity (blank) was analyzed in parallel to this procedure. The immobilization yield and retained activity were calculated using Equations 6.1 and 6.2.

For further characterization, the four selected derivatives such as mNC-NH_2-${}_{n}$CPO (ionic), mNC-NH_2-${}_{n}$CPO (covalent by two steps), mNC-NH_2-${}_{ox}$CPO (Schiff base complex), and mNC-C≡CH-${}_{n}$CPO (non-covalent) were prepared according to the described protocol at a final concentration of 1 mg mNC mL^{-1}. For the zeta potential measurements, the derivatives were diluted 10-times in 10 mM phosphate buffer pH 5.0.

The conjugated mNC were characterized following the same techniques and protocols as synthesized mNC (Section 6.2.3.3).

6.2.5.3 FSA on CoIDA-agarose

To immobilize FSA on CoIDA-agarose, 0.1 mL of support was suspended in 50 mM sodium phosphate buffer with 300 mM NaCl and 20 mM imidazole, at pH 8.0 in a total volume of 1 mL. The salt concentration was used to avoid the non-specific electrostatic interactions enzyme–support; imidazole was added to limit the interactions from the metal exclusively to His-tag residues. 0.8–20 U FSA was used and left to immobilize for 30 min, at 1000 rpm, 25 °C. Immobilization parameters were determined by measurements of SN and SUSP activities.

6.2.5.4 mNC-FSA

The immobilization screening for FSA onto mNC was designed similarly to the previous CPO experiments. Again, for all conjugations, 0.5 mg of functionalized mNC was suspended in 10 mM phosphate buffer in 1 mL of total volume. The buffer pH was set at 5.0. Although FSA can precipitate at this pH (no activity loss was observed in the previous chapters), it could be useful for an eventual co-immobilization with CPO. pH was also set at 8.0 in order to evaluate the immobilization at a more basic pH, more adequate for the enzyme. For the immobilization of FSA, prior BSA-blocking of tubes was not required, as not binding to the tube was observed.

FSA was not chemically modified to add more functional groups. The enzyme loading was kept at 0.02 U mL^{-1} (or 0.01 U mL^{-1} where specified). For a preliminary screening, FSA was left to immobilize for 60 min to mNC-Si, mNC-PEG, mNC-NH_2, mNC-COOH, mNC-CHO, mNC-SH, mNC-C≡CH, mNC-N_3, mNC-EDTA. Onto mNC-N3, 0–0.1 mg CuBr mL^{-1} catalyst was added. Before the immobilization, mNC-EDTA was incubated with 0–0.2 M $CoCl_2$ for 12 hours.

To perform the covalent bonding between mNC-NH_2 and FSA, carbodiimide was employed. To this end, 1–25 mM EDAC was added for 3 h. All immobilizations were performed at 25 °C under mild orbital stirring. 0/0.25/1 M NaCl (indicated in the text) was added at the end of the immobilization and left for 60 min to validate the bonding strength by the elimination of electrostatic interactions between the enzyme and particles. Final mNC-FSA conjugates were washed with buffer in order to eliminate the remaining reagents.

In this case, the immobilization parameters were not determined as described for mNC-CPO experiments. The enzyme load was too low to be detected using the spectrophotometric activity test. Thus, to determine the immobilization yield, samples from the supernatant were withdrawn and analyzed by Bradford quantification.[59] 150 µL of sample was mixed with 150 µL of Coomassie reagent for 10 min. After that, absorbance at 595 nm was analyzed and used for protein calibration, using a prior calibration curve with BSA, at a protein concentration range of 0–4 µg protein mL^{-1}. The immobilization yield was determined as the difference between the calculated initial protein concentration (from the FSA stock quantification) and the protein concentration at the SN. The retained activity was calculated from a new activity test analyzed by HPLC, as it is described in Section 6.2.2.2. In this case, the percentage of FSA activity retained on the mNC is determined.

6.2.6 Application of immobilized derivatives

6.2.6.1 β-OH oxidation by $_n$CPO on MANA-agarose

In order to catalyze the oxidation of β-OH with $_n$CPO immobilized on MANA-agarose, a high enzymatic load immobilization was carried out. Due to diffusional limitations, the intrinsic retained activity could not be truly calculated. The quantified mean retained activity after immobilization was calculated to be 40.9% (Section 6.3.1.1), and taken into account a reaction volume of 5 mL, 5625 CPO U were offered to 0.5 mL of agarose to achieve a final activity of 450 U mL^{-1} of the reaction medium.

β-OH solutions were prepared by dissolving the reagent in 100 mM sodium acetate buffer pH 5.0 in a final volume of 5 mL. Initial substrate concentration was 38 mM. Reactions were performed at 25°C, with magnetic stirring for soluble $_n$CPO, and orbital stirring (700 rpm, MHR 13, HLC BioTech, Bovenden, Germany) for immobilized enzyme. 450 $_n$CPO U mL^{-1} of the reaction medium was employed. Initial *t*-BuOOH concentration was zero, and its addition was carried out by the semi-continuous addition of a 5 µL pulse from a stock solution every 10^3 s, using a single-syringe automatic microburette (Crison Instruments, Barcelona, Spain). The concentration of the peroxide stock solution was 0.832 M in order to achieve a peroxide addition rates of 3 mM h^{-1}.

During the reaction, the enzyme half-life time ($t_{1/2}$) was determined by evaluation of the activity of the immobilized CPO on a simultaneous CPO activity assay (MCD chlorination). Concentrations of substrates and products were monitored along the reaction.

6.2.6.2 β-OH oxidation by mNC-NH_2-$_{ox}$CPO

Enzyme release to supernatant from the ionic mNC-NH_2-$_n$CPO and the covalent mNC-NH_2-$_{ox}$CPO biocatalysts was estimated at the initial reaction conditions for β-OH oxidation: 27 mM β-OH in 100 mM sodium acetate buffer pH 5.0. 4 U $_n$CPO or $_{ox}$CPO was immobilized onto 0.5 mg mNC-NH_2 in accordance with the established procedure (ionically or through a Schiff base bond). Final derivatives were washed with buffer and kept in a final volume of 0.3 mL. Then 0.7 mL of the reagents solution (38 mM β-OH, acetate buffer) was added. Several biocatalysts were identically prepared for studying the $_n$CPO desorption from the support through time (24 h), by measuring the enzyme activity in supernatant and suspension.

High $_{ox}$CPO load was immobilized onto mNC-NH_2 to catalyze the oxidation of β-OH. 90 mg mNC-NH_2 was suspended in 10 mM phosphate buffer pH 5.0 in 1 mL of total volume. A biocatalyst with final activity of 450 U $_{ox}$CPO mL^{-1} was employed according to the retained activity after immobilization (62.5%, Section 6.3.1.2). The final mNC-NH_2-$_{ox}$CPO derivative was washed with buffer and kept in a final volume of 0.3 mL.

β-OH (38 mM) was dissolved in 100 mM sodium acetate buffer pH 5.0 in a final volume of 0.7 mL. 0.3 mL mNC-NH_2-$_{ox}$CPO was added with final concentrations of 450 U $_{ox}$CPO mL^{-1}, 90 mg mNC mL^{-1} and 27 mM β-OH. Initial *t*-BuOOH concentration was 3 mM. Oxidation was carried out by the addition of a 3 mM pulse of *t*-BuOOH every hour, using a single-syringe automatic microburette at 25 °C, 1000 rpm of orbital stirring. The same procedure was also carried out using 450 U mL^{-1} of soluble $_n$CPO or $_{ox}$CPO instead of the immobilized biocatalyst. In order to avoid false-positive results, two reaction controls were carried out at 25 °C, 1000 rpm for 24 h: (a) 27 mM β-OH incubation in reaction buffer with 90 mg mNC-NH_2 mL^{-1} and 30 mM *t*-BuOOH, without enzyme in a final volume of 0.2 mL. This control accounted for the chemical oxidation of the amino alcohol catalyzed by mNC. (b) 11 mM β-CHO (expected amount of the aldehyde in reaction) and 90 mg mNC-NH_2 mL^{-1} incubation in reaction buffer without enzyme nor peroxide, in a final volume of 0.2 mL. This control accounted for a chemical reaction between β-CHO and the support. β-CHO stability in pure buffer was also examined.

$t_{1/2}$ was determined as indicated in Section 6.2.6.1.

6.2.6.3 Aldol addition by FSA on CoIDA-agarose

The aldol addition of DHA to β-CHO was catalyzed by FSA immobilized on Co-IDA agarose and compared to the one catalyzed by the soluble enzyme. Assuming a retained activity of 96.4%, a final derivative of 4.7 U FSA mL^{-1} was prepared. The final activity was confirmed by the F6P cleavage. The derivative was washed with 50 mM HEPES pH 8.0 to remove undesired salts for the reaction.

The reaction mixture contained 30 mM β-CHO, 45 mM DHA, and 4.7 U FSA mL^{-1} in 50 mM HEPES pH 8.0 in a total volume of 1 mL. The reaction was carried out at 25 °C, under orbital stirring (1000 rpm).

6.2.6.4 Aldol addition by mNC-NH2-FSA

High load of FSA was immobilized onto $mNC-NH_2$ for the aldol addition of DHA to β-CHO. According to a final retained activity of 29.1%, 3.4 U FSA was immobilized onto 85 mg $mNC-NH_2$ in 10 mM phosphate buffer pH 5.0 with 5 mM EDAC, using the same protocol described above, followed by several washing cycles with buffer. It was concentrated to a final volume of 0.3 mL, and then the reaction medium was added to perform the reaction. The activity of the derivative was 1.0 U mL^{-1} of reaction, which initially contained 30 mM β-CHO and 45 mM DHA, in 50 mM HEPES pH 8.0. The reaction was carried out under orbital stirring (1000 rpm) at 25 °C.

6.2.7 HPLC analysis

Concentrations of β-OH, β-CHO, β-COOH, *t*-BuOOH, DHA, and preFagomine were measured by HPLC analysis according to the protocol described in Chapter 4. The standard deviation was calculated from duplicated measurements from a single sample.

6.3 Results and discussion

There is not a universal immobilization method for all the enzymes, and therefore the optimization of the process is a rather complicated task. Here, both CPO and FSA are intended to be immobilized on agarose and mNC through different procedures. The most promising derivatives are further investigated to find the adequate conditions for the immobilization, such as incubation time and reagents concentrations.

6.3.1 CPO immobilization

6.3.1.1 MANA-agarose

In order to extend the $_n$CPO $t_{1/2}$, the enzyme was immobilized on MANA-agarose following the conditions reported in the literature.[40] According to this study, $_n$CPO was immobilized on MANA-agarose at a relative low enzymatic load –20 U mL^{-1} of MANA-agarose– intending to quantify both immobilization yield and retained activity. In this work, diffusional limitations were minimized immobilizing at this enzyme load or below that value. EDAC concentration was set in 12.5–50 mM range, and the incubation time at 2–3 h (Table 6.1). The best conditions were found to be 25 mM EDAC for a 3-hour incubation, with an immobilization yield of 96.6%, and a retained activity of 40.9% (similar values to those previously reported).[40]

The immobilization course of the experiment performed at these conditions is plotted in Figure 6.2. Almost all the enzyme was adsorbed on the support in 15 min; at this time, supernatant activity was nearly zero. Then 25 mM carbodiimide was added to form the covalent attachment. During this 3-hour incubation, there was the major loss of enzymatic activity. A final incubation with 1 M NaCl was used to eliminate the non-covalently attached enzyme molecules.

Table 6.1. Yield and activity from $_n$CPO immobilizations on MANA-agarose depending on EDAC concentration and incubation time. 20 U mL^{-1} of MANA-agarose was used in 10 mM sodium phosphate (pH 5.0) in 10 mL of total volume (10% v/v), 25 ºC.

EDAC (mM)	Incubation time (h)	Immobilization yield ± S.D. (%)	Retained activity ± S.D. (%)
12.5	3	76.3 ± 2.9	32.3 ± 1.9
25	2	92.5 ± 0.9	39.0 ± 2.3
25	3	96.6 ± 1.6	40.9 ± 3.4
50	3	97.6 ± 1.4	29.5 ± 3.5

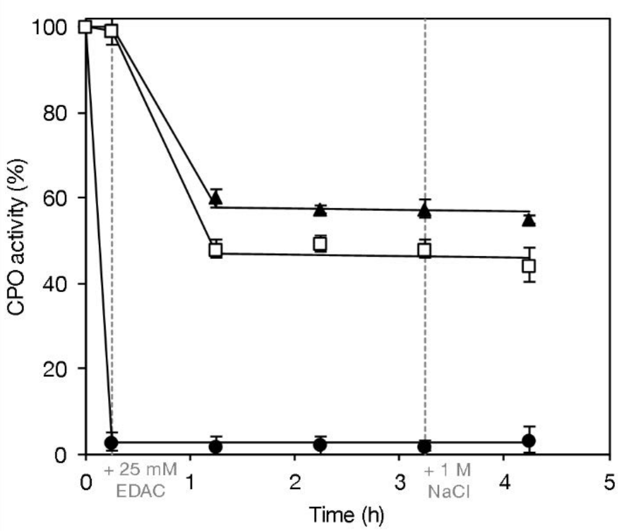

Figure 6.2. Covalent immobilization of CPO on MANA-agarose. 20 U mL^{-1} of MANA-agarose was used in 10 mM sodium phosphate (pH 5.0) in 10 mL of total volume (10% v/v), 25 ºC. 25 mM EDAC was used to form the covalent bond; 1 M NaCl was employed to remove electrostatic interactions. Blank (▲), suspension (□), supernatant (●).

In order to catalyze the oxidation of β-OH with immobilized $_n$CPO, a high enzymatic load immobilization was performed to get a derivative to render 450 U mL^{-1} of the reaction medium. Results from this reaction were compared with another one catalyzed by the same activity of soluble $_n$CPO. Figure 6.3 shows the remaining amino alcohol amount during the reaction, as well as the enzyme operational stability for the two reactions performed with soluble and immobilized $_n$CPO.

$t_{1/2}$ of soluble $_n$CPO was 3.4 h, whereas it was 2.6-fold higher when the enzyme was immobilized (9 h). Thus, immobilization on MANA-agarose stabilized the enzyme against *t*-BuOOH inactivation. Note that the measured activity for the immobilized enzyme could not correspond with the intrinsic one because of diffusional limitations, but it is a qualitative tool to study the inactivation rate of that enzyme.

The initial β-OH oxidation rate was slightly lower when the enzyme was immobilized. Nevertheless, as the immobilized enzyme was active for a longer period, the final conversion of β-OH was higher. Consequently, the formation of β-CHO increased 1.4-fold with $_n$CPO attached to MANA-agarose. Therefore, $_n$CPO immobilized on MANA-agarose is a candidate catalyst for the oxidation of the amino alcohol.

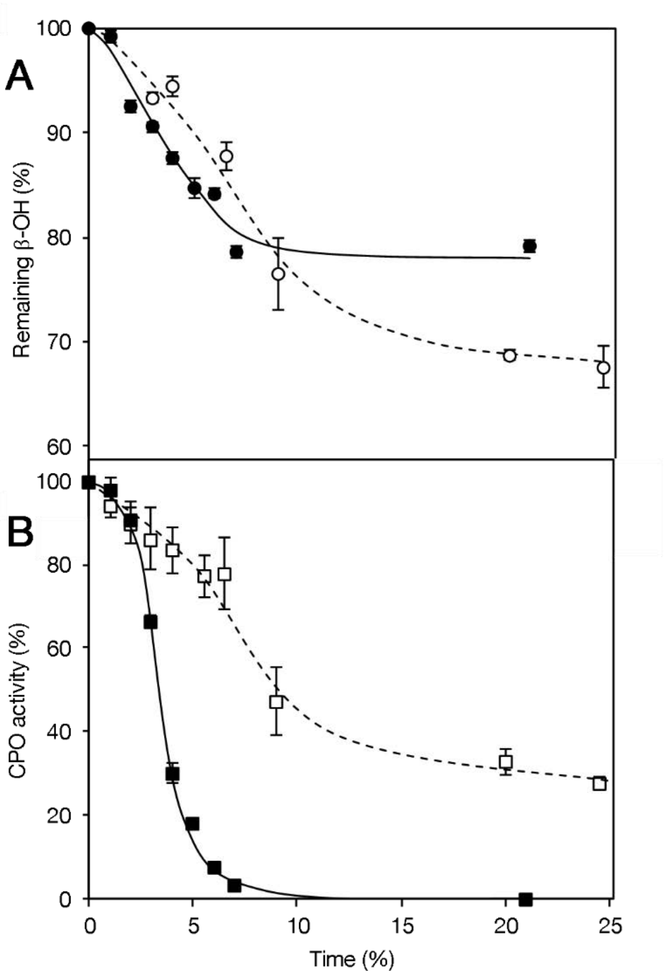

Figure 6.3. Remaining β-OH (**A**) and $_n$CPO activity (**B**) on the β-OH oxidation catalyzed by soluble $_n$CPO and $_n$CPO immobilized on MANA-agarose. Soluble $_n$CPO: β-OH (●), activity (■); immobilized $_n$CPO: β-OH (○), activity (□). Oxidation conditions: 38 mM β-OH, 450 U $_n$CPO mL^{-1}, 3 mM h^{-1} *t*-BuOOH in 100 mM acetate buffer pH 5.0, 25 ºC.

6.3.1.2 mNC

The conjugation/immobilization of CPO through its various functional groups to differently functionalized mNC was also investigated (Figure 6.4). The reactivity and abundance of functional groups, as well as their specific location on the tridimensional structure of the enzyme, are key factors for its binding efficiency. To enable linking of different functional groups of the CPO with the mNC surface and ensuring the colloidal stability of conjugates various functional groups/molecules were introduced on the mNC surface. The OH groups at the silica surface of mNC-Si are only appropriate for non-covalent linking while PEG functionalization is, at the same time, responsible for improved colloidal stability. Amino functionalization of mNC enables covalent binding with the carboxylic moieties of the CPO. Carboxyl functionalization of mNC is essential for the covalent binding with the CPO amines. CHO groups at the mNC surface enable the formation of a Schiff base with the CPO amines. SH-functionalized mNC reacts with the CPO sulfhydryls while N_3 and C≡CH groups are essential for click chemistry with the CPO. The latter reaction is frequently used for bioconjugation in medicinal chemistry due to its great selectivity and efficiency.[60]

Not only the mNC surface but also the CPO enzyme was modified to introduce reactive groups such as aldehyde that was obtained by oxidation of enzyme’s sugar moieties. These aldehyde groups are potentially reactive to mNC-NH_2. Alkyne groups on the CPO were provided by modification of its amino and carboxyl groups in order to perform click chemistry with mNC-N_3. The immobilization yield and activity recovery screening were performed for all types of mNC-CPO conjugates. The most promising conjugates were further studied and characterized. Finally, the best-performing conjugate was used as a magnetic biocatalyst in a proof of concept reaction of β-OH oxidation.

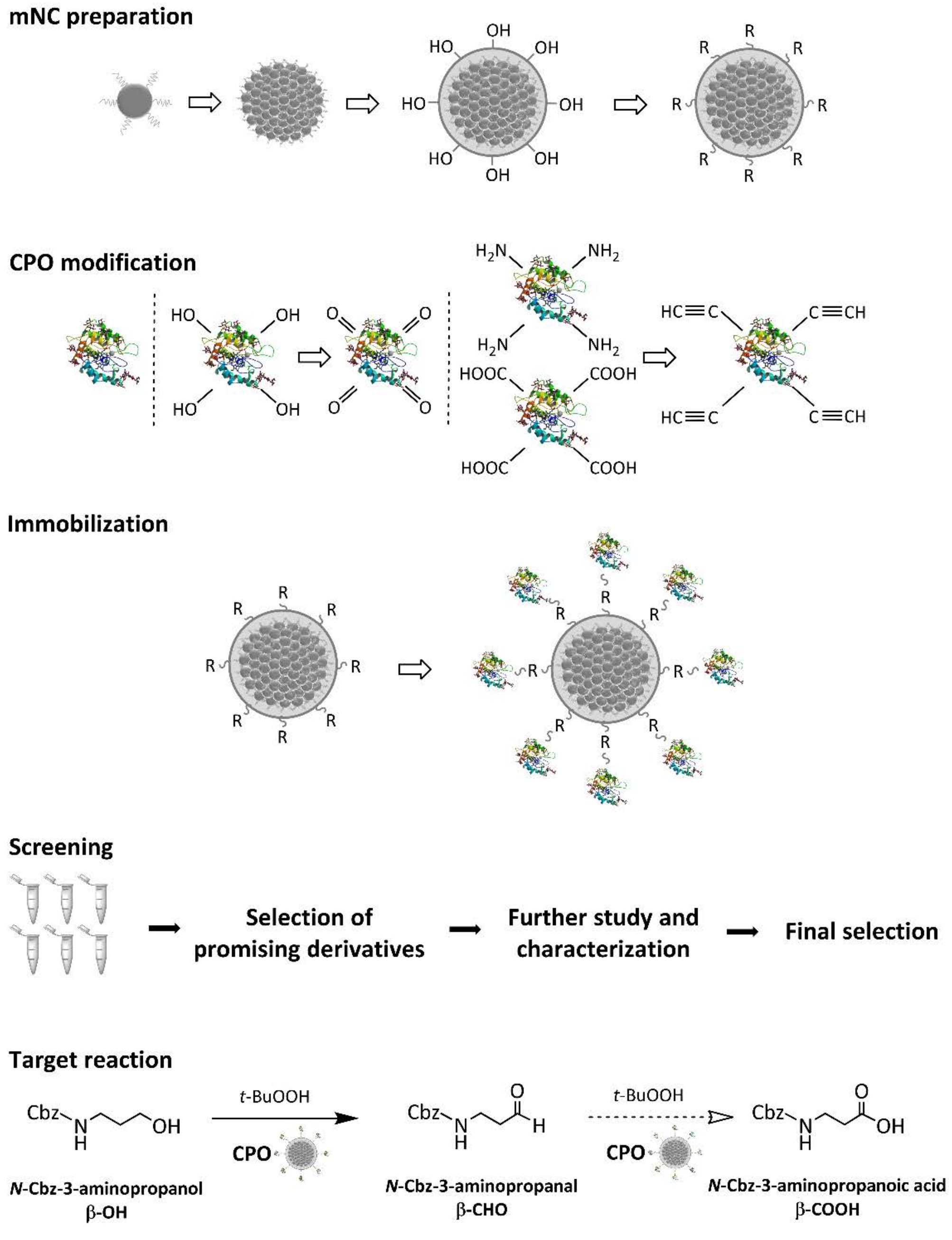
mNC preparation
OH
HO
OH
HO
OH
HO
OH
OH
R
CPO modification
HO
OH
HO
OH
O
H2N
NH2
HOOC
COOH
HC≡C
C≡CH
Immobilization
R
Screening
Selection of promising derivatives
Further study and characterization
Final selection
Target reaction
Cbz
N
H
OH
t-BuOOH
CPO
O
N-Cbz-3-aminopropanol
β-OH
N-Cbz-3-aminopropanal
β-CHO
N-Cbz-3-aminopropanoic acid
β-COOH

Figure 6.4. Methodology outline. On the mNC surface, R represents the introduced functional group (PEG, NH_2, COOH, CHO, SH, N_3, C≡CH).

Clusters characterization

As magnetic carriers for enzyme immobilizations, the nanoparticle clusters mNC with 15–20 nm thick silica shell were provided by Nanos SCI (commercially available as iNANOvative™|BIO). In the TEM image of the silica-coated mNC (mNC-Si) (Figure 6.5A), the cluster core composed of tightly packed primary maghemite nanoparticles is clearly resolved from the amorphous silica shell. The size of mNC-Si was measured from the TEM images (300 magnetic nanoparticle clusters measured) to be 140 nm $\pm$ 25 nm. DLS measurement of mNC-Si in an aqueous suspension (1.0 mg mL^{-1}, pH 7.4) showed narrow hydrodynamic-size distribution between approximately 110 and 180 nm with the average at ∼142 nm (Figure 6.5B). DLS measurements showed no significant differences in the hydrodynamic sizes of mNC-Si after they were functionalized with different molecules; the hydrodynamic sizes remained in the narrow range between 140–210 nm, which confirmed the good colloidal stability of the functionalized magnetic nanoparticle clusters without any notable aggregation. mNC-Si showed superparamagnetic properties with a saturation magnetization Ms of ∼41 Am^{2}kg^{-1} (Figure 6.5C).

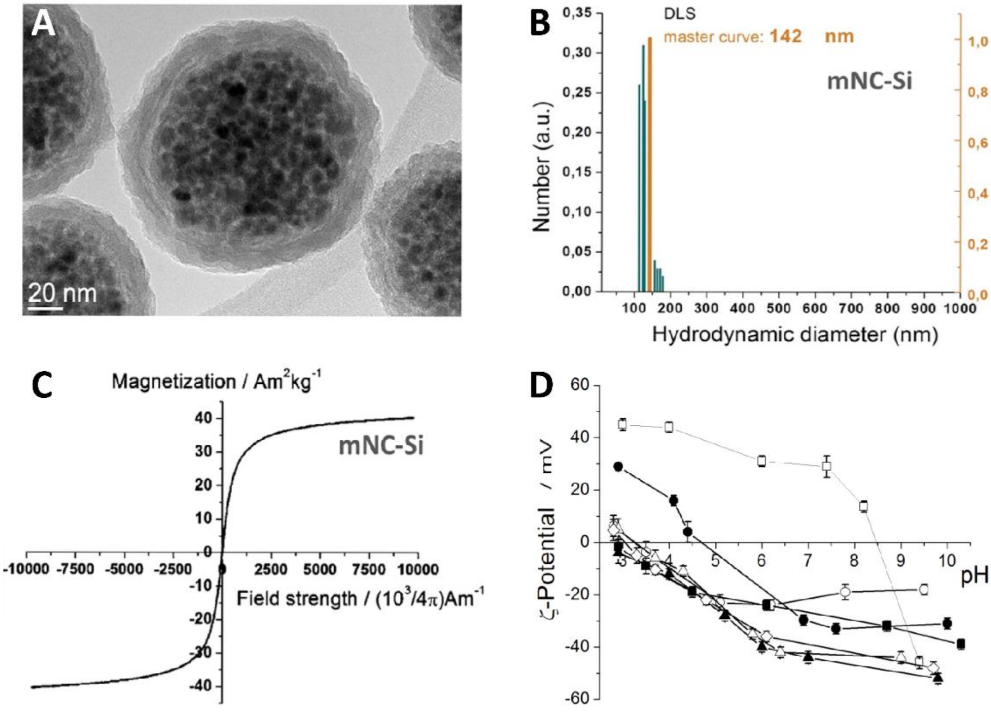

Figure 6.5. TEM images of mNC-Si (**A**), number-weighted distribution of the mNC-Si hydrodynamic diameters obtained from the DLS measurements in aqueous suspension (pH 7.4; 1 mg mL^{-1}) (**B**), and room-temperature measurements of the magnetization as a function of magnetic field strength for mNC-Si (**C**). Zeta-potential curves of the functionalized mNC versus pH in H$_2$O (**D**): mNC-Si (■), mNC-PEG (○), mNC-NH$_2$ (□), mNC-COOH (●), mNC-SH (▲), mNC-N$_3$ (◇), mNC-C≡CH (△).

The efficiency of the functionalization was followed using measurements of the zeta-potential of the functionalized mNC in the aqueous suspensions. The zeta-potential was measured as a function of the operational pH. mNC-CHO zeta-potential was the only one not determined, however, its functionalization efficiency was calculated below in terms of immobilization yield. Figure 6.5D shows the changes in the zeta-potential of mNC after various types of functionalization. The silica surface shows a relatively acidic character because its structure is terminated with negatively charged silanol groups at pH values above the isoelectric point (IEP) of approximately 3. Once the silanol groups react with alkoxysilanes, both the values of zeta potential and the shift of the IEP occurred. As expected, the functionalization of mNC-Si with -SH, -N_3, and -C≡CH had almost no effect on the IEP, however, the absolute values of zeta-potential at the neutral pH somewhat increased. After functionalization with –COOH the IEP shifted to higher pH of approximately 4.5. The highest influence of the functionalization was observed when silane-NH_2 was grafted onto the surfaces of mNC-Si. The zeta potential was positive at neutral pH as the IEP was shifted to pH of 8.5. The concentration of -NH_2 on the surfaces of the functionalized mNC-Si was estimated using conductometric titration to be approximately 2 silane-NH_2 molecules per nm^2. The surface density of other functional groups is assumed to be similar because the same functionalization protocol was applied for all surface modifications. The high absolute values of zeta potentials of around 30 mV or higher provide strong electrostatic repulsive forces between the nanoparticle clusters ensuring a good colloidal stability of the suspension.[61]

On the other hand, grafting of silane-PEG molecules onto the nanoparticles clusters does not significantly affect the zeta potential value, but it sterically improves the colloidal stability of the suspension. The steric stabilization of the suspensions is especially important when the colloidal particles are applied in reaction mixtures, where increased ionic strength decreases the electrostatic repulsive forces. For the improved colloidal stability, mNC-Si were therefore grafted with mixed layer of silane molecules, composed of ~83 mol.% functional silanes, providing different types of specific functional groups for conjugation with the CPO, and ~17 mol. % of the silane-PEG for the additional steric stabilization of the suspensions.

Immobilization screening

A primary screening of the CPO immobilization was carried out by mixing the native form of the enzyme with different functionalized mNC for an incubation time indicated in

Section 6.2.5.2. For all the immobilization runs, several CPO loads (U CPO / mg mNC) were assayed to ensure that the enzyme load was not over the maximum capacity per mg mNC, and to realize the absence of diffusional restrictions. No significant differences were found for CPO loads below 8 U CPO (mg mNC)$^{-1}$; these data are reported in Table 6.2.

Table 6.2. Immobilization yield and retained activity for the primary screening of the $_{n}$CPO immobilization onto functionalized mNC. Immobilization conditions: 4 U mL^{-1}, 0.5 mg mNC mL^{-1} in 10 mM phosphate buffer (pH 5.0), 25 ºC. Incubation time is detailed in Section 6.2.5.2. Standard deviations (S.D.) were determined by two replica experiments in each case.

#	Reactive group		Bond chemistry		Immobilization	Retained
	mNC	$_{n}$CPO	Non-covalent	Covalent	yield ± S.D. (%)	activity ± S.D. (%)
1	Si	OH	X		21.9 ± 0.2	<1
2	PEG	OH	X		19.2 ± 1.6	3.1 ± 1.6
3	NH_2	COOH	X		90.0 ± 0.7	87.6 ± 0.6
4	NH_2	COOH		X	55.0 ± 1.0	29.8 ± 0.8
5	COOH	NH_2	X		14.3 ± 3.2	9.1 ± 3.1
6	COOH	NH_2		X	37.6 ± 1.0	8.0 ± 2.9
7	CHO	NH_2		X	25.7 ± 2.2	3.2 ± 2.5
8	SH	SH	X		12.8 ± 0.9	2.9 ± 4.3
9	C≡CH	OH	X		60.7 ± 2.8	58.7 ± 4.0

The experiments with mNC-Si and mNC-PEG (#**1** and #**2**, Table 6.2) gave low immobilization yields that could be explained by moderate interaction with hydroxyls at the $_{n}$CPO surface; retained activities were even lower due to activity loss. However, the ionic immobilization yield onto mNC-NH_2 (#**3**) was very high, up to 90%, probably due to a lot of carboxyl residues on the enzyme surface; the activity loss was less than 5%. In order to covalently attach the enzyme (#**4**), EDAC was used as a carboxyl activating agent for amide bonding with primary amines. As indicated in Materials and Methods, a final incubation step with NaCl was employed to remove the non-covalent attached enzyme molecules. An immobilization yield of 55.0% was achieved; it is lower than in the ionic immobilization probably due to chemical modification of the enzyme. The final activity of the derivative was 29.8% of the initial one. Activity loss was attributed to a distortion of the 3D CPO structure due to chemical bond and by inter/intramolecular enzyme cross-linking.

In the case of intending to bind the enzyme NH_2 groups to mNC-COOH (#**5**), the yield and retained activity were very low. For the covalent bond (#**6**), EDAC was again employed following a similar procedure: the immobilization yield increased to 37.6%, probably because EDAC led to amide bond formation between CPO and mNC; however, final activity was again very low, only 8.0%. A hypothesis on the low yield and activity might be formulated according to the $_{n}$CPO 3D-structure (Figure 6.6). The structure representation on this figure has been obtained using UCSF Chimera software.[62] On that, colored in yellow, Glu69–Thr238–Glu266 are surrounding the entrance of the channel to the active site, in which the heme group is present.[63] Throughout the entire enzyme surface, only a few positively charged amino acid residues (Arg, Lys) are present, leading to a low immobilization yield. These groups are uniformly distributed and some of them are close to the active site. This could explain the low retained activity, due to the steric hindrance caused by the attachment to mNC. On the other hand, carboxyl groups are more abundant and non-uniformly distributed. Although two Glu are at the channel entrance, a higher COOH density is observed in the face opposite to the active site (Figure 6.6D). This could explain the negligible activity loss when attaching CPO to mNC-NH_2 (#**3**).

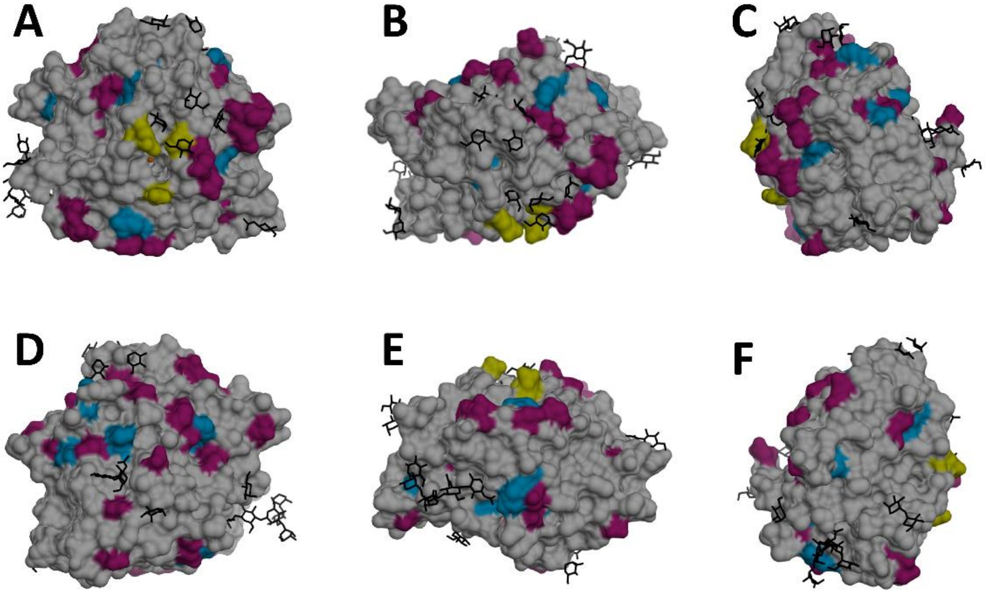

Figure 6.6. Tridimensional structure of native CPO. The entrance to the active site is located between the three amino acids in yellow. Acid residues are colored in red; basic residues are in blue; sugar moieties are in black. Multiple captions of the enzyme structure are pictured: (A) front, (B) top, (C) right, (D) back, (E) bottom, (F) left.

The binding of $_{n}$CPO onto mNC-CHO was also aimed through Schiff base formation (#**7**). For the preparation of mNC-CHO, mNC-PEG oxidation using $NaIO_4$ was intended, but no meaningful results were obtained. An alternative approach was the prior mNC-PEG etherification employing glycidol, followed by periodate oxidation. mNC-CHO #**b** (Materials and Methods) led to the best results in terms of yield and activity: 50.1% yield and 19.6% retained activity, before Schiff base reduction with $NaBH_4$. After bond reduction, mNC-CHO-$_n$CPO yield and activity decreased to 25.7% and 3.2%. Again, covalent binding through amino groups on the $_n$CPO surface led to low retained activity of the derivative.

CPO was also intended to be immobilized onto mNC-SH (#**8**), but it was discarded as a suitable immobilization support due to the low yield obtained. Finally, one of the most promising and unexpected results was achieved using mNC-C≡CH (#**9**). These particles were primarily designed for click chemistry between the support and the modified enzyme. Before enzyme modification, $_n$CPO was immobilized through non-covalent interactions with 60.7% yield and 58.7% retained activity. The enzyme was completely released from the support when increasing the ionic strength.

Primary selection of biocatalysts: further immobilization study

According to the previous discussion, some immobilization methods were worthy to be optimized: #**3**, #**4**, #**6**, #**7**, #**9** (Table 6.2). Regarding the ionic immobilization onto mNC-NH_2 (#**3**), the maximum $_n$CPO load per mg mNC was estimated to be near 10 U CPO (mg mNC)$^{-1}$ (Table 6.3*).* After this load, the yield dropped. For lower loads, the retained activity values were almost the same, confirming the absence of diffusional restrictions. An example of the immobilization time course is plotted in Figure 6.7A. As can be seen, the binding was very fast: the maximum yield was reached after only 5-10 min. Thus, in further experiments on this immobilization, the incubation time was set at 15 min, enough time to ensure a complete binding. After the attachment, no activity loss was observed for 60 min.

Table 6.3. Ionic $_n$CPO immobilization onto mNC-NH_2: yield and retained activity versus enzyme load per mg mNC. Immobilization conditions: 0.5 mg mNC mL^{-1} in 10 mM phosphate buffer (pH 5.0), 25 ºC.

$_n$CPO (U/mg mNC)	Immobilization yield ± S.D. (%	Retained activity ± S.D. (%)
4	89.2 ± 0.8	77.4 ± 1.5
6	88.0 ± 3.1	87.9 ± 2.6
8	90.0 ± 0.7	87.6 ± 0.6
10	81.4 ± 2.2	81.3 ± 0.5
20	58.2 ± 1.4	51.2 ± 3.1
40	32.1 ± 1.8	25.8 ± 3.0
100	18.1 ± 0.8	11.2 ± 1.1
200	12.2 ± 4.2	10.9 ± 2.4

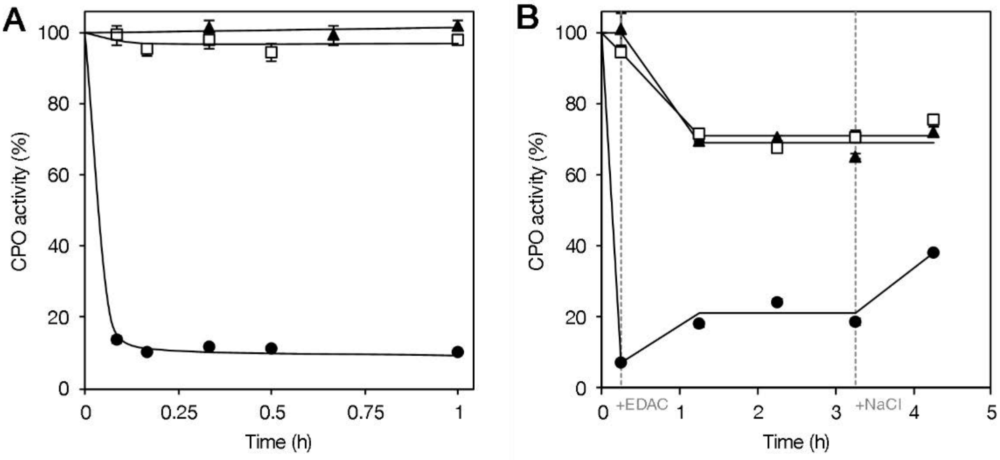

Figure 6.7. Activity of $_n$CPO immobilized onto mNC-NH$_2$ using 4 U CPO mL^{-1}, 0.5 mg mNC mL^{-1} in 10 mM phosphate buffer (pH 5.0), 25 ºC. (**A**) through ionic interactions; (**B**) by a two-step procedure (ionic, covalent), 10mM EDAC. Blank (▲), suspension (□), supernatant (●).

In order to reduce the activity loss when $_n$CPO was covalently attached to mNC-NH$_2$ (#**4**), a new two-step procedure was established: covalent bonding after prior ionic immobilization. Results could be improved as the enzyme is previously oriented on the support (ionic step) and then the covalent bonding is performed. By this procedure, intermolecular cross-linking of the enzyme could also be avoided. According to previous results, after 15 min of incubation for ionic attachment, EDAC was added to form the covalent bond. Different concentrations of EDAC were employed and the several derivatives were evaluated in terms of yield and activity (Table 6.4). Since the immobilization yield is determined by measuring the remaining supernatant activity, there might be some interference in yield values by the activity loss due to intermolecular cross-linking of soluble $_n$CPO. To avoid that, the EDAC concentration was selected in accordance with the higher retained activity values. Thus, the chosen concentration was 10 mM with a final activity of 37.2% (after NaCl step). Another variable in the process is the incubation time with EDAC. The highest activity was after 3 h, although not much increment was observed after 2 h. Thus, in comparison to the one-step covalent derivative (#**4**), final activity increased from 29.8% to 37.2% by the previous ionic step. A representative time course of the two-step immobilization is plotted in Figure 6.7B. It shows that a fraction of the ionically immobilized $_n$CPO was released to the supernatant when EDAC was added, presumably due to an increase in the ionic strength or a more specific binding. The non-covalently attached enzyme was released when NaCl was added.

Table 6.4. Effect of the EDAC concentration and the incubation time on the two-step $_n$CPO immobilization onto mNC-NH_2. Immobilization conditions: 4 U mL^{-1}, 0.5 mg mNC mL^{-1} in 10 mM phosphate buffer pH 5.0. NaCl 1M was used to remove non-covalent interactions.

EDAC (mM)	Incubation time (h)	Immobilization yield ± S.D. (%)	Retained activity ± S.D. (%)
0	3	<1	<1
1	3	11.7 ± 2.3	13.5 ± 0.2
5	3	37.3 ± 2.9	33.7 ± 0.8
10	1	52.7 ± 1.7	27.9 ± 2.5
10	2	60.8 ± 1.8	36.6 ± 0.1
10	3	61.8 ± 0.6	37.2 ± 0.6
25	3	66.8 ± 1.8	36.6 ± 0.1
50	3	68.7 ± 0.1	22.6 ± 2.3

According to these results, immobilization #**6** was also performed by this procedure. In this case, enzyme and support were incubated for 60 min. Then EDAC was added at 25 mM for 3 h. However, the activity was not improved and almost no activity was observed in the final derivative. As an alternative, prior carboxyl activation of mNC-COOH using EDAC followed by incubation with the enzyme was assayed. Several incubation times of mNC-COOH with EDAC were evaluated. With 30 min activation, the immobilization yield was raised to 66.9% with 44.7% retained activity. However, non-covalent binding was achieved.

Onto mNC-C≡CH (#**9**), the enzyme-support binding was observed to be fast: in 15 min the final yield was achieved. Regarding the maximum $_n$CPO load per mg mNC, it was again estimated around 10 U CPO (mg mNC)$^{-1}$. Although the binding was in principle thought to occur through the alkyne group, this hypothesis was discarded as follows. Two types of mNC-C≡CH were prepared according to the silane-C≡CH: (a) synthesized silane-C≡CH (Appendix) with an addition sugar moiety for an increased colloidal stability; ~60% retained activity was achieved. (b) Commercial silane from Gelest, lacking the sugar moiety; no $_n$CPO immobilization was detected. Thus, the important contribution to the binding of $_n$CPO and the first type of mNC-C≡CH is thought to be mediated through hydrogen bonds between the surface of $_n$CPO and sugar moieties on the mNC-C≡CH surface.

Immobilization of modified $_n$CPO

As mentioned above the yield of #**7** was 50.1% before the $NaBH_4$ incubation (value not shown in Table 6.2), high enough to suggest intending a similar immobilization but interchanging the groups to react: aldehyde groups on $_{n}$CPO surface with mNC-NH_2. To form this Schiff base, a previous enzyme modification was required. Thus, several $_{ox}$CPO derivatives were prepared by oxidation of the sugar moieties on the $_{n}$CPO surface. Different variants #**A**-**F** were obtained regarding the concentration of $NaIO_4$ used for the hydroxyl oxidation, according to Materials and Methods. Almost no activity loss was observed after the modification for concentrations lower than 50 mM $NaIO_4$. All the $_{ox}$CPO #**A**-**F** were incubated with mNC-NH_2 to be immobilized (Table 6.5). After Schiff base bond reduction and NaCl incubation to remove ionic interactions, the immobilization yields were truly high (95-98%) for variants #**C**-**F**, with retained activities of 46-63%. Although many of the sugar residues are located far from the active site, one mannose is bound to Thr238 at the active site entrance (Figure 6.6); this could lead to steric hindrance causing the activity loss. The most positive derivative was #**C** (95% yield, 63% activity). Results indicated that the immobilization requires enough amount of periodate to ensure a certain oxidation degree of $_{n}$CPO, but increasing this concentration lowers the retained activity.

Table 6.5. Oxidation of $_{n}$CPO sugar moieties: effect of periodate concentration on activity and immobilization onto mNC-NH_2. Oxidation conditions: 232 U mL^{-1} in 50 mM phosphate buffer pH 5.0. Immobilization conditions: 4 U mL^{-1}, 0.5 mg mNC mL^{-1} in 10 mM phosphate buffer (pH 5.0), 25 ºC. 0.1 mg $NaBH_4$ mL^{-1} was added to reduce the Schiff base.

#	$NaIO_4$ (mM)	Post-modification activity ± S.D. (%)	Immobilization yield ± S.D. (%)	Retained activity ± S.D. (%)
A	0	99.5 ± 2.4	50.9 ± 0.8	4.8 ± 3.6
B	5	99.7 ± 4.3	67.7 ± 1.2	23.9 ± 1.4
C	25	99.2 ± 5.0	95.0 ± 1.0	62.5 ± 0.1
D	50	91.5 ± 2.1	97.5 ± 0.8	56.8 ± 3.4
E	100	77.4 ± 2.0	97.8 ± 0.7	48.9 ± 2.1
F	200	53.3 ± 0.7	97.1 ± 0.5	45.7 ± 1.9

The mNC-NH_2-$_{ox}$CPO binding was very fast (Figure 6.8): in 15 min almost all the enzyme was linked to the support. However, the interference from the binding between mNC-NH_2 and COOH groups from the enzyme should be considered. NaCl was introduced to the mixture after 2.5 h incubation. Before this time, Schiff base complexes CHO-NH_2 were being formed as well as the ionic interactions COOH-NH_2. After NaCl addition, only the covalent bonding can be observed.

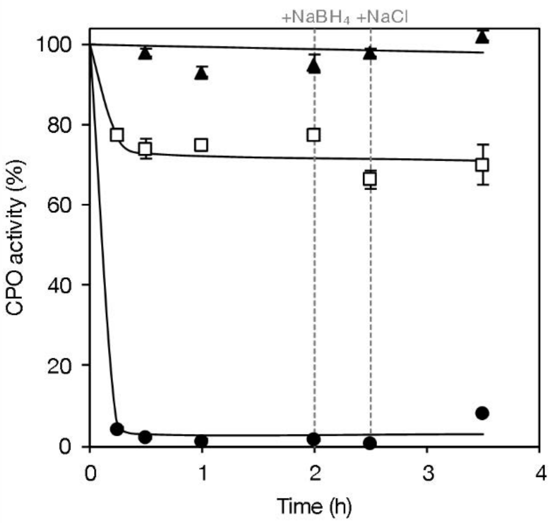

Figure 6.8. Activity of $_{ox}$CPO immobilized onto mNC-NH_2 using 4 U mL^{-1}, 0.5 mg mNC mL^{-1} in 10 mM phosphate buffer (pH 5.0), 25 ºC. 0.1 mg $NaBH_4$ mL^{-1} was added to reduce the Schiff base (**A**): blank (▲), suspension (□), supernatant (●).

Other CPO derivatives ($_{PA}$CPO, $_{PG}$CPO) were prepared by modification of amino and carboxyl groups on the $_{n}$CPO surface using PA or PG to introduce an alkyne group, which is reactive towards mNC-N_3. Several variants were prepared in each case (#**G**-**L,** Section 6.2.4). For the immobilization, catalytic amount of copper(I) salt was used to start the click reaction; without the copper catalyst, all the immobilization yields were lower. By incubation of the enzyme (native or any modified variant) and copper, no negative effect on the CPO activity was observed. Best immobilization results were accomplished using $_{PA}$CPO #**H** and $_{PG}$CPO #**K** with yields of 52% and 43%, respectively. However, almost no activity was present in the immobilized biocatalyst.

Selection and physical characterization of the mNC-CPO

According to the attachment achieved in each case and the previous results on yield and final activity, four immobilized derivatives were chosen as the most promising biocatalysts for the target amino alcohol oxidation: **i**) mNC-NH_2-$_{n}$CPO: ionic, **ii**) mNC-NH_2-$_{n}$CPO: covalent by two-step, **iii**) mNC-NH_2-$_{ox}$CPO: Schiff base complex, **iv**) mNC-C≡CH-$_{n}$CPO: non-covalent.

All four selected derivatives were further fully characterized. Zeta-potential and hydrodynamic sizes of the mNC-CPO suspensions were determined. The values of the zeta-potential measured in buffer at pH 5.0 were very similar for all four samples (**i**: (9.3

± 1.0) mV; **ii**: (11.7 ± 1.2) mV; **iii**: (4.8 ± 1.6) mV; **iv**: (10.3 ± 0.6 mV)), despite the fact that zeta potentials of the primary mNC-NH_2 (~35 mV) and mNC-C≡CH (~–20 mV) measured in aqueous suspensions were very different (Figure 6.5D). We can assume that the outermost surface of all selected derivatives might be very similar due to full coverage of the particle surface by enzymes. Thus, these measurements are in agreement with the presence of attached enzyme at the mNC surface.

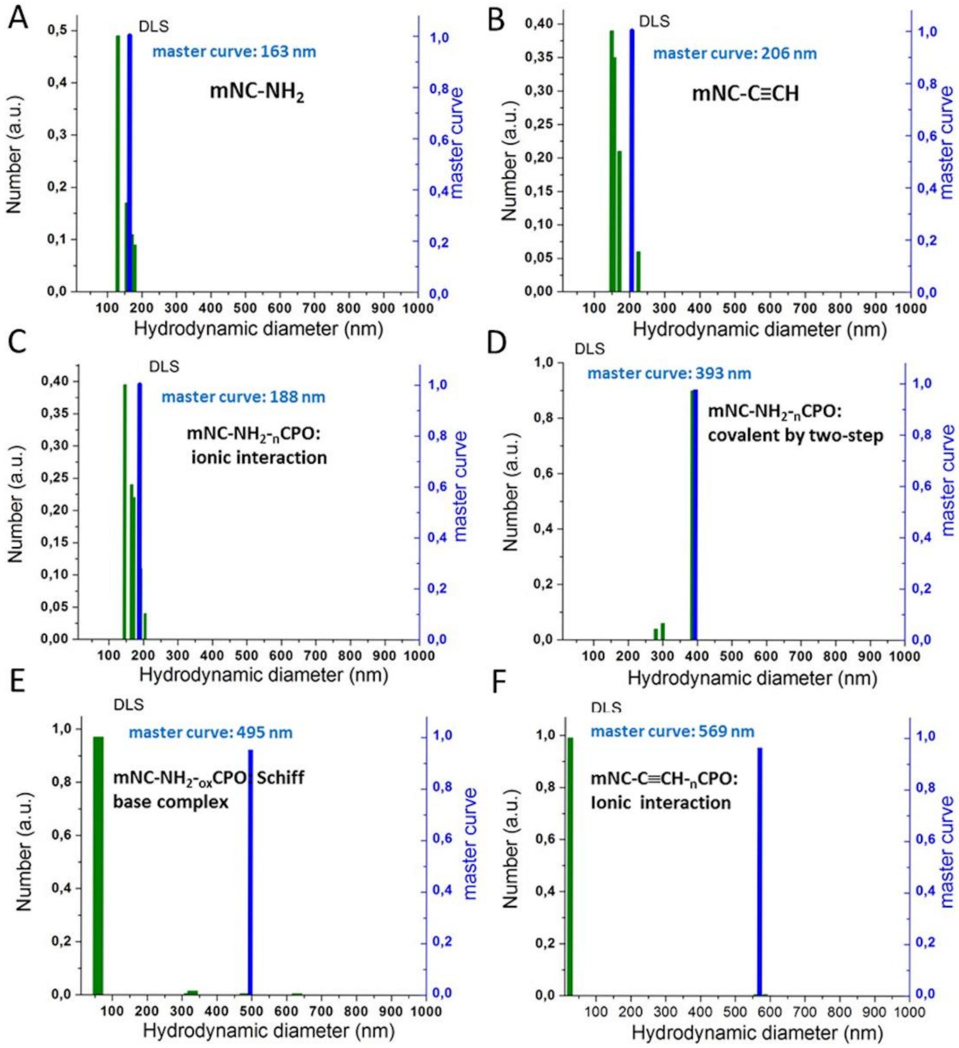

Figure 6.9. Number-weighted distribution of hydrodynamic diameters obtained from the DLS measurements for the primary mNC-NH_2 (**A**) and mNC-C≡CH (**B**), and all four selected derivatives **i**, **ii**, **iii**, **iv** (**C-F**).

DLS measurements (Figure 6.9) showed that the hydrodynamic sizes of functionalized mNC-Si increased significantly after conjugation with enzymes in agreement with the presence of CPO at their surfaces. Except for the sample **i**, the size distributions showed two size populations – smaller corresponding to the individual mNC-Si-CPO derivatives and larger for small aggregates composed of few conjugates (sizes between 390–570 nm). The average hydrodynamic sizes of individual derivatives were significantly larger (**ii**: 393 nm; **iii**: 495 nm; **iv**: 569 nm) to the size of the original **mNC-C≡CH** (206 nm). The distribution for the sample **i** showed only the individual derivatives with the average hydrodynamic size of 188 nm (the size of **mNC-NH$_2$** was 163 nm). The suspension containing the derivatives i remained completely stable, whereas other derivatives spontaneously settled in a few hours. This relatively fast sedimentation of the derivatives is in good agreement with the presence of small aggregates detected by DLS results. TEM analyses showed that all the clusters deposited on the specimen support were co-located with organic material (enzymes), sensitive to the electron beam. The conjugates of the sample **i** were well dispersed over the TEM grid (Figure 6.10A), whereas the conjugates of the other three selected derivatives are located on the TEM grid in a form of small agglomerates (Figure 6.10B-D). The presence of the small agglomerates in suspensions of those derivatives was also confirmed by DLS (Figure 6.9).

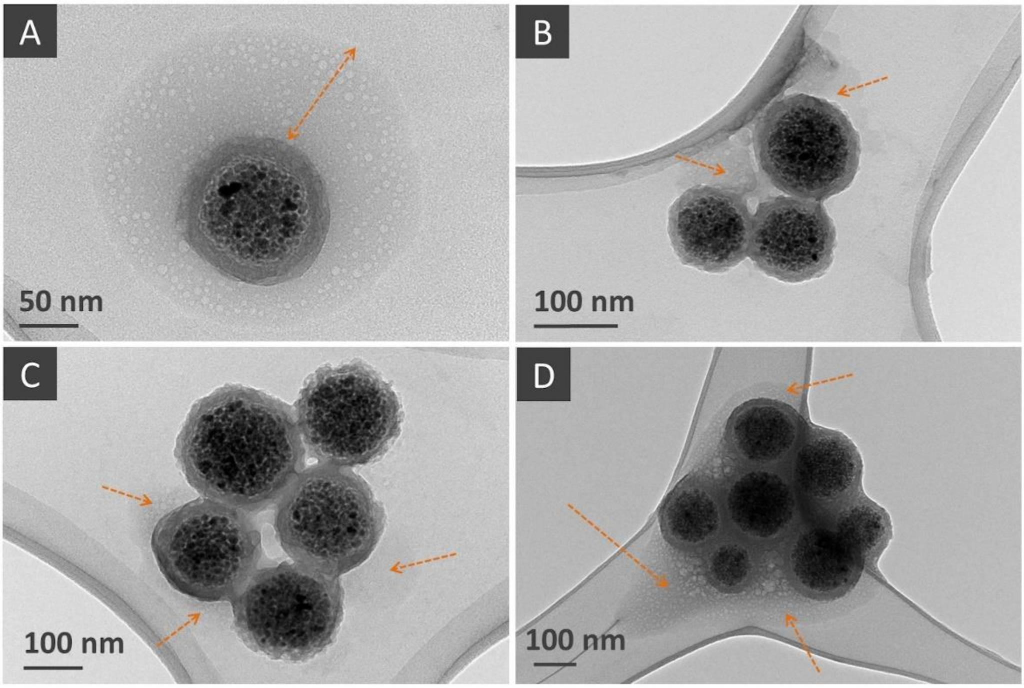

Figure 6.10. TEM images of the ionic derivative mNC-NH$_2$-$_n$CPO (A), the two-step covalent mNC-NH$_2$-$_n$CPO (B), the Schiff base-bound mNC-NH$_2$-$_{ox}$CPO (C), and the non-covalent mNC-C≡CH-$_n$CPO (D). The arrows indicate the presence of organic material co-located with the mNC.

Final derivative selection for β-OH oxidation

The biocatalyst prepared by immobilization of $_{n}$CPO onto mNP-NH$_2$ by ionic attachment was the one with the highest yield and retained activity. It was also the only one of the four chosen derivatives that did not agglomerate. For that, it was first selected as the biocatalyst for the β-OH oxidation. Nevertheless, when the hybrid biocatalyst was incubated in the reaction medium (27 mM β-OH in acetate buffer pH 5.0), the enzyme was rapidly desorbed to the supernatant. Only 27.1% remained attached to the support. To avoid the enzyme desorption, a covalent bond was required, which meant that only two possible derivatives were left: mNC-NH$_2$-$_{n}$CPO (covalent by two-step), mNC-NH$_2$-$_{ox}$CPO (Schiff base complex). In accordance with activity results, the latter was finally selected. Enzyme release in the reaction medium was evaluated and no desorption was observed after 24 h.

In parallel to the biotransformation, two controls were performed to avoid false-positive results, as described in Section 6.2.6.2. No β-OH oxidation catalyzed by the mNC-NH$_2$ in presence of peroxide was observed after 24 h. However, some binding of the product β-CHO to the support was measured (18% from an initial concentration of 11 mM), which has to be taken into account when evaluating the reaction yield. For a cascade biotransformation, eventually coupling the CPO-catalyzed reaction with the aldol addition of dihydroxyacetone catalyzed by FSA, β-CHO loss would be reduced, driven to the target product.

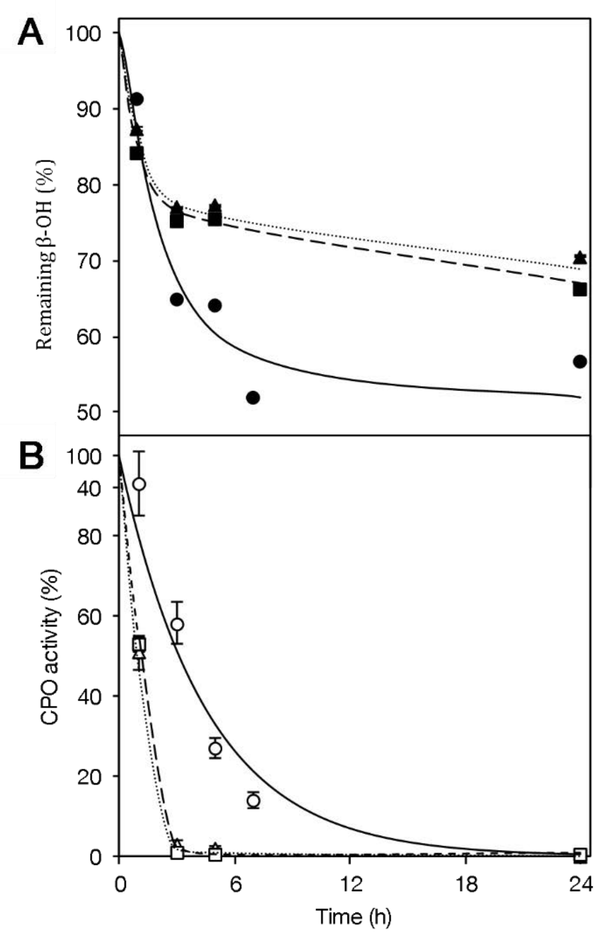

Figure 6.11. Remaining β-OH (**A**) and CPO activity (**B**) on the β-OH oxidation catalyzed by soluble $_n$CPO –β-OH (▲), activity (△)–, soluble $_{ox}$CPO –β-OH (■), activity (□)–, and immobilized mNC-NH$_2$-$_{ox}$CPO –β-OH (●), activity (○). Oxidation conditions: 27 mM β-OH, 450 U CPO mL^{-1}, 3 mM h^{-1} *t*-BuOOH in 100 mM acetate buffer (pH 5.0), 25 ºC.

The time course of the β-OH oxidation reaction catalyzed by mNC-NH$_2$-$_{ox}$CPO is plotted in Figure 6.11. In the same figure, two more reactions can be observed: a) one performed with soluble $_{ox}$CPO to check the immobilization effect on the reaction course and enzyme stability; b) another one catalyzed by soluble $_n$CPO to check the effect of the sugar moieties oxidation. All reactions were performed at the same initial CPO activity. The results showed that the oxidation of sugar moieties did not affect the amino alcohol oxidation activity, and similar initial reaction rates and final β-OH conversion (ca. 32% in 24 h) were obtained. Moreover, the immobilized derivative mNC-NH$_2$-$_{ox}$CPO exhibited the same initial rate confirming the absence of diffusional limitations, and a higher substrate conversion (ca. 45%). Thus, the immobilization onto mNC allowed the enzyme to be more stable towards the peroxide inactivation, with $t_{1/2}$ 4-fold higher than free CPO leading to a higher substrate conversion.

6.3.2 FSA immobilization

6.3.2.1 CoIDA-agarose

FSA was rapidly inactivated in the presence of CPO and *t*-BuOOH. To reduce this effect, FSA was immobilized on CoIDA-agarose, leveraging the His-tag that was added by a genetic modification. To this end, various enzyme loads were offered to the same amount of support in order to observe the presence of diffusional limitations and to determine the immobilization parameters (Table 6.6).

No diffusional limitations were identified at an enzyme load below 40 U mL^{-1} of support. No activity loss was observed: the immobilization yield was 97–99% and the retained activity of the derivative was 93.8–99.0%. Regarding the course of the immobilization of 20 U FSA on 1 mL of support that is plotted in Figure 6.12, all the enzyme was already attached to the support after 2 min of incubation.

Table 6.6. Immobilization yield and retained activity from FSA experiments on CoIDA-agarose, with different enzyme load.

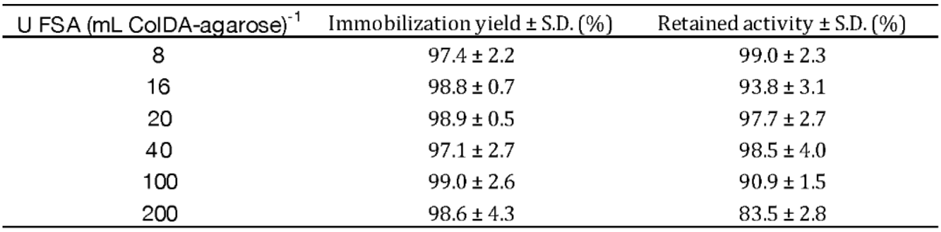

U FSA (mL CoIDA-agarose)$^{-1}$	Immobilization yield ± S.D. (%)	Retained activity ± S.D. (%)
8	97.4 ± 2.2	99.0 ± 2.3
16	98.8 ± 0.7	93.8 ± 3.1
20	98.9 ± 0.5	97.7 ± 2.7
40	97.1 ± 2.7	98.5 ± 4.0
100	99.0 ± 2.6	90.9 ± 1.5
200	98.6 ± 4.3	83.5 ± 2.8

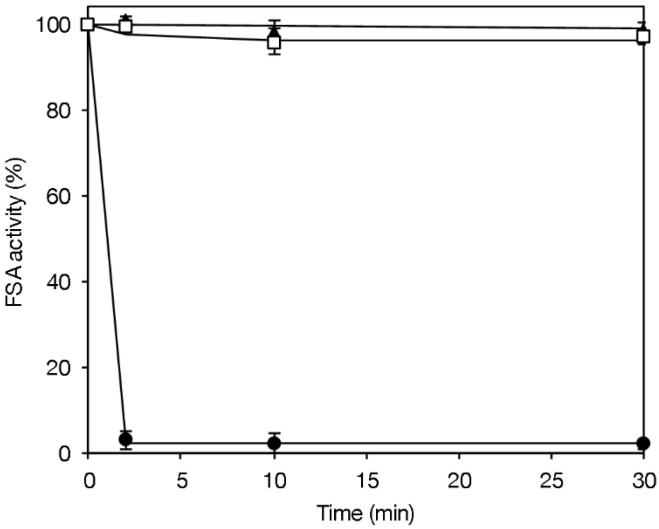

Figure 6.12. Affinity immobilization of FSA on CoIDA-agarose. 20 U mL^{-1} of support was used in 50 mM phosphate buffer (pH 8.0) in 5 mL of total volume, 25 ºC. Blank (▲), suspension (□), supernatant (●).

The applicability of FSA immobilized on CoIDA-agarose was evaluated by the comparison with soluble FSA on the catalysis of the DHA aldol addition. Both reactions were performed using 4.7 U FSA mL^{-1} of reaction medium. At this enzyme load (49 U mL^{-1} of support, no diffusional limitations were expected. Figure 6.13 confirmed this hypothesis; both aldol addition rates were very similar, achieving 92.8% and 91.8% aldehyde conversion after 60 min with immobilized and soluble enzymes, respectively. DHA interfered in the activity test of F6P cleavage, as it is an intermediate product. For that reason, no activity results are shown; however, no inactivation of the enzyme is expected.

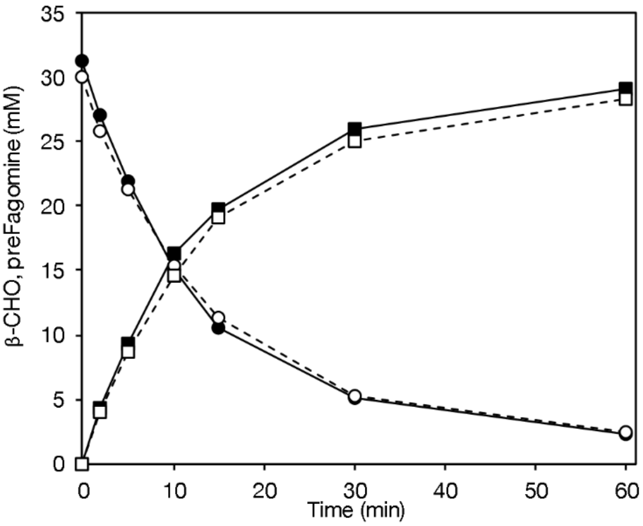

Figure 6.13. DHA aldol addition to the amino aldehyde catalyzed by soluble FSA and immobilized FSA on CoIDA-agarose. Reaction conditions: 30-31 mM β-CHO, 45 mM DHA, 4.7 U FSA mL^{-1} in 50 mM HEPES (pH 8.0), 25 °C. Soluble: β-CHO (○), preFagomine (□); FSA-CoIDA: β-CHO (●), preFagomine (■).

6.3.2.2 mNC

Immobilization of FSA was also intended onto magnetic nanoparticle clusters. The same type of clusters for CPO was also used for FSA, including mNC-Si, mNC-PEG, mNC-NH_2, mNC-COOH, mNC-CHO, mNC-SH, mNC-C≡CH, mNC-N_3. Furthermore, in this case, another mNC was designed: mNC-IDA in order to achieve the attachment of FSA to mNC through the histidine residues. However, no successful production of these clusters was accomplished. Instead, mNC functionalized with ethylenediaminetetraacetic acid (EDTA) was prepared. EDTA also acts as a metal chelator, so it could allow the immobilization. Nevertheless, EDTA consists of two IDA molecules, which means that EDTA can establish up to six coordination linkages with the metal, in contrast to the three ones from IDA (Figure 6.14).[64] Because of this, with EDTA, there are no other free coordination sites to the metal; the His-tag from the protein should compete with EDTA. Despite that, mNC-EDTA was evaluated as a carrier.

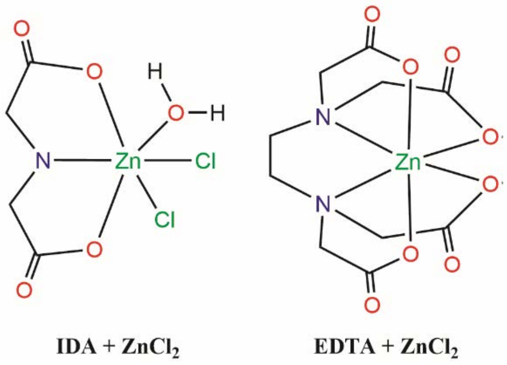

$IDA + ZnCl_2$ $EDTA + ZnCl_2$

Figure 6.14. Metal coordination complexes with IDA and EDTA. It has been adapted from literature.[64]

Enzyme activity quantification

The specific activity of FSA is very low in comparison to CPO: 15 U mg^{-1} and 1400 U mg^{-1} for FSA and CPO, respectively. In CPO immobilizations, the maximum enzyme load per mNC was observed to be approximately 10 U CPO mg^{-1} mNC. In all immobilizations, 0.5 mg mNC mL^{-1} was used; that means an initially offered CPO activity of 5 U mL^{-1}. That was enough activity to be measured with the spectrophotometric activity test of CPO (MCD chlorination). This activity corresponds to 7.1 µg CPO mg^{-1} mNC.

In the case of FSA, a correct initial activity would be around 2 U mL^{-1}. This is the same as 133.3 µg FSA mg^{-1} mNC, much higher than for CPO. First immobilization trials were performed at this enzyme load and, as expected, the immobilization yield and activity were negligible. Therefore, the initial FSA activity was lowered to 0.02 U mL^{-1} (2.7 µg FSA mg^{-1} mNC), to ensure an enzyme load below the maximum value (mNC amount was not increased because of economic reasons). However, the spectrophotometric test for FSA activity (F6P cleavage) is not sensitive enough to properly quantify this activity. Besides, mNC was observed to affect the test, lowering the absorbance (interaction with NADH).

In collaboration with PhD student L. Vázquez, a new activity test was developed. First of all, the decoupling of the spectrophotometric activity test was proposed. The standard test involves the cleavage of F6P into DHA and G3P. The latter compound is converted to DHAP by the isomerase, and DHAP is reduced to glycerol 3-phosphate by GPD using NADH. The aim of the decoupling is to avoid the incubation of mNC with NADH. It was successfully decoupled, first obtaining a Lineweaver Burk calibration curve from the reduction reaction of DHAP (Figure 6.15).[65] Michaelis-Menten kinetics was assumed.

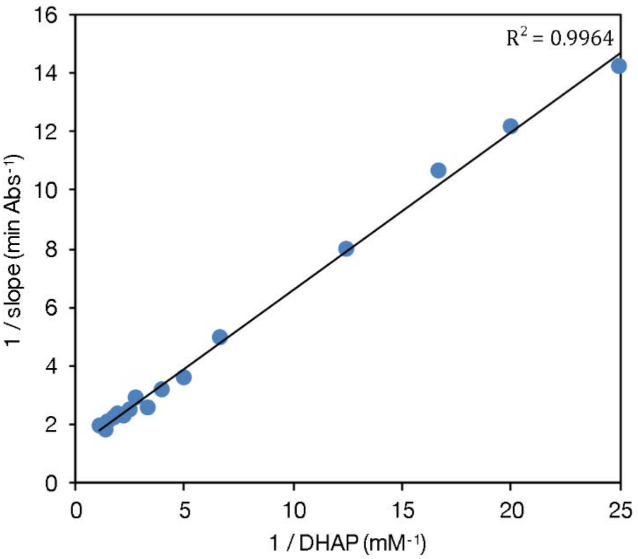

Figure 6.15. Lineweaver Burk plot for the DHAP conversion into NADH catalyzed by GPD. Various concentrations of DHAP in the cuvette with 5 U TPI/GPD mL^{-1} were employed. The slope was calculated from the decrease in absorbance at 340 nm resulting from the conversion of NADH to NAD$^+$ at 30 ºC.

This linearization was used to estimate the FSA activity. After FSA incubation with F6P and imidazole, the enzyme was separated, and the formed G3P was converted into glycerol 3-phosphate by TPI/GPD. The linearity (also inverse axes) of the newly developed test was confirmed by using several amounts of FSA to catalyze the cleavage of F6P, analyzing the resulting conversion of NADH (Figure 6.16). All these trials were carried out using soluble enzyme. However, in a posterior screening using immobilized enzymes, the error between measurements of the same sample was large, probably caused by too many experimental steps (immobilization, mNC-FSA concentration, reactants addition for the F6P cleavage, mNC elimination, ultrafiltration, NADH test). Because of that, this test was discarded and another activity test was developed.

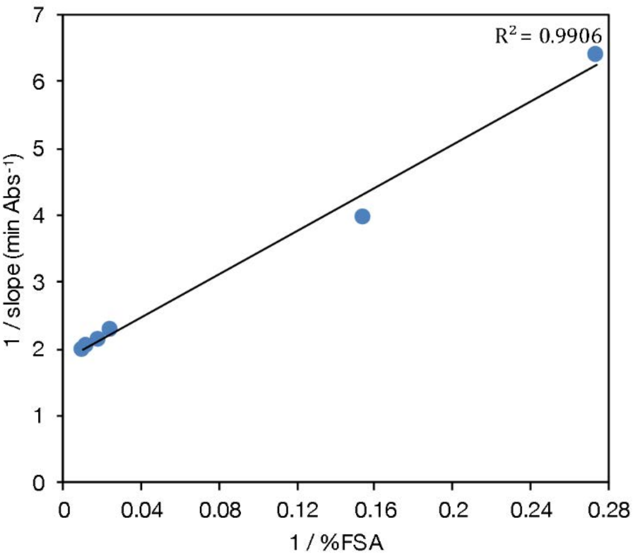

Figure 6.16. A linear relation between the FSA activity and the slope observed in the spectrophotometric test of the reaction of G3P to glycerol 3-phosphate. Assay conditions are detailed in Section 6.2.2.2.

This second test consists in the target aldol addition of DHA to β-CHO catalyzed by FSA, measuring the formation of preFagomine on HPLC. This test shows great linearity (Figure 6.17). In the immobilization screening reported in the following pages, it was the selected activity test, as the reproducibility was enough to characterize each derivative.

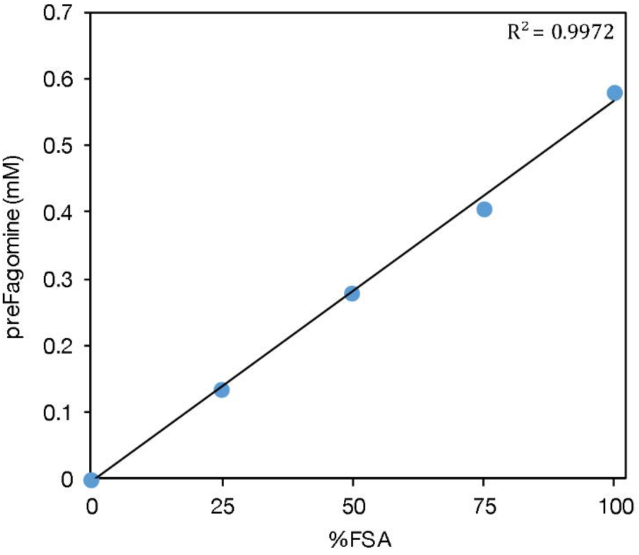

Figure 6.17. The relation between percentage of FSA activity and product formation in the activity test consisting in the DHA aldol addition to β-CHO.

Primary immobilization screening by protein quantification

A primary screening on the immobilization of FSA onto mNC was performed by incubation of the enzyme with each type of cluster, analyzing the protein concentration in the supernatant by the Bradford method. Protein concentration can be assumed to be FSA concentration, as the FSA stock was previously purified using CoIDA agarose, and eluted with 300 mM imidazole. This hypothesis was confirmed by SDS-PAGE (Figure 6.18), following the protocol detailed in the Appendix.

Table 6.7 shows the results from the immobilization screening. S.D. from the table are not statistically valid, since they are too large. This is caused by the low protein concentration to quantify; Bradford method is not sensitive enough. However, the range of the yields is enough to evaluate the immobilization derivatives and select the most promising candidates for further study.

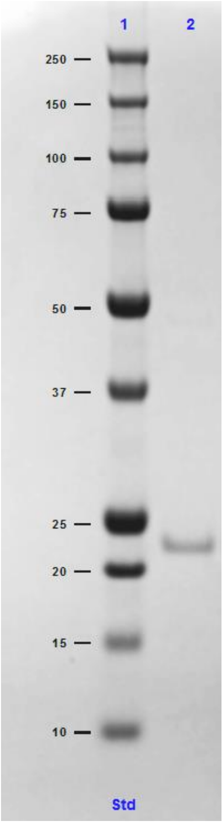

Figure 6.18. SDS-PAGE gel from FSA sample purified using CoIDA agarose. Lane 1: molecular weight marker in kDa. Lane 2: FSA band of approximately 23 kDa.

Table 6.7. Results from the screening of the FSA immobilization onto functionalized mNC. S.D. is calculated from 4 replicas in each case. Immobilization conditions: 0.5 mg mNC and 0.02 U FSA in 10 mM phosphate buffer in 1 mL of total volume, 25 ºC. No NaCl was added. n.d.: not determined.

#	Reactive group		Immobilization yield ± S.D. (%)	
	mNC	FSA	pH 5.0	pH 8.0
1	Si	OH	77.5 ± 7.6	20.5 ± 14.6
2	PEG	OH	15.8 ± 19.3	6.1 ± 10.0
3	NH_2	COOH	>99 ± 19.5	>99 ± 15.8
4	COOH	NH_2	>99 ± 11.3	9.8 ± 15.1
5	CHO	NH_2	>99 ± 17.1	67.2 ± 5.6
6	N_3	n.d.	88.8 ± 11.4	6.5 ± 8.3
7	N_3 (+CuBr)	n.d.	97.3 ± 13.1	90.8 ± 9.2
8	SH	SH	<1 ± 5.2	<1 ± 2.8
9	$C\equiv CH$	OH	26.1 ± 5.9	<1 ± 6.1
10	EDTA	NH_2	>99 ± 12.0	86.2 ± 7.1

Up to eleven derivatives achieved an immobilization yield near or above 50%: #**1** (pH 5.0), #**3** (pH 5.0), #**3** (pH 8.0), #**4** (pH 5.0), #**5** (pH 5.0), #**5** (pH 8.0), #**6** (pH 5.0), #**7** (pH 5.0), #**7** (pH 8.0), #**10** (pH 5.0), and #**10** (pH 8.0). In all cases, the binding support–enzyme was electrostatic since all the enzyme was released to the supernatant when a high concentration of NaCl was added and left for 60 min. Although #**5** was expected to be covalent through a Schiff base formation, this type of bond was not accomplished. An improved preparation of this type of mNC (e.g. higher reactivity) could enhance this binding.

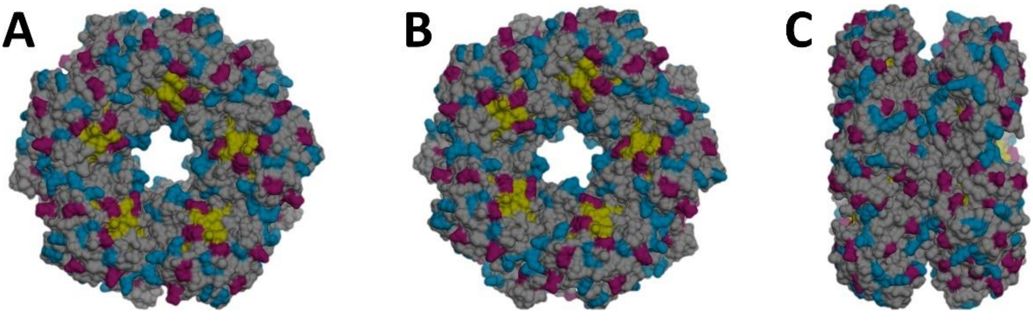

Figure 6.19. Tridimensional structure of FSA. The entrances to the two active sites are located between the Lys85 from five subunits, in yellow. Acid residues are colored in red; basic residues are in blue. Some captions of the enzyme structure are pictured: (A) front, (B) back, (C) side. His-tag is not represented since this modification has not been included in the literature used for the Protein Data Bank (PDB) file.[66]

As shown in the table, the immobilization was successful (in terms of yield) through both amino and carboxylic groups from the enzyme. This is caused by the enzyme structure, which is represented in Figure 6.19, by the use of UCSF Chimera software. Many NH_2 and COOH are present along the FSA surface. They are equally distributed; their immobilization is not favored in detriment to the other.

In the case of mNC-N_3, it was not determined which one was the reactive group from FSA. At first, it was thought to be some particular interaction with the His-tag of the enzyme, however it was expected that the enzyme was not released when increasing the ionic strength, but with a competitor as imidazole. The binding was broken with NaCl, therefore it was supposed an electrostatic interaction driven by the positive charge of the azide. The same mNC was employed in the presence of a catalytic amount of CuBr (#**7**), similarly to the study with CPO. Especially at pH 8.0, the immobilization yield notably increased.

Results from derivative #**10** were also not expected. As above mentioned, these particles were firstly prepared for the binding of the enzyme through polyhistidine tag. To this end, these particles were intended to be chelated with cobalt in order to further attach the enzyme. Various concentrations of the metal were used to charge this mNC (Table 6.8). As plotted in Figure 6.20, the more metal was offered to mNC, the less enzyme was attached in the immobilization. 0.2 mM was enough to charge almost completely the particles. Above this value, no significant values in the immobilization yield were observed. This could be explained according to the assumption that both EDTA and the metal can form up to six coordination bonds. If no metal is present, EDTA has four carboxylic groups available to interact with FSA, probably by the amino groups of the enzyme. When the metal is offered, these COOH groups form coordination bonds with cobalt. Hence, this metal chelation reduces the formation of bonds between COOH from mNC and NH_2 from the enzyme. Instead, the metal is charged on the surface of the cluster. Nevertheless, as EDTA is a very strong metal chelator, the His-tag from the enzyme cannot compete with EDTA. This could explain the low immobilization yield when the metal concentration has been increased.

Table 6.8. Dependence on the cobalt charge in the immobilization of FSA onto mNC-EDTA. Metal concentration is referred to the mNC-EDTA preparation detailed in Materials and Methods. The immobilization was performed in 10 mM phosphate buffer (pH 8.0), 25 ºC. No NaCl was added. S.D. is calculated from 2 replicas in each case.

$CoCl_2$ (mM)	Immobilization yield ± S.D. (%)
200	33.1 ± 10.2
100	31.5 ± 7.4
4	43.4 ± 6.8
0.4	49.3 ± 2.4
0.2	48.6 ± 6.9
0	86.2 ± 7.1

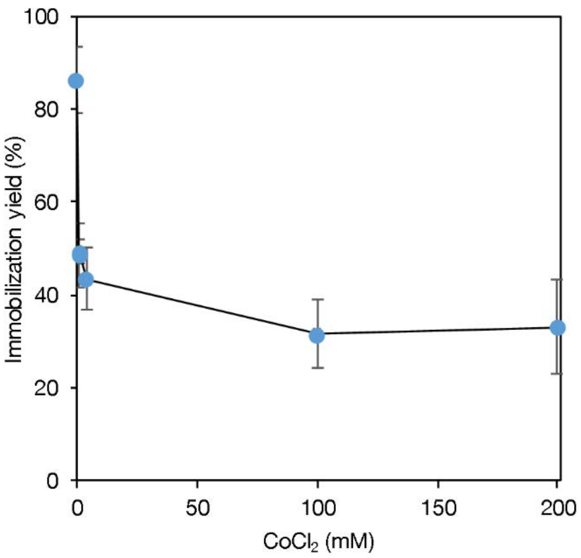

Figure 6.20. Graphical representation of the data on Table 6.8 for a better understanding.

Activity screening of selected derivatives

The eleven derivatives with immobilization yields above 50% were further investigated. The activity of all eleven derivatives was analyzed using the newly developed activity test (preFagomine formation measured by HPLC) (Table 6.9). The activity of derivative #**7** at both pH was not calculated, because CuBr affected the HPLC analysis, even after washing with buffer, altering the peak separation and quantification.

Table 6.9. Activities of the selected derivatives from the primary screening. The activity was calculated using the HPLC test involving the preFagomine formation. No NaCl was added. S.D. is calculated from 2 replicas in each case.

# Derivative	pH	Retained activity ± S.D. (%)
1	5	59.5 ± 5.6
3	5	61.0 ± 12.8
3	8	21.0 ± 3.9
4	5	2.1 ± 2.4
5	5	60.0 ± 14.3
5	8	9.8 ± 2.8
6	5	94.0 ± 20.8
10	5	20.0 ± 9.3
10	8	55.5 ± 3.1

The activity screening reduced the candidate derivatives to five (with retained activity >50%): #**1** (pH 5.0), #**3** (pH 5.0), #**5** (pH 5.0), #**6** (pH 5.0), and #**10** (pH 8.0). The attachment through the amino groups of the enzyme (#**4**, Table 6.7) produced a total loss of activity. This could be explained by a possible linkage between mNC-COOH and Lys85 of FSA (Figure 6.19), which has a key role in the catalysis of this enzyme.[67] In other cases when attaching to the amino groups of the enzyme (#**5**, #**10**), some activity loss was also observed.

In the five mentioned derivatives, FSA was only immobilized through electrostatic interactions. After incubation in the target reaction buffer (50 mM HEPES pH 8.0), most of the enzyme was released to the supernatant. Thus, a covalent attachment was required. Covalent binding between NH_2–COOH has been extensively used in this chapter. Here, this EDAC technology could be used for derivatives #**3** pH 5.0, and #**10** pH 8.0. The first one was a bit more active; besides, EDAC binding is strongly recommended to be performed in acidic conditions (pH 4.5–5).[68] Therefore, biocatalyst #**3** was the one selected for further study.

Covalent attachment onto mNC-NH_2

A screening regarding the EDAC concentration was designed to find the more suitable immobilization conditions. Nanobiocatalyst repeated washing with NaCl was employed to ensure the formation of covalent bonds. 1 M NaCl was first used, but it was seen some loss of activity due to this incubation with salt. Instead, two washing cycles with 0.25 M NaCl were found to be enough to remove the electrostatic interactions, without any activity loss.

An EDAC amount between 2.5 and 10 mM was found to be the proper concentration, leading to a final mean retained activity close to 29% (Table 6.10). It was set to 5 mM EDAC in further experiments. The activity loss in comparison the electrostatically-immobilized derivative can be related to higher bond rigidity, and also to some cross-linking of the enzyme (through its NH_2 and COOH groups).

Table 6.10. Screening of the EDAC concentration for the covalent immobilization of FSA onto mNC-NH_2. Immobilization conditions: 3 h in 10 mM phosphate buffer (pH 5.0), 25 ºC. *Washing* corresponds to two 5-minute consecutive washing cycles with 0.25 M NaCl.

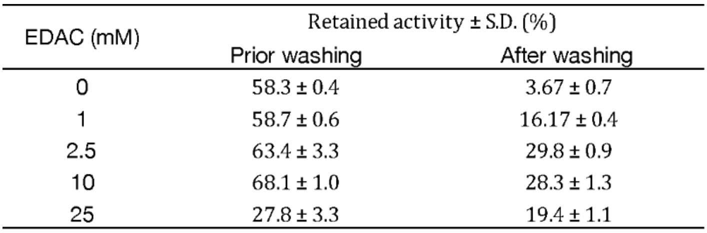

EDAC (mM)	Retained activity ± S.D. (%)	
	Prior washing	After washing
0	58.3 ± 0.4	3.67 ± 0.7
1	58.7 ± 0.6	16.17 ± 0.4
2.5	63.4 ± 3.3	29.8 ± 0.9
10	68.1 ± 1.0	28.3 ± 1.3
25	27.8 ± 3.3	19.4 ± 1.1

Aldol addition catalyzed by mNC-NH_2-FSA

The covalent derivative mNC-NH_2-FSA was selected to be evaluated in the target reaction of FSA, the aldol addition of DHA to β-CHO. The reaction course was compared to another reaction catalyzed by the same units of soluble enzyme (Figure 6.21). As the immobilized enzyme was onto mNC with easy magnetic recovery, reaction cycles were proposed.

Comparing the first cycle of the immobilized enzyme with the soluble form, it can be seen that the reaction course was quite similar in both cases, with very similar final product yields in both cases: after 5 h, 90.4% for mNC-NH_2-FSA, and 86.5% for soluble FSA. The main problem was observed after the first cycle. The derivative was washed with buffer, and the substrates for the second cycle were added. Nevertheless, the second reaction rate was much lower than the first one, leading to a product yield of only 19.4% in the same reaction time. The yield from the third reaction cycle was even lower: 2.0%. This means that the immobilized derivative is somehow being inactivated, and the buffer washing between cycles does not reduce this inactivation.

A possible explanation of this inactivation could be derived from the surface amino groups from this mNC-NH_2. The amino aldehyde (β-CHO) enters the active site of FSA in order to be converted into preFagomine. Once inside the enzyme, it could be linked to mNC-NH_2 by a Schiff base formation. The enzyme could then be attached to the support through the aldehyde, modifying its tridimensional structure. This likely modification, or the blocking of the enzyme active site by double-attachment of the aldehyde to mNC and FSA, could explain the inactivation of the enzyme.

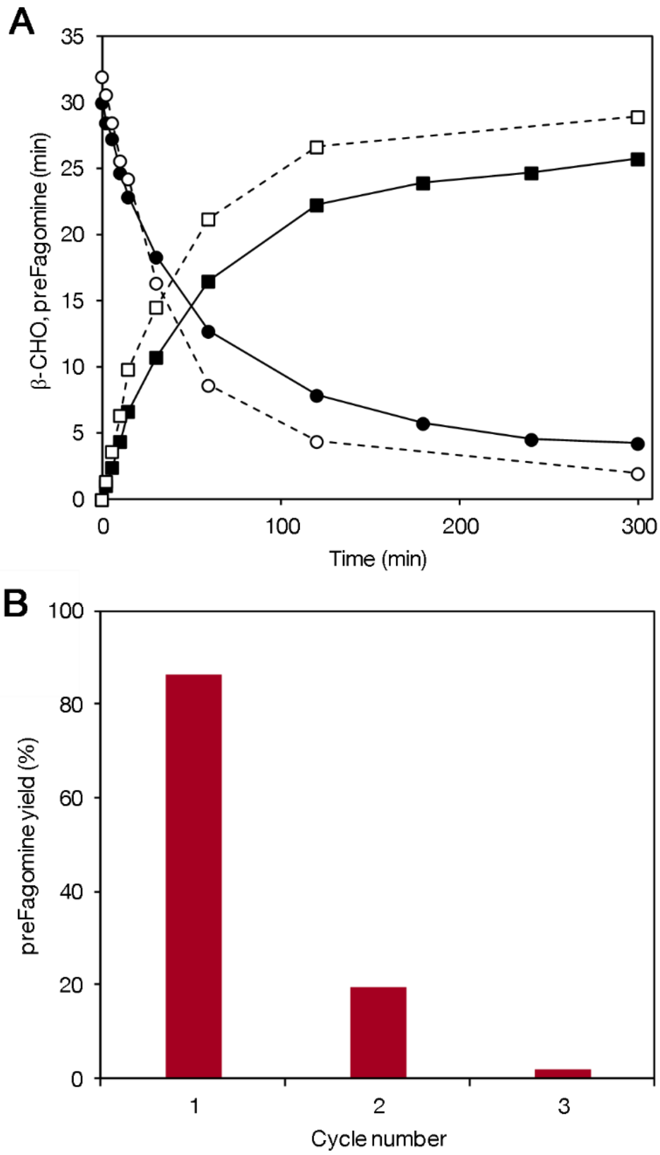

Figure 6.21. DHA aldol addition to the β-CHO catalyzed by soluble FSA and immobilized mNC-NH_2-FSA. (**A**) Reaction course of the first cycle with immobilized FSA, and the reaction catalyzed by soluble FSA. Soluble: β-CHO (○), preFagomine (□); mNC-NH_2-FSA: β-CHO (●), preFagomine (■). (**B**) Reaction cycles. Reaction conditions: 30-31 mM β-CHO, 45 mM DHA, 1.0 U FSA mL^{-1} in 50 mM HEPES (pH 8.0), 25 °C.

6.4 Conclusions

The immobilization of $_n$CPO on MANA-agarose has been performed, increasing the biocatalyst stability to peroxide inactivation. This allowed a higher final *N*-Cbz-3-aminopropanol conversion. Functionalized magnetic nanoparticle clusters (mNC) have demonstrated to be a promising material for the preparation of hybrid enzyme-mNC biocatalysts. The systematic study of CPO immobilization onto mNC by covalent or non-covalent bonds led to several hybrid biocatalysts that could be employed in biotransformations. The selected biocatalyst (mNC-NH_2-$_{ox}$CPO) catalyzes the β-OH oxidation, is 4-fold more stable than soluble native or oxidized enzyme leading to higher conversion and exhibits magnetic response sufficient for derivative recovery.

FSA has been immobilized on agarose functionalized with IDA and chelated with cobalt, leveraging the His-tag included in its recombinant form. High immobilization yield and activity were obtained, as well as a similar reaction rate to the soluble enzyme in the DHA aldol addition to the amino aldehyde. FSA has been also immobilized in variously functionalized mNC. Similarly to CPO, an exhaustive screening has been performed to select the most promising derivatives, which have been characterized using a newly developed activity test. Finally, the selected conjugate (mNC-NH_2-FSA) has been used in the aldol addition reaction, with similar results as the soluble enzyme. However, the derivative was not stable enough, and its activity dropped fast in the second reaction cycle. This could be enhanced by preparation of another covalent derivative, with different functionalization on the mNC surface; the use of mNC-EDTA with EDAC could be an alternative. Besides, successful preparation of mNC-IDA could be an important enhancement.

Thus, the preparation of active immobilized derivatives from CPO and FSA has been achieved, employing some conventional (functionalized agarose) and other more trending supports (magnetic nanoparticle clusters). The described methodology for nanobiocatalysts could easily be extended to many other enzymes for the preparation of efficient and reusable biocatalysts.

6.5 Contributions from the collaborations

Dr. Slavko Kralj (*Department for Materials Synthesis, Institut Jožef Stefan –IJS–, Ljubljana, Slovenia; Nanos SCI, Ljubljana, Slovenia; Department of Chemical and Pharmaceutical Sciences, Trieste, Italy*) performed all the mNC syntheses and characterizations, with the exception of mNC-CHO that was modified by Gerard Masdeu.

Physical characterization of final immobilized mNC derivatives was also carried out by Dr. Kralj.

Dr. Stane Pajk (*Condensed Matter Physics Department, IJS; Faculty of Pharmacy, Ljubljana, Slovenia*) did the synthesis of silane-N_3 and silane-C≡CH.

Prof. Darko Makovec (*Department for Materials Synthesis, IJS)* supervised the research stay of G. Masdeu at his institute, regarding the first trials in CPO and FSA immobilization onto mNC.

Luis Miguel Vázquez (*Department of Chemical, Biological and Environmental Engineering, UAB*), together with G. Masdeu, worked on the development of an alternative activity test for FSA, as well as in the activity screening of the selected derivatives. Finally, they both performed the reaction cycles with mNC-NH_2-FSA.

G. Masdeu did the preparation of MANA-agarose and CoIDA-agarose and all the immobilizations of CPO on MANA-agarose, CPO onto mNC, and FSA on CoIDA-agarose. Besides, he did the primary FSA immobilization screening on mNC.

6.6 References

[1] C. Mateo, J. M. Palomo, G. Fernandez-Lorente, J. M. Guisan, R. Fernandez-Lafuente, *Enzyme Microb. Technol.* **2007**, *40*, 1451–1463.

[2] R. A. Sheldon, S. Van Pelt, *Chem. Soc. Rev.* **2013**, *42*, 6223–6235.

[3] L. Cao, in *Carrier-Bound Immobil. Enzym. Princ. Appl. Des.*, Wiley-VCH, Weinheim, Germany, **2006**, pp. 1–52.

[4] S. Datta, L. R. Christena, Y. R. S. Rajaram, *3 Biotech* **2013**, *3*, 1–9.

[5] W. Tischer, F. Wedekind, in *Biocatal. - From Discov. to Appl.* (Eds.: W.D. Fessner, A. Archelas, D.C. Demirjian, R. Furstoss, H. Griengl, K.E. Jaeger, E. Morís-Varas, R. Öhrlein, M.T. Reetz, J.L. Reymond, et al.), Springer, Berlin, Germany, **1999**, pp. 95–126.

[6] R. A. Meryam Sardar, *Biochem. Anal. Biochem.* **2015**, *4*, 1–8.

[7] J. Porath, R. Axén, *Methods Enzymol.* **1976**, *44*, 19–45.

[8] P. Zucca, R. Fernandez-Lafuente, E. Sanjust, *Molecules* **2016**, *21*, 1–25.

[9] J. C. S. Dos Santos, O. Barbosa, C. Ortiz, A. Berenguer-Murcia, R. C. Rodrigues, R. Fernandez-Lafuente, *ChemCatChem* **2015**, *7*, 2413–2432.

[10] P. F. Builders, O. O. Kunle, M. U. Adikwu, *Int. J. Pharm.* **2008**, *356*, 174–180.

[11] H. Tian, G. Xu, B. Yang, G. Guo, *J. Food Eng.* **2011**, *107*, 21–26.

[12] H. W. M. de Koning, R. A. F. M. Chamuleau, A. Bantjes, *J. Biomed. Mater. Res.* **1984**, *18*, 1–13.

[13] A. Awadhiya, D. Kumar, V. Verma, *Carbohydr. Polym.* **2016**, *151*, 60–67.

[14] C. Mateo, J. M. Palomo, M. Fuentes, L. Betancor, V. Grazu, F. López-Gallego, B. C. C. Pessela, A. Hidalgo, G. Fernández-Lorente, R.

Fernández-Lafuente, et al., *Enzyme Microb. Technol.* **2006**, *39*, 274–280.

[15] J. Guisán, *Enzyme Microb. Technol.* **1988**, *10*, 375–382.

[16] R. Fernandez-Lafuente, C. M. Rosell, V. Rodriguez, C. Santana, G. Soler, A. Bastida, J. M. Guisan, *Enzyme Microb. Technol.* **1993**, *15*, 546–550.

[17] I. Ardao, M. D. Benaiges, G. Caminal, G. Álvaro, *Enzyme Microb. Technol.* **2006**, *39*, 22–27.

[18] Y. Deng, C. Deng, D. Qi, C. Liu, J. Liu, X. Zhang, D. Zhao, *Adv. Mater.* **2009**, *21*, 1377–1382.

[19] L. Lei, Y. Bai, Y. Li, L. Yi, Y. Yang, C. Xia, *J. Magn. Magn. Mater.* **2009**, *321*, 252–258.

[20] X. Liu, Y. Guan, R. Shen, H. Liu, *J. Chromatogr. B* **2005**, *822*, 91–97.

[21] S. P. Gubin, *Magnetic Nanoparticles*, Wiley-VCH, **2009**.

[22] A. K. Gupta, M. Gupta, *Biomaterials* **2005**, *26*, 3995–4021.

[23] E. Katz, I. Willner, *Angew. Chemie - Int. Ed.* **2004**, *43*, 6042–6108.

[24] P. G. Tratnyek, R. L. Johnson, *Nano Today* **2006**, *1*, 44–48.

[25] B. Xin, S. Si, G. Xing, *Chem. Asian J.* **2010**, *5*, 1389–94.

[26] H. F. Lo, H. Y. Hu, C. P. Hung, S. C. Chen, L. L. Lin, *Biocatal. Biotransformation* **2009**, *27*, 318–327.

[27] Q. Zhang, J. Kang, B. Yang, L. Zhao, Z. Hou, B. Tang, *Chinese J. Catal.* **2016**, *37*, 389–397.

[28] Q. Zhang, X. Han, B. Tang, *RSC Adv.* **2013**, *3*, 9924–9931.

[29] S. Kralj, D. Makovec, *RSC Adv.* **2014**, *4*, 13167–13171.

[30] U. Häfeli, W. Schütt, J. Teller, M. Zborowski, *Scientific and Clinical Applications of Magnetic Carriers*, Plenum Press, New York, USA, **1997**.

[31] A. Ditsch, P. E. Laibinis, D. I. Wang, T. A. Hatton, *Langmuir* **2005**, *21*, 6006–6018.

[32] L. De Matteis, R. Germani, M. V. Mancini, G. Savelli, N. Spreti, L. Brinchi, G. Pastori, *J. Mol. Catal. B Enzym.* **2013**, *97*, 23–30.

[33] L. De Matteis, R. Germani, M. V. Mancini, F. Di Renzo, N. Spreti, *Appl. Catal. A Gen.* **2015**, *492*, 23–30.

[34] S. Hudson, J. Cooney, B. K. Hodnett, E. Magner, *Chem. Mater.* **2007**, *19*, 2049–2055.

[35] Y. J. Han, J. T. Watson, G. D. Stucky, A. Butler, *J. Mol. Catal. B Enzym.* **2002**, *17*, 1–8.

[36] M. Andersson, B. K. Samra, H. Holmberg, P. Adlercreutz, *Biocatal. Biotransformation* **1999**, *17*, 293–303.

[37] D. I. Perez, F. Van Rantwijk, R. A. Sheldon, *Adv. Synth. Catal.* **2009**, *351*, 2133–2139.

[38] C. Roberge, D. Amos, D. Pollard, P. Devine, *J. Mol. Catal. B Enzym.* **2009**, *56*, 41–45.

[39] D. R. Morris, L. P. Hager, *J. Biol. Chem.* **1966**, *241*, 1763–1768.

[40] M. Pešić, C. López, G. Álvaro, J. López-Santín, *J. Mol. Catal. B Enzym.* **2012**, *84*, 144–151.

[41] W. Wang, Y. Xu, D. I. C. Wang, Z. Li, *J. Am. Chem. Soc.* **2009**, *131*, 12892–3.

[42] R. Cui, C. Bai, Y. Jiang, M. Hu, S. Li, Q. Zhai, *Chem. Eng. J.* **2015**, *259*, 640–646.

[43] L. Horváth, M. Ábrahám, L. Boross, B. Szajáni, *Appl. Biochem. Biotechnol.* **1989**, *22*, 223–235.

[44] S. E. D'Souza, W. Altekar, S. F. D. D'Souza, *World J. Microbiol. Biotechnol.* **1997**, *13*, 561–564.

[45] S. Reinicke, H. C. Rees, P. Espeel, N. Vanparijs, C. Bisterfeld, M. Dick, R. R. Rosencrantz, G. Brezesinski, B. G. de Geest, F. E. Du Prez, et al., *ACS Appl. Mater. Interfaces* **2017**, *9*, 8317–8326.

[46] T. Suau, J. Calveras, P. Clapés, M. Dolors Benaiges, G. Álvaro, *Biocatal. Biotransformation* **2005**, *23*, 241–250.

[47] I. Ardao, G. Álvaro, M. D. Benaiges, *Biochem. Eng. J. j* **2011**, *56*, 190–197.

[48] I. Ardao, J. Comenge, M. D. Benaiges, G. Álvaro, V. F. Puntes, *Langmuir* **2012**, *28*, 6461–6467.

[49] C. Guérard-Hélaine, B. Légeret, C. Fernandes, V. Prévot, C. Forano, M. Lemaire, *New J. Chem.* **2011**, *35*, 776.

[50] R. Mahdi, C. Guérard-Hélaine, C. Laroche, P. Michaud, V. Prévot, C. Forano, M. Lemaire, *J. Mol. Catal. B Enzym.* **2015**, *122*, 204–211.

[51] S. Kralj, T. Potrč, P. Kocbek, S. Marchesan, D. Makovec, *Curr. Med. Chem.* **2016**, *23*, 1–16.

[52] S. Kralj, D. Makovec, *ACS Nano* **2015**, *9*, 9700–9707.

[53] L. Kopanja, S. Kralj, D. Zunic, B. Loncar, M. Tadic, *Ceram. Int.* **2016**, *42*, 10976–10984.

[54] M. Tadic, S. Kralj, M. Jagodic, D. Hanzel, D. Makovec, *Appl. Surf. Sci.* **2014**, *322*, 255–264.

[55] S. Kralj, D. Makovec, S. Čampelj, M. Drofenik, *J. Magn. Magn. Mater.* **2010**, *322*, 1847–1853.

[56] S. Kralj, M. Drofenik, D. Makovec, *J. Nanoparticle Res.* **2011**, *13*, 2829–2841.

[57] P. L. Felgner, J. E. Wilson, *Anal. Biochem.* **1976**, *74*, 631–635.

[58] N. M. Giles, A. B. Watts, G. I. Giles, F. H. Fry, J. A. Littlechild, C. Jacob, *Chem. Biol.* **2003**, *10*, 677–693.

[59] M. Bradford, *Anal. Biochem.* **1976**, *72*, 248–254.

[60] G. C. Tron, T. Pirali, R. A. Billington, P. L. Canonico, G. Sorba, A. A. Genazzani, *Med. Res. Rev.* **2008**, *28*, 278–308.

[61] T. F. Tadros, *Solid/liquid Dispersions*, Academic Press, London, UK, **1987**.

[62] E. F. Pettersen, T. D. Goddard, C. C. Huang, G. S. Couch, D. M. Greenblatt, E. C. Meng, T. E. Ferrin, *J. Comput. Chem.* **2004**, *25*, 1605–1612.

[63] M. Sundaramoorthy, J. Terner, T. L. Poulos, *Structure* **1995**, *3*, 1367–1378.

[64] S. Sylvie, K. Pavel, C. Kristyna, N. Lukas, M. Rodrigo, M. Angel, S. Zbysek, K. Rene, in *Mendelnet*, **2015**, pp. 595–599.

[65] H. Lineweaver, D. Burk, *J. Am. Chem. Soc.* **1934**, *56*, 658–666.

[66] S. Thorell, M. Schürmann, G. A. Sprenger, G. Schneider, *J. Mol. Biol.* **2002**, *319*, 161–171.

[67] I. Sánchez-Moreno, L. Nauton, V. Théry, *J. Mol. …* **2012**, *84*, 9–14.

[68] G. T. Hermanson, *Bioconjugate Techniques*, Academic Press, Rockford, USA, **2013**.

7 Kinetic model exploitation for the determination of the coupled reaction conditions

7.1 Introduction

Understanding the mechanism of an enzyme-catalyzed reaction is essential for its correct application in industry, especially when dealing with a very complex system of reactions.[1] Computation tools complement experimental techniques in order to facilitate the interpretation of the enzyme behavior and the formulation of a mathematical model, which can speed the pharmaceuticals development.[2,3] In the case of a multi-enzyme system, a decomposition of the whole system is required for the model formulation, understanding each reaction separately. This methodology was followed in Chapter 5, as the system was too complex to be resolved experimentally, without the use of modeling.

The use of modeling becomes essential in biocatalytic processes when inhibition effects of substrates and products can alter the system productivity.[4] In that sense, modeling techniques enable the evaluation of possibilities for process intensification, as they allow the simulation of alternative processes, tuning the operational variables of the system, without further experimental work.[5] Because of this, they are used in industry, although not widely implemented yet, for example by the Swiss company Lonza in the production of fine chemicals.[6,7]

In the case of study, the developed kinetic model of the CPO/FSA-catalyzed synthesis of preFagomine is used in this chapter to study the initial operating conditions for the coupled reaction. Previously, the restrictions of the system were found: (1) the oxidation of DHA catalyzed by CPO, (2) the inhibition of CPO reactions by DHA, (3) the inactivation of FSA by the radical formed in the degradation of *t*-BuOOH by CPO, and (4) the inactivation of FSA by a product of the undesired oxidation of DHA by CPO. Using the reaction model, the reaction conditions are optimized to try to increment the negligible preFagomine yield that was obtained in the preliminary study presented in Chapter 4. The reaction performance is tested in two configurations (one-pot or in two consecutive reaction vessels looking for the best conditions in each case.

In this thesis work, immobilized biocatalysts of each enzyme have been obtained and characterized. Four derivatives were selected ($_n$CPO-MANA-agarose, mNC-NH$_2$-$_{ox}$CPO, FSA-CoIDA-agarose, mNC-NH$_2$-FSA) and will be tested in the above mentioned optimized reaction conditions. However, it is worth to note that when immobilized enzymes are used to catalyze the reaction, the kinetics parameters can differ from the ones found for the soluble catalysts.[8] This is, the optimal reaction conditions determined from an optimization of the *soluble-enzyme* model cannot surely be the optimal conditions for a reaction employing immobilized derivatives, due to mass transfer effects or altered inactivation rates due to immobilization .

7.2 Materials and methods

7.2.1 Materials

All the reagents used in this chapter have been already presented in previous chapters.

7.2.2 CPO/FSA activity

The enzymatic activities of CPO and FSA were measured following the activity test detailed in Materials and Methods in Chapter 3 and Chapter 4, respectively. The activity test for a low concentration of FSA is discussed in Chapter 6.

7.2.3 Enzyme immobilization

$_n$CPO sugar moieties were oxidized to render $_{ox}$CPO, which was covalently immobilized on mNC-NH$_2$. $_n$CPO was also attached to MANA-agarose. FSA was covalently immobilized on mNC-NH$_2$ and by affinity to CoIDA-agarose. All immobilization protocols are fully described in Chapter 6.

7.2.4 HPLC analysis

Concentrations of β-OH, β-CHO, β-COOH, *t*-BuOOH, DHA, and preFagomine were measured by HPLC analysis according to the protocol described in Chapter 4.

7.2.5 Model calculations

All simulations and optimization calculations have been performed using PSE gPROMS® Model Builder 5.0.0. Various scenarios were simulated to maximize the formation of preFagomine. Different concentrations of substrates and enzymes were assayed. The optimization algorithm of the software was employed to this end.

7.2.6 Coupled reactions

The one-pot reaction was carried out at the following initial concentrations: 16 mM β-OH, 39.9 mM *t*-BuOOH, 72.6 mM DHA. 3.57 mg CPO mL^{-1} and 13.33 mg FSA mL^{-1} were used. The initial two-step reaction mixture was 5.0 mM β-OH, 10.0 mM *t*-BuOOH, and 312.5 U CPO mL^{-1} for the β-OH oxidation, and 0.5 mM β-CHO, 20.0 mM DHA, and 0.58 U FSA mL^{-1} for the aldol addition. The reaction medium after the oxidation was separated by a magnetic field (if applicable), filtrated to remove the agarose (if applicable), and ultrafiltrated to remove the soluble enzyme (all cases). Finally, it was left under mild agitation for 60 min before starting the second reaction, to degrade the peroxy radical.

All reactions were performed in 100 mM MES buffer (pH 6.5) at 25 °C, 1000 rpm of orbital stirring, in 1 mL of total volume. Withdrawn volume was always kept below 10%.

7.3 Results and discussion

The mathematical model developed for the CPO-oxidation of β-OH coupled to the DHA aldol addition of FSA to produce preFagomine was used to find the optimal initial conditions for this reaction, in one-pot approach. The variables to optimize are then the initial concentrations of *t*-BuOOH, β-OH, DHA, CPO and FSA. Their optimal value to render the higher preFagomine yield was found using the gPROMS® software. Considering a time horizon of 5 h, the highest preFagomine yield was found to be 14.6%, although no significant increment in conversion was observed after the first 30 min of reaction. The values of the variables are detailed in Table 7.1. Y_{CPO} and Y_{FSA} values were found to be at the upper bound of the variable range used in the optimization. That range was not further increased since both upper bound already correspond to a high amount of enzyme. Therefore, the simulations predict that a high quantity of both enzymes is required to obtain a preFagomine yield around 15%.

Since the main problem of the coupled reaction is the inactivation of FSA, a (semi)continuous addition of the peroxide and DHA was thought as a solution, keeping both concentrations at a low level to reduce the inactivation. Enzyme additions were also considered. However, when simulating, it was observed that the optimization value was not close to that point. The model predicts a higher preFagomine yield if the amino alcohol oxidation is fast, producing amino aldehyde to be converted into the aldol adduct. This requires a high concentration of peroxide at the beginning of the reaction to speed this oxidation. Then, a higher DHA concentration is required for the aldol addition, before FSA becomes inactivated.

Table 7.1. Optimal values of the variables from the CPO/FSA-catalyzed synthesis of preFagomine.

Variable	Value	Units	Optimization interval
$[t\text{-BuOOH}]_0$	39.9	mM	0-100
$[\beta\text{-OH}]_0$	16.0	mM	5-40
$[\text{DHA}]_0$	72.6	mM	0-200
Y_{CPO}	3.57	$g \cdot L^{-1}$	0-3.57
Y_{FSA}	13.33	$g \cdot L^{-1}$	0-13.33

The values from Table 7.1 were experimentally checked by performing a coupled reaction at these initial conditions using both soluble CPO and FSA. A comparison table between the conversions/yields predicted from the model and the experimentally measured values is shown in Table 7.2. Similar values were obtained, confirming the applicability of the model and the unfeasibility of the coupled system. This coupled reaction was not performed employing immobilized biocatalysts, as it represents an enzyme load too high to be immobilized on the support if the relation 10% v/v of support/reaction medium is maintained.

Table 7.2. Predicted and measured values at the end-point of the CPO/FSA-catalyzed synthesis of preFagomine performed in the optimal initial conditions according to the kinetic model. $[t\text{-BuOOH}]_0 = 39.9$ mM, $[\beta\text{-OH}]_0 = 16.0$ mM, $[\text{DHA}]_0 = 72.6$ mM, $Y_{CPO} = 3.57$ mg mL^{-1}, $Y_{FSA} = 13.33$ mg mL^{-1}. Reaction time = 60 min.

Variable	Units	Predicted value	Measured value
t-BuOOH conversion	%	100.0	>99
β-OH conversion	%	27.8	22.4
β-CHO yield	%	10.3	8.3
β-COOH yield	%	2.9	2.8
DHA conversion	%	46.7	48.7
preFagomine yield	%	14.6	11.4
CPO activity	%	73.6	66.1
FSA activity	%	≈0	<1

Hence, the coupled reaction is not feasible to be operated in one-pot configuration. An alternative operation is to separate both reactions, performing the overall reaction as two consecutive cascade reactions. That avoids the above mentioned four problems: (1) DHA is not oxidized and (2) does not inhibit the CPO oxidations, (3,4) FSA is not inactivated. However, the two latter points are not trivial: the inactivating agent (products from r_4, CPO) should be completely removed from the reaction medium before adding FSA for the second reaction. According to the FSA inactivation equation detailed in Chapter 5 (Equation 5.48), the inactivation is related to r_4, not to its products concentration which is considered to be negligible along time (degradation). Nevertheless, their removal should be ensured. CPO should be also removed, since *t*-BuOOH would remain in the reaction mixture.

7.3.1 Two-step coupled reaction

The two-step coupled reaction was performed in two separate vessels with an intermediate step of ultrafiltration to remove CPO from the reaction medium. The filtered mixture was left under mild agitation for 60 min in order to ensure the degradation of the formed radical.

The software was used again to find the initial conditions. In this case, the optimization procedure was different. To enable the further use of immobilized CPO and FSA in the reaction, the enzyme concentration was fixed at the maximum enzyme load maintaining the 10% v/v support/medium. This is, considering 1 mL of reaction volume, 50 mg of support for each enzyme can be used; in an eventual one-pot coupling, 100 mg (50 + 50) are used. For CPO immobilization, the enzyme capacity was close to 10 U (mg mNC)$^{-1}$. Assuming a retained activity of 62.5%, 312.5 U can be immobilized onto 50 mg mNC. This corresponds to 0.223 active mg CPO. For FSA immobilization, the maximum enzyme load was near 0.04 U (mg mNC)$^{-1}$. The retained activity is 29.1%; therefore, 0.58 U (0.039 active mg FSA) can be immobilized.

After setting the enzyme concentrations, the optimization of the first reaction has two variables: amino alcohol and peroxide concentrations. The best initial conditions were found at 5.0 mM β-OH and 5.5 mM *t*-BuOOH. The value for β-OH was found at the lower bound of the variable interval. It was not further decreased as it is already a low concentration of the target substrate. By simulation of alternative reactions, it was observed that the β-CHO yield does not substantially differ using 5.5–10.0 mM *t*-BuOOH as an initial value. The yield is 24.2% (5.5 mM) or 18.4% (10 mM), after 5 hours. The selected value to perform the reaction was 10.0 mM *t*-BuOOH, in order to facilitate the comparison with the one-pot reaction performed with high amount of enzyme, in which the peroxide concentration was nearly the double as the β-OH concentration.

For the aldol addition reaction, the enzyme concentration has been fixed, and the initial amino aldehyde concentration corresponds to the formed product in the β-OH oxidation. Assuming an initial β-OH concentration of 5.0 mM and a β-CHO yield of 18.4%, the expected initial β-CHO concentration in aldol addition is 0.92 mM. However, due to the filtration step and the addition of FSA and DHA to perform the second reaction, the initial β-CHO was reduced to 0.5 mM. Using model simulations, the initial value of DHA concentration was set at 20.0 mM, to ensure a preFagomine yield of the second reaction of 79.3%. Below that value (e.g. 5 mM DHA), yields lower than 70% are obtained; above that, no meaningful increment is observed.

7.3.1.1 Soluble biocatalysts

First, the two-step reaction was carried out using both soluble CPO and FSA. The oxidation of β-OH is plotted in Figure 7.1, in which the model simulation is also represented. The experimental data fit the prediction of the model, leading to a β-CHO yield of 17.9% (expected: 18.4%). The reaction was stopped after 5 hours when the measured activity of CPO was negligible. The reaction mixture was filtered, and after 60 min the aldol addition was started (Figure 7.2).

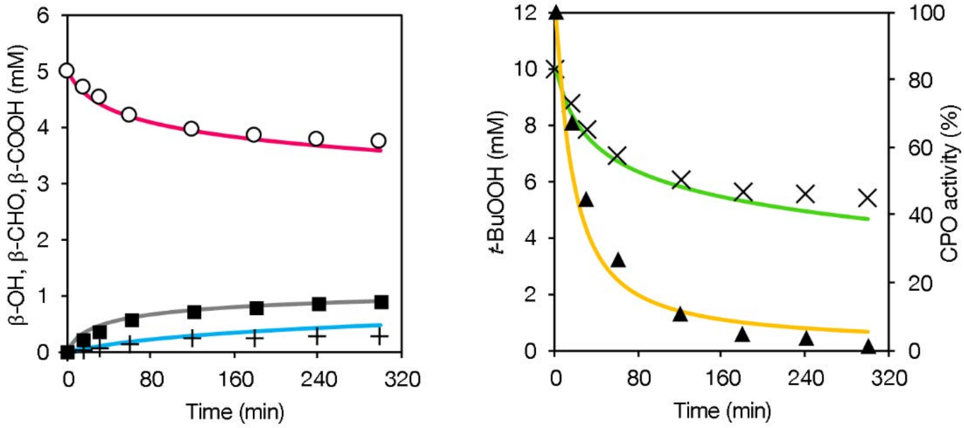

Figure 7.1. β-OH oxidation catalyzed by soluble CPO in the two-step synthesis of preFagomine. 312.5 U CPO mL^{-1} was used in 100 mM MES pH 6.5, 25 ºC. Initial concentrations: 5.0 mM β-OH, 10.0 mM *t*-BuOOH. Experimental data: β-OH (○), β-CHO (■), β-COOH (+), *t*-BuOOH (×), CPO activity (▲); model simulation: β-OH (➡), β-CHO (➡), β-COOH (➡), *t*-BuOOH (➡), CPO activity (➡).

In the FSA-catalyzed reaction, the experimental data did not fit the predicted values (not shown in the graph). The measured preFagomine yield was 38.4%, whereas the predicted one was 79.3%. The latter value was confirmed by performing an aldol addition reaction using commercial β-OH at the same reaction conditions (Figure 7.3) with a preFagomine yield of 81.1%. Therefore, the difference is likely caused by inactivation of FSA in the two-step reaction. Although no inactivation was expected, the soluble FSA activity dropped to less than 20% in 3 hours, probably because some inactivating agent was not removed from the mixture, and it inactivated FSA. Further stabilization was expected by using immobilized enzymes, either onto nanoparticles or conventional supports.

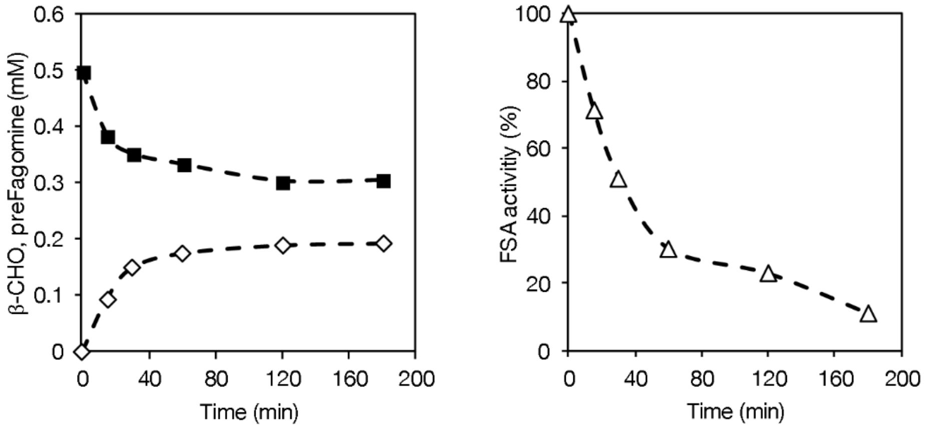

Figure 7.2. DHA aldol addition catalyzed by soluble FSA in the two-step synthesis of preFagomine. 0.58 U FSA mL^{-1} was used in 100 mM MES pH 6.5, 25 ºC. Initial concentrations: 0.5 mM β-CHO, 20.0 mM DHA. β-CHO (■), preFagomine (◇), FSA activity (△).

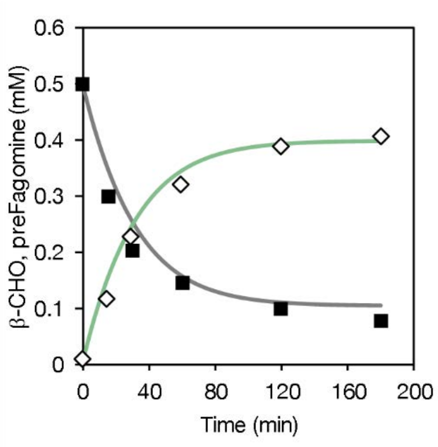

Figure 7.3. DHA aldol addition catalyzed by soluble FSA using commercial β-CHO. 0.58 U FSA mL^{-1} was used in 100 mM MES pH 6.5, 25 ºC. Initial concentrations: 0.5 mM β-CHO, 20.0 mM DHA. Experimental data: β-CHO (■), preFagomine (◇); model simulation: β-CHO (➡), preFagomine (➡).

7.3.1.2 CPO/FSA onto mNC

The immobilized nanobiocatalysts selected in previous chapters were tested in the two-step synthesis of preFagomine. The reaction was performed at the same initial conditions. Figure 7.4 shows the β-OH oxidation catalyzed by mNC-NH_2-$_{ox}$CPO, with similar results than soluble CPO. The amino aldehyde yield was 19.0% at the same reaction time (5 h). No improvement in the operational stability of the enzyme was observed, in contrast to the results in Chapter 6, where a different strategy for the peroxide addition was employed.

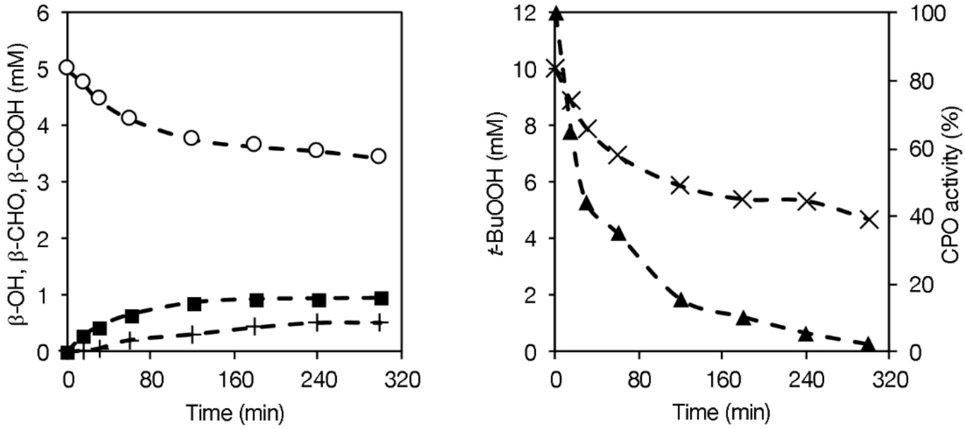

Figure 7.4. β-OH oxidation catalyzed by mNC-NH_2-$_{ox}$CPO in the two-step synthesis of preFagomine. 312.5 U CPO mL^{-1} was used in 100 mM MES pH 6.5, 25 ºC. Initial concentrations: 5.0 mM β-OH, 10.0 mM *t*-BuOOH. β-OH (○), β-CHO (■), β-COOH (+), *t*-BuOOH (×), CPO activity (▲).

In the aldol addition catalyzed by mNC-NH_2-FSA, a low yield of preFagomine was obtained: 15.0% (Figure 7.5). It is likely related to the rapid inactivation of FSA, similar to the results detailed in the previous chapter. It is then confirmed that mNC-NH_2-FSA is not an appropriate biocatalyst for this reaction.

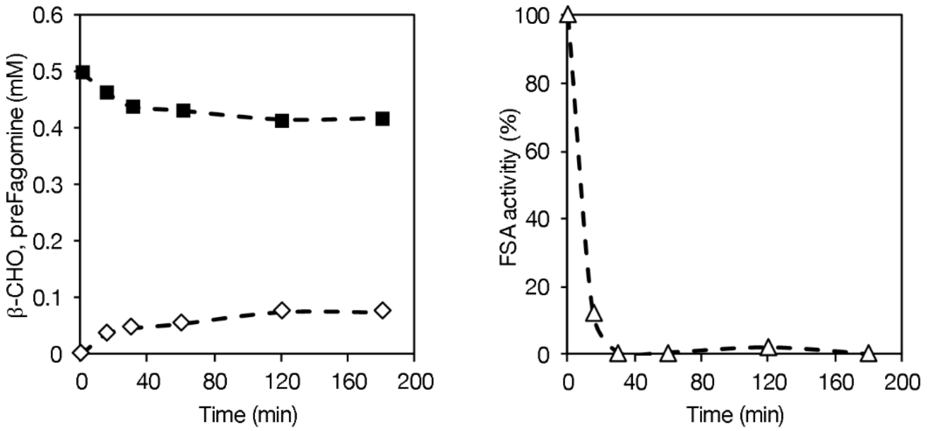

Figure 7.5. DHA aldol addition catalyzed by mNC-NH_2-FSA in the two-step synthesis of preFagomine. 0.58 U FSA mL^{-1} was used in 100 mM MES pH 6.5, 25 ºC. Initial concentrations: 0.5 mM β-CHO, 20.0 mM DHA. β-CHO (■), preFagomine (◇), FSA activity (△).

7.3.1.3 CPO/FSA on agarose support

Finally, the immobilized derivatives of CPO and FSA on an agarose support were tested in the two-step reaction. The oxidation of CPO on MANA-agarose (Figure 7.6) gave similar results with a β-CHO yield of 20.2%. Although the enzyme remained active after 5 h, the reaction was stopped because the amino aldehyde concentration started to drop. Note that the percentage of CPO activity from Figure 7.6 can be altered due to the presence of diffusional limitations.

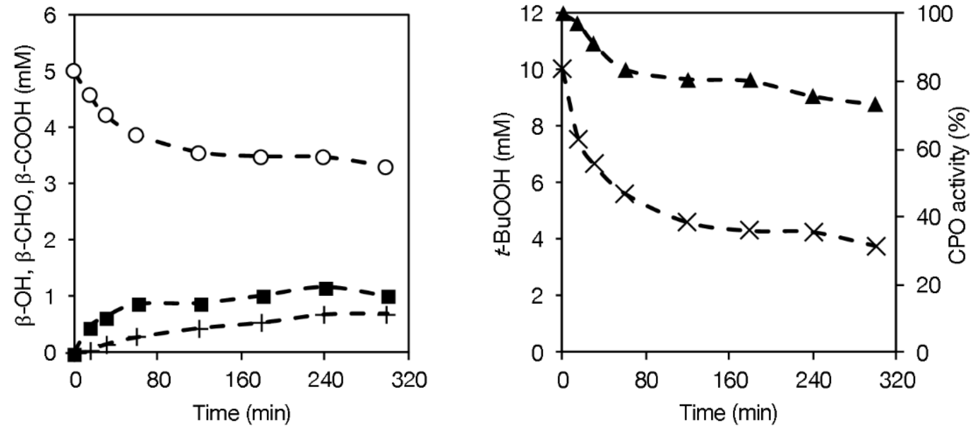

Figure 7.6. β-OH oxidation catalyzed by CPO immobilized on MANA-agarose in the two-step synthesis of preFagomine. 312.5 U CPO mL^{-1} was used in 100 mM MES pH 6.5, 25 ºC. Initial concentrations: 5.0 mM β-OH, 10.0 mM *t*-BuOOH. β-OH (○), β-CHO (■), β-COOH (+), *t*-BuOOH (×), CPO activity (▲).

The aldol addition catalyzed by FSA on CoIDA-agarose led to the best results in the second reaction (Figure 7.7), with a preFagomine yield of 96.3% (this reaction was left for 4 h since FSA remained active). Although diffusional limitations can hinder its interpretation, FSA stability is truly enhanced by the immobilization of the enzyme of CoIDA-agarose, and a final overall yield of 19,5% is reached.

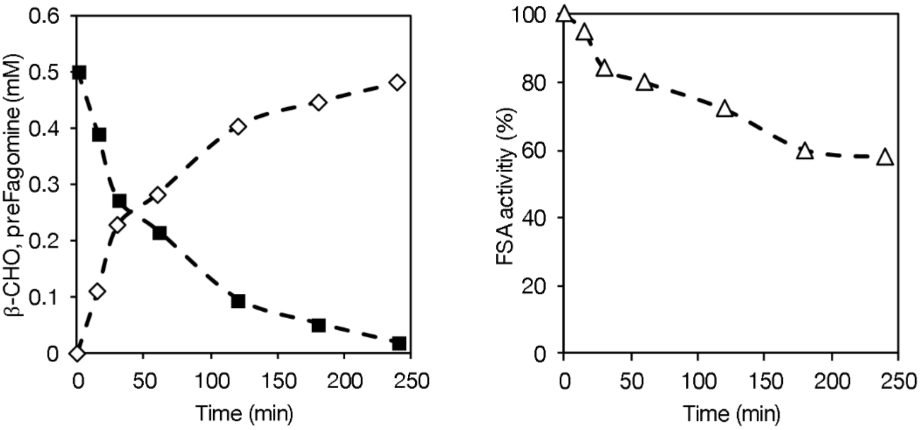

Figure 7.7. DHA aldol addition catalyzed by FSA immobilized on CoIDA-agarose in the two-step synthesis of preFagomine. 0.58 U FSA mL^{-1} was used in 100 mM MES pH 6.5, 25 ºC. Initial concentrations: 0.5 mM β-CHO, 20.0 mM DHA. β-CHO (■), preFagomine (◇), FSA activity (△).

Another extra reaction was performed using CPO-MANA-agarose and FSA-CoIDA at the same initial conditions in one-pot configuration. However, the stability improvement of FSA was not enough, and no meaningful concentration of preFagomine was measured (data not shown).

7.4 Conclusions

The kinetic model for the CPO-catalyzed β-OH oxidation and the FSA-catalyzed DHA aldol addition has been exploited to find the optimal conditions of operation. First of all, the coupled reaction was thought to be operated in one-pot configuration. However, the reaction performed at the optimal values gave a low preFagomine yield (11.4%) using a high amount of CPO and FSA. The experimental yield was similar to the value predicted by the model.

In order to improve the preFagomine yield, the reaction was performed as two consecutive cascade reactions, lowering the enzyme amount more than 1 order of magnitude. The best initial conditions were predicted by the model, and the reaction was performed using soluble and immobilized CPO/FSA. The best results were obtained with

CPO-MANA-agarose and FSA-CoIDA-agarose, with an overall preFagomine yield of 19.5%, in comparison to 6.9% (soluble CPO/FSA) or 2.8% (mNC-CPO/FSA).

These results could be enhanced using 100 mg of support per mL (here only 50 mg were used to compare with an eventual one-pot coupling). Besides, a further study with the immobilized biocatalysts on agarose would enable the correction of the model parameters, which are different from the soluble enzymes due to diffusional limitations and improved stability. With this, optimized initial conditions might be determined.

7.5 References

[1] R. Lonsdale, J. N. Harvey, A. J. Mulholland, *Chem. Soc. Rev.* **2012**, *41*, 3025–3038.

[2] R. Heinrich, S. Schuster, H.-G. Holzhütter, *Eur. J. Biochem.* **1991**, *201*, 1–21.

[3] J. L. van Roon, C. G. P. H. Schroën, J. Tramper, H. H. Beeftink, *Biotechnol. Adv.* **2007**, *25*, 137–147.

[4] J. M. Woodley, *Comput. Chem. Eng.* **2017**, *105*, 297–307.

[5] D. J. Pollard, J. M. Woodley, *Trends Biotechnol.* **2007**, *25*, 66–73.

[6] D. Vasić-Rački, Z. Findrik, A. Vrsalović Presečki, *Appl. Microbiol. Biotechnol.* **2011**, *91*, 845–856.

[7] I. Gosling, *Ind. Biotechnol.* **2005**, *1*, 106–109.

[8] A. Illanes, *Enzyme Biocatalysis: Principles and Applications*, **2008**.

8 Overall conclusions. Future perspectives

The feasibility of a multi-enzymatic cascade to synthesize iminocyclitols using amino alcohols as the starting material has been investigated in this thesis work. A two-enzyme system has been presented to render the precursor of a model iminocyclitol, D-fagomine. Particularly, the coupled CPO-catalyzed β-OH oxidation and FSA-catalyzed DHA aldol addition that renders preFagomine is introduced. First of all, a preliminary study on the amino alcohol oxidative capacity of CPO regarding substrate structure has been discussed, confirming the acceptance of β-amino alcohols as substrates for this enzyme.

Experimental trials on the β-OH oxidation have been performed to determine the main operating conditions for the first assays of the coupled reaction in one-pot configuration. The reaction medium, pH, temperature and the peroxide were selected. However, many side reactions were identified, hindering the coupling of reactions: peroxide degradation, further oxidation of the amino aldehyde, DHA oxidation, and also a chemical reaction aldehyde–peroxide. Besides, inactivation of both enzymes was measured. The yield of preFagomine was negligible.

Two strategies were proposed to work out a solution: kinetic modeling and enzyme immobilization. A mathematical model for the whole system was developed by an exhaustive study of each reaction separately. This enabled a better understanding of the coupled reaction mechanism, showing the inhibitions between substrates and products from the different reactions. Finally, the kinetic model has been validated, although a very low amount of preFagomine has been obtained.

Concurrently, the effort has been made in enzyme immobilization to reduce the inactivation of CPO and FSA. Both enzymes have been immobilized on functionalized conventional supports of agarose. Furthermore, mNC has been used for the preparation of magnetic hybrid biocatalysts. A systematic study of the immobilization of CPO and FSA onto mNC has led to the preparation of several derivatives that could be employed in biotransformations. Hence, four biocatalysts were selected for further experimentation in the current system: CPO on MANA-agarose, FSA on CoIDA-agarose, mNC-NH_2-$_{ox}$CPO, and mNC-NH_2-FSA.

Finally, the kinetic model has been used for process intensification, determining the optimal conditions for the coupling in two reactor configurations: one-pot or two-consecutive vessels. Both strategies were investigated using soluble and immobilized CPO/FSA. The best results were obtained in the two-step reaction catalyzed by CPO-MANA-agarose and FSA-CoIDA-agarose, with an overall preFagomine yield of 19.5%.

Although the above-mentioned yield could be increased if using a higher amount of enzymes, results have demonstrated the limitations of the coupling of CPO and FSA reactions. The selection of another peroxidase to catalyze the oxidation of the amino alcohol could be an alternative. This peroxidase should not accept a broad range of different substrates like CPO does. Another alternative is regarding the genetic modification of the enzymes to increase their stability in the reaction.

In the case of the operation with the current CPO and FSA, the separation of the two reactions appears to be the proper solution, with both enzymes in immobilized form. The immobilization on functionalized agarose used in the work gave the best results in terms of the target yield. Besides, mNC can also be used if the immobilization of FSA on mNC with functionalization different from NH_2 is achieved.

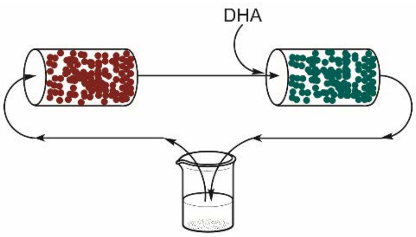

Figure 8.1. Schematic representation of the proposed operating mode. CPO (●); FSA (●).

Then, in both cases, another reactor configuration is proposed: two plug flow reactors, each one with an immobilized enzyme (CPO or FSA) (Figure 8.1). The output of the CPO-reactor connects with the input of the FSA-reactor, whose output is recycled to the input of the first reactor looking for full conversion of the initial substrate. With this, CPO and FSA are not in contact, so the inactivation of FSA is minimized. DHA is added at a low flow directly into the FSA-reactor, avoiding reaching the first reactor before its reaction to preFagomine. A third reactor after the CPO-reactor can be added to ensure the degradation of the peroxy radical, by an eventual addition of antioxidants. In the case of mNC, the plug flow reactor can be substituted by a magnetic separator; i.e. only the tube with the peristaltic pump for the recirculation, with two magnetic separators: one retaining CPO, another one with FSA. Nevertheless, in any case, the formation of the by-product β-COOH would be completely avoided.

If the system succeeds, other steps could be added in the cascade reaction, such as the *in-situ* formation of peroxide and β-amino alcohol. The β-amino alcohol synthesis from β-keto alcohols may be carried out by an amino alcohol dehydrogenase using NADH as cofactor and NH^{4+} as amino group donor.

9 Acknowledgments

This work was supported by Spanish MINECO (project No. CTQ2014-53114R), co-financed by European Regional Development Fund. The Department of Chemical, Biological and Environmental Engineering of UAB constitutes the Biochemical Engineering Unit of the Reference Network in Biotechnology, and the research group 2014SGR452, Generalitat de Catalunya. Financial support from Spanish MINECO for the PhD scholarship of Gerard Masdeu is acknowledged. The authors acknowledge the financial support for the research stay in the host institutions (Jožef Stefan Institute, University of Zagreb) from the European Comission (Erasmus pràctiques) and the COST-STSM-CM1303.

10 Scientific contributions

- Gerard Masdeu, Míriam Pérez-Trujillo, Josep López-Santín, Gregorio Álvaro, **Chloroperoxidase-catalyzed amino alcohol oxidation: Substrate specificity and novel strategy for the synthesis of *N*-Cbz-3-aminopropanal**, Process Biochemistry, Volume 51, Issue 9, 2016, Pages 1204-1211.

  Author contribution:
  Masdeu performed all the CPO-catalyzed oxidations and experimental analyses, apart from the experimental design, results interpretation and manuscript drafting.
  Pérez-Trujillo identified the products from the chemical reaction by NMR analysis.
  López-Santín and Álvaro contributed to the experimental design, results interpretation and manuscript revision.

- Gerard Masdeu, Míriam Pérez-Trujillo, Josep López-Santín, Gregorio Álvaro, **Data on the identification and characterization of by-products from N-Cbz-3-aminopropanal and *t*-BuOOH/H_2O_2 chemical reaction in chloroperoxidase-catalyzed oxidations**, Data in Brief, Volume 8, 2016, Pages 659-665.

  Author contribution:
  Masdeu performed the preparation of all the compounds from the chemical reaction aldehyde-peroxide, and their concentration analyses, apart from the manuscript drafting.
  Pérez-Trujillo did the NMR characterization of the products from the chemical reaction, and contributed to the manuscript drafting.
  López-Santín and Álvaro contributed to the manuscript revision.

- Gerard Masdeu, Slavko Kralj, Stane Pajk, Josep López-Santín, Darko Makovec, Gregorio Álvaro, **Hybrid chloroperoxidase-magnetic nanoparticle clusters: effect of functionalization on biocatalyst performance**, Journal of Chemical Technology and Biotechnology, 2017.

  Author contribution:
  Masdeu performed the experimental design, all the immobilization assays, and oxidation reactions, apart from the results interpretation and manuscript drafting.
  Slavko Kralj did the preparation and characterization of the magnetic nanoparticle

clusters, and contributed to the manuscript drafting.

Stane Pajk did the alkynes synthesis, and contributed to the manuscript drafting.

Darko Makovec contributed to the manuscript drafting.

López-Santín and Álvaro contributed to the experimental design, results interpretation and manuscript drafting.

11 Appendix

11.1 Products from the chemical reaction aldehyde-peroxide

Three preparative reactions were carried out in order to obtain sufficient amounts of compounds **6**-**8** (Figure 3.6) for NMR and MS analyses. β-CHO (17 mM, maximum solubility) was dissolved in 10 mL of water. The selected peroxide was added to the reaction medium and incubated for 24 h. To prepare compound **6**, 250 mM *t*-BuOOH was used (ca 50% yield); for **7**, 600 mM H_2O_2 (ca 65% yield); and for **8**, 72 mM H_2O_2 (ca 99% yield). All reactions were performed at 25°C and 1000 rpm of orbital stirring orbital stirring. Compounds **6–7** were carefully filtered prior to the analysis to eliminate impurities. Compound **8** was isolated by filtration and carefully dried at 35 °C.

Compounds **6–8** were identified by MS and NMR spectroscopy. The exact mass of compound **6** was obtained by MS: 320.1469 (ESI+, positive electrospray ionization). The chemical structure of molecule **6** was elucidated by ^{1}H NMR spectroscopy, via one-dimensional (1D)-selective nuclear Overhauser effect spectroscopy (NOESY) experiments. The reaction intermediate **7** was detected, and its mass was identified by HPLC-MS (264.0842). By HPLC–MS/MS, the main ion fragment was identified (201.0769), which confirmed the presence of the Cbz substituent. The concerted analysis of 1D and 2D NMR experiments allowed full ^{1}H and ^{13}C NMR characterization of **7**, confirming its molecular structure. Finally, the compound **8** was analyzed by MS–ESI+ (471.1744). The chemical structure of **8** was obtained by 1D, 2D, and diffusion-ordered spectroscopy (DOSY) NMR experiments.

The NMR experiments conducted for the structural elucidation of the products were performed at *Servei de Ressonància Magnètica Nuclear* from *Universitat Autònoma de Barcelona (UAB)*. The masses of products **6**–**8** were confirmed by mass spectrometry (Figure 11.1, Figure 11.2, Figure 11.3): HPLC–MS/MS or MS at *Servei d'Anàlisi Química, UAB*.

The complete characterization of the three compounds is presented as follows:

Benzyl (3-(tert-butylperoxy)-3-hydroxypropyl)carbamate (6): Colorless; ^{1}H NMR (600 MHz, H_2O–D_2O 67:33): δ = 7.39–7.29 (br m, 5H), 5.13 (t, J=5.8, 1H), 5.03 (br s, 2H), 3.17 (br m, 2H), 1.75 (m, 1H), 1.69 (m, 1H), and 1.15 (s, 9H); MS-ESI+: *m*/*z* = 320.1469, calculated for $C_{15}H_{23}NO_5$: 320.1468.

Benzyl (3-hydroperoxy-3-hydroxypropyl)carbamate (7): Colorless; ^{1}H NMR (600 MHz, H_2O–D_2O 67:33): δ = 7.39–7.29 (br m, 5H), 5.09 (t, *J* = 5.8, 1H), 5.04 (br s, 2H), 3.17 (br m, 2H), 1.74 (m, 1H), 1.69 (m, 1H); ^{13}C NMR (150 MHz, $CDCl_3$): δ = 158.1, 136.4, 128.9, 128.5, 128.3, 99.3, 66.8, 36.5, and 32.4; HPLC–MS–ESI+: *m*/*z* = 264.0856, calculated for $C_{11}H_{15}NO_5$: 264.0842.

Dibenzyl (peroxybis(3-hydroxypropane-3,1-diyl))dicarbamate (8): White solid; ^{1}H NMR (600 MHz, $CDCl_3$): δ = 7.39–7.29 (br m, 10H), 5.39 (br m, 2H), 5.09 (br m, 4H), 3.36 (br m, 4H), and 1.79 (br m, 4H); ^{13}C NMR (150 MHz, $CDCl_3$): δ = 157.0, 136.2, 128.9, 128.5, 128.3, 99.4, 66.7, 36.1, and 33.6; MS–ESI+: *m*/*z* = 471.1744, calculated for $C_{22}H_{28}N_2O_8$: 471.1738.

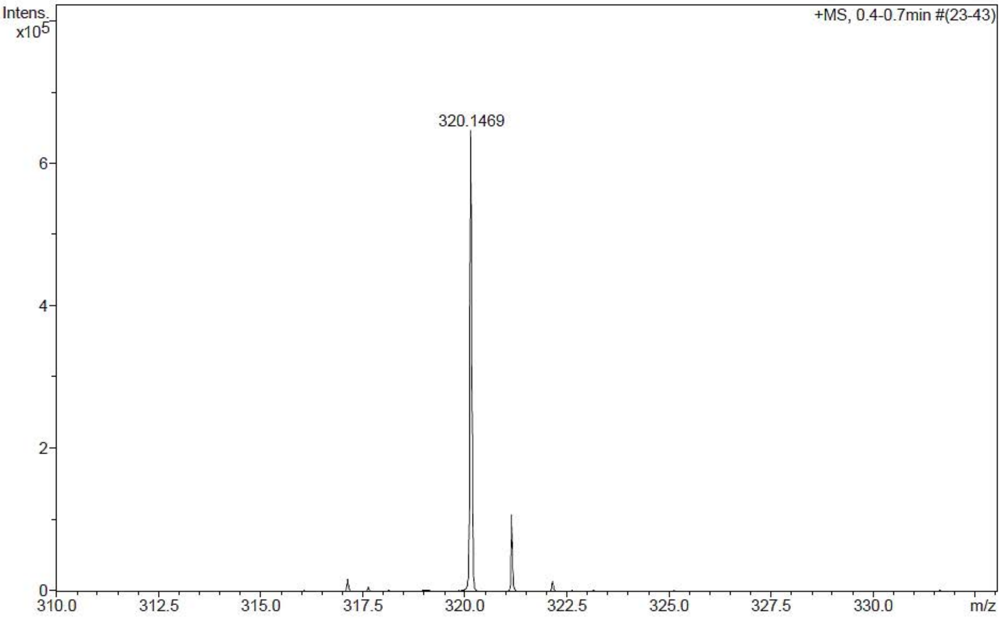

Figure 11.1. MS–ESI+ spectra of the identified compound **6** (m/z = 320.1469), obtained by the chemical reaction between *N*-Cbz-3-aminopropanal and *t*-BuOOH.

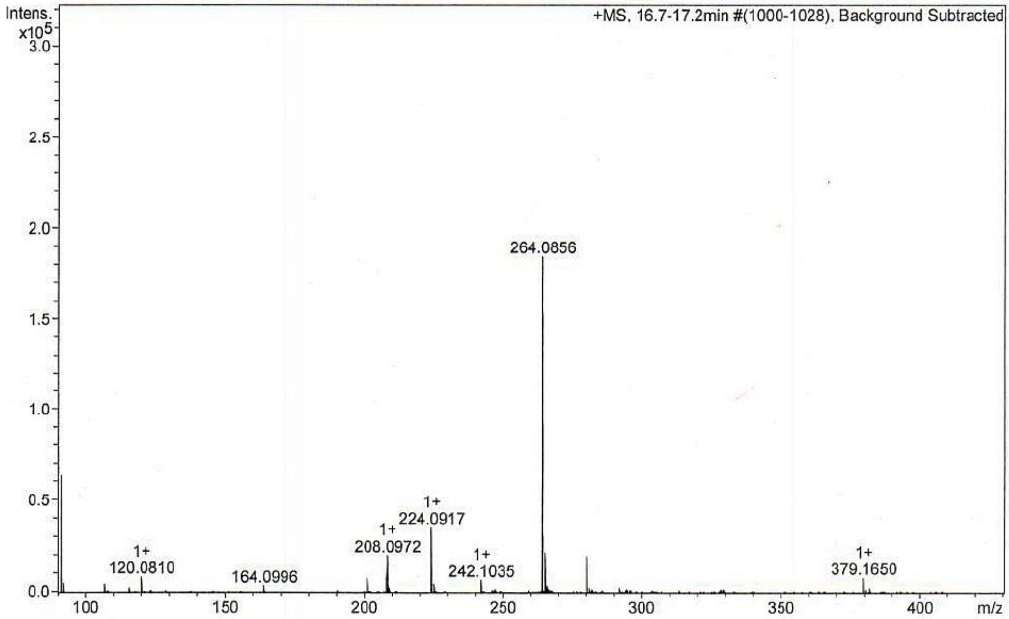

Figure 11.2. HPLC–MS–ESI+ spectra of the identified compound **7** (m/z = 264.0856), obtained by the chemical reaction between *N*-Cbz-3-aminopropanal and H_2O_2.

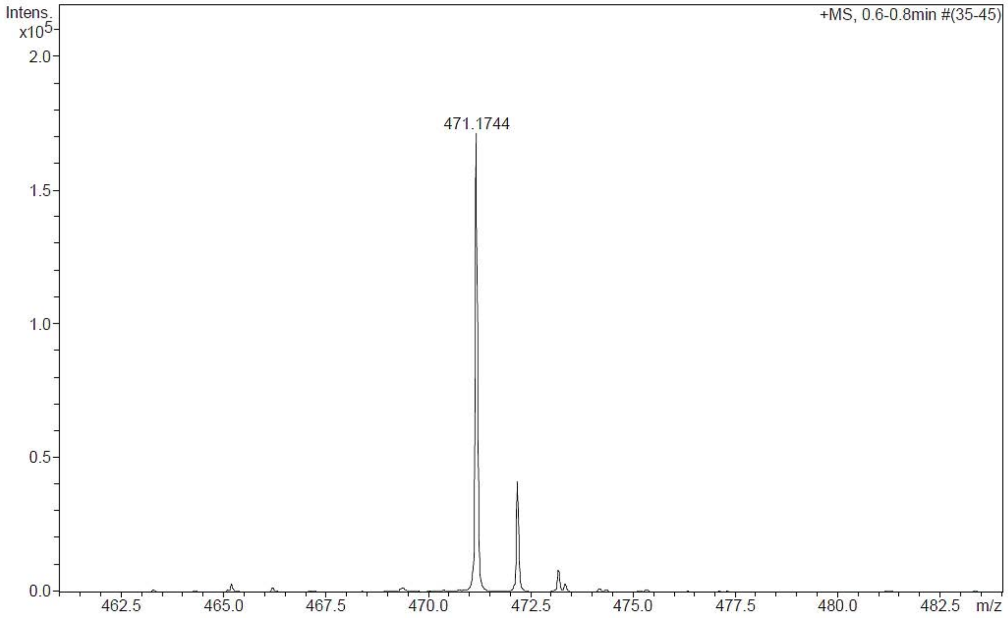

Figure 11.3. MS–ESI+ spectra of the identified compound **8** (m/z = 471.1744), obtained by further chemical reaction between *N*-Cbz-3-aminopropanal and the product from the reaction of *N*-Cbz-3-aminopropanal and *t*-BuOOH.

11.2 FSA production

FSA was produced in high-cell density fed-batch *E. coli* cultures employing a modification of previously published procedures.[1] Preinoculum cultures of *E. coli* BL21(DE3) containing the plasmid pET22-fsaA with the single mutation A129S were grown from Cryobilles stocks in 50 mL falcon tubes, containing 15 mL of Lysogeny Broth (LB) medium (10 g peptone L^{-1}, 5 g yeast extract L^{-1}, 10 g NaCl L^{-1}) and supplemented with ampicillin at a final concentration of 100 mg L^{-1}. An overnight incubation (14–16 hours) was performed at 37 °C on a rotator shaker at 150 rpm.

To prepare the inoculum culture, a determined amount of preinoculum was transferred into a 100 mL shake flask containing 100 mL of defined minimal (DM) medium to reach a final OD_{600nm} (optical density) of 0.1. 100 mL of DM medium consisted of glucose (5.0 g L^{-1}), K_2PO_4 (2.97 g L^{-1}), KH_2PO_4 (0.60 g L^{-1}), NaCl (0.46 g L^{-1}), $(NH_4)_2SO_4$ (0.75 g L^{-1}), $MgSO_4$ (0.025 g L^{-1}), $FeCl_3$ (0.0025 g L^{-1}), and ampicillin (0.0125 g L^{-1}), with 22 µL of the Microelements solution (Table 11.1). The shake flask was incubated 3–4 hours to reach an OD_{600nm} of 1.2.

Table 11.1. The composition of Microelements solution.

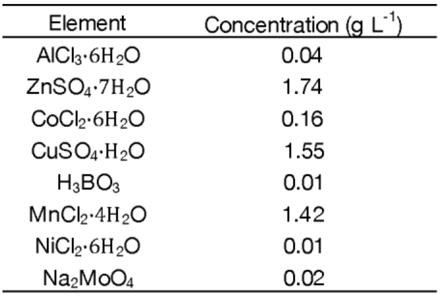

Element	Concentration (g L^{-1})
$AlCl_3 \cdot 6H_2O$	0.04
$ZnSO_4 \cdot 7H_2O$	1.74
$CoCl_2 \cdot 6H_2O$	0.16
$CuSO_4 \cdot H_2O$	1.55
H_3BO_3	0.01
$MnCl_2 \cdot 4H_2O$	1.42
$NiCl_2 \cdot 6H_2O$	0.01
Na_2MoO_4	0.02

For the batch phase, 80 mL of the inoculum culture were transferred to the bioreactor containing 720 mL of DM medium. 1 L of DM medium consisted of glucose (20.0 g L^{-1}), K_2PO_4 (11.9 g L^{-1}), KH_2PO_4 (2.4 g L^{-1}), NaCl (1.8 g L^{-1}), $(NH_4)_2SO_4$ (3.0 g L^{-1}), $MgSO_4$ (0.1 g L^{-1}), $FeCl_3$ (0.01 g L^{-1}), and ampicillin (0.05 g L^{-1}), with 90 µL of the microelements solution (Table 11.1). The growth was carried out using a Biostat® B bioreactor (Braun Biotech, Berlin, Germany) equipped with 2 L jar. 19 OD_{600nm} were reached at the end of this phase (Figure 11.4). When glucose was consumed after the batch step (10.7 h after inoculation), substrate feeding was initiated. 500 mL feeding solution consisted of glucose (478.0 g L^{-1}), $MgSO_4$ (9.56 g L^{-1}), $FeCl_3$ (0.49 g L^{-1}), ampicillin (0.05 g L^{-1}), and

$CaCl_2$ (0.089 g L^{-1}), with 31.5 µL of the microelements solution (Table 11.1). Fed-batch phase was performed using a predetermined exponential feeding profile to keep constant the specific growth rate at $\mu=0.22$. Glucose was the limiting substrate. Feeding solution was supplied in a discrete way using an automatic microburette of 2.5 mL capacity.

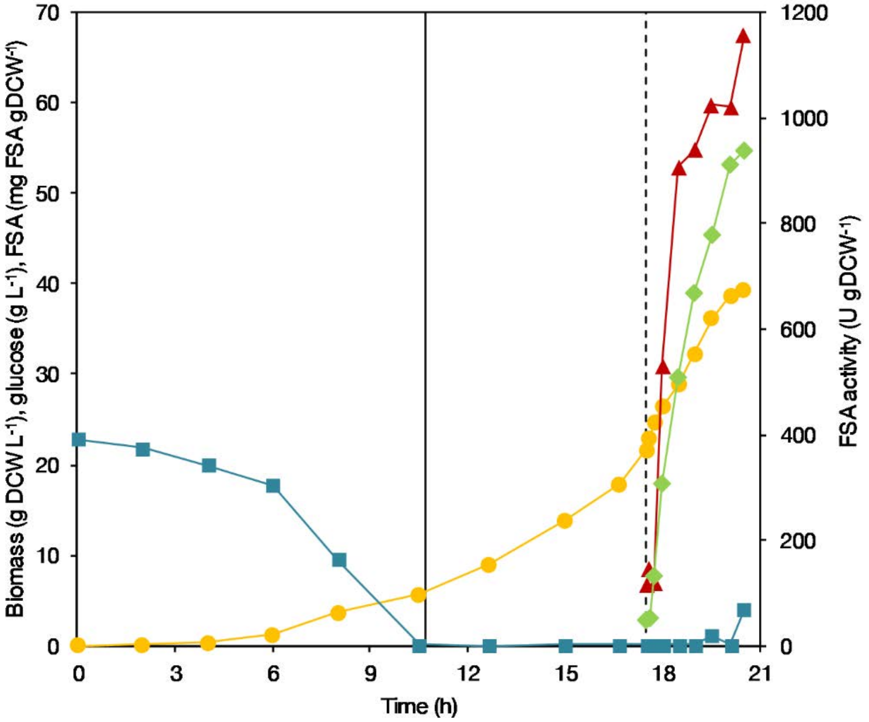

Figure 11.4. Time course of FSA production during fed-batch cultivation. Glucose (■), biomass (●), FSA activity (◆), FSA mass units (▲). The vertical continuous line indicates the moment in which the feeding started (t=10.7 h), while the vertical dashed line indicates the time when the pulse of IPTG is added into the culture in order to induce the overexpression of FSA (t_{ind} = 17.5 h).

Induction of the recombinant FSA was initiated when a high cell density was achieved (OD_{600nm}=72) by a pulse of a 100 mM IPTG stock solution to obtain a final concentration of IPTG inside the reactor of 100 µM.

The pH was maintained at 7,00±0,05 by adding 15% (w/v) NH_4OH solution to the reactor. The temperature was kept at 37ºC. The pO_2 value was maintained at 60% saturation by adapting the stirrer speed between 450 and 1150 rpm (pO_2 controlled by cascade through the stirring) and supplying air and/or pure oxygen at a flow rate of 1.5 L min^{-1} according to biomass requirements. When the stirring reached the maximum speed which is 1194 rpm, the proportion of air and pure oxygen is altered. 20 µL of antifoam –

50% (v/v) silicone-antifoam– was added at the beginning of the batch step. Few drops of antifoaming were added once along the fermentation. Inducer was added to the reactor by a single pulse using a stock solution of 100 mM.

The feeding solution did not contain phosphates because at high concentrations they may precipitate, so a concentrated solution of phosphates 500 g L^{-1} K_2HPO_4 and 100 g g L^{-1} KH_2PO_4 was prepared. Single pulses of 5 mL of this solution were added to the reactor every 30 OD_{600nm} increase of biomass.

Cellular concentration in the cultivation broth was determined by measurement of OD at a wavelength of 600 nm in the linear range 0.1-0.8 absorbance. One unit of OD_{600nm} is estimated as 0.3 g DCW L^{-1}. Glucose concentration in the culture medium was determined enzymatically (Biochemistry analyzer 2700 Select, YSI, Ohio, USA). The sample was withdrawn from the reactor and the biomass was eliminated by centrifugation at 14000 rpm for 5 minutes. Supernatant was filtered using a 0.45 µm Ø filter.

The expression of the recombinant protein is intracellular. Hence, for its analysis it is necessary to disrupt the biomass. The lysis procedure is based on the sonication of a sample adjusted to an OD_{600nm}=4 in 100 mM Tris-HCl buffer (pH 7.5) using a Vibracell CV50 sonicator (Sonics & Materials, Newtown, USA) for 4 cycles of 15 seconds, and two minutes between cycle. Samples were kept on ice. Afterwards, the disrupted sample was centrifuged at 14000 rpm for 10 minutes in order to separate the cell debris. The quantification of the specific activity of the target protein was carried out by the enzyme activity according to activity test, and by mass determination using Bradford method together with SDS-PAGE and densitometry using the specific software Image Lab© (Bio-Rad Laboratories). The protocol for gel electrophoresis is detailed below.

After the fermentation, the biomass was separated from the cultivation medium by centrifugation, and the pellet was kept at -20 °C for further experiments. As shown in Figure 11.4, the final biomass was 39.4 g DCW L^{-1}, with total protein production of 306.2 mg L^{-1} and FSA activity of 937.8 U (g DCW)$^{-1}$. Using gel densitometry (Figure 11.5), calculated FSA specific activity was 13.9 U (mg FSA)$^{-1}$. After FSA purification (below), it increased to 15.0 U (mg FSA)$^{-1}$, probably by removal of other proteins and salts that may interfere in the protein and activity analyses.

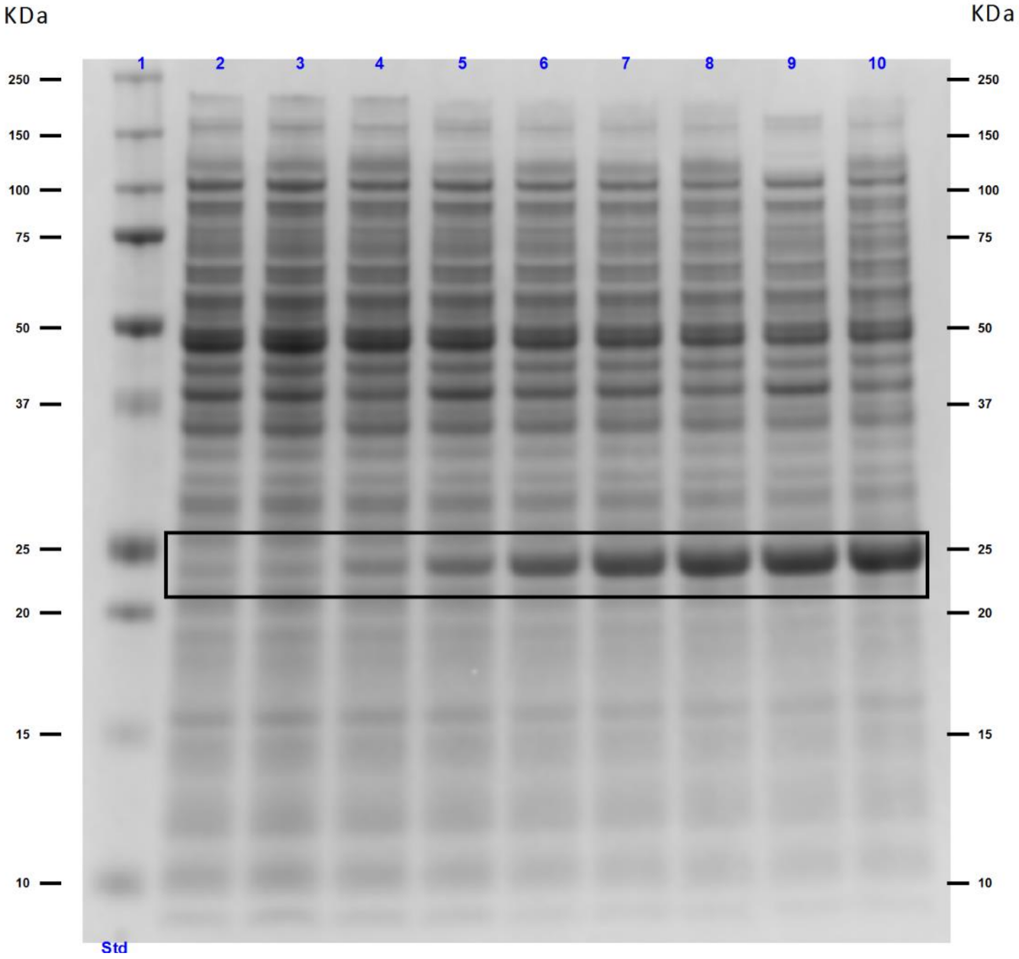

Figure 11.5. SDS-PAGE from the FSA A129S fermentation. The lanes correspond, from left to right, to (1) molecular marker, (2) pre-induction sample, and after-induction samples: (3) 5 min, (4) 15 min, (5) 30 min, (6) 1 h, (7) 1.5 h, (8) 2 h, (9) 2.5 h, (10) 3 h. The drawn rectangle indicates the FSA band (23 KDa).

11.3 SDS-PAGE

Electrophoresis was employed to determine the percentage of FSA among the rest of intracellular soluble proteins. NuPAGE® 12 % Bis Tris gels (Invitrogen, US) with MES-SDS as running buffer were used. Samples were prepared with 5 µL of sample buffer 4X, 3 µL of milliQ water, 2 µL of reducing agent, and 10 µL of the sample. Mixtures were incubated for 10 min at 70°C and 300 rpm in a dry bath.15 µL of each sample were loaded into the gel. One of the wells of the gels was loaded with 5 µL of protein standard marker (Bio-Rad®). After 40min running at 200 V, gels were rinsed with distilled water and then covered with gel fixation solution (40 % methanol, 10 % acetic acid in water) for 1 hour. Finally, gels were covered with Bio-SafeTM Comassie (BioRad®) for 1-2 hours to dye the protein bands.

11.4 FSA purification

The purification of FSA was performed by affinity separation employing agarose functionalized with iminodiacetic acid and chelated with cobalt (CoIDA-agarose). To this end, ¼ of the fermentation pellet was unfrozen and suspended in 50 mM sodium phosphate buffer (pH 8.0) to the corresponding final volume to achieve an OD_{600nm} close to 100 (approximately 300 mL). This volume was disrupted using a mechanical disruptor (Constant Cell Disruption Systems, Northamptonshire, UK), with 1 single step at 2.76 kBar. 8 mL were disrupted in every step. The final disrupted volume (approximately 300 mL) was incubated with 15 g CoIDA-agarose, and left under mild agitation for 60 min. Then 300 mM imidazole was added and left for incubation for 60 min to elute the protein to the supernatant. Finally, purified FSA was recovered by filtration.

11.5 Analysis of preFagomine

For the preparation of preFagomine sample, 20 mM β-CHO, 30 mM DHA, and 0.13 mg FSA mL^{-1} were incubated for 120 min in distilled water (no buffer was used to reduce the amount of salts for the analyses). Figure 11.6 shows the HPLC-MS results that confirm the proposed preFagomine structure. These analyses were performed at *Servei d'Anàlisi Química, UAB.*

preFagomine: colorless; MS-ESI+ (Na^+): *m/z* = 320.1106, calculated for $C_{14}H_{19}NO_6$: 320.1105.

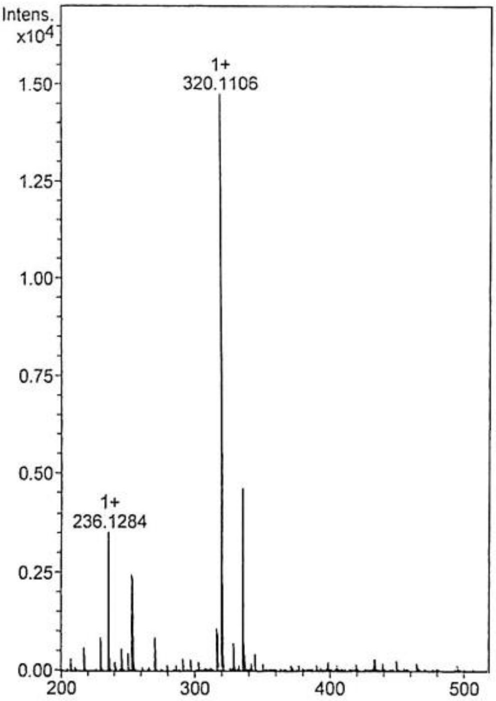

Figure 11.6. MS–ESI+ (Na^+) spectra of preFagomine (m/z = 320.1106).

11.6 Analysis of the product of DHA oxidation

For the preparation of $_{ox}$DHA (1,1,3-trihydroxypropan-2-one), 100 mM *t*-BuOOH, 100 mM DHA, and 1.79 mg CPO mL^{-1} were incubated for 120 min in distilled water (no buffer was used to reduce the amount of salts for the analyses). Figure 11.7 shows the HPLC-MS results that confirm the proposed structure. These analyses were performed at *Servei d'Anàlisi Química, UAB.*

1,1,3-trihydroxypropan-2-one: colorless; MS-ESI+ (Na^++H_2O): *m*/*z* = 147.0267, calculated for $C_3H_6O_4$: 147.0264.

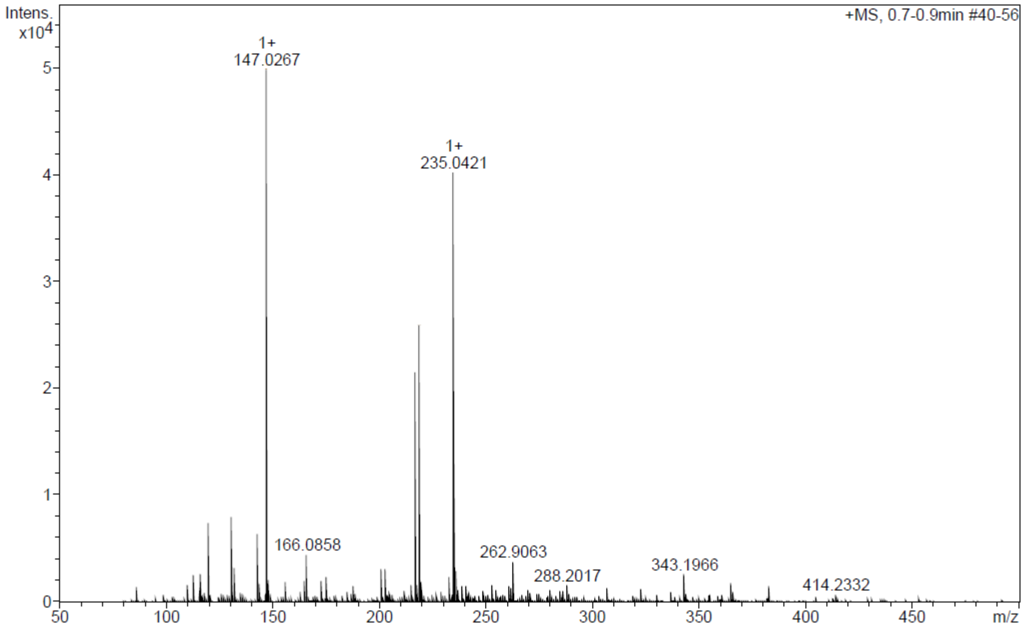

Figure 11.7. MS–ESI+ ($Na^{+}+H_2O$) spectra of **1,1,3-trihydroxypropan-2-one** (m/z = 147.0267).

11.7 Silane-C-C≡H/N$_3$ synthesis

This synthesis was carried out by Dr. Stane Pajk. All reactions (**a**, **b**, **c** from Figure 11.8) were performed under argon atmosphere, unless otherwise stated. Analytical TLC was performed on Merck silica gel (60 F_{254}) plates (0.25 mm) and visualized with 20% sulphuric acid in ethanol and ninhydrin detection reagents. ^{1}H NMR spectra were recorded on a Bruker AVANCE III 400 MHz NMR spectrometer in $CDCl_3$, MeOH-d_4 and DMSO-d_6 solution, with TMS or residual non-deuterated solvent as the internal standards. Mass spectra were recorded using an Advion expression CMS mass spectrometer.

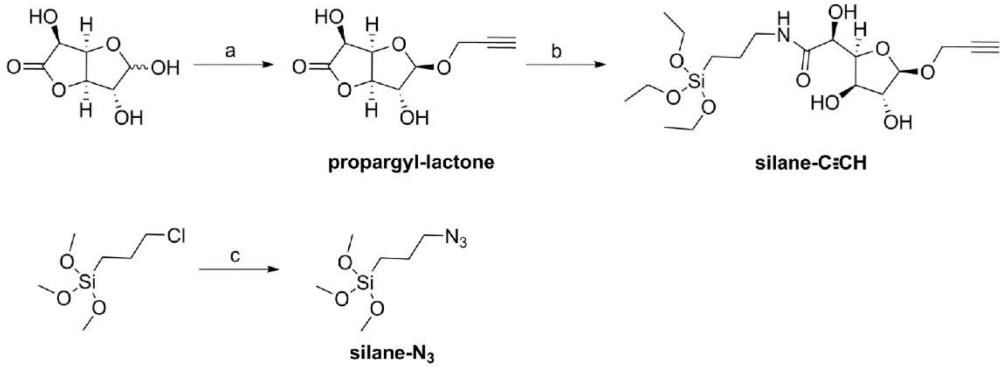

Figure 11.8. Reagents and conditions: (**a**) propargyl alcohol, H_2SO_4, 0 °C to 55 °C, 65%; (**b**) (3-amino propyl)triethoxysilane, ethanol, 60 °C; (**c**) NaN_3, DMF, 60 °C, 55%.

Propargyl-β-D-glucuronic acid γ-lactone (propargyl-lactone) was synthesized as described in the literature[2] with modifications. The D-(+)-glucuronic acid γ-lactone (4 g, 22.6 mmol, 1 equiv.) was suspended in propargyl alcohol (6.70 mL, 113 mmol, 5 equiv.) and cooled to 0 °C on an ice bath. Sulphuric acid (96 µL, 1.8 mmol, 0.08 equiv.) was added dropwise to the vigorously stirred reaction mixture. The reaction mixture was then stirred at 85 °C for 2 hours, when TLC analysis showed complete consumption of the starting lactone. $NaHCO_3$ (380 mg, 4.6 mmol, 0.2 equiv.) was added to the cooled down reaction mixture and the propargyl alcohol was removed under reduced pressure. The crude product was purified by flash chromatography (CH_2Cl_2:MeOH, 10: to 7:1), to give the desired product (3.14 g, 14.7 mmol, 65%) as a brownish syrup. α and β isomers were present; however, β isomer was the major product and the only one isolated after purification by flash chromatography. NMR data is in accordance with the literature.[2] NMR (DMSO-d_6, 400 MHz): δ (ppm) 5.94 (d, 1H, *J* = 6.0 Hz, OH), 5.79 (d, 1H, *J* = 3.6 Hz, OH), 5.12 (s, 1H, H-1), 4.80 (dd, 1H, *J* = 6.0, 4.8 Hz, H-4), 4.73 (d, 1H, *J* = 4.8 Hz, H-3), 4.44 (dd, 1H, *J* = 6.0, 6.0 Hz, H-5), 4.22 (dd, 1H, *J* = 15.6, 2.4 Hz, OCH_{ab}-C≡), 4.15 (dd, 1H, *J* = 15.6, 2.4 Hz, OCH_{ab}-C≡), 4.08 (d, 1H, *J* = 3.6 Hz, H-2), 3.36 (t, 1H, *J* = 2.4 Hz, ≡CH). MS (ESI): 237 $(M+Na)^+$.

For the synthesis of the (S)-2-((2S,3R,4R,5R)-3,4-dihydroxy-5-(prop-2-yn-1-yloxy) tetrahydro-furan-2-yl)-2-hydroxy-*N*-(3-(triethoxysilyl)propyl)acetamide (silane-C≡CH), to the solution of propargyl-β-D-glucuronic acid γ-lactone (318 mg, 1.61 mmol, 1 equiv.) in anhydrous ethanol (3 mL) was added (3-aminopropyl)triethoxysilane (393 µL, 1.61 mmol, 1 equiv.), and the reaction mixture was stirred at 50 °C for 2 hours (TLC analysis showed complete consumption of the starting propargyl-β-D-glucuronic acid γ-lactone). The solvent was removed under reduced pressure and the crude product was obtained in quantitative yield as brown oil. The product was used without further purification. NMR (MeOH-d_4, 400 MHz): δ (ppm) 5.11 (s, 1H, H-1), 4.46 (dd, 1H, *J* = 5.6, 4.8 Hz, H-4), 4.35 (d, 1H, *J* = 5.6 Hz, H-5), 4.27 (d, 2H, *J* = 2.4 Hz, OCH_2-C≡), 4.11 (dd, 1H, *J* = 4.8, 1.6 Hz, H-3), 4.04 (d, 1H, *J* = 1.6 Hz, H-2), 3.82 (q, 6H, *J* = 6.8 Hz, 3 × CH_2), 3.29-3.16 (m, 2H, CH_2), 2.84 (t, 1H, *J* = 2.4 Hz, ≡CH), 1.69-1-56 (m, 2H, CH_2), 1.21 (t, 9H, *J* = 6.8 Hz, 3 × CH_3), 0.70-0.60 (m, 2H, CH_2). MS (ESI): 458 $(M+Na)^+$.

(3-Azidopropyl)trimethoxysilane (silane-N_3) was synthesized as described previously[3] with modifications. To the suspension of NaN_3 (1,43 g, 20.8 mmol, 4 equiv.) and KI (455 mg, 2.6 mmol, 0.5 equiv.) in anhydrous dimethylformamide (10 mL) was added (3-chloropropyl)trimethoxysilane (1 mL, 5.5 mmol, 1 equiv.) and the obtained suspension was stirred for 24 h at 60 °C. The solvent was then removed under reduced pressure and the residue was suspended in diethyl ether. Solids were filtered off and diethyl ether removed under reduced pressure to give the desired product (712 mg, 3.4 mmol, 63%) as colorless oil. The product was used without further purification. NMR data is in accordance with the literature.[3] NMR ($CDCl_3$, 400 MHz): δ (ppm) 3.58 (s, 6H), 3.31-3.24 (m, 2H), 1.77-1.67 (m, 2H), 0.75-0.67 (m, 2H).

11.8 References

[1] D. Calleja, J. Kavanagh, C. de Mas, J. López-Santín, *Biotechnol. Bioeng.* **2016**, *113*, 772–782.

[2] A. Richel, F. Nicks, P. Laurent, B. Wathelet, J.-P. Wathelet, M. Paquot, *Green Chem. Lett. Rev.* **2012**, *5*, 179–186.

[3] S. S. Lee, S. N. Riduan, N. Erathodiyil, J. Lim, J. L. Cheong, J. Cha, Y. Han, J. Y. Ying, *Chem. - A Eur. J.* **2012**, *18*, 7394–7403.